The Role and Signaling Mechanism of IQGAP2 in Breast Cancer Tumorigenesis and Angiogenesis

By

Dinesh Kumar

LIFE11201404002

National Institute of Science Education and Research (NISER)

Bhubaneswar

A thesis submitted to the

Board of Studies in Life Sciences

In partial fulfillment of requirements

for the Degree of

DOCTOR OF PHILOSOPHY

Of

HOMI BHABHA NATIONAL INSTITUTE

October, 2020

Homi Bhabha National Institute

Recommendations of the Viva Voce Committee

As members of the Viva Voce Committee, we certify that we have read the dissertation prepared by Mr. Dinesh Kumar entitled "The role and signaling mechanism of IQGAP2 in breast cancer tumorigenesis and angiogenesis" and recommend that it may be accepted as fulfilling the thesis requirement for the award of Degree of Doctor of Philosophy.

Chairman – Dr. Sanjib Kar	Sanjib Kar	**Date:** 23/12/2020
Guide / Convener - Dr. Manjusha Dixit	Manjusha	**Date:** 23/12/2020
Examiner – Dr. Sandhya Sitasawad		**Date:** 23-12-2020
Member 1- Dr. Asima Bhattacharyya		**Date:** 23.12.20
Member 2- Dr. Tirumala Kumar Chowdary		**Date:** 23.12.2020
Member 3- Dr. Rajeeb Kumar Swain		**Date:** 23/12/2020

Final approval and acceptance of this thesis is contingent upon the candidate's submission of the final copies of the thesis to HBNI.

I/We hereby certify that I/we have read this thesis prepared under my/our direction and recommend that it may be accepted as fulfilling the thesis requirement.

Date: 23/12/2020

Place: NISER, Jatni

Manjusha

Dr. Manjusha Dixit

(Thesis Supervisor)

STATEMENT BY AUTHOR

This dissertation has been submitted in partial fulfillment of requirements for an advanced degree at Homi Bhabha National Institute (HBNI) and is deposited in the Library to be made available to borrowers under rules of the HBNI.

Brief quotations from this dissertation are allowable without special permission, provided that accurate acknowledgment of source is made. Requests for permission for extended quotation from or reproduction of this manuscript in whole or in part may be granted by the Competent Authority of HBNI when in his or her judgment the proposed use of the material is in the interests of scholarship. In all other instances, however, permission must be obtained from the author.

Dinesh Kumar

Dinesh Kumar

DECLARATION

I, hereby declare that the investigation presented in the thesis has been carried out by me. The work is original and has not been submitted earlier as a whole or in part for a degree/diploma at this or any other Institution/University.

Dinesh Kumar

Dinesh Kumar

List of Publications arising from the thesis

- **Kumar, D.**, Hassan, M. K., Pattnaik, N., Mohapatra, N., & Dixit, M. (2017). Reduced expression of IQGAP2 and higher expression of IQGAP3 correlates with poor prognosis in cancers. PLOS ONE, 12(10), e0186977. https://doi.org/10.1371/journal.pone.0186977

- **Kumar D**, Hassan MK, Patel SA, Pattanaik N, Mohapatra N, Dixit M., Reduced IQGAP2 expression promotes EMT and inhibits apoptosis by modulating the MEK-ERK and p38 signalling in breast cancer irrespective of ER status. (Communicated)

- **Kumar D**, Chawla S, Mohapatra N, Dixit M., Reduced expression of IQ motif-containing GTPase-activating protein 2 activates VEGF-A/VEGFR2-AKT signaling and regulates angiogenesis in breast cancer. (Communicated)

Other publications (as co-author)

- Hassan, M. K., **Kumar, D.**, Naik, M., & Dixit, M. (2018). The expression profile and prognostic significance of eukaryotic translation elongation factors in different cancers. PLOS ONE, 13(1), e0191377. https://doi.org/10.1371/journal.pone.0191377

- Hassan, M. K., **Kumar, D.**, Patel, S.A., Pattnaik, N., Mohapatra, N., & Dixit, M. (2020). Expression pattern of EEF1A2 in brain tumors: Histological analysis and functional role as a promoter of EMT. Life Sci. 4:117399. doi: 10.1016/j.lfs.2020.117399

- Hassan, M.K., **Kumar, D.**, Patel, S.A., & Dixit, M. EEF1A2 triggers stronger ERK mediated metastatic program in ER negative breast cancer cells than in ER positive cells. Life Sci. 2020:262:118553

Conferences

- **Kumar D**, Hassan MK, Dixit M. IQGAP2 regulates breast cancer progression, independent of molecular subtypes via. MEK/ERK pathway "XLII All India Cell Biology Conference"- BITS Pilani Dec 21-23, 2018, Goa, India. (P160)

- **Kumar D**, Hassan MK, Dixit M. Mechanistic studies to elucidate effect of IQGAP3 expression on ER signalling in Breast cancer. "International Congress of Cell Biology"- CCMB Jan 27-31, 2018, Hyderabad, India. (P044)

Dinesh Kumar

Dinesh Kumar

Dedicated to My Family

Acknowledgements

I would avail this opportunity to acknowledge all those who made this project successful. With humble gratitude and great respect, I would like to thank my project supervisor Dr. Manjusha Dixit for her guidance, constant support and encouragement. I am always indebted to for her immense help and valuable advice for the initiation and successful completion of the thesis. I am thankful to the National Institute of Science Education and Research (NISER), Department of Atomic Energy (DAE), Department of Science and Technology (DST), Science and Engineering Research Board (SERB) for funding the project. I would like to express my sincere thanks to the former Director of NISER, Prof. V. Chandrashekhar and present Director Prof S. Panda for permitting me to avail all the facilities in the institute related to my thesis work. I am highly obliged to my doctoral committee members Dr. Sanjib Kar, Dr. Asima Bhattacharyya, Dr. Tirumala Kumar Chowdary and Dr. Rajeeb Kumar Swain for their critical evaluation and valuable suggestions. I would also like to acknowledge Dr. Nagendra Sharma for his immense support and encouragement.

I am also grateful to Chairperson SBS NISER, and all other faculty members of SBS, NISER, for their support during my project. Special thanks to Dr. Niharika Pattanaik, Senior pathologist, AMRI Hospitals, and Dr. Nachiketa Mohapatra, Senior pathologist Apollo Hospital Pvt Ltd. for their help with clinical studies related to this project. I am highly obliged to Dr. Saurabh Chawla, Veterinarian and In-charge of Animal house, NISER, and other staff member of animal house for their continuous support in conducting experiments on laboratory animals. I wish to thank Md. Azijul Rehman, Surya Narayan Singh, Sumit, for their active support in the collection of samples and patient data.

My special acknowledgement to my senior lab member Dr. Khurshidul Hassan for his guidance, discussion and sincere cooperation which enabled me to execute this work. I am thankful to my lab members Dr. Ankit Tiwari, Bratati Mukherjee, Vinay J, Saket A Patel, Ananya Palo, Neha Ramani, Kirti Sinha, Deepa Kumari, Rishi, Arman, Pratush, Monali, Bishwahiree and other younger member of the lab for their interactive discussion and maintain a healthy research environment. It is my great pleasure to thank my batchmates Bushra, P. Sanjai, Himani, Pragesh, Durga, Somdatta, Shashank, Pratiksha, Subhant and friends Abhash, Ranjay Om, Prabhat, Asim, Tapan, Bibek, Yakub Pasha, Minu for their immense love and support.

Lastly, I thank my family for their continuous support, and care. I am highly indebted to my wife Nirmala for her unconditional love, constant support, encouragement and inspiration at every phase of my life.

I would like to apologise to anyone for omissions in this brief acknowledgement, it doesn’t mean, in anyway my lack of gratitude towards them.

CONTENTS

SUMMARY

IQGAP family of scaffolding proteins comprises three members namely, IQGAP1, IQGAP2 and IQGAP3. While IQGAP1 and IQGAP3 proteins show overexpression in many cancers and promote tumor growth and metastasis, IQGAP2 is a putative tumor suppressor, with some contradictory indications. The role of IQGAP1 and IQGAP3 as an oncogene is well established in breast cancer, while that of IQGAP2 remained unexplored. This work was carried out to investigate the role of IQGAP2 in breast cancer progression, by studying its expression levels in breast cancer patients, in affecting tumorigenic properties of breast cancer cells, and in EMT and angiogenesis. We report that IQGAP2 plays a tumor suppressive role in breast cancer progression. In breast tumor tissues, the level of IQGAP2 was reduced compared to normal tissues, which was associated with higher tumor stage and increased lymphovascular invasion. Depletion of IQGAP2 protein in breast cancer cells using shRNAs, resulted in drastic increase in proliferative, migratory and invasive properties of the cells, irrespective of their molecular subtype, primarily via abrogation of MEK-ERK pathway. IQGAP2 knockdown reduced apoptosis, induced EMT and increased expression of pro-inflammatory cytokines. Further, using *in vitro*, ex-ovo and *in vivo* models, we showed that IQGAP2 reduces angiogenesis via attenuation of VEGF-VEGFR2-AKT cascade and vice versa. In breast cancer cells, IQGAP2 was found to interact with IQGAP1. Manipulation of ratio of IQGAP isoforms *in vitro* revealed that IQGAP2 can restrict IQGAP1 mediated oncogenic potential, via reduction of cellular phospho-ERK pool. Datamining analysis showed that enhanced IQGAP3 and reduced IQGAP2 mRNA levels were frequently observed in multiple cancers, with the former predicting poor survivability and the latter predicting the opposite. Overall, we have shown that IQGAP2 plays a protective role by inhibiting multiple processes associated with breast carcinogenesis.

ABBREVIATIONS

IHC	Immunohistochemistry
ER+	Estrogen receptor positive
PR+	Progesterone receptor positive
HER2+	Human epidermal growth factor receptor 2 positive
TNBCs	Triple negative breast cancers
EMT	Epithelial to mesenchymal transition
ECM	Extracellular matrix
MMPs	Matrix metalloproteinases
EGF	Epidermal growth factor
FGF	Fibroblast growth factors
VEGF	Vascular endothelial growth factor
VEGFR	Vascular endothelial growth factor receptor
EndoMT	Endothelial-to-mesenchymal transition
ROS	Reactive oxygen species
IL	Interleukin
EC	Endothelial cell
BRCA	Breast cancer gene
mTOR	Mammalian target of rapamycin
EGFR	Epidermal growth factor receptor
CHD	Calponin homology domain
GRD	Gap-related domain
GAP	GTPase-activating proteins
GTP	Guanosine-5'-triphosphate
siRNA	Small interfering RNA
HCC	Hepatocellular carcinoma
mRNA	Messenger RNA
DFS	Disease free survival
TNM	Tumor (T), Nodes (N), and Metastases (M).
FFPE	Formalin-fixed paraffin-embedded
KD	Knock-down
Sc	Scrambled
EV	Empty vector
GAPDH	Glyceraldehyde 3-phosphate dehydrogenase
qRT-PCR	Quantitative real-time polymerase chain reaction
TCGA	The Cancer Genome Atlas
MAPK	Mitogen-activated protein kinase
GST	Glutathione S-transferases
CCL	Chemokine (C-C motif) ligand
MVD	Microvascular density
HUVECs	Human umbilical vein endothelial cells
CAM	Chick chorioallantoic membrane
ELISA	Enzyme-linked immunosorbent assay
KM Plotter	Kaplan-Meier plotter
OS	Overall survival
FP	First progression

PPS	Post-progression survival
DMFS	Distance metastasis free survival
RFS	Relapse free survival
CI	Confidence interval
HR	Hazard ratio
IRS	Immunoreactive score
VE-cadherin	Vascular endothelial cadherin
DMEM	Dulbecco's modified eagle medium
RPMI	Roswell park memorial institute
EGM-2	Endothelial cell growth medium-2
DPBS	Dulbecco's phosphate-buffered saline
FBS	Fetal bovine serum
PBS	Phosphate-buffered saline
ERalpha	Estrogen receptor alpha
ERK	Extracellular signal-regulated kinase 1/2
AKT	Protein kinase B

LIST OF FIGURES

LIST OF TABLES

INTRODUCTION

DINESH KUMAR

NISER, Bhubaneswar

1. INTRODUCTION

Breast cancer is the leading cause of cancer related mortalities in women (GLOBOCAN, 2018) [1]. Many environmental, lifestyle and genetic factors including pollutants, old age, poor BMI, alcohol consumptions, smoking, intake of oral contraceptives, mutations in genes (BRCA1 and BRCA2), favour breast tumor development [2, 3]. The treatment of this disease is primarily based on surgery, chemotherapy, endocrine therapy, radiation therapy and targeted therapy [4]. While surgical treatment is limited to the localised breast cancer; chemotherapy and radiation therapy restrict the growth and spread of localised as well as metastatic breast cancer, but have many side effects [5]. With the latest advancement in molecular biology and immunotherapy, very specific targeted therapies against ER, HER2, EGFR, mTOR and others have been developed that limit the growth and spread of breast cancer in more efficient manner [6]. However, the main challenge with the targeted therapy is the emergence of resistance, leading to relapse of metastasis [4, 5, 7].

To improve the survivability of the patient, search for additional molecular targets is the need of the hour for restricting the growth and metastatic spread of cancer [6]. Moreover, if they work irrespective of breast cancer molecular subtype, a single therapeutic regimen can be applied to all breast cancer patients [8]. These new targets could be proteins, which control multiple processes including apoptosis, cell cycle, EMT and angiogenesis. Use of molecules which regulate multiple molecular signaling pathways, as therapeutic target, can reduce the possibility of drug resistance and cancer can be targeted in more effective manner [8].

One of such molecules could be IQGAP2, which is a member of the IQGAP family. IQGAP is a family of scaffold proteins, evolutionarily conserved and expressed in various

organisms including fungi, protists, and animal cells [9]. IQGAPs had been the subject of intensive research in the last decade, owing to their involvement in affecting a wide array of cellular processes ranging from cytokinesis to vesicle trafficking [10-15]. There are three members of the IQGAP family, which have been named IQGAP1, IQGAP2 and IQGAP3, in order of their discovery. All the members of this family share a homologous multidomain structure, consisting of N-terminal CHD domain, IQ domain, WW domain, GAP-related domain and RasGAP C domain. It is worth mentioning that IQGAPs have many interacting partners and show variable functions specific to each member of this protein family, which could be attributed directly or indirectly to the role of these individual domains. Although IQGAPs have a highly homologous multidomain protein structure, yet the expression pattern shows uniqueness. This uniqueness in expression (tissues specific microenvironment) might be the determinant of their unique functions [16].

All three IQGAPs have role in tumorigenesis but in differing manner [17]. The role of IQGAPs in the process of carcinogenesis became evident largely due to studies carried out on IQGAP1, which showed that it takes part in the maintenance of various cellular processes like cytokinesis [10, 11, 18], cell cycle regulation [19] and, cytoplasmic remodelling [12, 20, 21]. Many of these processes have been linked with tumorigenesis. Multiple studies in a variety of cancers suggested that IQGAP1 mRNA and protein levels were elevated in tumor tissue compared to normal tissue [22-28]. The overexpression of IQGAP1 was associated with poor overall survival (OS) of patients. At the functional level the role of IQGAP1 was established as an oncogene. It affected crucial processes, identified as hallmarks of cancer, such as evasion of apoptosis, induction of EMT and triggering angiogenesis [29-32]. Another oncogenic member of this family is IQGAP3, which has garnered attention in recent times owing to its overexpression in numerous

human cancers and subsequent association with worse survival rate [33-37]. The oncogenic attributes of IQGAP3 are in sync with IQGAP1, which is reflected in the activation of oncogenic cell properties and signaling pathways. The third isoform IQGAP2 was reported as a tumor-suppressor, first in hepatocellular carcinoma (HCC) [38]. This protein has not been explored as extensively as IQGAP1 and, till date very limited literature is available. In HCC [39], gastric [40], prostate [41] and ovarian cancers [42] a reduced expression of IQGAP2 was reported. Functionally, the increase in expression of this gene was found to restrict the progression of cancer and higher expression of IQGAP2 was associated with better survivability of the HCC, ovary, gastric, and prostate cancer patients [40, 42-44].

In HCC, IQGAP2 showed an opposite expression pattern and function, compared to IQGAP1. IQGAP2 null mice had increased IQGAP1 protein levels in the liver, along with a concomitant decrease of membrane E-cadherin [38]. Subsequent study strengthened the opposite role of IQGAP1 and IQGAP2 in tumor progression, where it was observed that patients with elevated IQGAP2 and reduced IQGAP1 level had better overall survival rate in HCC [39]. On the contrary, a couple of studies showed increased expression of this gene at transcript levels in prostate [45] and colorectal cancer [46]. These contradictory observations require further study to establish the role of IQGAP2, which could be tissue specific.

Additionally, limited studies showing the opposite expression pattern of IQGAP2 and IQGAP1 in HCC, warrants further investigation in other cancer types, to strengthen the function of this gene in cancer overall. Similarly, the analysis of IQGAP2 and IQGAP3 relative expression levels in various cancers will be helpful in differentiating the role of IQGAP2 from the other two members.

In breast cancer the role of IQGAP1 as an oncogene, in initiation, development and maintenance, is well established. Increased IQGAP1 protein level is associated with a poor survival rate; it induces EMT, thereby triggering the metastatic cascade required for the invasive spread of breast tumor to remote sites [27, 32, 47]. Similarly, IQGAP3 has recently been found to have elevated expression in breast cancer tissues [48]. Like IQGAP1, IQGAP3 also assists the breast tumor cells to proliferate and invade via activation of key signaling pathways [48, 49]. Despite the crucial role of IQGAP2 in restricting the oncogenic activities of IQGAP1 in HCC, IQGAP2 has not been able to attract much needed research; specifically, its role in breast cancer is completely unexplored.

It is worth mentioning that IQGAP1 clearly functions as an oncogene in breast cancer, so exploring the role of IQGAP2 in the perspective of IQGAP1 driven breast tumors becomes even more relevant. Multiple studies have established that IQGAP1 regulates EMT [29, 50-52] and angiogenesis [53-55] in solid tumors, both of these processes are essential for tumor growth and metastasis, including breast cancer [56, 57]. Prospecting the role of IQGAP2 in EMT and angiogenesis can be highly beneficial to discover its therapeutic potential, which might be independent, or IQGAP1 related. As discussed previously, breast cancer is a complex and heterogeneous disease wherein therapeutic management of patients is closely linked with the histological subtype and the stage of cancer. Thus, it is required to look for potential targets, which could aid as a biomarker or therapeutic intervention, regardless of the histological subtype of the tumor. IQGAP2 could be a potential candidate owing to its known tumor-suppressive role in other cancers, significant endogenous levels in normal breast tissue and observation of IQGAP1 opposing role in HCC.

A comprehensive literature review regarding the involvement of IQGAP2 in breast cancer showed various gaps in the understanding of the role of this putative tumor suppressor. Firstly, the status of IQGAP2 expression and its association with different clinicopathological parameters of breast cancer is not established. Secondly, the function of this protein in the progression of breast cancer and the underlying molecular mechanism is not reported. Moreover, its effect on IQGAP1 mediated tumorigenesis is unknown. Thirdly, the role of IQGAP2 towards the process of tumor angiogenesis is completely unexplored. Lastly, there is a clear-cut lack in the knowledge of the relative differential expression pattern of both IQGAP2 and IQGAP3 isoforms in different cancers. Therefore, we took up this study to establish the prognostic value and role of IQGAP2 in breast cancer progression.

In the first chapter, we have established the role and molecular mechanism of IQGAP2 in breast cancer progression. In this chapter, we have initially analysed the expression pattern of IQGAP2 in breast cancer tissues and examined the association with different clinicopathological parameters of the patient. Next, using *in vitro* model system, we have checked the role of IQGAP2 in cell proliferation invasion and migration in breast cancer cell lines. Thereafter, we inspected the signaling molecules associated with these processes, focusing on EMT and apoptosis. We validated the function of IQGAP2 using *in vivo* tumor xenograft mouse model system. Finally, we checked the expression of IQGAP2 and IQGAP1 in the same set of clinical tissues and examined the role of one over the other in breast cancer progression.

The second chapter discusses our findings to elucidate the role of IQGAP2 in affecting breast cancer angiogenesis. In this chapter, we have used primary endothelial cells, HUVECs, as *in vitro* angiogenesis model and checked the angiogenic properties like,

proliferation, migration and tubule formation of HUVECs with change in IQGAP2 expression in breast cancer cell lines. Further, the IQGAP2 mediated signaling mechanism of tumor angiogenesis is explored. The *in vitro* findings are then validated by different animal based assays like matrigel plug assay, CAM assay and wound healing assay. Finally, the association study between IQGAP2 expression levels and microvessel density, has been carried out in large number of breast cancer tissue samples.

In final chapter, we investigated the previously unexplored relative expression pattern and survival analysis of IQGAP2 and IQGAP3 across different cancer types using publicly available databases. Besides, we also looked for mutation and methylation status for the changes in expression of the two isoforms.

REVIEW OF LITERATURE

DINESH KUMAR

NISER, Bhubaneswar

2. REVIEW OF LITERATURE

2.1 Breast cancer

Breast cancer is the most prevalent cancer worldwide (GLOBOCAN, 2018) [1], responsible for the maximum mortalities among cancer-associated deaths in women (Fig. 2.1.1). The incidence rate is higher in developed countries (89.7 per 100,000 women), than in developing countries (19.3 per 100,000 women). In India, breast cancer accounts for 14 percent of cancer incidences with 1,62,468 new registered cases and 87,090 reported deaths in 2018 [1].

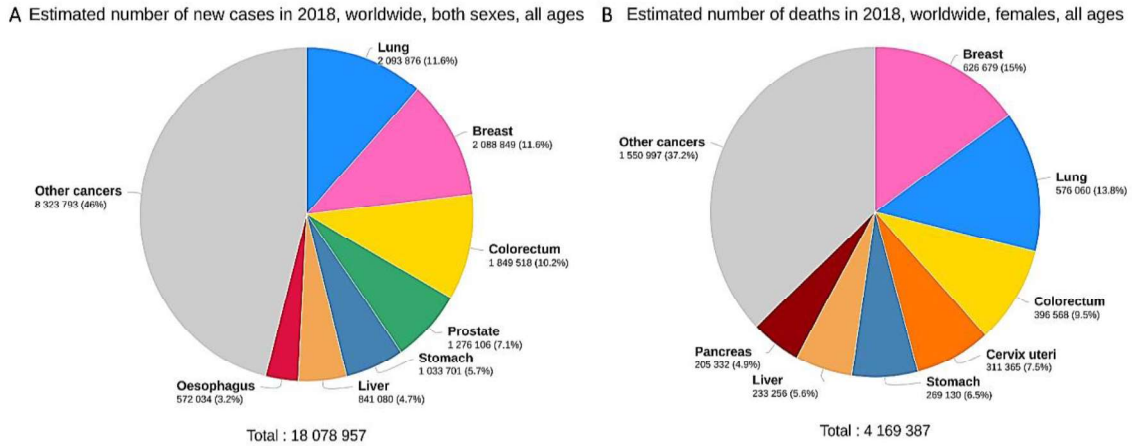

Figure 2.1.1. The estimated number of incidences and deaths of breast cancer patients, worldwide, GLOBOCAN 2018. A) Pie chart showing the number and percentage of the new cancer cases diagnosed in both sexes as per GLOBOCAN cancer Observatory 2018 data. **B)** Pie chart showing the estimated number of all types of cancer deaths in 2018 in females, according to the GLOBOCAN cancer Observatory 2018 data.

Breast cancer has been divided into multiple types and subtypes, some of these are quite common, while others are relatively rare in occurrence (Fig. 2.1.2). The majority of reported breast cancer cases worldwide are of the ductal and lobular types, with the former accounting for 40-75% of overall diagnosed cases [58]. IHC studies have classified human mammary carcinomas broadly into three categories. These subtypes are primarily based on the presence or absence of certain receptors on the tumor cells, which include estrogen receptor (ER), progesterone receptor (PR) and the HER2. Breast tumors with ER and PR positivity, are a common occurrence and exhibit a more differentiated

appearance. This group of tumors are regulated by specific hormones and respond well to drugs that interfere with the interaction between such hormones and their receptors, tamoxifen being a drug of such kind [59]. The next major subtype is HER2+ tumor which constitutes 30% of all diagnosed breast cancers and is associated with more aggressiveness and unfavourable prognosis, as compared to the ER/PR+ve breast tumors [60]. Tumors that do not harbour any of the hormone receptors and no amplification of HER2, have been named as triple negative breast cancer (TNBC) [60].

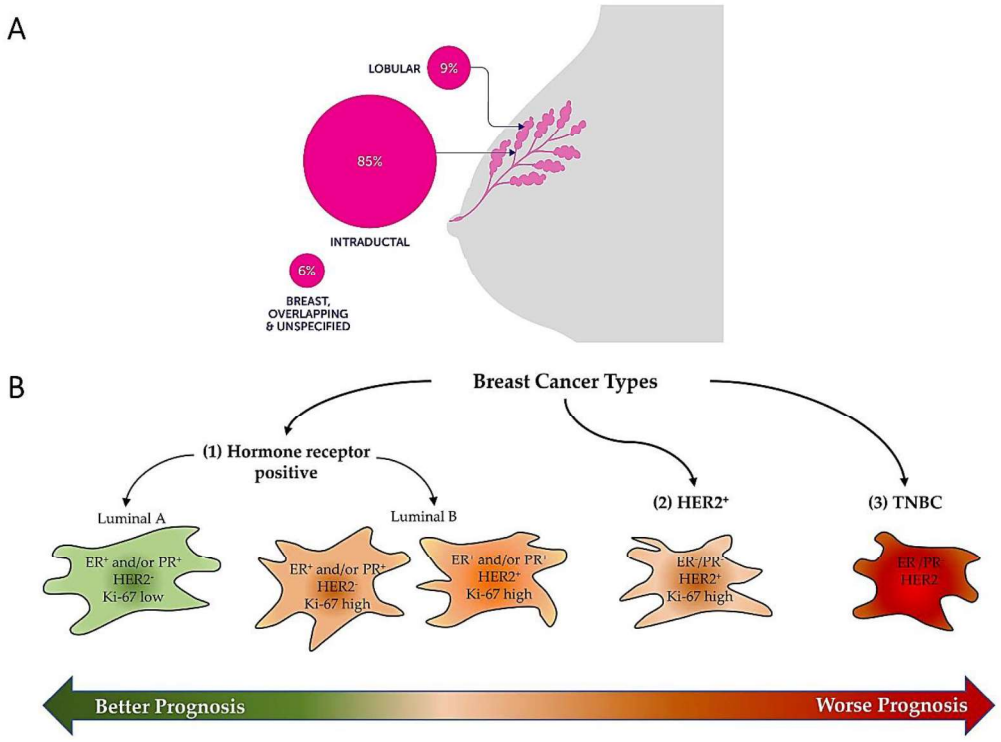

Figure 2.1.2. Breast cancers classification depending upon the site of origin or ER/PR/HER2 expression. A) The two breast cancer types ductal and lobular on the basis of the site of origin. A small population shows overlapping properties of ductal and lobular types, considered as Mixed type/ Unspecified. This figure is based on a graphic created by Cancer Research UK Trust [61]. **B)** Breast cancer categorised into three major subtypes, Hormone receptor positive (Lum A, Lum B), HER2+ and triple-negative types based on ER/PR/HER2 expression. Figure is adapted from [62].

2.1.1 Breast cancer pathogenesis

Tumorigenesis in humans is a multistep event that initiates with abnormal cell growth and progressive conversion of normal cells into highly malignant cells [63]. The malignant cells acquire more genetic changes and lead to metastasis in distant organs of the patient.

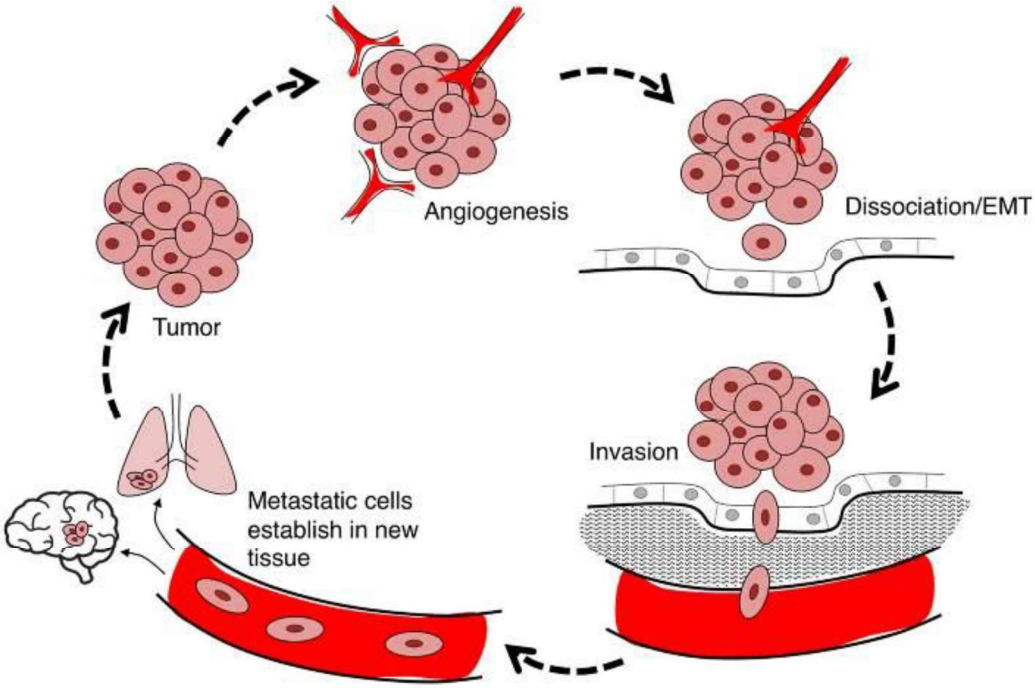

Figure 2.1.1.1. Flow diagram representing the process of cancer metastasis. During metastasis, cells from the primary tumor migrate to distant organs. Tumors grow in size and nourished with angiogenesis. Primary tumor cells loose cell-cell adhesions and invade the nearby ECM, followed by intravasation into the circulatory or lymphatic system. Circulating tumor cells then escape to secondary sites to reinitiate the process. Figure is taken from [64].

Metastasis process includes a series of sequential steps which involve detachment of cancer cells from the primary site followed by entry into the circulatory systems, extravasation at distant capillary beds, and invasion and proliferation within distant organs [57, 64, 65]. The process of metastasis is supported by epithelial to mesenchymal transition (EMT) and angiogenesis [57] (Fig. 2.1.1.1).

Epithelial-Mesenchymal Transition

Epithelial-Mesenchymal Transition (EMT), a classical hallmark of cancer, which is essential for the distant spread of tumor and is a major culprit for cancer-associated mortality. EMT in cancer cells is characterised by certain events that include reduction of adherence junctions, loss of apical-basal polarity, attainment of a mesenchymal phenotype, leading to increased migratory and invasive characteristic (Fig. 2.1.1.2).

Epithelial cells undergoing EMT, respond to a number of EMT inducing signals present in their environment and upregulate a group of transcription factors (Twist, Snail, Slug, ZEB1). These transcription factors in turn orchestrate all the major morphological, cellular, and molecular changes during EMT [65].

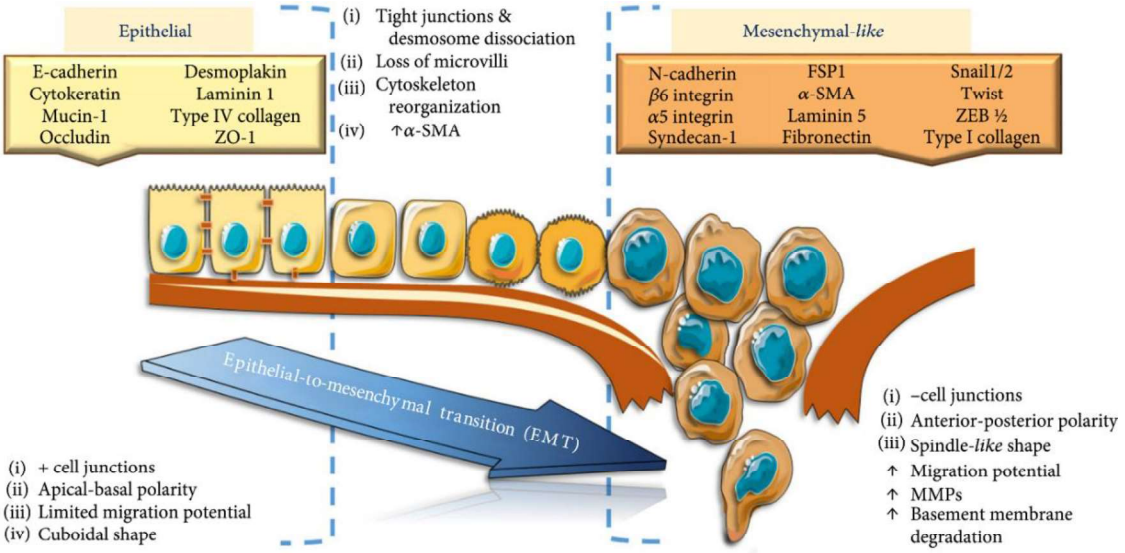

Figure 2.1.1.2. Different steps of Epithelial to Mesenchymal Transition (EMT) and signaling molecules involved with this process. Figure is taken from [65].

EMT in breast cancer: The association with molecular subtypes

Classical histological and molecular subtypes of breast cancers show association with EMT and breast cancer prognosis. The most aggressive basal-like breast cancers show predominant mesenchymal features compared to the non-basal tumors [66-68]. Multiple pathways control EMT program, however a common theme of all of these pathways is the activation of transcriptional factors Snail, Zeb, Slug and Twist. Furthermore, increased expression of N-cadherin, which is a key mesenchymal marker, in parallel with E-cadherin loss, marks the reduction in cell-cell adhesion. This particular phenomenon takes centre stage in the metastatic spread of basal-like and HER2+ breast cancers. However, one should be cautious as the expression of such markers is non-uniform across tumors. Increase in the production of matrix metalloproteinases (MMPs), that degrade the

surrounding basement membrane, contributes to a more invasive phenotype during EMT. An increased expression of certain metalloproteinases such as MMP14 (MT1), MMP2, MMP9, and ADAMTS1 are prerequisites for increased invasive and metastatic character obtained during EMT programming [69]. It is important to mention that multiple studies have found progressive loss of ER activity leads to epithelial to mesenchymal transition, characterized by amplified metastatic ability. Moreover, luminal A/B and HER2+ show a more epithelial phenotype, compared to their non-luminal counterparts [66, 70].

Angiogenesis

Angiogenesis, another hallmark of cancer, is the process of formation of new blood vessels from the existing ones. Angiogenesis plays a key role in processes which include embryo nourishment, normal growth and wound repair. The angiogenic process commences with the interaction of pro-angiogenic factors (VEGF, EGF, FGF) released from tumor cells with the receptors (VEGFR1/2/3, TGFBR1/2) present on to the endothelial cells (Fig. 2.1.1.3). This interaction stimulates the growth signals that induce endothelial cells to release proteases and similar enzymes to dissolve the basement membrane around blood vessels. The degradation of the basement membrane and surrounding ECM is facilitated by the matrix metalloproteinases (MMPs) secreted from the tumor cells and the supporting cells. Hereafter, numerous proangiogenic factors are released that lead to a change in endothelial cell junctions. The cell projections move through the newly formed spaces and new sprouts grow towards the source of pro-angiogenic stimulus. The endothelial cells reach the tumor mass after invasion into the matrix, organize themselves into hollow tubes (canalization) and form a fresh basement membrane for further vascular stability. These newly formed blood vessels, then regulate the flow of blood in tumor.

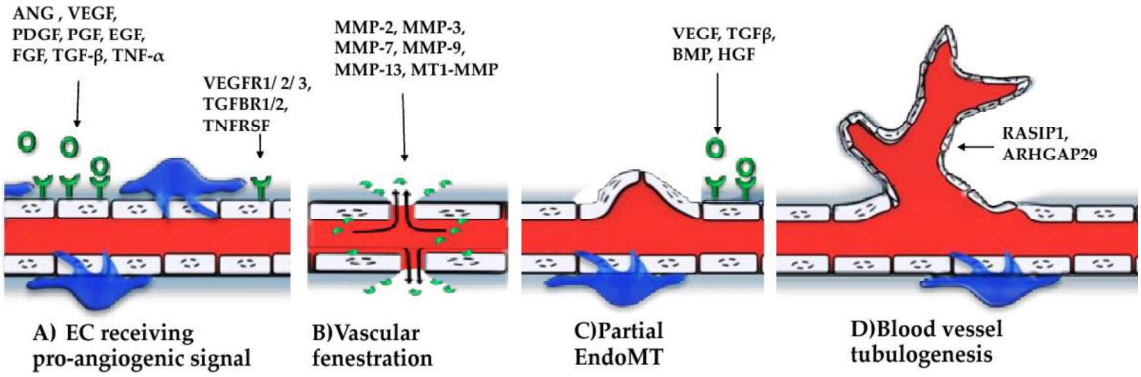

Figure 2.1.1.3. Angiogenesis process. Angiogenesis is multistep process which includes **A)** Receiving of pro-angiogenic signals by endothelial cells. **B)** Vascular fenestration and basement membrane degradation by MMPs. **C)** A partial endothelial to mesenchymal transition (partial EndoMT) drives endothelial cell migration, which undergo further rounds of proliferation at the site of fenestration, resulting in the new blood vessel budding. **D)** Tubulisation of blood vessels. Figure is taken from [71].

Angiogenesis is delicately regulated by maintaining the balance between angiogenic activators and repressors [72, 73]. However, this process is exploited by cancerous cells to facilitate tumor growth and metastatic spread. This involves intricate signaling between stromal and tumor cells. Specific tumor cells carry out the task of producing both pro-angiogenic, as well as anti-angiogenic proteins, which could stimulate and restrict angiogenesis, respectively [74, 75] (Fig. 2.1.1.4). It is a well established notion that tumors trip the angiogenic switch by perturbing the balance between pro and anti angiogenic factors [76]. While some tumors trip the angiogenic switch via activation of pro-angiogenic factors, others inhibit the anti-angiogenic ones. Meanwhile, some tumors could simuntaneously increase the level of pro-angiogenic factors and decrease the activity of anti-angiogenic factors to the desired effect [77]. However, the intricate mechanism that directs the shift in the balance between activators and inhibitors of angiogenesis remains a fascinating scientific question.

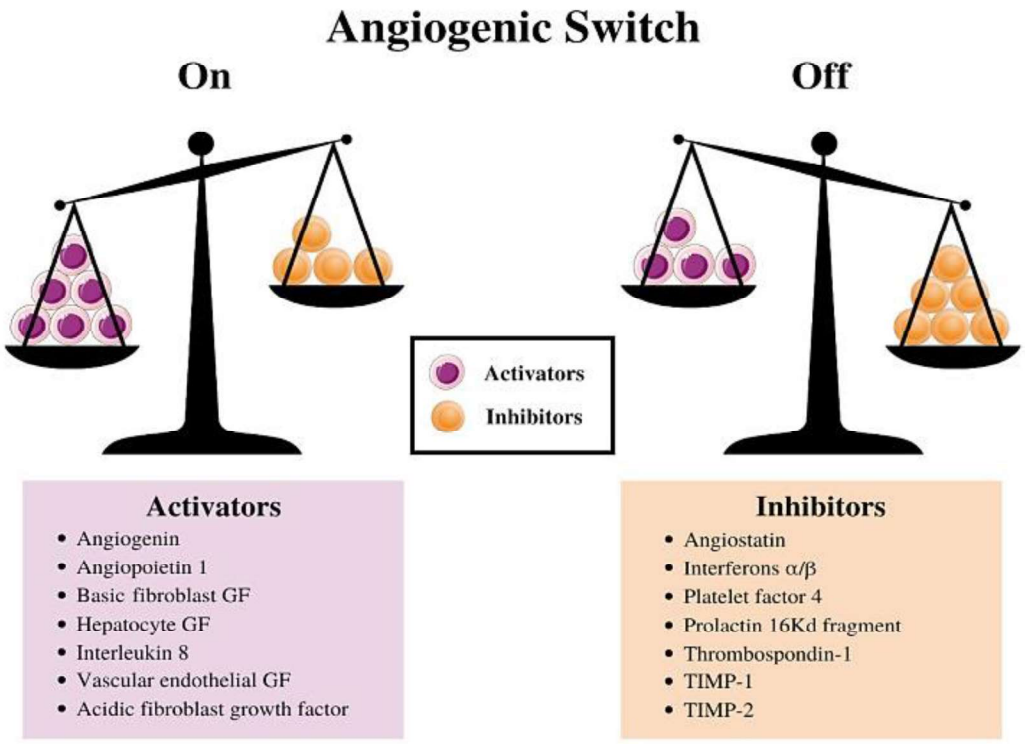

Figure 2.1.1.4. The balance of the angiogenic switch. An angiogenesic switch controls normal angiogenesis (formation of new capillaries). In pathological conditions, including cancer, this balance can be tripped to either facilitate increased blood vessel or to inhibit blood vessl formation by changing the concentration of inducers and inhibitors of angiogenesis. Adapted from reference [78].

A list of inducers and inhibitors of angiogenesis has been given in Table 2.1.1.1 and 2.1.1.2, respectively. The activities of both pro and anti-angiogenic factors could be controlled at transcriptional level, level of secretion, or by proteolytic activation. Such regulation can be brought about by hypoxia, glucose deficiency, ROS formation, and deficiency of iron. In the case of cancer, gain of function of oncogenes and/or loss of function of tumor suppressor genes has a major role in controlling the balance of pro-and anti-angiogenic factors [79-82]. For example, oncogene, H-Ras activates the angiogenic signaling in endothelial cells by upregulating the expression of VEGF and MMPs.

Table 2.1.1.1. List of known pro-angiogenic factors*

PRO-ANGIOGENIC FACTORS	
1. 1- Butyryl glycerol	2. Cytokines-Interleukin 8
3. Acid fibroblast growth factor	4. Laminin
5. Adenosine	6. Leptin
7. Angiogenin	8. Midkine
9. Angiopoietin	10. Nicotinamide
11. Collagen	12. Perfecan
13. Del-1	14. Phospholipids (SPP, LPA)
15. Entactin	16. Placental Growth Factor
17. Epidermal Growth Factor	18. Platelet Derived endothelial Growth Factor
19. Ephrins	20. Pleiotropin
21. Acid Fibroblast Growth Factor	22. Proliferin
23. Basic Fibroblast Growth Factor	24. Prostaglandins E1 and E2
25. Fibronectin	26. Scatter Factor
27. Follistatin	28. Transforming Growth Factor- α
29. Granulocyte Colony-Stimulating Factor	30. Transforming Growth Factor- β
31. Heparin- Heparan sulphate	32. Tumor Necrosis Factor- α
33. Hepatocyte Growth Factor	34. Vascular Endothelial Growth Factor

*Adapted from [83]

On the other hand, p53 (wild type), a major tumor suppressor inhibits the expression of pro-angiogenic factor VEGF [84, 85], FGF [86, 87], MMP1 [88] and Cox2 [89] and activate anti-angiogenic factors such as TSP1 [90, 91], BAI1 [92] and MMP2 [93]. The switching of angiogenesis is supplemented by the increased level of VEGF and MMPs. The source of these factors could be the cancer cells themselves. Alternatively, tumor-infiltrating inflammatory cells also secrete angiogenic factors. Hence, genetic and epigenetic changes inside cancer cells, in cooperation with other intra-tumoral stromal cells, prepare the ultimate blend of both pro and anti-angiogenic factors in the tumor microenvironment. This in effect, could tilt the balance in favor of formation of new blood vessels.

Table 2.1.1.2. List of known anti-angiogenic factors*

ANTI-ANGIOGENIC FACTORS	
1. 2- Methoxy-estradiol	2. Maspin
3. 1-25-Dihydroxyvitamin D_3	4. Metalloproteinase inhibitor (TIMP 1-3)
5. ADAMTS1	6. METH-1
7. Angiopoietin-2	8. PEDF
9. Angiostatin	10. Pex
11. Antiangiogenic antithrombin III	12. Pigment-epithelium-derived factor
13. Calreticulin	14. Placental ribonuclease inhibitor
15. Canstatin	16. Plasminogen fragment Kringle 5
17. Cartilage Derived Inhibitor	18. Platelet factor 4
19. CD59 complement fragment	20. Prolactin 16 kDa fragment
21. Decorin	22. Proliferin-related protein
23. Endostatin	24. Retinoids
25. Fibronectin fragment	26. Soluble VEGF receptor
27. Gro-β	28. Tetrahydrocortisol-S
29. Heparinases	30. Thrombospondin-1 and 2
31. Heparin hexasaccharide fragment	32. Human chorionic gonadotropin
33. Interferons- α, β, γ	34. Interferon inducible protein (IP-10)
35. Vasculostatin	36. Interleukin- 4, 12
37. Vasostatin	38. Ligands of PPARγ

*Adapted from [83]

Angiogenesis in Breast Cancer

Abnormal angiogenesis is important for mediating metastasis in multiple cancer types, including breast cancer [94-99]. To induce tumor angiogenesis, growth factors such as VEGF, transforming growth factor beta-1 (TGFβ-1), platelet-derived EC growth factor, basic fibroblast growth factor (bFGF) and many other growth factors [100-102], are released by tumor and stromal cells in the tumor microenvironment. Chief among these factors is VEGF, which has been frequently characterised as being the major players of tumor angiogenesis in breast cancer [103]. Breast cancer cell lines with elevated VEGF levels also show high level of interleukin-8 (IL-8), suggesting its crucial role in the

promotion of angiogenesis. Signaling pathways regulating VEGF and IL-8 expression in breast cancer have been implicated as therapeutic targets [104-106].

Bindng of VEGF-A to its cognate receptors VEGFR-1 or 2 facilitates the process of angiogenesis in breast cancer [107-111]. For the angiogenesis cascade to contribute significantly to invasion and metastatic spread of the tumor, an interplay of pro-angiogenic growth factors like VEGF, IL-8, bFGF/FGF-2, and MMPs is required [112-114]. IL-8 could stimulate VEGF production in endothelial cells by binding with its receptor and thereby activating VEGF receptors [115]. Furthermore, IL-8 itself can directly enhance angiogenesis by inducing the proliferation and promoting survival of endothelial cells and stimulating tubulogenesis *in vitro*. MMPs are involved in angiogenesis owing to their prominent role in remodelling the ECM matrix by degrading its constituent proteins [116]. The degradation of proteins in the ECM leads to destabilisation of existing blood vessel wall, leading to intiation of angiogenesis event [117-119].

Apoptosis in cancer

Evading cell death is one of the key necessities for a cell undergoing malignant transformation [120]. Since Kerr et al [121] had first found apoptosis responsible for the elimination of potentially malignant cells, in the early 1970's, the crucial role of resistance to apoptosis as a contributing factor towards carcinogenesis has taken centre stage. A malignant cell is able to achieve reduction in apoptosis or becomes resistant to apoptosis in a number of ways. The mechanisms to evade apoptosis have been broadly divided into the following categories 1) loss in the balance of pro and anti-apoptotic proteins, 2) decreased function of caspases and 3) diminished signaling associated with death receptor. All these mechanisms have been pictorially represented in Figure 2.1.1.5.

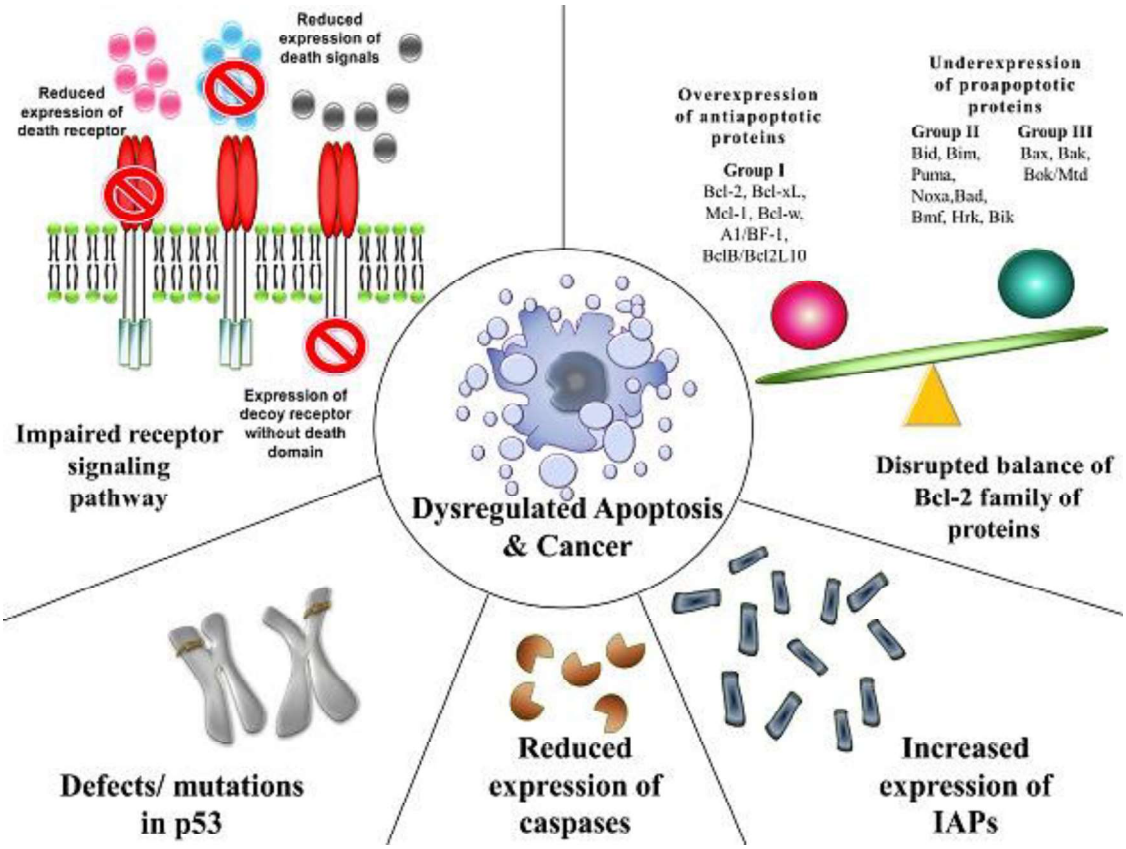

Figure 2.1.1.5. The events favoring evasion of apoptosis and carcinogenesis. Figure is adapted from [122].

In a cell, there are certain proteins which play a pro-apoptotic role and many others play an anti-apoptotic role. Here it is important to mention that it is not the total quantity but rather the ratio between these two groups of proteins which determines the regulation of cell death. An important family of such proteins is Bcl-2. Likewise, it has been reported that silencing of p53 mutant leads to reduced colony growth in human cancer cells via induction of apoptosis [123]. Abnormal activity of p53 owing to mutation in the same contributes to cell proliferation via evasion of apoptosis [124].

Another key mechanism of evading apoptosis is reduced caspase activity. Caspases are broadly divided into two major groups. In the first group, there are caspases which are related to caspase 1 (caspase-1, -4, -5, -13, and -14), and are involved in cytokine processing during inflammation [125]. The second group includes the caspases which

play crucial roles in regulating apoptosis. These include caspase-2, -3, -6, -7, -8, -9 and -10. This group of caspases has been further subdivided into 1) initiator caspases (caspase-2, -8, -9 and -10), required for the initiation of the apoptotic process and 2) effector caspases (caspase-3, -6 and -7), which facilitate the actual cleavage of cellular components during the apoptotic process [126]. Reduced levels of caspases or faulty caspase function may manifest in the reduction of apoptosis, thereby facilitating carcinogenesis across a wide spectrum of human cancers [127-129].

Apoptosis in breast cancer

In breast cancer, extensive investigation has been carried out to identify novel biomarkers related to apoptosis, which include the caspases [130]. Till date, 11 caspases have been identified in humans, which contribute to breast cancer progression. Breast cancer pathology has so far indicated that reduced caspase 3, 6, and 8 expression correlates with low apoptosis rate and high histological grade [131-133].

2.1.2 Risk factors of breast cancer

Development and progression of breast cancer are influenced by a number of genetic and environmental factors. Some of them are older age, sex, race, obesity, alcohol, oral contraceptives, mutations on the BRCA1 and BRCA2 genes [2]. Breast cancer is less frequent in women aged below 40 years but increases linearly between the age of 40 and 59 years. More than eighty percent of the incidence of this disease is recorded in women aged 50 and above [134]. This disease is predominant in female and sporadic incidences are reported in male that account for less than 1% of the total diagnosed breast cancer [135].

Race is another important risk factor for the occurrence of breast cancer. According to the GLOBOCON 2018 data, the occurrence of this disease is very prevalent in the

population of women having Australian, New Zealand, and European origin compared to African and South-central Asia origin [1]. The dietary habits also increase the risk of breast cancer. Eating fat rich food increases obesity, and consuming processed products that use flavour enhancers may help in neoplastic transformation [134]. The consumption of even small amount of alcohol increases the level of estrogen-related hormones and risk of the disease [136]. The use of oral contraceptives is another risk factor that increases the exogenous level of estrogen and, risk of breast cancer [137, 138]. Apart from all the above risk factors, mutations and abnormal amplification of some genes have been noticed in the onset and development of breast cancer. For instance, mutation in BRCA1 or BRCA2 gene [139, 140] and overexpression of HER2 [141, 142], EGFR [143], and c-Myc [144, 145] proteins are associated with breast cancer.

2.1.3 Survival and therapy of breast cancer

The survival of breast cancer patients differs substantially by the stage of the patient. The 5-year overall survival rate varies from 98% for stage I to 27% for stage IV [146]. The survival rate also varies greatly depending on the economic status of the country and ethnicity. For example, the 5-year survival rate of this cancer in developed countries like North America, Japan and Sweden is much higher than the survival rate in poor and low-income countries [147]. The reason behind this may be, the lack of early detection programmes, in-sufficient diagnosis and treatment facilities.

With the advancement in cancer research, many treatment options are currently available for breast cancer therapy. These include traditional methods like surgery, chemotherapy, radiotherapy and modern techniques including hormone-based therapy, immunotherapy, and targeted therapy [148]. The treatment strategy works depending on many factors like the physical condition of patient, cancer type and tumor stage. The surgical therapy is the

first choice for localised non-metastatic tumor in which the tumor region and the axillary lymph nodes surgically resected out from the patient followed by postoperative treatment with radiation, hormonal therapy or chemotherapy. The selection of chemotherapy, radiation therapy or hormonal therapy or their combination is primarily determined by the stage and subtype of breast cancer. For instances, endocrine therapy works well in ER+ tumors [149], the combination of trastuzumab-based ERBB2-directed antibody and chemotherapy is recommended for HER2+ tumors [150-152] whereas the chemotherapy shows better results in triple-negative breast cancer [153]. In high risk and advanced stage patients the chemotherapy alone or in combination with radiation therapy have profound effect on survival. But these treatments also result in many side effects because of their non-specific action on cancerous as well as normal cells [5]. This limitation of specificity is sorted out with the development of targeted therapy. The drugs block the specific pathway of cancer cells by targeting the key signaling molecules like ER, HER2, EGFR, mTOR that reduces the growth and spread of the cancerous cells in more efficient manner [6]. This option also shows lesser side effects in patients but there are reports that have shown the relapse of metastasis after its long use. This is due to resistance developed during the course of treatment [4, 5, 7]. Thus identification of newer molecular targets may be helpful in this regard [6].

2.2 IQGAP family of scaffold proteins

IQGAP is a family of scaffold proteins, evolutionarily conserved and expressed by broad range of protists, fungi and animal cells. There are three known members of the IQGAP family in human, namely IQGAP1, IQGAP2 and IQGAP3 [17]. Each member of this protein family possesses five conserved domains in its structure (Fig. 2.2.1.A). All of these members show significant sequence homology and possess comparable structures [17].

IQGAP1 was the first to be identified [154], and subsequently implicated in a number of cellular processes including cell proliferation [13], cytokinesis [10, 11], vesicle trafficking [14, 15], cell migration [12], intracellular signaling [13, 14], , and cytoskeletal dynamics [20, 21]. The conserved domains of these isoforms are reported to interact with various signaling molecules. CHD towards the N-terminus facilitates interaction with the actin cytoskeleton and also binds calmodulin and Ca^{2+} [155, 156]. A middle IQ region comprising of 4 IQ motifs, these motifs bind with calcium and calmodulin, myosin essential light chain (essential MLC) and S100B [157]. Furthermore, the IQ motif is essential for mediating interaction with EGFR and MEK, and also in IQGAP1 homodimerisation [158, 159]. The WW domain is responsible for interaction with ERK [160, 161]. A C-terminus GAP related domain (GRD) binds the Rho family members Rac1 and Cdc42, thereby assisting their active GTP bound state [155, 156]. Lastly, a unique RasGAP C-terminal domain is present exclusively in IQGAPs. This domain has been found to mediate multiple interactions for example with E-cadherin, APC and CLIP-170 [162] (Fig. 2.2.1B).

The multiple interacting partners and variable properties of IQGAPs can be attributed to the differences present in structural domains [156]. For example, calcium-sensing protein CaM (calmodulin) binds to all the IQGAPs through IQ-motifs, but its stability differs among all the members. In presence of calcium ions, the IQGAP2 shows a weak binding affinity for CaM compared to IQGAP1 and IQGAP3. The reason behind this difference can be explained in terms of the participation of four IQ motifs with CaM. It has been shown that CaM interacts with IQGAP2 through second and third binding site of IQ motif whereas all four IQ-motifs of IQGAP1 and IQGAP3 take part in interaction with CaM. The nature of the binding in the case of IQGAP2 is transient whereas IQGAP3 shows

long-lived binding with its last three IQ motifs and a transient binding for the first IQ motif [163].

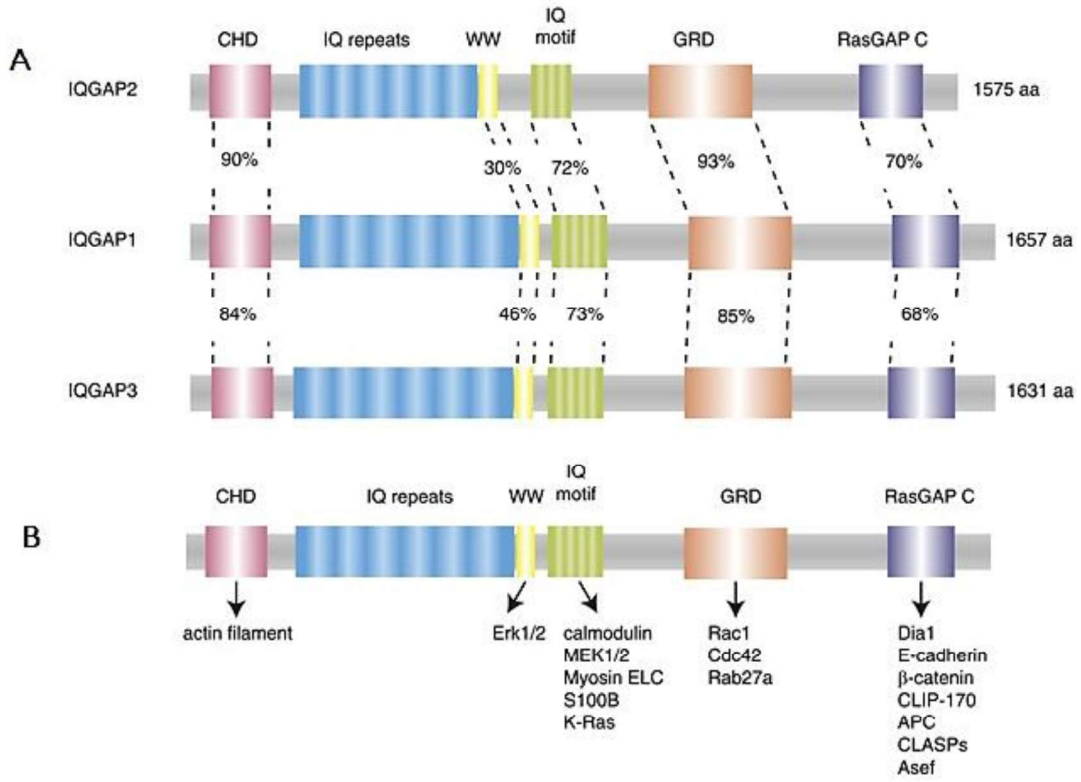

Figure 2.2.1. Five conserved domains of IQGAPs and their interacting partners. A) Schematic presentation of domain wise structure of IQGAPs. Percentages denote the identity of IQGAP2 and IQGAP3 domains to the equivalent domains of IQGAP1, at an amino acid level. **B)** The IQGAP binding proteins have been represented with their respective domains. Adapted from [16].

Similarly, the binding affinity of IQGAPs with myosin essential light chain and S100B shows differences. On one hand, the binding affinity of IQGAP1 with myosin essential light chain and S100B is high, on the other hand, IQGAP2 and IQGAP3 show a transient or no binding affinity for these proteins [163-165]. The previous studies have also shown that IQGAP1 and IQGAP3 show specificity for ERK. Although both are associated with ERK, IQGAP1 interacts with both, ERK1 and ERK2 [160] whereas IQGAP3 specifically binds with ERK1 [33]. Additionally, Anillin proteins co-immunoprecipitate with IQGAP3 but do not show co-immunoprecipitation with IQGAP1 or IQGAP2 [166].

IQGAP1 shows higher binding affinity for the active GTP-Cdc42 and GTP-Rac1 than for the inactive, GDP-bound form of the GTPases [167, 168]. A similar affinity was also observed with IQGAP3 for active Rac1 and Cdc42 [169]. But the IQGAP2 has been reported to interact with both the GDP and the GTP-bound forms [170, 171]. Inspite of their observed homology, IQGAPs do not exhibit a uniform expression pattern (Table 2.2.1). While IQGAP1 is expressed ubiquitously, expression of IQGAP3 and IQGAP2 is tissue specific [17]. IQGAP2 is majorly present in the liver but also shows expression in, kidney, stomach, testis, prostate, thyroid, salivary glands and platelets. The expression of IQGAP3, on the other hand, is witnessed in the brain, lung, small intestine, colon and testis [17].

Table 2.2.1. The tissue specific expression pattern of IQGAPs

	IQGAP1	**IQGAP2**	**IQGAP3**
Brain	+	+	+++
Heart	++		+
Lung	+++	+	++
Liver	+++	+++	
Stomach	+++	++	
Spleen	+++	+	+
Kidney	+++	+	
Skeletal muscle			+
Testis	+++	++	+
Breast*	++	+	++

This table is adapted from [16]. * data adapted from GeneCards database.

The unique expression pattern of IQGAP isoforms hints at the differential function roles of each isoform, despite sharing a highly homologous structure [17].

2.3 IQGAPs in cancer

IQGAP1 is an oncogene

Among all the members of this protein family, IQGAP1 has garnered the most attention, primarily due to its role in a wide spectrum of functions traditionally linked with cancer.

IQGAP1 interacts with more than 130 binding partners that include Cdc42, Rac1, Ca2+/calmodulin, clip-170, PIP2, PIPKIy, KRas, ERK1/2, PI3K, AKT, β-catenin, sp1 etc. [9]. The interaction between IQGAP1 and its binding partners has immense functional significance. Overexpression of IQGAP1 at the mRNA and protein level is observed in various cancers including ovary [22], pancreases [23], gastric [24], thyroid [25], colorectal, head and neck, laryngeal squamous cell carcinoma (LSCC) [26], breast [27], lung [28] and liver cancers [17]. Elevated levels of IQGAP1 in these cancers correlate with poor prognosis of the patients, underlining the prognostic significance of IQGAP1 across a variety of cancers. Multiple studies with *in vitro* manipulation of IQGAP1 levels have established that IQGAP1 plays a positive role in the proliferation, migration and invasion of several cancer cell types, ultimately facilitating tumor progression [29-32, 172]. Further, *in vivo* studies with genetically engineered transgenic mice for IQGAP1 or xenograft have substantiated the oncogenic potential of this gene for breast [32], lung [173], head and neck [174], pancreatic ductal adenocarcinoma [175], colorectal cancer [176] and hepatocellular carcinoma [177].

IQGAP3: a putative oncogene

Apart from IQGAP1, the less studied IQGAP3 has also become known for enhancing malignancy, in recent years. Elevated IQGAP3 protein levels in lung tumours have been shown to drive tumorigenesis by interacting with ERK1. This interaction was found to increase the cancerous properties of A-549 lung cancer cells [33]. Depletion of IQGAP3 protein by siRNA significantly reduced invasion and also anchorage-independent growth of gastric cancer cell lines. Pull-down based studies further showed that IQGAP3 induces the active Rac1, Rho and Cdc42, Ras GTPases [34]. High IQGAP3 levels are also present in high-grade serous ovarian cancer (HGSOC), which when silenced were found to have a negative effect on tumorigenic properties of ovarian tumor lines *in vitro*. This was

further supported by studies using *in vivo* mouse model system [35]. In HCC patients, the plasma was found to contain high levels of IQGAP3 protein. Amount of IQGAP3 protein in plasma of HCC patients showed a significant correlation with increasing tumor size, highlighting the prognostic significance of IQGAP3 [36]. IQGAP3 functions as a potential oncogene in pancreatic cancer, owing to high mRNA levels in pancreatic tumors [37]. In breast cancer, a recent study has found that IQGAP3 mRNA and protein levels are elevated in tumor tissues compared to adjacent normal tissue. The same study reported that ectopic expression of IQGAP3 in breast cancer cell lines led to drastic increase in the tumorigenic properties of the cell lines [49]. Furthermore, association of IQGAP3 with poor survival rate and with radiation therapy resistance hints at the crucial role of IQGAP3 as a prognostic marker in breast cancer progression [178].

IQGAP2: a putative tumor suppressor gene

The role of IQGAP2 as a putative tumor suppressor was first brought to the forefront by a study in IQGAP2 deficient mice model of HCC. Mice lacking IQGAP2 showed concomitant increase of IQGAP1 levels and loss of membrane E-cadherin and developed hepatocellular carcinoma [38]. Mice lacking both IQGAP1 and IQGAP2 had reduced HCC occurrence and better survival rate, indicating that loss of IQGAP2 alone may not be sufficient to drive a malignant phenotype, rather it is dependent on the oncogenic IQGAP1 [38]. A further extension of these findings led to the observation that IQGAP1 is overexpressed, while IQGAP2 shows reduced expression in human HCC compared to the control tissue [39]. Examination of the prognostic value of these IQGAPs in HCC led to the conclusion that IQGAP1-high or IQGAP2-low tumors had significantly poor overall survival [43].

IQGAP2 was identified as a deterrent to tumor progression in gastric cancer. IQGAP2 promoter hypermethylation and subsequent reduction of its expression in gastric cancer led to increased tumorigenesis [179]. Hypermethylation of IQGAP2 promoter was positively associated with enhanced tumor invasion and a poor overall survival rate in gastric cancer patients [40]. In gastric cancer cells, IQGAP2 was found to interact with and increase the phosphatase activity of SHIP2. This subsequently resulted in inactivation of AKT and reduction in EMT [179]. The association of IQGAP2 and prostate cancer was brought to the limelight by the study carried out by Xie Y et al., wherein they reported elevated IQGAP2 protein levels in normal prostate tissues and prostate cancer tissues of early stages, as opposed to reduced IQGAP2 levels in advanced and androgen independent prostate cancer tissues [41]. The tumor suppressive role of IQGAP2 in prostate was further supported by study of xenograft tumours originated from the stem-like DU145 cells, which displayed reduced IQGAP2 levels in comparison to non-stem like DU145 cells-derived tumors. Ectopic IQGAP2 expression in DU145 cells inhibited AKT activation, which in turn abrogated the proliferative and invasive abilities of cells via up-regulated E-cadherin expression [41]. Subsequent studies in prostate cancer showed that reduced IQGAP2 mRNA levels are linked with shorter disease free survival (DFS) in patients [44].

Similar to gastric cancer, low expression of IQGAP2, along with a hyper-methylated promoter, was observed in ovarian cancer. Survival analysis in a cohort of ovarian cancer patients revealed that reduced IQGAP2 level as an indicator of poor progression-free survival. Functionally, IQGAP2 was able to inhibit ovarian cancer cell EMT, primarily via inhibition of nuclear translocation of β-catenin and subsequent transcriptional activity [42].

Although the above studies have found the low expression of IQGAP2 in HCC, ovary, prostate and gastric cancer, an inverse expression pattern of this gene has also been reported in colorectal and prostate cancers. Ohmachi et al., 2006 [1] , analysed the expression profile of upregulated gene in colorectal cancer cells compared to the normal epithelial cells by cDNA microarray and laser microdissection based methods. They observed 84 genes that were overexpressed which included the higher expression of IQGAP2 (fold change- 2.50). A similar expression pattern of IQGAP2 was also observed in prostate cancer. The microarray data of prostate cancer and the normal adjacent tissue performed by Ernst T et al., 2002 [2] showed the elevated expression level of IQGAP2 (fold change- 2.6) in prostate cancer tissues.

2.4 IQGAPs relative expression pattern

IQGAP1 and IQGAP2

The oncogenic IQGAP1 and the tumor suppressive IQGAP2 have been reported to show opposing expression pattern and contrasting functions in hepatocellular carcinoma (HCC). Reduced IQGAP2 levels were reported in 78% (64/82) of primary HCC. At the same time, IQGAP1 was significantly upregulated [39]. The reciprocal expression pattern between these two isoforms becomes even more significant because of its association with HCC progression. While IQGAP1 shows a positive correlation with TNM staging, grade and large tumor size, IQGAP2 is inversely correlated with the same. Higher IQGAP1 levels predict worse survival, whereas with increase in IQGAP2 expression, disease-free survival and overall survival are significantly improved [43]. These observations hint at the possibility of a functional interplay between IQGAP2 and IQGAP1, in which the former acts as a roadblock for latter's oncogenic activity. This is

corroborated by the discovery of protein complexes formed with the interaction of IQGAP1, β-catenin, IQGAP2 and E-cadherin in the mouse liver [38].

To summarise, literature supported the notion that low IQGAP2 expression marked in HCC, gastric, prostate and ovarian cancers is associated with a more invasive phenotype and worse survival of cancer patients, in spite of the pro-tumorigenic role of IQGAP1 [156].

IQGAP2 and IQGAP3

The relative expression pattern of these isoforms has not been explored in any study. The knowledge of relative expression of both the isoforms in various cancers will help in deciding the prognostic values of these isoforms in cancer.

2.5 IQGAPs in breast cancer

In breast cancer, the role of IQGAP1 as an oncogene in initiation, development and maintenance is well established. IQGAP1 protein levels associate with a poor patient survival rate. IQGAP1 induces EMT, thereby triggering the metastatic cascade required for the invasive spread of breast tumor to remote sites [27, 47, 180]. The same could be said about IQGAP3, which has recently been found to show elevated level in breast cancer tissues. Like IQGAP1, IQGAP3 also assists the breast tumor cells to proliferate and invade via activation of key signaling pathways [48, 178].

Despite the crucial role of IQGAP2 in restricting the oncogenic activities of IQGAP1 in HCC, IQGAP2 has not yet drawn the attention of researchers overall and, specifically the role of IQGAP2 in breast cancer is completely unexplored. It is noteworthy that IQGAP1 acts a very potent oncogene in breast cancer, so inspecting the role of IQGAP2 in the perspective of IQGAP1 driven breast tumors becomes even more relevant. IQGAP1 as

an oncogene has been known to regulate EMT and also aids in vascularisation of solid tumors. In breast cancer, both EMT and tumor vascularisation are essential prerequisites for the growth and metastatic spread of tumor. Prospecting the role of IQGAP2 in this regard could be highly beneficial. As discussed previously, breast cancer is a complex and heterogeneous disease wherein therapeutic management of patients is closely linked with the aggressiveness and subtype of the tumor. Thus, it is very crucial to look for potential targets, which could work as biomarker and can be targeted for therapeutic intervention, regardless of the histological subtype of the tumor. IQGAP2 could be a potential candidate due to its known strong tumor-suppressive effect in other cancers and anti-IQGAP1-oncogenic activity.

2.6 Role of IQGAP2 in cancer related processes

Role of IQGAP2 in EMT

As expected of a tumor-suppressor, IQGAP2 has previously been associated negatively with EMT in multiple cancers. In prostate cancer, IQGAP2 was found to upregulate E-cadherin, and thereby inhibit tumorigenesis [41]. E-cadherin is a well known epithelial marker, frequently reexpressed in cells undergoing a mesenchymal to epithelial transition, rendering them less invasive in the process. In another study in ovarian cancer, IQGAP2 was found to actively suppress ovarian cancer EMT via regulation of Wnt/β-catenin pathway [42]. This was not surprising, as IQGAP2 had been previously established to be an interacting partner of β-catenin, and anchored together with E-cadherin, in hepatocytes [38]. Further, in gastric cancer cells, IQGAP2 was found to interact with and enhance the phosphatase activity of SHIP2, reducing EMT, as a consequence [179].

IQGAP2 in apoptosis

Only a couple of studies have found the role of IQGAP2 in apoptosis, but their findings are contradictory to each other. The role of IQGAP2 in apoptosis was first highlighted by Schmidt et al., wherein they showed that IQGAP2 knockout mice show age-dependent hepatocellular apoptosis. In this study, the authors showed that targeted elimination of IQGAP2 gene in mice results in the progress of mitochondial pathway mediated apoptosis in an age-dependent manner, which led to hepatocellular carcinoma [38]. In contrast, another study shows a positive association between the pro-apoptotic molecules, Bax and Caspase-3 with IQGAP2, and negative association of IQGAP2 with the anti apoptotic BCL2 in the same study, further highlighted the crucial role of IQGAP2 in mediating cell death via regulation of apoptosis [181].

Role of IQGAP2 in Angiogenesis

While the role of IQGAP2 in mediating tumor angiogenesis is unheard of, the role of the oncogenic IQGAP1 in promoting tumor vascularisation is well documented. IQGAP1 bind to VEGFR2 and activate B-Raf to stimulate proliferation of endothelial cells [53]. IQGAP1 silencing in endothelial cells lead to reduced *in vivo* angiogenesis in presence of VEGF. Overexpression of IQGAP1 on the other hand promotes the angiogenesis of esophageal cancer process via AKT and ERK mediated activation of the VEGF/VEGFR2 signaling pathway [54]. The effect of IQGAP1 in cell to cell detachment in quiescent endothelial cells has also been reported. IQGAP1 provides a scaffold and helps in the formation of a complex (VEGFR2, VE-cadherin and β-catenin) at the adherent junction. This results in ROS-dependent loss of cell-cell contact [55]. Since IQGAP2 has been reported to play an opposite role to IQGAP1 in tumor progression, we prospect the role of IQGAP2 in tumor angiogenesis.

IQGAP2 maintains metabolic homeostasis

Vaitheesvaran and his group examined the effects of IQGAP2 deficiency on the overall metabolic phenotype and proteomics changes associated with the cellular metabolism of Iqgap2 −/− C57BL/6J mice [182]. The loss of IQGAP2 expression in Iqgap2 −/− C57BL/6J mice results in obesity, fasting hyperglycemia and metabolic inflexibility. These physiological conditions are linked with abnormal regulation of metabolic processes like lipid homeostasis, glycolysis, glycogenolysis, gluconeogenesis in liver. The change in these metabolic cycles results in a proteomic change in mitochondrial and cytosolic compartments. The above mentioned metabolic processes also get deregulated in metabolic reprogramming during carcinogenesis. For instance, change in TCA cycle, glycolytic flux, de novo lipogenesis are hallmarks for cancer metabolism [183]. The function of IQGAP2, in metabolism and cancer, makes this protein a potential protein linking the etiology of diabetes and carcinogenesis.

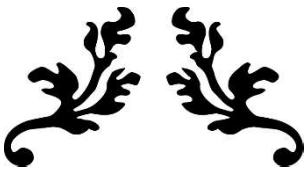

HYPOTHESIS

DINESH KUMAR

NISER, Bhubaneswar

3. HYPOTHESIS

The review of existing literature regarding the differential roles of IQGAP isoforms in processes related to carcinogenesis enlightens their importance. There is universal consensus regarding the pro-oncogenic attributes of the well-studied IQGAP1, as well as the relatively less-studied IQGAP3. The role of IQGAP2 in cancer progression remains less clear, although a majority of studies indicate a tumor-suppressive function to this protein, yet there are exceptions. We identified certain lacunae in the existing knowledge regarding the role of IQGAP2 protein, which necessitated an investigation to answer some crucial scientific questions, specifically, 1) How does IQGAP2 function in breast cancer pathology? 2) Does it affect the prognosis of patients, and can it serve as a biomarker in breast cancer? 3) What role does IQGAP2 play in modulating EMT and angiogenesis cascade in breast cancer? 4) Does the cellular IQGAP2 pool affect IQGAP1 mediated cellular processes in breast tissues as well, like it did in HCC? 5) How are IQGAP2 and IQGAP3 expression levels varied across different cancers, is there a relation between them? If yes, how do they affect prognosis in cancers?

We hypothesized that IQGAP2 affects tumorigenesis in breast cancer through EMT and angiogenesis processes, which might be independent or IQGAP1 mediated. IQGAP2 may have opposite role and expression pattern relative to IQGAP3 in cancers.

To answer the above-mentioned questions and to validate our hypothesis, we carried out this work applying various *in vitro*, *in vivo*, in-silico methods, to achieve following objectives;

Objective 1. To understand the effect of altered IQGAP2 expression in breast cancer progression and its molecular mechanism.

Objective 2. To decipher the role and molecular signaling of IQGAP2 in tumor

angiogenesis.

Objective 3. To find out the relative differential expression pattern of IQGAP2 and IQGAP3 in cancers.

The result section describes each objective as one chapter.

MATERIALS AND METHODS

DINESH KUMAR

NISER, Bhubaneswar

4. MATERIALS AND METHODS

4.1 Materials

Human FFPE tumor tissue blocks collection

The archival formalin-fixed paraffin-embedded (FFPE) blocks of 126 breast cancer, 53 colorectal cancer, 32 prostate cancer, 19 benign prostate hyperplasia (BHP), 47 stomach cancer and 49 brain cancer were collected from the Department of Pathology, Apollo hospital, Bhubaneswar and SRL Diagnostic Lab, Bhubaneswar with the ethical approval from Institutional Ethics Committee, NISER, Bhubaneswar (protocol no. NISER/IEC/2016-02). The requirement for informed consent was waived by Institutional Ethics Committee, National Institute of Science Education and Research (NISER), Bhubaneswar, India, based on waiver of consent policy of Ethical Guidelines for Biomedical Research on Human Participants, ICMR, 2006. The clinicopathological characteristics like age, histological type, tumor size, Tumor-Node-Metastasis (TNM) stage and lymphovascular invasion etc. of each patient were recorded.

Human breast cancer tissue arrays

The human breast cancer tissue microarray (BC081120c) was purchased from BioMax, MD, USA. In this array, 5 µm thin sections of 100 breast cancer tumor tissues and 10 normal adjacent tissues of breast were available. The histopathological and clinical information of the patient, namely age, histological grade, lymph node status, TNM staging were supplied with the array datasheet.

Experimental animals

Three strains of 6-8 weeks old mice namely Balb/c, C57/BL6 and Balb/c- nude mice were used in our study. All experiments related to animals were performed in our Institutional Animal House central facility. Animals were housed in well-adjusted climatic conditions

with clean drinking water, food, controlled temperature, humidity and a 12-12-h light-dark cycle. Balb/c, C57/BL6 mice were provided from Animal House Facility, NISER. Nude mice were procured from the Central Animal Facility, Centre for Cellular and Molecular Biology, Hyderabad, India. First, they were put in quarantine for seven days and then experiments were performed. All the animal experiments were approved by the Institutional Animal Ethics Committee (IAEC) as per CPCSEA guidelines. Efforts were made to minimize animal suffering.

Cell lines

The detailed information of cell lines used in this study are summarised in the table below;

Table 4.1.1 List of cell lines used in this study, their features and particulars

Cell line	Details	Source
MCF7	Luminal A type, Origin- Adenocarcinoma, mammary gland, breast; derived from metastatic site: pleural effusion	NCCS, Pune
T-47D	Luminal A type, Origin- Adenocarcinoma,mammary gland; derived from metastatic site: pleural effusion	NCCS, Pune
MDA-MB-231	Basal type, Origin- Adenocarcinoma, mammary gland/breast; derived from metastatic site: pleural effusion	NCCS, Pune
MDA-MB-468	Basal type, Origin- Adenocarcinoma, mammary gland/breast; derived from metastatic site: pleural effusion	NCCS, Pune
MDA-MB-453	HER2 positive type, Origin- Adenocarcinoma, mammary gland/breast; derived from metastatic site: pericardial effusion	NCCS, Pune
MCF10A	Basal type, Origin- Mammary epithelia; breast immortalised long-term culture	Dr. M Lahiri, IISER, Pune
HUVEC	Human umbilical vein endothelial cells (HUVEC), from pooled donors	Lonza, USA

Plasmid vectors, antibodies and primer sequences

A list of all Expression and shRNAs plasmid vectors, antibodies and primers used in this study are described in Appendix I, II and III respectively.

4.2 Reagents

Immunohistochemistry (IHC): Poly-L-Lysine (Merck, USA), Xylene (Merck, USA), Fibrinogen (Instrumentation laboratory, USA), Formalin solution (HiMedia, India), Paraffin (Thermo Fisher Scientific, USA), Acetone (Merck), Eosin (HiMedia), EnVision™ Flex Wash Buffer (Dako, Denmark), EnVision™ Flex Substrate Buffer (Dako), EnVision™ Flex DAB+ Chromogen (Dako), EnVision™ Flex HRP secondary antibody (Dako), Ethanol (Merck), EnVision™ Flex peroxidase blocking reagent (Dako), DPX mountant (Fisher Scientific), Haematoxylin (HiMedia), EnVision™ Flex target Retrieval solution, high pH (Dako), EnVision™ Flex target Retrieval solution, low pH (Dako).

Cell culture: RPMI1640 (HiMedia), DMEM (Hi-media), DPBS – pH 7.4 (HiMedia), DMEM Phenol-red free (HiMedia), Trypsin- EDTA solution 0.25% (HiMedia), EGM™-2 Endothelial Cell Growth Medium-2 (Lonza, USA), Antibiotic solution with Penicillin, Streptomycin and Amphotericin B (HiMedia), Trypan blue (0.4% in PBS) (HiMedia), VEGFR2 inhibitor (Calbiochem, Merck, USA), ERK inhibitor II (Calbiochem), P38 inhibitor (Calbiochem), Fetal Bovine Serum (HiMedia), Charcoal treated FBS (HiMedia), DMSO (MP Biomedicals, India), Ethanol (Merck).

Transfection and stable cell-line generation: Opti-MEM (Thermo Fisher Scientific, USA), Lipofectamine 3000 (Thermo Fisher Scientific, USA), G418 (50 µg/ml) (HiMedia), Puromycin (1mg/ml) (Sigma).

ELISA: Human VEGF Quantikine ELISA Kit (R&D Systems).

Immunocytochemistry: Microscopic glass slides (Riviera, India), 12 mm coverslips (Fisher Scientific), Paraformaldehyde (HiMedia), Triton-X 100 (Sigma), Anti goat-Alexa fluor 488 secondary antibody (Invitrogen) (Appendix II), ProLong Antifade

Mountant (Thermo Fisher Scientific), DAPI (HiMedia), Fluoromount-G (Thermo Fisher Scientific).

Cell proliferation assay: CellTiter 96 Aqueous One solution reagent (Promega, USA).

Transwell migration and invasion assay: Growth factor reduced Matrigel (Corning, USA), Millicell Hanging Cell Culture Insert (8 µm, 12 mm) (Millipore, USA), Phosphate Buffered Saline (pH- 7.4), Paraformaldehyde (HiMedia), Methanol (Merck), Crystal violet (HiMedia), Giemsa (Thermo Fisher Scientific).

Tubule formation assay: Matrigel matrix (Corning), µ slide angiogenesis (ibidi, Germany).

Bacterial culture: LB Broth- Miller (HiMedia), LB Agar- Miller (Lonza), Kanamycin (50 mg/ml) in autoclaved milli-Q water (Sigma), Ampicillin (100 mg/ml) in autoclaved milli-Q water (Sigma).

Plasmid preparation: 10X TE (Genei, India), Plasmid mini kit (Qiagen, Germany), Plasmid midi kit (Qiagen), Nuclease Free Water (Genei), Isopropanol (Sigma).

Competent Cell preparation: Inoue Buffer [15 mM $CaCl_2.2H_2O$ (HiMedia), 55 mM $MnCl_2.4H_2O$ (HiMedia), 250 mM KCl (Sigma), 10 mM PIPES (Sigma)].

Agarose gel electrophoresis: 50X TAE (Appendix V), LE Agarose (Lonza), 100 bp DNA ladder (NEB, USA), 1Kb DNA ladder (NEB), 6X DNA loading dye (Genei).

SDS-PAGE Electrophoresis and Western blotting: Pierce Protease Inhibitor Mini Tablets (Thermo Fisher Scientific), RIPA Lysis and Extraction Buffer (Thermo Fisher Scientific), Halt™ Protease and Phosphatase Inhibitor Single-Use Cocktail (100X) (Thermo Fisher Scientific), Tris (MP Biomedicals), Acrylamide (Invitrogen), Glycine

(MP Biomedicals), Bis-acrylamide (Sigma), SDS (MP Biomedicals), TEMED (Sigma), Bromophenol blue (Sigma), APS (MP Biomedicals), β-Mercaptoethanol (MP Biomedicals), Glycerol (MP Biomedicals), Polyvinylidenedifluoride membrane (PVDF) membrane (Millipore, Merck), BlueElf Prestained Protein Marker (BR Biochem), Tween® 20 (MP Biomedicals), PageRuler Prestained Protein Ladder (Thermo Fisher Scientific), Skim milk powder (MP Biomedicals), Ponceau-S stain (HiMedia), Restore™ Plus Stripping Buffer (Thermo Fisher Scientific), Bovine Serum Albumin Fraction V (BSA) (MP Biomedicals), Pierce™ BCA Protein Assay Kit (Thermo Fischer Scientific), SuperSignal™ West Femto Maximum Sensitivity Substrate (Thermo Fischer Scientific), 4X Laemmli Sample Buffer (BioRad, USA). All primary and seconady antibodies used in Western blot are listed in Appendix II.

RNA extraction and cDNA synthesis: Verso cDNA Synthesis Kit (Thermo Fisher Scientific), Nuclease Free Water (Genei), RNeasy Mini Kit (Qiagen).

Quantitative- Real-time PCR: PowerUp™ SYBR™ Green Master Mix (Thermo Fisher Scientific), Nuclease Free water (Genei), Primers (Integrated DNA Technologies). The sequences of primers have been listed in Appendix III.

Caspase activity assay: Caspase-Glo® 3/7 Assay System (Promega).

Cellular ROS activity assay: DCFDA / H2DCFDA - Cellular ROS Assay Kit (Abcam).

Apoptosis assay: FITC Annexin V Apoptosis Detection Kit I (BD Pharmingen™).

Skin wound healing assay: Isoflurane - USP (Halocarbon, USA), Silicon splints (Generic, lab made), Tegaderm (3M, India), 4-6mm biopsy puncture, Tramadol (Bestochem Formulations Ltd, India), Sutures (Johnson & Johnson, USA).

4.3 Methodology

4.3.1 Cell culture and cell-based assays

4.3.1.1 Culture of human breast cancer cells

MCF7 cell line was cultured and maintained in DMEM supplemented with 10% v/v heat inactivated FBS, 0.025 µg/ml Amphotericin B, 100 units/ml of Penicillin and 50 µg/ml Streptomycin. Other breast cancer cell lines like MDA-MB-468, MDA-MB-453 and T-47D were maintained in RPMI1640 with 10% heat inactivated FBS, 100 units/ml of Penicillin, 0.025 µg/ml Amphotericin B and 50 µg/ml Streptomycin. To culture MDA-MB-231, RPMI 1640 supplemented with 15% FBS, 100 units/ml of Penicillin, 0.025 µg/ml Amphotericin B and 50 µg/ml Streptomycin was used. For Estradiol/Tamoxifen based treatment, MCF7 cells were cultured in phenol red-free DMEM with 10% charcoal-treated FBS, 100 units/ml of Penicillin, 0.025 µg/ml Amphotericin B and 50 µg/ml Streptomycin. All these cell lines were cultured and maintained in T-25/ T-75 flasks at 37ºC temperature, 5% CO_2 and 95% humidity in an incubator.

4.3.1.2 Culture of human primary HUVECs

Primary cells, HUVECs were cultured and maintained in complete EGM-2 endothelial cell growth medium. To prepare the complete EGM-2 endothelial cell growth medium, EBM-2 Basal Medium and EGM-2 SingleQuots Supplements were mixed according to the manufacturer's protocol. The complete medium was further passed through 0.2 µm filter and stored at 4ºC. HUVECs were maintained in a humidified chamber at 37ºC temperature and 5% CO_2.

4.3.1.3 Subculture, trypsinization and passage of cells

In order to subculture, first the cells were allowed to reach 80-90% confluence in healthy conditions. Washing with 1X DPBS was carried out after decanting the old medium. The

cells were incubated with pre-warmed trypsin-EDTA solution for 2-10 minutes at 37ºC in the incubator, for detachment of cells from the flask surface. Further, complete medium was added to the flask to neutralize the action of trypsin. The cell-suspension was then aspirated in 15 ml sterile centrifuge tube and spun at 300g for 5 minutes at room temperature. The supernatant was discarded and the remaining pellet was resuspended in complete growth medium. A small volume of cell suspension was mixed with trypan-blue dye and loaded in a hemocytometer. The hemocytometer was kept under 10X objective lens of an inverted microscope to calculate the total number of viable cells. Finally, 1 x 10^6/ 2 x 10^6 viable cells were seeded in T-25/T-75 flask containing pre-warmed medium.

4.3.1.4 Cell storage and revival

For long time storage, the cells of low passage number were grown to 80-90% confluence in T-75 flask. Cells were detached and pelleted down, according to the protocol mentioned in the previous section. The total number of viable cells was counted using trypan-blue method and 1 x 10^6 cells/ml were resuspended in a freezing mix solution (DMSO-FBS solution in 1:9 ratio v/v). The cell-suspension was kept in sterile and airtight cryovials and kept overnight at -80ºC in a cryo 1 degree cooler (Tarsons, India). The next day, vials were transferred to liquid nitrogen for long-term storage.

To revive the cryopreserved cells from liquid nitrogen, first distilled water was warmed at 37ºC in a glass beaker (volume should be sufficient to reach the 2/3rd part of the vial) and few drops of iodine solution were added in it. Next, cryovials were immediately transferred from liquid nitrogen to the warm water for quick recovery of cell suspension. Pre-warmed complete growth medium was added to the cell suspension and the tube was centrifuged at 200g for 5 minutes at room temperature. The supernatant was further discarded and the pellet was resuspended in a 5-6 ml of complete growth medium and

cultured in a T-25 flask at 37ºC temperature, 5% CO_2 and 95% humidity in a sterile chamber.

4.3.1.5 Stable and transient transfection of cells

In our study, we used Lipofectamine 3000 reagent for the transfection of expression/shRNA vectors of IQGAP2 in MCF7 and MDA-MB-468 cells. The ratio of DNA: Lipofectamine 3000 (L3000): P3000, used for the optimum transfection of cells have been summarised in Table 4.3.1.5.1. In brief, cells were first allowed to grow to 70-80% confluence. The old medium was removed and cells were washed twice with 1X DPBS. Fresh growth medium was added to the plates/flasks and was kept back in the incubator for an hour. In between, the transfection master mix was prepared; for that, two solutions were prepared, first the solution of Opti-MEM, DNA and P3000 and the other one of Opti-MEM and L3000. After 5 minutes both the solutions were mixed and incubated at room temperature for 20-30 minutes. The transfection complex was subsequently added to the cells in a drop-wise manner and gently swirled for uniform distribution of the complex. The plate/flask was kept in the incubator for 24-48 hours to get the optimum transfection efficiency. Cells were then used for cell based assay or allowed to prepare stable cells as described below.

To get the stable MCF7/ MDA-MB-468 line with IQGAP2 ectopic expression or knock down, the cells were kept in antibiotic selection post 48 hours of transfection.

Table 4.3.1.5.1 Reaction setup of mammalian cell line transfection*

Culture plate	Vol. of growth medium	Components of mix I			Components of mix II	
		Opti-MEM (µl)	P3000 (µl)	DNA (µg)	Opti-MEM (µl)	L3000 (µl)
6-well	2 ml	125 µl	5.0	2.5	125 µl	7.5
12-well	1 ml	50 µl	2.0	1.0	50 µl	3.0
24-well	500 µl	25 µl	1.0	0.5	25 µl	1.5
96-well	100 µl	5 µl	0.2	0.1	5 µl	0.3

*Adapted from Lipofectamine™ 3000 Reagent user guide, Invitrogen, Thermo Fisher Scientific

The information of cell line, plasmid vector and antibiotic used for selection to prepare stable cell line is summarised in Table 3. Now onward, these stable cell-lines will be referred as per Table 4.3.1.5.2.

Table 4.3.1.5.2 Details of stable cell line preparation

Name of stable cell line	Description	Cell line	Plasmid used for transfection	Antibiotic used for selection
MCF7_IQGAP2_Ex	MCF7 cell line with IQGAP2 over expression	MCF7	pCMV6-IQGAP2-Myc	G418 (1000 µg/ml)
MCF7_Control_EV	MCF7 cell line with vehicle control	MCF7	pCMV6	G418 (1000 µg/ml)
MCF7_IQGAP2_KD	MCF7 cell line with IQGAP2 knockdown	MCF7	pLKO.1_IQGAP2-shRNA	Puromycin (1 µg/ml)
MCF7_Control_Sc	MCF7 cell line with scrambled control	MCF7	pLKO.1_Scrambled	Puromycin (1 µg/ml)
MDA-MB-468_IQGAP2_KD	MDA-MB-468 cell line with IQGAP2 knockdown	MDA-MB-468	pLKO.1_IQGAP2-shRNA	Puromycin (1 µg/ml)
MDA-MB-468_Control_Sc	MDA-MB-468 cell line with scrambled control	MDA-MB-468	pLKO.1_Scrambled	Puromycin (1 µg/ml)

The confirmation of positive stable colonies was done by Western blotting. The positive clones were then maintained at 500 µg/ml G418 concentration or at 0.5 µg/ml puromycin concentration for ectopic expression and knock down, respectively.

4.3.1.6 Cell proliferation assay

To perform cell proliferation in MCF7 and MDA-MB-468 cell lines, 2000 cells/well were seeded in a 96 well plate with 200 µl of complete growth medium. For HUVECs, 5000 cells/well were seeded in a 96 well plate with 200 µl of complete EGM-2 growth medium. The cells were allowed to settle down on the surface of the plate and then the old medium was replaced with 200 µl of new 2-5% FBS supplemented medium. Further, cells were kept inside a humidified incubator maintaining 37ºC temperature and 5% CO_2 level for

24 hours to 96 hours. The cells were then taken out at an interval of 24 hours and the old growth medium was replaced with 100 µl pre-warmed fresh growth medium and 20 µl MTS (CellTiter 96® AQueous One Solution) reagent. The cells were then incubated for 1-4 hours inside the incubator. Finally, the absorbance at 490 nm wavelength was recorded in Varioskan™ LUX multimode microplate reader (Thermo Fisher Scientific). The assay was carried out with three replicates in each group.

4.3.1.7 Colony formation assay

1000 cells were seeded into each well of a 6-well plate at a density of 1000 cells/well in complete growth medium. The plates were kept inside the humidified incubator maintained at 37ºC temperature and 5% CO_2 for 10-15 days. After the incubation period is over, the plates were taken out from the incubator and cells were washed gently, twice with 1X DPBS buffer. Subsequently, cells were fixed with cold fixation solution of methanol and acetic acid (3:1) for 5 minutes. The fixation solution was decanted and cells were further washed with 1X DPBS buffer. The cells were stained with 0.5% crystal violet solution for 20 minutes followed by washing under tap water. Thereafter, plates were dried and photographs of cell colonies were captured using a digital camera (Nikon, Japan). The size and number of cell colonies were counted using ImageJ software (NIH, USA). The assay was performed in triplicates.

4.3.1.8 Scratch wound healing assay

In a 12 well plate approx. 0.3 x 10^6 cells were seeded with complete growth medium. The plates were swirled slowly on the surface of hood so that the cells are distributed evenly in the wells. Plates were then kept back inside the incubator at 37ºC till the confluence reached 90-100%. Thereafter, the growth medium was aspirated off from the culture plates and washed twice with pre-warmed 1X DPBS. In the middle of each well, a fine

scratch was created using P200 pipette tip. The wells were further washed with pre-warmed 1X DPBS buffer to remove the detached cells. Thereafter, 2 ml of complete medium was added to each well and plates were kept back inside the incubator. Images of wound were captured using an inverted microscope (Nikon, 10X objective lens) at an interval of 12 hours till the complete closure of the wound. The area of wound closure was analyzed in ImageJ software. This assay was performed in triplicates.

4.3.1.9 Transwell migration assay

Millipore transwell chambers (8 μm pore size) were used for the transwell migration assay. Initially, the cells were grown for 12 hours in a reduced serum medium for serum-starvation. Cells (0.05×10^6) were seeded with 0.5 ml of reduced serum medium in the upper chamber of a 12-well plate. In order to induce cell migration, the lower chamber of the well was filled with 1 ml of complete growth medium. The plate was kept back in the incubator for another 16-24 hours. After the incubation period, the plates were taken out and insert were removed very carefully from the plate using forceps. The medium in the insert was decanted and cells were washed twice with 1X PBS. Cells were fixed by adding 4% paraformaldehyde to the top of each insert for 10 minutes. The fixation reagent was decanted and cells were washed twice with 1X PBS. To permeabilised the cells, ice-chilled methanol was added to each insert and incubated for 20 minutes. Cells were washed twice with 1X PBS and then 0.5% Crystal Violet solution or Giemsa solution was applied on top of the inserts for 15 minutes, in dark. Thereafter, the cells were washed twice with 1X PBS and the non-migrated cells from upper chamber were wiped off using cotton swab. Images were captured from five different fields of each chamber using 10X objective lens of an upright bright field microscope (Olympus, Japan). The number of migrated cells was recorded and analysed using ImageJ software. The experiment was performed in triplicates.

4.3.1.10 Transwell matrigel invasion assay

To perform transwell matrigel invasion assay, all the steps of transwell migration assay were followed except the initial step where a pre-coating of Corning® Matrigel® (Growth Factor Reduced Basement Membrane Matrix) (Corning) was done in the upper chamber of Millipore transwell inserts (8 µm pore size). For pre-coating, 100 µl of 1 mg/ml growth factor reduced Matrigel was added on the upper chamber of the insert and allowed to settle down for 4-6 hours in incubator at 37ºC. The rest of the method is the same as mentioned in above section (Section 3.3.2.9).

4.3.1.11 Cell apoptosis assay

To measure apoptosis of cells, we used FITC Annexin V Apoptosis Detection Kit I (BD Biosciences, USA). To perform this assay, initially 1×10^6 cells were grown in complete medium at 37ºC temperature and 5% CO_2 for 48 hours. Afterward, the cells were trypsinized and centrifuged at 300g for 5 minutes at room temperature. The cell pellet was washed twice with cold PBS and resuspended in 1X Binding Buffer at a concentration of 1×10^6 cells/ml and then 5 µl of Propidium iodide (PI) solution and Annexin V-FITC solutions were added. The cell suspension was incubated for 20 minutes in the dark. The samples were then analysed using FACS Calibur (BD Biosciences, USA) flow cytometry with 488 nm excitation and 647 nm emission filters. Data was analysed using cell quest pro software (BD Biosciences).

4.3.1.12 Measurement of caspase activity

Caspase-Glo 3/7 Assay Kit (Promega, USA) was used to check the caspase activity of cells. In a white-walled 96-well plate, 1×10^4 cells were seeded and incubated in CO_2 incubator at 37ºC for 48 hours. Then, the Caspase-Glo® 3/7 reagent was prepared by mixing the two components of kit, Caspase-Glo® 3/7 Buffer and Caspase-Glo® 3/7

substrate. The 96-well plates were taken out from the incubator and allowed to equilibrate to room temperature; 100 µl of this reagent was added to each well of the 96 well plate and mixed gently at 300-500 rpm for 30 seconds. The plate was kept back to the incubator at room temperature for 1 hour and luminescence was recorded in a Varioskan™ LUX multimode microplate reader (Thermo Fisher Scientific). The results were shown as relative light units (RLU). This assay was performed in triplicates.

4.3.1.13 Pulldown Assay

2×10^6 cells were grown in complete medium in T-75 flask in a humidified incubator at 37ºC, 5% CO_2 for 24 hours. The flask was taken out and cells were washed twice with cold PBS. Thereafter, cells were lysed in lysis buffer (1% Triton X-100, 150 mM Sodium chloride, 200 mM Tris-HCl, Phosphatase Inhibitor and Halt Protease, pH 7.4) by sonication for 15 seconds. Pre-clearing of cell lysate was carried out with glutathione-Sepharose at 4^0C for 1 hour. The equal volume of lysate was incubated with glutathione-Sepharose beads attached GST or GST tagged IQGAP1 at 4^0C for 3h. Finally, samples were washed thrice with wash buffer followed by SDS-PAGE and Western blotting for GST, IQGAP1 and IQGAP2.

4.3.1.14 Measurement of Reactive Oxygen Level

DCFDA/H2DCFDA Cellular Reactive Oxygen Species Detection Assay Kit (Abcam) was used to detect the reactive oxygen level (ROS) level. Approx. 20000 cells were plated in each well of a flat bottom 96-well plate in phenol red free complete growth medium and incubated at 37°C for 24 hours. The plate was taken out and cells were washed twice with 1X wash buffer. The cells were stained with the diluted DCFDA Solution. The plate was kept back in incubator and incubated for 45 minutes at 37°C in the dark. The cells were washed twice with 1X wash buffer. Finally, 100 µl of 1X buffer was added to each

well and images were captured immediately in an inverted microscope with FITC filter at constant light exposure using 4X objective lens. The intensity of fluorescence was then analysed using ImageJ software. The experiment was performed with three replicates.

4.3.1.15 Conditioned media preparation

Breast cancer cell lines, MCF7 and MDA-MB-468 were grown (2×10^6 cells) in 10 cm dishes in complete growth media (10 ml) for 24 hours.

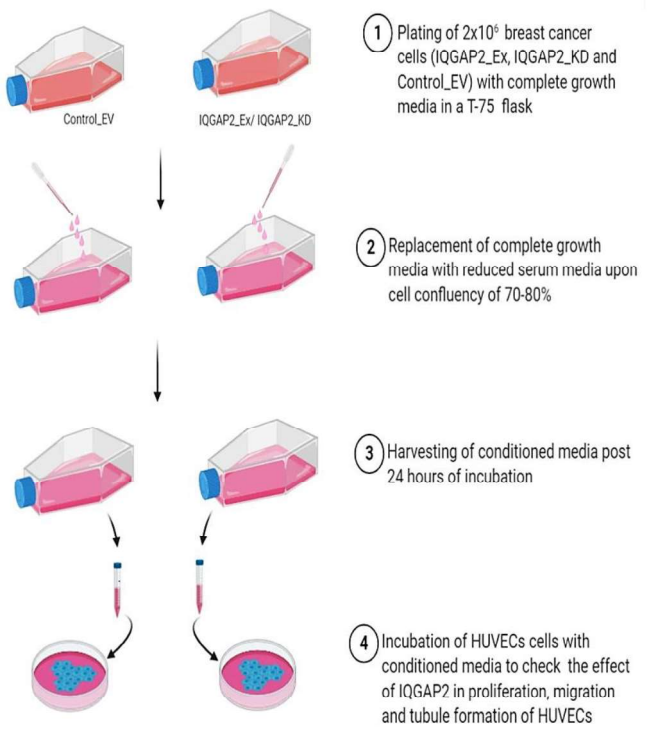

Figure 4.3.1.15.1. A pictorial representation of conditioned media preparation from breast cancer cells.

The media was collected into 15 ml centrifuge tube and spin at 1000 rpm for 5 minutes at 4^0C. The supernatant was then transferred into fresh tube, labelled and stored at -80^0C till use. The media was replaced with serum free media (10 ml) and cells were incubated for the next 48 hours.

4.3.1.16 Tubule formation assay

96 well-plate or μ-Slide Angiogenesis (Ibidi) were used to carry out Matrigel tubule formation assay. Conditioned medium from MCF7 (MCF7_IQGAP2_Ex, MCF7_Control_EV, MCF7_IQGAP2_KD, MCF7_Control_Sc) or MDA-MB-468 (MDA-MB-468_IQGAP2_KD, MDA-MB-468_Control_Sc) cells were used for the assay. Matrigel matrix was thawed overnight at 4ºC for the assay in 96-well plate. Pre-chilled 96-well plate and 200 μl tips were used for pipetting Matrigel matrix. 50 μl of Matrigel matrix was pipetted into each well of the 96-well plate followed by centrifugation at 200g, 4ºC for 5 minutes. The Matrigel matrix was then allowed to solidify by keeping the plate in the incubator at 37ºC for one hour. For experiments with conditioned medium, HUVECs were resuspended in a mixture of conditioned medium and EGM2 (1:1) and plated at a density of 20 x 10^4 cells/well, in a total volume of 100 μl. The culture plate was then incubated at 37ºC, 5% CO_2 and 95% humidity.

We acquired the first images 2-hour after the incubation and at regular intervals of 2-hours thereafter using Nikon inverted microscope (using 4X and 10X objective lenses), till completion of the assay. For tubule formation assay with μ-Slide Angiogenesis, the inner wells of μ-Slide Angiogenesis were filled with 10 μl of Matrigel matrix carefully so that no air bubbles were formed for the assay using the slide. The μ-Slide was then incubated at 37ºC for 1 hour, to allow the Matrigel matrix to solidify. Similar to prior experiments, harvested HUVECs were resuspended in a mixture of conditioned medium and EGM2 (1:1), for experiments with conditioned medium, and plated at a density of 2 x 10^4 cells/well, in a total volume of 50 μl. The μ-Slide was then incubated at 37ºC, 5% CO_2 and 95% humidity followed by imaging at regular intervals as described previously. Angiogenesis Analyser plugin of ImageJ software was used to analyse the images. The experiments were performed in triplicates or more.

4.3.1.17 Immunocytochemistry

Cells were grown on sterile glass coverslips to 50% confluency in an incubator at 37ºC, 5% CO2 and 95% humidity, for immunocytochemistry. Culture medium was removed from the dish and washed gently with 1X PBS at room temperature. To fix the cells, freshly prepared 4% PFA solution was used on the coverslips and then incubated for 10 minutes at room temperature. The coverslips were then washed gently with 1X PBS thrice to remove the remaining fixative. After the fixation, 0.1% Triton-X 100 in PBS was used on the coverslips followed by incubation for 20 minutes at room temperature. The cover slips were then washed thrice in 1X PBST. 2% BSA in 1X PBS was used for blocking for one hour at room temperature to minimize the background fluorescence. The cells were then incubated with primary antibody diluted in 2% BSA and 0.1% PBST (1:1) solution, for 4 hours at room temperature in a humidified chamber followed by washing thrice with 1X PBST. The cells were then incubated with Alexa fluor-conjugated secondary antibody diluted in the same solution as the primary antibody for 1 hour at room temperature. After washing the coverslips thrice in PBST, DAPI (1:2000 in PBS) was used or directly proceeded to mount with ProLong™ Gold Antifade Mountant (Life technologies). After washing thrice with 1X PBS, DAPI stained slides were mounted with Fluoromont-G (Thermo Fisher Scientific). A confocal microscope (Leica) was used to analyse the cells. The primary and secondary antibody dilutions have been listed in Appendix II. Buffers used have been listed in Appendix V.

4.3.2 Western blotting

4.3.2.1 Whole cell lysate preparation

Cells were grown up to 70-80% confluency in cell culture plates and dishes in an incubator at 37ºC, 5% CO2 and 95% humidity. After washing the cells with ice-cold 1X PBS, lysis was done by adding ice-cold RIPA buffer (Thermo Fisher Scientific) at a

suitable volume. Ice- cold scrapers were used to maximize the lysis efficiency. The lysate was then collected in cold-microcentrifuge tubes followed by centrifugation at ~14,000g, 4ºC for 15 minutes to pellet down the cell debris and supernatant collection. An aliquot of the sample was separated and kept immediately in -80ºC freezer for protein estimation by BCA method. 4X Laemmli Sample Buffer (BioRad) was added to a final concentration of 1X to the remaining samples and boiled at 95ºC for 5 minutes. The protein samples thus prepared were kept at -80ºC till further use.

4.3.2.2 Protein estimation by BCA method

BCA protein assay kit (Pierce) was used for protein estimation. Standards were prepared by making serial dilutions of Bovine Serum Albumin (BSA) at 1.5-fold from 2 mg/ml (stock solution) to 20 µg/ml. BCA reagent A and BCA reagent B were mixed at a ratio of 50:1 to prepare working reagent. 10 µl each of samples and BSA standards were dispensed in a 96 well plate in triplicates. 200 µl of working reagent was then added to each well followed by incubation at 37ºC for 30 minutes. The plate was then cooled to room temperature for 10 minutes followed by absorbance measurement at 562 nm using Varioskan™ LUX multimode microplate reader (Thermo Fisher Scientific).

4.3.2.3 Sodium dodecyl sulfate-polyacrylamide gel electrophoresis (SDS-PAGE)

SDS-PAGE method was used for the separation and visualization of proteins based on their molecular mass. Various stock solutions and buffers required for the entire procedure have been described in Appendix V. Gel electrophoresis was conducted in Mini-PROTEAN tetra system (Biorad). 5% stacking gel and 10% or 12% resolving gels were prepared for SDS-PAGE. The volume and concentration of components required to cast a gel of predetermined volume are given in Table 4.3.2.3.1. 1X TGS electrophoresis buffer was used in electrophoresis chamber and connected to a power pack. Protein

samples stored in -80ºC freezer were thawed on ice followed by boiling at 95ºC for 5 minutes. 20 µg of protein lysates were loaded into each well along with prestained protein ladder, as size standard and ran at a constant voltage of 100V, till the bromophenol blue dye front exits from the base of the gel.

Table 4.3.2.3.1. The volumes and concentrations of components to prepare SDS-PAGE gels*

Resolving gel (12%)		**Stacking gel (5%)**	
Components	**Vol. for 10 ml (ml)**	**Components**	**Vol. for 3ml (ml)**
Milli Q water	3.3	Milli Q water	2.1
1.5 M Tris (pH 8.8)	2.5	1 M Tris (pH 6.8)	0.38
30% acrylamide	4	30% acrylamide	0.5
10% APS	0.1	10% APS	0.03
10% SDS	0.1	10% SDS	0.03
TEMED	0.004	TEMED	0.003

*Adapted from [184]

4.3.2.4 Immunoblotting

After SDS-PAGE, the gel was placed onto the methanol activated PVDF membrane and assembled into the transfer cassette. Transfer module of Mini Trans-Blot® Electrophoretic Transfer Cell (BioRad) was filled with chilled transfer buffer and transfer cassette was placed inside the module. After the entire assembly was connected to a power-pack, it was transferred to 4ºC room. A constant voltage of 30V for the duration of 16 hours was used for transfer followed by Ponceau staining of the membrane to visualize the transferred protein. Subsequently, the stain was removed by washing with 1X TBST for 5 minutes. Blocking solution (either 5% BSA or 5% skim milk powder in 0.01% TBST) was used to block the non-specific binding of IgG by incubating the membrane in blocking solution for one hour in a shaker. Primary antibody solution at appropriate dilution (Appendix II), was then used to incubate the membrane at room temperature for 1 hour followed by overnight incubation at 4ºC. The following day, membrane was washed thrice with 1X TBST, for 5 minutes each and, subsequently

membrane was transferred to corresponding HRP-conjugated secondary antibody solution. For the incubation with secondary antibody, membrane was kept at constant shaking at room temperature for 1 hour followed by washing of the membrane thrice with TBST, for 5 minutes each. Immunoblots were detected using SuperSignal™ West Femto Maximum Sensitivity Substrate (Thermo Fischer Scientific) and Chemidoc XRS equipped with Quantity 1-D analysis software version 4.6.9 (Bio-rad Laboratories) was used for imaging.

4.3.2.5 Stripping and reprobing of the PVDF membrane

The PVDF membranes were reprobed with a different antibody, for which stripping was done using Restore™ Plus Stripping Buffer (Thermo Fisher Scientific). The membrane was washed thrice with 0.1% TBST for 5 minutes each, thereafter the membrane was incubated with Restore™ Plus Stripping Buffer for 15- 20 minutes with constant shaking at 37ºC. The washing was done with TBST, thrice for 10 minutes each, at room temperature. Subsequently blocking of the membrane, incubation with antibodies and detection was carried out, as described in section 3.3.2.4.

4.3.3 Quantitative- Real-time PCR

4.3.3.1 RNA extraction and cDNA synthesis

Cells were grown in 6-well plate until 70-80% confluence is reached, prior to cell harvest and RNA isolation. RNAeasy Mini Kit (Qiagen) was used for RNA extraction and the procedure has been described in Appendix IV. The quality of the extracted RNA was checked by agarose gel electrophoresis on 1% agarose gel for 15 minutes at 120V. The quality was considered as good when the presence of two intact bands, indicating 28S and 18S rRNA were observed. Nanodrop 2000 (Thermo Fisher Scientific) was used to determine the concentration of RNA. Subsequently, 1 µg of total RNA was aliquoted and

Verso cDNA Synthesis Kit (Thermo Fisher Scientific) was used for single-strand cDNA synthesis. The reaction mixture and cycling conditions for the same are given in Table 4.3.3.1.1.

Table 4.3.3.1.1 Components of cDNA synthesis reaction mix for a single reaction

Components	**Volume (µl)**
5X cDNA synthesis buffer	4
Template RNA (1 µg)	1-5
Anchored Oligo dT (500 ng/µl)	0.25
Random hexamer (400 ng/µl)	0.75
dNTP mix (500 µM each)	2
Nuclease free water	To 20 µl

The cycling program for reverse transcription included one cycle at 42 ºC for 30 minutes (cDNA synthesis), followed by inactivation at 95 ºC for 2 minutes. The prepared cDNA was kept in -20 ºC freezer until further use.

4.3.3.2 Real-time PCR

The real-time PCR primers were designed using Primer3 BLAST tool (NCBI). The qRT-PCR reaction was set up in optically clear 96-well plate or 8-well strip. A final concentration of 10 ng/µl of the cDNA was prepared in nuclease-free water. Reaction set up conditions are mentioned in Table 4.3.3.2.1. For each experimental condition, reaction was set up in triplicates, along with a non-template control (NTC). GAPDH was used as internal control. The 96 well plate was sealed with an optically clear film after the completion of reaction setup followed by centrifugation at 1000 rpm for 10 minutes in a swinging bucket rotor. The reaction was performed either in ABI7500 real-time PCR machine (ABI) or QuantStudio 7 Flex Real-Time PCR Systems (Thermo Fisher Scientific), using cycling conditions as mentioned in Table 4.3.3.2.2. Relative expression was calculated using the $2^{-\Delta\Delta CT}$ method.

Table 4.3.3.2.1 Components of qPCR reaction mix for QuantStudio 7 Flex and ABI 7500 Real-Time PCR System

Components	**QuantStudio 7 Flex System**		**ABI 7500 System**	
	Reaction mix with template	No template control (NTC)	Reaction mix with template	No template control (NTC)
2X SYBR Green	6 µl	6 µl	10 µl	10 µl
Template cDNA (10 ng/µl)	2 µl	0	2 µl	-
Forward Primer (2.5 µM)	1 µl	1 µl	1 µl	1 µl
Reverse Primer (2.5 µM)	1 µl	1 µl	1 µl	1 µl
NFW	2 µl	4 µl	6 µl	8 µl
Total	12 µl	12 µl	20 µl	20 µl

Table 4.3.3.2.2. QuantStudio 7 Flex and ABI 7500 Real-Time PCR System cycling conditions

Stage	**QuantStudio 7 Flex System**		**ABI 7500 System**	
	Temperature	Time	Temperature	Time
Holding			50ºC	2 minutes
Holding	95ºC	2 minutes	95ºC	10 minutes
Melting (40 cycles)	95ºC	3 seconds	95ºC	15 seconds
Annealing and extension (40 cycles)	60ºC	30 seconds	60ºC	1 minute

4.3.4 Immunohistochemistry

3.3.4.1 Poly-L-Lysine coating of slides

Soap was used to clean the glass slides, subsequently slides were immersed in 1% acetic acid (acetic acid: ethanol in 1:99 ratio) for 20 minutes. The slides were then washed twice with tap water, followed by two consecutive washes in distilled water. Slides were transferred in an incubator and left to dry. The dried slides were then immersed twice inside 0.01 % poly-L-lysine solution in a staining kit for five minutes each. The coated slides were then left to dry overnight at 37ºC.

4.3.4.2 Staining for immunohistochemistry

5 μm thin tumor sections and matched control were cut from FFPE tissue blocks and placed on poly L-lysine coated glass slides. Sections were deparaffinized by heating on a heating plate at 80ºC for 1 hour, followed by two consecutive washes with xylene. Afterward, alcohol gradient from 100% to 50% was used to rehydrate the tissue sections followed by heat-induced epitope retrieval in low pH citrate buffer (pH-6.0) for IQGAP1, IQGAP2, IQGAP3, phospho-ERK, and high pH retrieval buffer (pH-9.0) for CD31. Envision Peroxidase Blocker (Dako) was then used to incubate all the slides for 15 minutes and were incubated with respective primary antibodies for 1 hour, in a humidified chamber at room temperature. The sections were washed and incubated with Envision Flex HRP secondary antibody (Dako) for 30 minutes. Liquid DAB substrate (Dako) was added at the final step. The counterstaining of sections was done with hematoxylin. Thereafter, the sections were dehydrated and, a cleaned glass coverslip with mounting media was placed to cover it. Human breast cancer tissue microarray was also used in this study for IQGAP2 and CD31 expression analysis by IHC. The IHC staining procedure for this array is the same as described above for FFPE tissue sections. Details of antibodies used for the entire procedure have been listed in Appendix II. Imaging was done using an upright light microscope (CX31, Olympus), using 10X and 40X objective lenses. To omit the non-specific background signals of secondary antibody, tissues were also stained with the HRP-secondary antibody only. Final intensity of primary antibodies were calculated after subtracting the background signal of secondary antibody.

4.3.4.3 Immunohistochemistry scoring

The expression levels of proteins were scored in tumor tissue and normal (uninvolved) tissue, as Immunoreactive Score (IRS) or Allred Score as described by Fedchenko et al, 2014 [185].

The IRS scores were determined from the brown signals appearing in the cell cytoplasm, nucleus or membrane, and subsequently categorized as weak, moderate and strong. The IRS score was finalized by multiplying the score of staining intensity and percentage cell positivity. The score of staining intensity was kept in a range of 0 to 3 based on: 0 for no staining, 1 for weak staining, 2 for moderate staining and, 3 for strong staining. The scores for cell positivity were given in the range of 1 to 4, based on: 1 for positive staining in 0–25% of cells, 2 for positive staining in 25–50% of cells, 3 for positive staining in 51–75% of cells and, 4 for positive staining in 75–100% of cells. For further analyses the IRS scores ranging from 0–4 were treated as weak staining, 5–8 as moderate staining and, 9–12 as intense staining.

In Allred scoring system, the intensity score (0 for negative, 1 for weak, 2 for moderate and, 3 for strong) and cell positivity score (0- 0% cell positivity, 1- ≤ 1% cell positivity, 2- 1%-10% cell positivity, 3- 11%-33% cell positivity, 4- 34%-66% cell positivity, 5- 67%-100% cell positivity) were added to get final Allred score of the tissue section. For analyses, the Allred scores of 0-2 were considered as negative/weak, 3-6 as moderate and, 7-8 as intense/strong expression levels.

4.3.4.4 Microvessel density analysis

IHC of FFPE tissue sections was carried out with CD31 (a vascular marker). Microvessel density (MVD) was determined from areas of highest vascularisation within the tumor or normal region. To check the most vascularised areas, microscopic slides were screened at low magnification (20X, 40X) using bright field microscope (Olympus). Vessel counting from the three most vascularised areas was done by pathologist (Dr. Nachiketa Mohapatra) at a magnification of 200X (microscopic field area 0.785 mm^2). An average of three counts reported in vessels per mm^2 was used as the MVD of the tissue sections.

4.3.5 Animal based assays

4.3.5.1 Xenograft tumor growth assay

This experiment was approved from the Institutional Animal Ethics Committee, NISER, India (Protocol No-NISER/SBS/AH/110). To perform xenograft tumor growth assay, the female athymic nude mice (age matched, 6-8 week, 15-18 gram) were used. MCF7_IQGAP2_KD and MCF7_Control_Sc cells (2×10^6) resuspended in 1X PBS, were mixed with 100 µl of ice-cold Matrigel matrix (1:1 ratio) and injected into the fourth mammary fat pad of mice. The dose of estradiol benzoate (10 µg with 1X PBS) was given to the mice at 7 day's interval, subcutaneously. The size of the tumor (length and width) was recorded at three day's interval using an electronic calliper (Ocean premium, India). To calculate the tumor volume of mice following formula was used: volume = length × width^2. The mice were euthanized on day 30 using CO_2 gas chamber. Next, the tumors were removed carefully, washed in 1X PBS and weight was taken on electronic weighing balance. The photographs of tumor were captured using a digital camera (Nikon) and immediately the tissues were placed in 4% paraformaldehyde for fixation. The fixed tissues were further used for paraffin embedding, sectioning followed by immunohistochemistry for phospho-ERK. This experiment was performed with four mice in each group.

4.3.5.2 Matrigel plug assay

This experiment was approved by the Institutional Animal Ethics Committee, NISER, India (Protocol No-NISER/SBS/AH/117). To perform Matrigel plug assay, 6-8 weeks old female C57BL/6 mice were used. On the very first day of experiment, a mix of conditioned medium from stable MCF7 cells for IQGAP2 knockdown/control and Matrigel matrix in 1:1 ratio was prepared and 200 µl of the mix was injected subcutaneously into the right flank of four mice (one injection site/mouse) using an ice-

cold syringe with a 24G needle. The mix was allowed to solidify into a gel plug and then mice were kept back into their cages with proper food, water and optimum environmental conditions. After 7-10 days of injection, mice were euthanized using CO_2 gas chamber and the matrigel plugs were excised out from the right flank of mice. The excised plugs were washed in 1X PBS buffer and photographed to visualise the presence of blood vessels. After capturing images of plugs, they were fixed in formalin for overnight followed by paraffin embedding and sectioning onto slides. Thereafter, hematoxylin and eosin (H&E) staining was carried out to ascertain microvessel density. Haemotoxylin positive cells arranged in circular manner were considered as micro vessels.

4.3.5.3 Wound healing assay in mice

Six to eight weeks old female Balb/c mice were used for this assay. Mice were excluded from the study if even any minor skin injury was present. This experiment was approved from the Institutional Animal Ethics Committee, NISER, India (Protocol No- NISER/SBS/AH/170). Mice were anesthetized using the isoflurane-oxygen based method. The hair from the dorsal region of mice was removed using trimmer and shaving blade. This area was cleaned with 70% ethanol and a wound of 4-6 mm diameter was created on right back skin of the mice using 4-6 mm biopsy puncture. A silicone splint (inner diameter- 8 mm, thickness- 0.5 mm) was fixed around the wound using topical skin adhesive (Dermabond) and 5.0 silk sterile suture. Finally, the wound was covered with a Tegaderm, dressing film. An intraperitoneal (IP) injection of Tramadol (40mg/kg body weight) was given to mice at an interval of 12 hours for 3 days as analgesic. Further, a mix of Matrigel matrix and conditioned medium from stable MCF7 cells with IQGAP2 knockdown or vehicle control were prepared in 1:1 ratio and 200 µl of the mix was injected in the centre of wound at an interval of every 24 hours for 3 days. The images of wound were taken every day with a digital camera till the complete closure of the wound.

The area of wound was measured with the help of ImageJ software. Wound healing rate was calculated using following equation: would healing rate = [(original wound area - current wound area)/original wound area] ×100%.

4.3.5.4 The chick chorioallantoic membrane (CAM) assay

The 3-days old embryonated eggs were purchased from Central Poultry Development Organisation, Bhubaneswar. The outer surface of eggs was cleaned using sterile water and incubated inside an incubator at 37^0C and 50% humidity. Eggs were taken out and placed inside a laminar flow hood. The eggs were broken with sharp edge of metal and the intact embryoes was placed carefully in transparent plastic cups. The cups were covered with the transparent cling-wrap and kept inside the incubator for 4 days. After completion of day 4, the cups containing embryos were taken out from the incubator and kept in laminar airflow. The conditioned media from IQGAP2 overexpression, knockdown and control were applied on circular filter paper discs (thickness 1 mm, 6.30 ± 0.04 mm in diameter). The soaked filter discs were then placed over the CAM with the help of sterile forceps. The cups were then re-covered with cling-wrap and kept inside the incubator for the next 7 days. After completion of 7 days, the cups were taken out and images of blood vessels around the filter disc were capture with the help of CCD digital camera. The small blood vessels arising from the major blood vessels and moving centrifugally towards the filter disc were considered as micro blood vessels and used for analysis.

4.3.6 Datamining

4.3.6.1 ONCOMINE based analysis

ONCOMINE is a cancer microarray database and web-based data-mining platform that helps in genome-wide expression analyses and facilitate rapid interpretation of a gene's

potential role in cancer. We have used ONCOMINE database [https://www.oncomine.org, Compendia biosciences, Ann Arbor, MI, USA] to analyse the differences in the expression of genes of interest (IQGAP2 and IQGAP3) in different subtypes of cancers [186]. The inclusion criteria for selection of the studies from the database were as follows- p-value ≤ 0.01, fold change ≥ 2 fold and gene rank $\leq 10\%$. For each gene, comparison of expression levels was performed between cancer and normal tissues.

4.3.6.2 Analysis of TCGA data using UCSC Xena browser

The Cancer Genome Atlas (TCGA) is an assemblage of web-based tools that can be used to visualize, integrate and analyze cancer genomics and accompanying clinical data [187]. The mRNA HiSeq expression data were downloaded with the help of UCSC Xena browser (http://xena.ucsc.edu/, version: 2016-08-16) to analyse the expression levels of different genes across multiple cancer types (lung, kidney, gastric, brain, breast, colorectal, prostate, and liver).

4.3.6.3 Kaplan-Meier plotter analysis

Kaplan-Meier (KM) Plotter (http://kmplot.com/analysis/) database assimilates gene expression data and clinical data, to calculate association of prognostic values for gastric, lung and breast cancer, with mRNA expression levels of different genes. Kaplan Meier plotter has data of 54,675 genes on survival by January 2018. The cancer cases include 5143 breast, 2437 lung and 1065 gastric cancer patients with a mean follow-up of 69 / 40 / 49 / 33 months, respectively. We first selected the best specific probes (JetSet probes) for our gene of interest, which were then individually entered to obtain survival plots to calculate the prognostic value. The analyses provide data related to overall patient survival (OS), first progression (FP), post-progression survival (PPS), distance

metastasis-free survival (DMFS) and relapse-free survival (RFS). Hazard ratios (HR) with 95% confidence intervals (CI) to determine the prognostic value of the gene were extracted. The threshold for statistical significance was set at $p \leq 0.05$.

4.3.6.4 SurvExpress database analysis

The prognostic value of other cancer types namely kidney, brain, liver, prostate and colorectal cancer was analysed using SurvExpress database (http://bioinformatica.mty.itesm.mx:8080/Biomatec/SurvivaX.jsp) [188], as KM plotter database did not have survival information for the aforementioned cancers. SurvExpress is a cancer-wide gene expression database with clinical outcomes and a web-based tool that provides survival analysis and risk assessment of cancer datasets. This database covered more than 20,000 samples and 130 datasets with censored clinical information of tumors over 20 tissues. TCGA datasets were selected for analysis because of the presence of both desirable probes and larger sample size (> 200 patients) in the SurvExpress database. The HR (Hazard ratio) with 95% confidence interval (CI) having $p \leq 0.05$ was considered statistically significant.

4.3.6.5 Somatic mutation and Copy number alteration analysis

TCGA datasets were used to find the somatic mutations and copy number alterations associated with IQGAP2 or IQGAP3 using cBioportal (http://www.cbioportal.org/) [189, 190]. To get the data for mutations or copy number variation, the information like specified TCGA name of cancer dataset and name of gene of interest were entered and results were analysed with the selection of mutation and copy number variation (CNV) query type option. Mutation assessor option was also selected to get an idea that a specific mutation has a potential role as a driver (changes protein function) or passenger (no role in fitness of a clone but associated with clonal expansion) or not. The mutations with FIS

ranges ≥ 1.93 were considered as pathological and neutral with FIS <1.93. 'mRNA vs copy number option' was used to check a correlation between the copy number changes with mRNA expression.

4.3.6.6 Methylation status analysis

To check the status of DNA methylation on the promoter region (mainly CpG islands) of IQGAP2 and IQGAP3, Wanderer web tool (http://maplab.imppc.org/wanderer/doc.html) [191] was used. Wanderer is a gene centered interactive web viewer for TCGA data. It allows data retrieval and visualization of DNA methylation and gene expression profiles in different tumor types. Here, we compared the methylation pattern of IQGAP2 and IQGAP3 in promoter region of normal vs cancer tissues for specific TCGA cancer dataset. To check the correlation between methylation and expression of IQGAP2 and IQGAP3 Pearson correlation test was applied. The only probes showing significant changes of methylation level at promoter region and mRNA expression of single exon were used for the correlation analysis. Pearson's correlation coefficient (r) showing values between 0.5 to 1.0 were considered strong positive correlation, -0.5 to -1.0 as strong negative correlation, 0.3 to 0.5 moderate positive correlation or -0.3 to-0.5 as moderate negative correlation, 0.1 to 0.3 weak positive correlation or -0.1 to -0.3 weak negative correlation.

3.3.7 Statistical Analysis

GraphPad Prism 6.0 Version (GraphPad Software Inc., USA), and Microsoft excel (Microsoft, USA) were used for all statistical analyses. Continuous data were presented as the mean ± standard deviation (SD) of the mean or SEM for cell-based assays. Student's t-test (2-tailed, unpaired) was used to calculate the significance of differences between the means. Non-parametric unpaired Mann-Whitney U test was utilised to determine the significance of difference in distribution frequency of IRS and Allred

scores, between tumor and control group for Immunohistochemistry data. Spearman correlation test was used in order to determine the correlation between clinicopathological parameters and Allred scores for IQGAP2 expression. $p \leq 0.05$, was considered to be significant for all the tests.

RESULTS AND DISCUSSION

DINESH KUMAR

NISER, Bhubaneswar

CHAPTER 1

To understand the effect of altered IQGAP2 expression in breast cancer progression and its molecular mechanism

Findings of this section have been communicated.

Kumar D, Hassan MK, Patel SA, Pattanaik N, Mohapatra N, Dixit M., Reduced IQGAP2 expression promotes EMT and inhibits apoptosis by modulating the MEK-ERK and p38 signalling in breast cancer irrespective of ER status.

5.1 Introduction

Breast cancer is the primary cancer type showing highest incident rate and mortality in women all around the world [1]. The survivability of breast cancer patients is better than other cancer types, but long-term survivability is still poor due to drug resistance [192]. The problem of drug resistance of currently targeted genes [193-196] demands identification of more molecular targets, and especially those which can function in subtype independent manner. IQ Motif Containing GTPase Activating Proteins (IQGAPs) belong to the scaffolding protein family and comprise three members, namely IQGAP1, IQGAP2 and, IQGAP3 in mammals. These members are highly identical in the presence of five conserved domains namely RasGAP_C-terminus, IQ domain, RasGAP-related domain (GRD), WW domain and calponin homology domain [14], but they differ in cellular functions [9]. High expression levels of IQGAP1 and IQGAP3 have been reported in several cancer types where they show their association with the poor survivability of patients and help in progression of tumor growth and metastasis [17, 197-200]. In contrast, studies have observed reduced expression of IQGAP2 in cancers [40, 201-203] and suggested its role as a tumor suppressor. Interestingly, there are few reports that also indicated the elevated level of IQGAP2 in some cancers [45, 46].

The two members, IQGAP1 and IQGAP3 function as oncogenes and associated with worse prognosis in breast cancer [27, 32, 180, 204] whereas the expression pattern, function and mechanism of IQGAP2, is yet to be explored. It is noteworthy, that IQGAP2 and IQGAP1 show inverse expression pattern and function in cancer, explicitly in HCC. IQGAP1 enhances AKT activation in HCC [205], on the other hand, IQGAP2 diminishes the activation of AKT in prostate cancer [41]. Similarly, IQGAP1 downregulates E-cadherin in oesophageal squamous cell carcinoma [29], IQGAP2 does the opposite in prostate cancer [41]. While, IQGAP1-facilitates reduction of cadherin-mediated cell-cell

adhesion [206], IQGAP2 stimulates this process [207]. From the studies of Carmon KS et al., 2014 [208] and Gnatenko DV et al., 2013 [209], it appears that IQGAP2 functions opposite to IQGAP1 in facilitating Wnt signaling. This reciprocal expression pattern was associated with stage/ grade and survival of HCC patients [39]. An increase in IQGAP1 expression has been observed in IQGAP2-/- mice. Interestingly, the mice deficient for both IQGAP2 and IQGAP1 show late onset of HCC [38]. These observations suggest a functional interplay between these two IQGAPs in which IQGAP2 may suppress IQGAP1's oncogenic activity.

Keeping these lacunae/information in mind, this chapter of the study was designed with the main aim to explore the: 1) expression pattern of IQGAP2 in breast cancer patients and it's association with clinicopathological parameters like tumors stage/grade, age, lymph node positivity and lymphovascular invasion of the patient; 2) function and molecular mechanism of IQGAP2 in breast cancer pathogenesis; 3) the relative expression pattern of IQGAP2 and IQGAP1 in breast cancer and its effect on regulation of breast cancer pathogenesis.

To achieve this aim, first, we examined the expression of IQGAP2 using immunohistochemistry in large number of breast cancer patients and performed association study between IQGAP2 protein levels and tumor stage, grade and other histopathological parameters of breast cancer patients. Furthermore, using representative cell-lines of different molecular subtypes, we assessed the role of IQGAP2 in affecting oncogenic potential of breast cancer cells, activation of key signaling pathways, and induction of EMT as well as regulation of inflammatory cytokine milieu in the local tumor microenvironment. *in vivo* xenograft models were used to validate the *in vitro* observations. Finally, the expression pattern of IQGAP2 with regards to IQGAP1, and

the significance of the ratio of these isoforms with regards to tumor progression in patients and induction of oncogenic pathways were explored.

5.2 Results

5.2.1 IQGAP2 expression is reduced in breast cancer tissues

In order to explore the role of IQGAP2 in breast cancer, we started by looking at its expression level in breast tumor tissues.

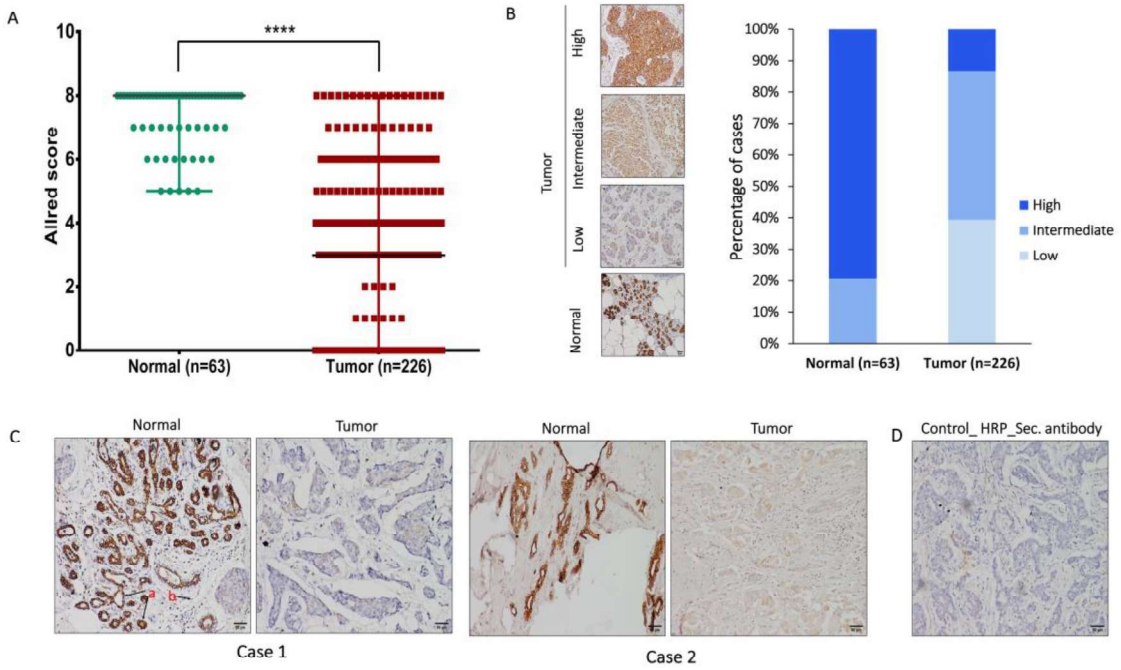

Figure 5.2.1.1. Reduced expression of IQGAP2 in breast cancer tissues. A) The comparison of Allred scores of IQGAP2 expression between tumor (n = 226) and adjacent normal tissue (n = 63) of breast cancer patients (Mann-Whitney U test). **B)** The percentage frequency distribution of normal versus cancer tissues according to the Allred score of IQGAP2. Y-axis represents percentage of patients positive with IQGAP2 low, intermediate or high Allred score. X-axis represents two groups; normal and tumor. **C)** The representative images of tumor tissue and adjacent normal tissue of two breast cancer patients, showing IQGAP2 expression and localization. **C-a)** Represents the glandular cells and **C-b)** represents the stromal region. **D)** Representative IHC image of breast tissue showing no signal for HRP-secondary antibody only. The images were captured using 10X objective lens of bright field microscope. Scale bar in all images is 50 µm, AS = Allred Score, **** represents $p \leq 0.0001$.

We performed IHC in 226 FFPE breast tumor tissues and 63 adjacent normal (uninvolved) regions of breast cancer patients. Comparing the IQGAP2 Allred score, we observed a significant ($p \leq 0.0001$) reduction of IQGAP2 expression in tumor tissue (median value = 3, range = 0-8) compared to normal (median value = 8, range = 5-8) (Fig. 5.2.1.1A).

Analysis of percentage distribution of IQGAP2 expression in the tissue samples showed that staining in tumor area was weak to negative in 39.38% (89 out of 226), moderate in 47.34% (107 out of 226) and strong only in 13.27% cases (30 out of 226) whereas, most of the normal tissue were positive for strong (79.36%, 50 out of 63) and moderate staining (20.63%, 13 out of 63) (Fig. 5.2.1.1B).

We then proceeded to examine the expression pattern specific to particular cell type (glandular/stromal) and localization of IQGAP2 (cytosolic/nuclear/membrane) in breast normal and tumor tissues. The glandular cells showed higher expression of IQGAP2 compared to the stromal region (Fig. 5.2.1.1C. a, b). The expression was predominant in the cytosolic region compared to the nucleus but we found no difference in the localisation pattern of IQGAP2 in normal versus tumor tissues (Fig. 5.2.1.1C). To rule-out the non-specific background signals raised with secondary antibody, the breast tissues were stained with only HRP-secondary antibody only, in each lot (Fig. 5.2.1.1D). Final IHC intensity of each primary antibody was calculated after subtracting background signal.

5.2.2 Low expression of IQGAP2 associates with poor clinical outcomes

In order to determine the association between IQGAP2 expression and clinicopathological features, we divided patients into two groups, IQGAP2 low and IQGAP2 positive based on IQGAP2 IHC score (Allred score 0-4 as negative, Allred score

5-8 as positive). We further compared the distribution of Allred scores with different categories of clinicopathological characteristics (age, tumor size, lymph node metastasis, lymphovascular invasion and histological grade). Our analysis showed that lower expression of IQGAP2 in breast cancer was significantly associated with higher age ($p \leq 0.01$), lymphovascular invasion ($p \leq 0.01$) and higher histological grade ($p \leq 0.001$); however, there was no significant association with lymph node metastasis and, tumor size (Table 5.2.2.1).

Table 5.2.2.1. Correlation of IQGAP2 expression with histopathological parameters of breast cancer

Characteristics	**No. of cases**	**IQGAP2 expression**		**p-value***
		Low N (%)	High N (%)	
Age (Years)				
≤40	44	32 (72.73)	12 (27.27)	0.002
>40	182	164 (90.1)	18 (9.89)	
Tumor Size (cm)				
≤5	125	107 (85.6)	18 (14.4)	0 .61
>5	99	87 (87.88)	12 (12.12)	
Lymphnode metastasis				
N0	111	93 (83.79)	18 (16.21)	0.20
N1-N2	114	102 (89.47)	12 (10.53)	
Lymphovascular invasion				
Yes	61	58 (95.08)	3 (4.92)	0.0017
No	64	48 (75)	16 (25)	
Histological grade				
I-II	116	93 (80.17)	23 (19.83)	0.00013
III-IV	101	98 (97.03)	3(2.97)	

*Chi-square test of independence

5.2.3 IQGAP2 expression doesn't correlate with breast cancer molecular subtype in cell lines

Further, we checked the correlation between IQGAP2 expression and molecular subtypes of breast cancer, by comparing the mRNA and protein levels of IQGAP2 in different

breast cancer cell types such as MCF7, T-47D, MCF 10A, MDA-MB-453, MDA-MB-468 and MDA-MB-231 representing different molecular subtypes.

T-47D, MCF 10A and MDA-MB-231 breast cancer cell lines showed a very low expression of IQGAP2 protein and higher expression was observed in MCF7, MDA-MB-453 and, MDA-MB-468 cell lines (Fig. 5.2.3.1A). Similar observations were made at mRNA level (Fig. 5.2.3.1B). Cells with higher and lower expression groups are a mixed population, containing ER/PR positive and triple negative cell lines. Therefore, IQGAP2 expression cannot be correlated with breast cancer molecular subtype.

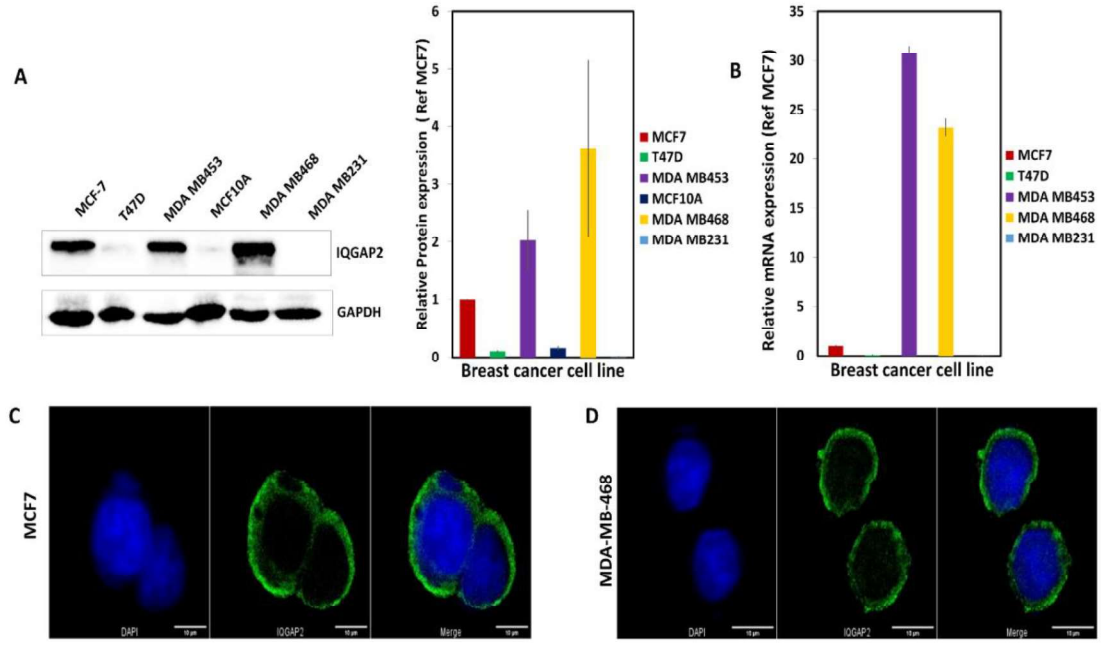

Figure 5.2.3.1. IQGAP2 expression doesn't correlate with breast cancer molecular subtype. **A)** The Western blot of IQGAP2 showing its endogenous expression in different breast cancer cell lines of specific molecular signature (left panel). Here, IQGAP2 expression is shown in MCF7 (ER/PR positive), T-47D (ER/PR/HER2 positive), MDA-MB-453 (HER2 positive), MCF 10A (ER/PR/HER2 negative normal like), MDA-MB-468 (ER/PR/HER2 negative) and MDA-MB-231 (ER/PR/HER2 negative and highly aggressive) cell lines. Right panel shows densitometry bar graph relative to the expression of MCF7, (n = 3). **B)** The endogenous mRNA level of IQGAP2 (relative to the endogenous expression of MCF7) in different breast cancer cell lines, (n = 3). **C)** ICC showing the endogenous expression and cytosolic localization of IQGAP2 (Green) in MCF7. DAPI (blue) staining was done for nucleus. **D)** ICC showing the cytosolic localization of IQGAP2 (Green) in MDA-MB-468. DAPI (blue) staining was done for nucleus.

The scale bar is 10 µm. Images were taken with 60X oil immersion objective lens in confocal microscope.

Additionally, we checked if there was any difference in the localization pattern of IQGAP2 between cell lines of different molecular subtypes. The immunocytochemistry (ICC) of MCF7 (ER/PR positive) and MDA-MB-468 (ER/PR/HER2 negative) cell lines revealed the predominant expression of IQGAP2 in the cytosolic region of the cell, same as observed in the patient tissues (Fig. 5.2.3.1C, 5.2.1.1C).

5.2.4 IQGAP2 expression affects proliferation of breast cancer cell line

To assess the role of IQGAP2 in tumorigenicity of breast cancer, we used MCF7 (ER positive) breast cancer cell line. First, we prepared MCF7 cell lines for stable IQGAP2 overexpression (MCF7_IQGAP2_Ex) and knockdown (MCF7_IQGAP2_KD) (Fig. 5.2.4.1A). Next, we examined the rate of proliferation, one of the hallmarks of tumorigenesis through MTS and colony formation assay.

The results of MTS assay showed that MCF7 cells with IQGAP2 depletion proliferate at significantly higher rate than the control group ($p \leq 0.01$, IQGAP2_KD/ Control_Sc = 42528 ± 3647/ 30082 ± 2319 cells post 96 hours) (Fig. 5.2.4.1B). The ectopic expression of IQGAP2 in MCF7 cells showed an opposite trend ($p \leq 0.0001$, IQGAP2_Ex/ Control_EV = 40288 ± 441/ 42633 ± 349 cells post 96 hours of cell plating) (Fig. 5.2.4.1C). The colony formation assay also resulted in a similar trend. More colonies were observed in MCF7 with IQGAP2 depletion group compared to the control ($p \leq 0.0001$, IQGAP2_KD/ Control_Sc = 96 ± 13/ 37 ± 12 colonies).

The colony's size was measured and found to be significantly larger ($p \leq 0.0001$) in MCF7 with reduced IQGAP2 expression in comparison to the controls (Fig. 5.2.4.1D). Ectopic expression of IQGAP2 in MCF7 showed significantly lesser number of ($p \leq 0.001$,

IQGAP2_Ex/ Control_ EV = 4.7 ± 0.6/ 48 ± 5 colonies) and smaller colonies, compared to the control group (Fig. 5.2.4.1E).

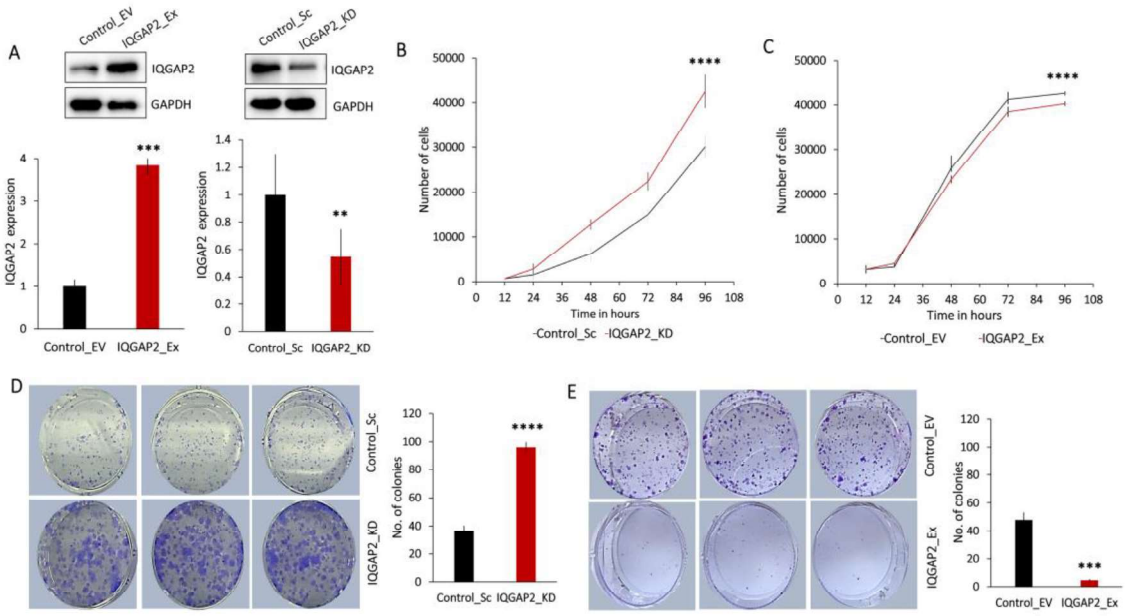

Figure 5.2.4.1. Reduced IQGAP2 expression promotes cell proliferation in MCF7 (ER positive) cell line. A) The upper panels show representative images of Western blot for IQGAP2 in stable MCF7_Control_EV, MCF7_IQGAP2_Ex, MCF7_Control_Sc and, MCF7_IQGAP2_KD cell lines respectively. In lower panels the relative densitometry bar graph of Western blots (upper panel) calculated using ImageJ software is shown (n = 3, 2-tailed unpaired t-test). **B)** The graph shows cell proliferation (MTS assay) of MCF7_IQGAP2_ KD and MCF7_Control_Sc at time intervals of 24-96 hours (n = 3, 2-tailed unpaired t-test). Here, Y-axis indicates the cell number and X-axis shows time in hours. **C)** The graph represents result of MTS assay, showing the cell number of MCF7 IQGAP2_Ex group and MCF7 Control_EV group (n = 3, 2-tailed unpaired t-test). **D)** The panel in left shows the images of colony formation assay in MCF7_IQGAP2_KD and MCF7_Control_Sc (after 10 days of cell plating) and the panel in right show illustrations bar graph (n = 3, 2-tailed unpaired t-test). **E)** Image showing the number of colonies in MCF7 IQGAP2_Ex group and MCF7 Control_EV group (left panel). The right panel illustrations bar graph, showing the differences of colony numbers between both the groups (n = 3, 2-tailed unpaired t-test). The colony number was calculated using ImageJ software. * represents $p \leq 0.05$, ** represents $p \leq 0.01$, *** represents ≤ 0.001, **** represents $p \leq 0.0001$, n represents experiment replicates.

These results corroborate the role of IQGAP2 as a tumor suppressor gene in ER positive MCF7 cells.

5.2.5 IQGAP2 affects breast cancer cell proliferation irrespective of ER status

Then, to confirm whether the effect of IQGAP2 is limited to ER positive cells or it may affect ER negative cells too, we performed the above assays in ER negative MDA-MB-468 cells. The Stable depletion of IQGAP2 was conducted in the MDA-MB-468 cell line (Fig. 5.2.5.1A) as the endogenous level of IQGAP2 was very high (Fig. 5.2.3.1A).

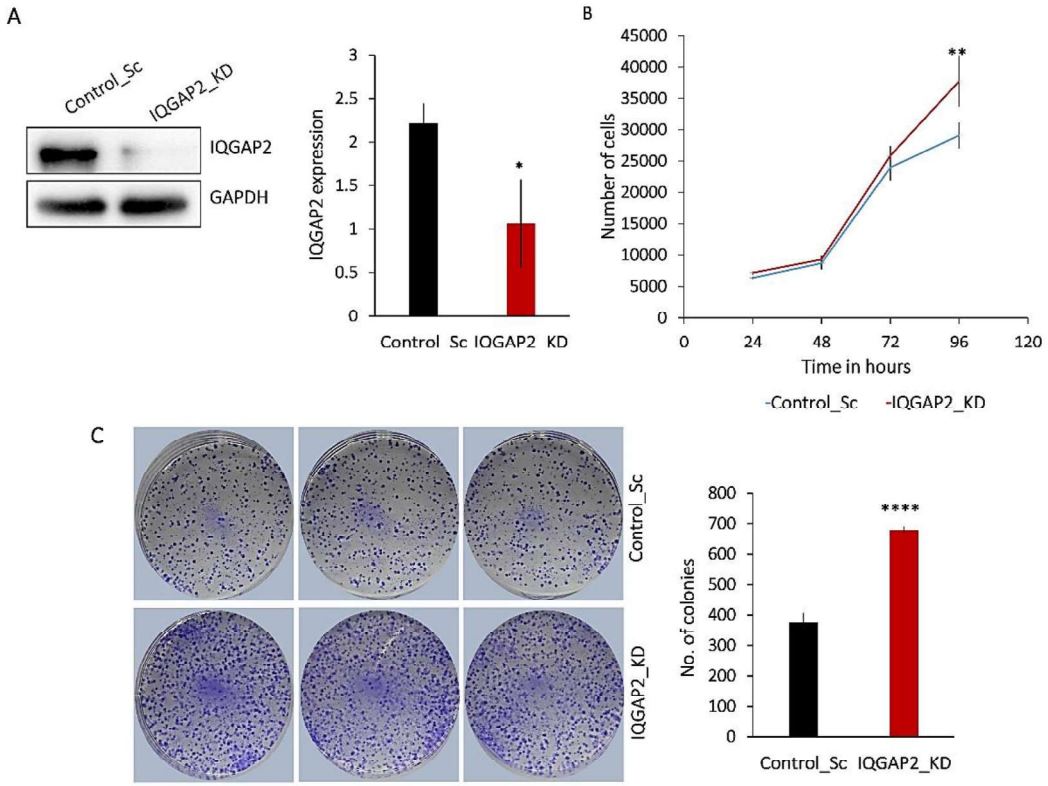

Figure 5.2.5.1. Reduced IQGAP2 expression promotes cell proliferation in MDA-MB-468 (ER negative) cell line. A) Western blot images (left panel) showing knockdown of IQGAP2 in MDA-MB-468 cells, densitometry bar graph (right panels) showing the relative expression of IQGAP2 in IQGAP2_KD and Control_Sc group (n = 3, 2-tailed unpaired t-test). **B)** Bar graph shows the comparison between cell number (MTS) in MDA-MB-468_IQGAP2_KD group and MDA-MB-468_Control_Sc group, from 24-96 hours of cell plating (n = 3, 2-tailed unpaired t-test). **C)** Representative images of colony formation assay (left panel) in MDA-MB-468 IQGAP2_KD and Control_Sc groups. In the right panel, bar graph shows the difference of colony

numbers between both the groups (n = 3, 2-tailed unpaired t-test). * represents $p \leq 0.05$, ** represents $p \leq 0.01$, **** represents $p \leq 0.0001$, n represents experiment replicates.

Depletion of IQGAP2 in MDA-MB-468 cell lines showed a significant higher cell proliferation rate in comparison to the control group ($p \leq 0.01$, IQGAP2_KD/ Control_Sc = 37738 ± 4000/ 29114 ± 2000 cells) (Fig. 5.2.5.1B). The colony formation assay also showed a significant more number of colonies in IQGAP2 knockdown group compared to the control group ($p \leq 0.0001$, IQGAP2_KD/ Control_Sc = 680.3 ± 10.2/ 377 ± 28.3 colonies) (Fig. 5.2.5.1C). These results indicate that IQGAP2 inhibits cell proliferation irrespective of ER status of cell lines.

5.2.6 IQGAP2 expression level regulates migration and invasion of breast cancer cells irrespespective of ER status

Epithelial to mesenchymal transition (EMT), a hallmark of cancer is characterised by higher migratory and invasive property of cancer cells. To examine the migration ability of cells, wound healing assay and transwell migration assay were performed with MCF7_IQGAP2_KD, MCF7_IQGAP2_Ex, MDA-MB-468_IQGAP2_KD and their respective controls. In wound healing assay, a wound was created and after 24 hours the percentage of wound recovery was calculated. The wound recovery was significantly faster in MCF7_IQGAP2_KD group compared to the control ($p \leq 0.0001$, IQGAP2_KD - 92 ± 5.22%, Control_Sc - 75 ± 7.05%) (Fig. 5.2.6.1A). Similarly, in transwell migration assay a significant increase in migration was observed in MCF7 IQGAP2 knockdown group compared to the control group ($p \leq 0.0001$, IQGAP2_KD - 128.6 ± 13.75 cells/field, Control_Sc - 50.2 ± 4.54 cells/field) (Fig. 5.2.6.1B). A similar result was also observed in MDA-MB-468. The reduction of IQGAP2 in MDA-MB-468 led to elevated cell migration in wound healing assay ($p \leq 0.05$, IQGAP2_KD - 48.45 ± 5.31%, Control_Sc- 32.69 ± 5.96%) (Fig. 5.2.6.1C).

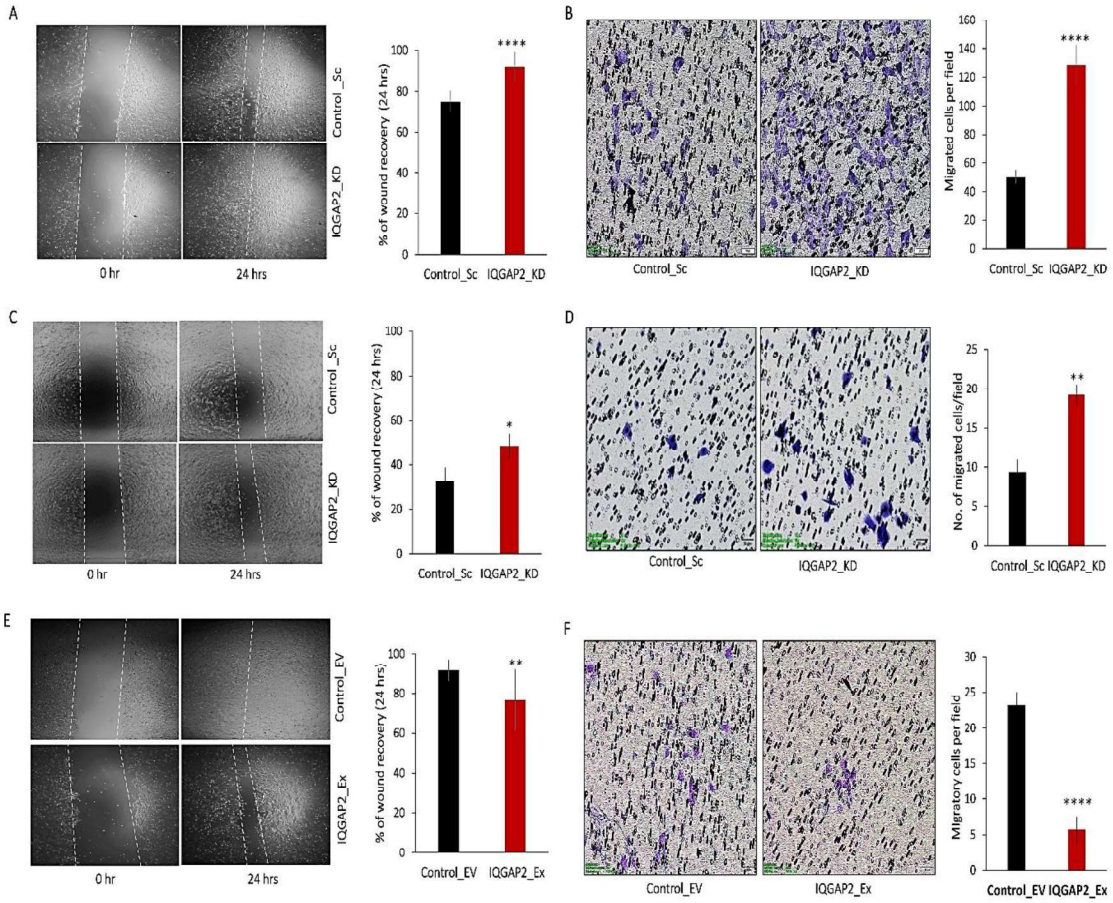

Figure 5.2.6.1. IQGAP2 expression levels alter migration in breast cancer cell lines. A) Representative images of wound healing assay in MCF7_IQGAP2_KD and MCF7_Control_Sc group, at 0 hour and 24 hours (left panel). The bar graph (right panel) showing the recovery rate of wound in IQGAP2 knockdown group vs control group (n = 3, 2-tailed unpaired t-test). **B)** Representative images (left panel) of transwell migration assay in MCF7_IQGAP2_KD and MCF7_Control_Sc group. The bar graph (right panel) showing statistical differences in migratory cells between two groups (n = 3, 2-tailed unpaired t-test). **C)** Left panel shows representative images of wound healing assay of MDA-MB-468 IQGAP2_KD and Control_Sc cells. The graph at right panel shows statistical differences in wound recovery between two groups (n = 3, 2-tailed unpaired t-test). **D)** Representative images (left panel) of transwell migration assay in MDA-MB-468 IQGAP2_KD and Control_Sc group. The bar graph is at right panel shows the statistical differences between the groups (n = 5, 2-tailed unpaired t-test). **E)** Left panel shows representative images of wound healing assay of MCF7 IQGAP2_Ex and MCF7 Control_EV cells at 0 hour and 24 hours. Bar graph in right panel shows statistical differences between the groups (n = 3, 2-tailed unpaired t-test). **F)** Representative images (left panel) of transwell migration assay in MCF7 IQGAP2_Ex and MCF7 Control_EV cells and bar graph, right panel (n = 3, 2-tailed unpaired t-test). * represents $p \leq 0.05$, ** represents $p \leq 0.01$, *** represents $p \leq 0.001$, **** represents $p \leq 0.0001$, n = 3. Scale bar in all images is 50 µm.

Likewise, the transwell migration assay showed an increased cell migration in IQGAP2 knockdown group compared to the control ($p \leq 0.0001$, IQGAP2_KD- 19.2 ± 1.3 cells/field, Control_Sc - 9.4 ± 1.5 cells/field) (Fig. 5.2.6.1D). In comparison to the IQGAP2 knockdown group of MCF7, the ectopic IQGAP2 expression group of MCF7 showed an opposite trend. The wound healing assay with MCF7 IQGAP2 _Ex group resulted in slow wound recovery compared to the control ($p \leq 0.01$, IQGAP2_Ex - 76.7 ± 15.1%, Control_EV - 91.6 ± 5.3%) (Fig. 5.2.6.1E).

The transwell migration assay also showed a decrease in cell migration in IQGAP2_Ex group compared to its control ($p \leq 0.0001$, IQGAP2_Ex - 5.75 ± 2.62 cells/field, Control_EV - 23.2 ± 1.78 cells/field) (Fig. 5.2.6.1F).

In order to investigate the role of IQGAP2 on cell invasiveness, a Matrigel based transwell invasion assay was carried out. In MCF7, the reduction of IQGAP2 significantly increased the invasiveness of MCF7 cells where more cells invaded to the bottom surface of the chamber, compared to the control group ($p \leq 0.0001$, IQGAP2_KD - 60.66 ± 1.15 cells/field, Control_Sc - 8.75 ± 0.5 cells/field) (Fig. 5.2.6.2A). A similar trend was observed in MDA-MB-468 IQGAP2_KD group where reduction of IQGAP2 level increased the invasiveness of cells ($p \leq 0.0001$, IQGAP2_KD - 21.4 ± 2.0 cells/field, Control_Sc - 9.0 ± 1.58 cells/field) (Fig. 5.2.6.2B).

In contrast to IQGAP2 knockdown group of MCF7 and MDA-MB-468, the increase in IQGAP2 expression in MCF7 resulted in reduction of cell invasiveness compared to its respective control ($p \leq 0.0001$, IQGAP2_Ex - 3 ± 1 cells/field, Control_EV - 26.2 ± 3.7 cells/field) (Fig. 5.2.6.2C).

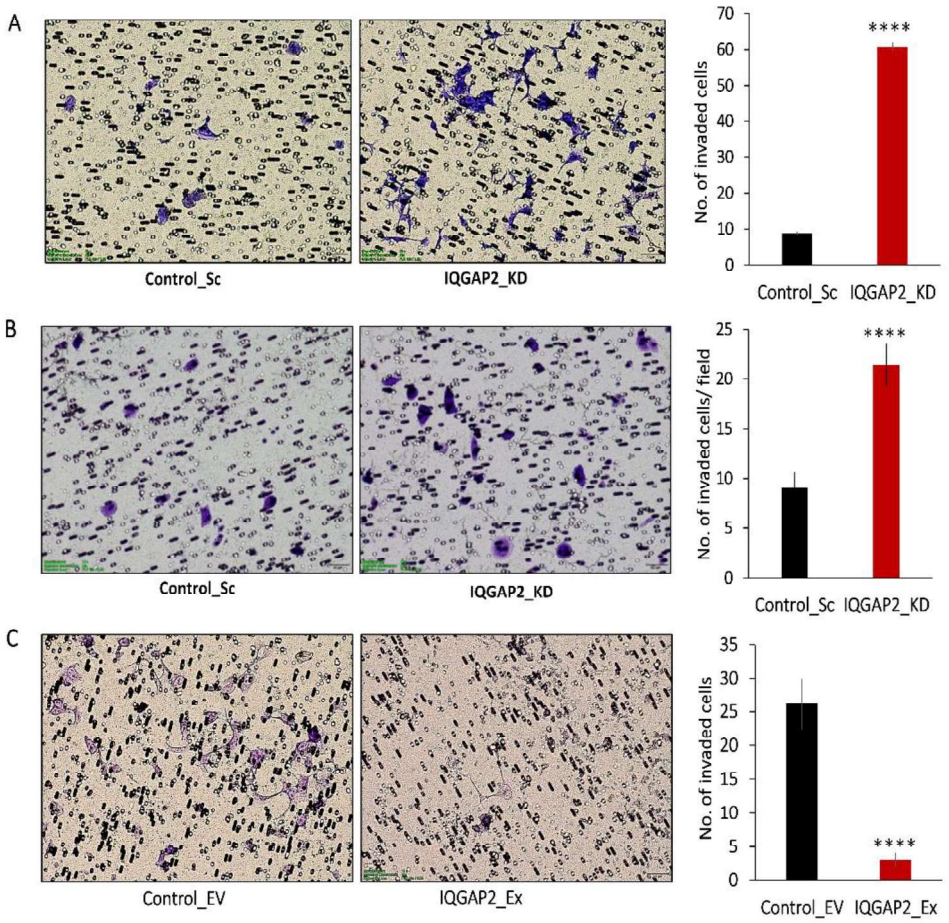

Figure 5.2.6.2. IQGAP2 expression levels alter invasion in breast cancer cell lines. A) Representative images (left panel) of transwell invasion assay in MCF7 IQGAP2_KD and Control_Sc group and bar graph at right (n = 3, 2-tailed unpaired t-test). **B)** Representative images (left panel) of transwell invasion assay in MDA-MB-468 IQGAP2_KD and Control_Sc group. In right panel the bar graph showing a significant difference in invasion between IQGAP2_KD and Control_Sc group of MDA-MB-468 (n = 5, 2-tailed unpaired t-test). **C)** Representative images of transwell invasion assay in MCF7 IQGAP2_Ex and MCF7 Control_EV groups (left panel). The bar graph in right panel, showing a significant difference in invasion between IQGAP2_Ex and Control_EV group of MCF7 (n = 3, 2-tailed unpaired t-test). * represents $p \leq 0.05$, ** represents $p \leq 0.01$, *** represents $p \leq 0.001$, **** represents $p \leq 0.0001$, scale bar in all images is 50 µm.

5.2.7 IQGAP2 expression regulate apoptosis in breast cancer cells

We next examined the effect of IQGAP2 in apoptosis, a hallmark of cancer, in breast cancer. Previous studies have indirectly indicated the connection between IQGAP2 in apoptosis in HCC [38, 181]. So, we hypothesised that expressional change of IQGAP2 may regulate cell growth by affecting the apoptosis in breast cancer. To check our

hypothesis, the change in apoptosis was investigated in MCF7 and MDA-MB-468 cell lines using Annexin- V-FITC- propidium iodide (PI) flow cytometry assay.

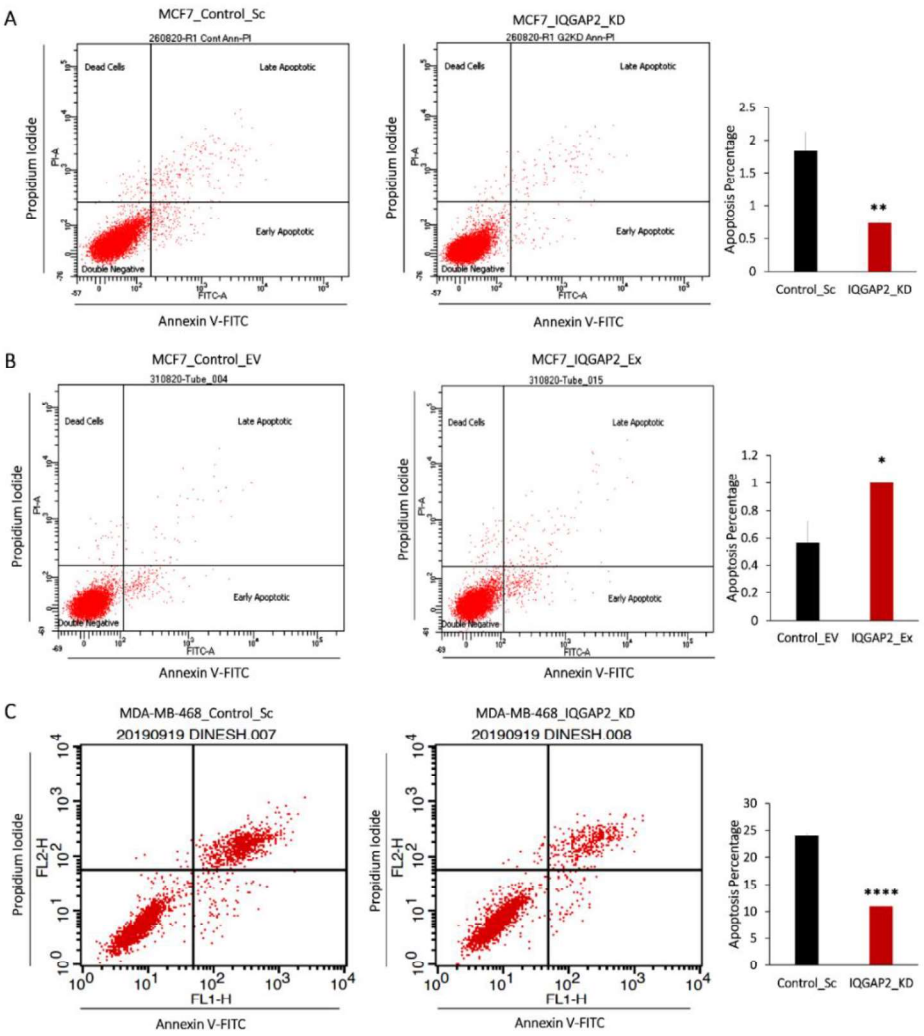

Figure 5.2.7.1. IQGAP2 expression levels affects apoptosis in breast cancer cell lines. Cell apoptosis was measured by Annexin V-FITC – PI based flow cytometry method. Flow cytometry images showing percentage of apoptotic cells in **A)** MCF7_Control_Sc and MCF_IQGAP2_KD group. **B)** MCF7_Control_EV and MCF_IQGAP2_Ex groups. **C)** MDA-MB-468_Control_Sc and MDA-MB-468_IQGAP2_KD groups. The bar graph in right panel of each flow cytometry image showing the difference in percentage of apoptosis between control and IQGAP2 perturbation groups (n = 3, 2-tailed unpaired t-test). The X-axis of flow cytometry graph represents the percentage cells positive for Annexin V-FITC stain and Y-axis represents the percentage cells positivity for propidium-iodide stain. In bar graph the X-axis shows control and IQGAP2 perturbation group and Y-axis shows the percentage of cell death due to apoptosis. For statistical calculation 2-tailed unpaired t-test was performed with n = 3. * represents $p \leq 0.05$, ** represents $p \leq 0.01$, **** represents $p \leq 0.0001$.

The reduction of IQGAP2 in MCF7 showed a significant decrease in apoptosis compared to its control group ($p \leq 0.01$, IQGAP2_KD - 0.73 ± 0.04, Control_Sc -1.83 ± 0.29) (Fig. 5.2.7.1A) whereas the opposite trend was observed with the over expression of IQGAP2 ($p \leq 0.05$, IQGAP2_Ex - 1.0 ± 0.1, Control_EV - 0.57 ± 0.15) (Fig. 5.2.7.1B). In MDA-MB-468 cell lines, depletion of IQGAP2 level show reduced apoptosis ($p \leq 0.0001$, IQGAP2_KD - 10.96 ± 0.28, Control_Sc - 24.05 ± 0.34), as observed in MCF7 cells lines (Fig. 5.2.7.1C).

The above results together suggest that decrease in IQGAP2 expression level reduces cellular apoptosis, which enhances protumorigenic properties of cells.

5.2.8 IQGAP2 affects apoptosis by affecting p38-p53 pathway triggered by increase in ROS

Next, we investigated the mechanism responsible for IQGAP2 mediated apoptosis. The activation of reactive oxygen species (ROS) is well known for the induction of apoptosis which ultimately activates p53, p38 MAPK and the downstream molecule caspase 3/7. Previous studies have reported association of IQGAP2 levels with ROS and apoptosis [38, 181]. So, the possibilities of IQGAP2 mediated ROS activity and apoptosis in breast cancer can't be overlooked.

To examine the effect of IQGAP2 in ROS activity, a DCFDA/H2DCFDA- Cellular ROS Assay Kit (Abcam), was used and assay was conducted in MCF7_IQGAP2_KD, MDA-MB-468_IQGAP2_KD, MCF7_IQGAP2_Ex, and their respective controls. The reduction in ROS level (green fluorescence signal) was observed in IQGAP2_KD group of MCF7 ($p \leq 0.01$, IQGAP2_KD - 6804.79 ± 1572.8, Control_Sc - 2488.62 ± 26.8) (Fig. 5.2.8.1A) and MDA-MB-468 ($p \leq 0.001$, IQGAP2_KD - 11461.70 ± 517.02, Control_Sc - 5991.13 ± 457.51) (Fig. 5.2.8.1B) cells compared to their controls. In contrast, the level

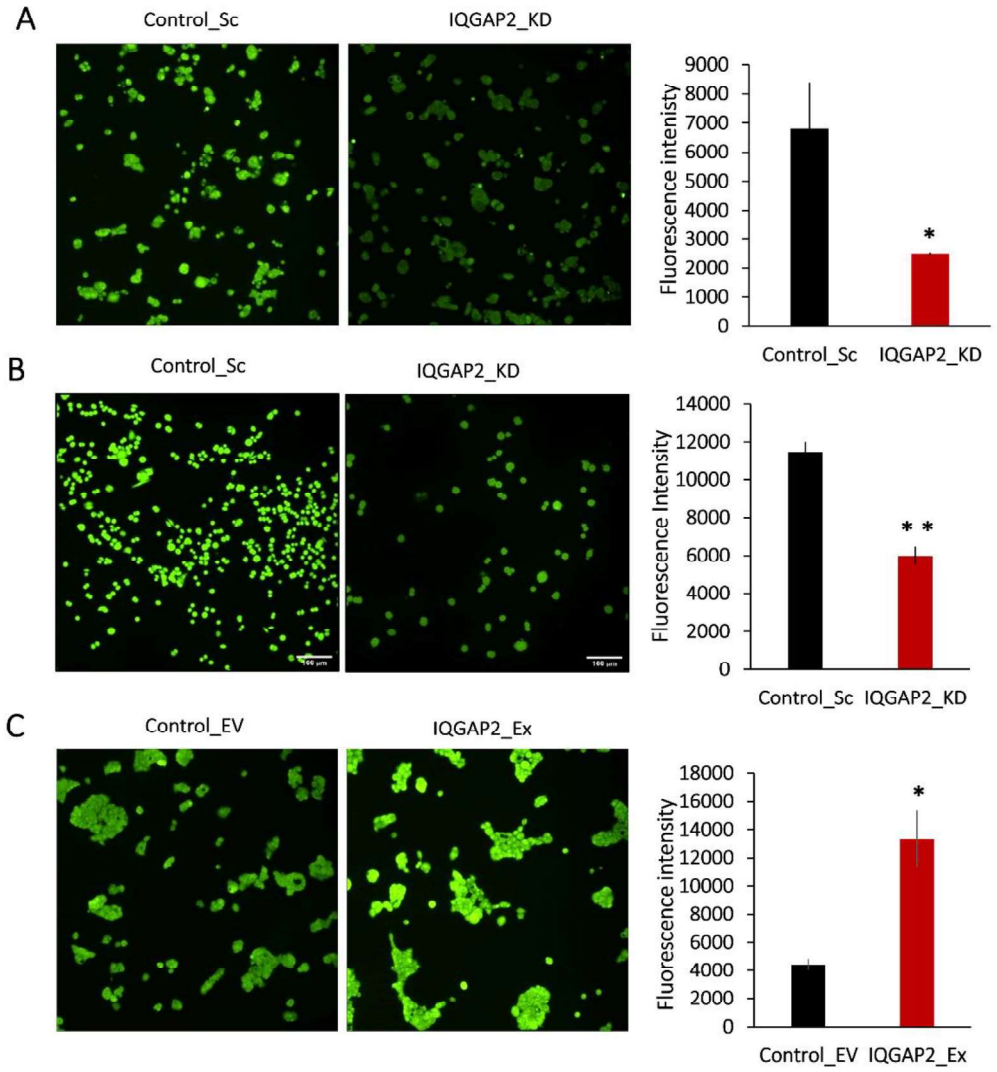

Figure 5.2.8.1. IQGAP2 increases reactive oxygen species levels (ROS) in breast cancer cell lines. ROS generation by the cells was measured using DCFDA / H2DCFDA - Cellular ROS Assay Kit. ROS generation was observed under a fluorescence microscope with 10X objective (Nikon). **A)** Representative fluorescent microscopy images showing the ROS levels (green fluorescent signals) in MCF7_IQGAP2_KD (left) and MCF7_Control_Sc groups (right). The bar graph showing the difference in ROS levels between both the groups (n = 3, 2-tailed unpaired t-test). **B)** Representative fluorescent microscopy images showing the ROS levels in MDA-MB-468_IQGAP2_KD (left) and MDA-MB-468_Control_Sc groups (right). The bar graph showing the difference in ROS levels between both the groups (n = 3, 2-tailed unpaired t-test). **C)** Representative fluorescent microscopy images showing the ROS levels in MCF7_IQGAP2_Ex (left) and MCF7_Control_EV groups (right). The bar graph showing the difference in ROS levels between both the groups (n = 3, 2-tailed unpaired t-test). * represents $p \leq 0.05$, ** represents $p \leq 0.01$. Scale bar in images is 100 µm.

of ROS increased in MCF7 cells with IQGAP2_Ex compared to its control ($p \leq 0.01$, IQGAP2_Ex - 4410.49 ± 365.9, Control_EV - 13348.05 ± 1993.3) (Fig. 5.2.8.1C).

After noticing a change in ROS level by IQGAP2 expression, we further examined the effect of IQGAP2 on downstream signaling molecules of ROS, namely phospho-p53 and phospho-p38 MAPK by Western blot.

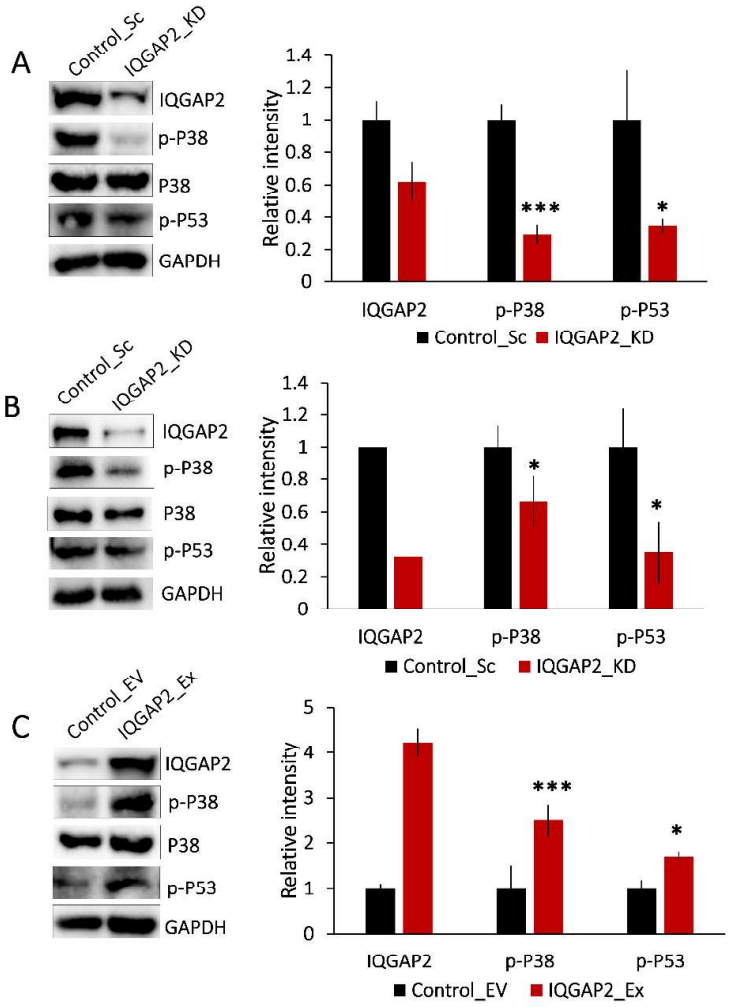

Figure 5.2.8.2 IQGAP2 increases expression of phospho-p53 and phospho-p38 MAPK in breast cancer cell lines. Representative Western blot images of phospho-p53 and phospho-p38 MAPK in **A)** MCF7_IQGAP2_KD and MCF7_Control_Sc group. **B)** MDA-MB-468_IQGAP2_KD and MDA-MB-468_Control_Sc group. **C)** MCF7_IQGAP2_Ex and MCF7_Control_EV group. The densitometric bar graph (right) showing the difference in expression of phospho-p53 and phospho-p38 MAPK between control and IQGAP2 perturbation groups (n = 3, 2-tailed unpaired t-test). * represents $p \leq 0.05$, *** represents $p \leq 0.001$.

We observed a reduced expression of phospho-p53 ($p \leq 0.05$, IQGAP2_KD - 0.35 ± 0.04, Control_Sc - 1.0 ± 0.30) and phospho-p38 MAPK ($p \leq 0.001$, IQGAP2_KD - 0.29 ± 0.06, Control_Sc - 1.0 ± 0.1) with depletion of IQGAP2 in MCF7 (Fig. 5.2.8.2A).

Similarly, in MDA-MB-468 cells the reduced level of phospho-p53 ($p \leq 0.05$, IQGAP2_KD - 0.35 ± 0.19, Control_Sc - 1.0 ± 0.23) and phospho-p38 MAPK ($p \leq 0.05$, IQGAP2_KD - 0.67 ± 0.15, Control_Sc - 1.0 ± 0.13) was observed in IQGAP2 knockdown group compared to the controls (Fig. 5.2.8.2B). On the other hand, an increased phospho-p53 levels ($p \leq 0.05$, IQGAP2_Ex - 1.71 ± 0.09, Control_EV - 1.0 ± 0.18) and phospho-p38 MAPK levels ($p \leq 0.001$, IQGAP2_Ex - 2.5 ± 0.34, Control_EV - 1.0 ± 0.5) were observed in MCF7 with over expression of IQGAP2 (Fig. 5.2.8.2C). These results indicate that IQGAP2 positively affects activation of p38 and p53.

Next, we checked the downstream apoptotic signaling molecules.

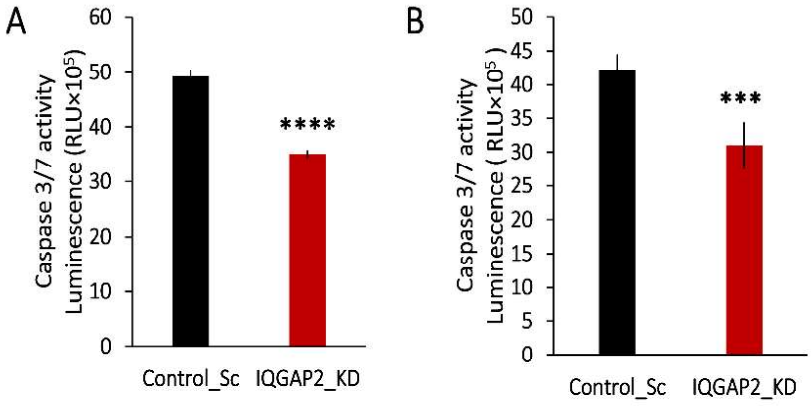

Figure 5.2.8.3. Caspase 3/7 levels in breast cancer cell line with IQGAP2 depletion. A) The bar graph showing the difference of caspase 3/7 levels between MCF7_IQGAP2_KD and MCF7_Control_Sc groups (n = 5, 2-tailed unpaired t-test). **B)** The bar graph showing the significant difference of caspase 3/7 levels between MDA-MB-468_IQGAP2_KD and MDA-MB-468_Control_Sc group (n = 5, 2-tailed unpaired t-test). Here X- axis representing both control and IQGAP2_KD groups, Y-axis showing the Caspase 3/7 luminescence activity of both the groups in relative light unit (RLU). *** represents $p \leq 0.001$, **** represents $p \leq 0.0001$.

Caspase 3 and 7 are the downstream targets of phospho-p38 and phospho-p53 and well established executioner caspases [210, 211]. They cleave a diverse array of protein substrates including nuclear enzyme poly (ADP ribose) polymerase (PARP) and facilitate apoptosis [212, 213]. Measurement of these caspases in cells indicates the state of apoptosis.

Therefore, we analysed the levels of caspase 3/7 in MCF7 IQGAP2_KD and MDA-MB-468 IQGAP2_KD and their respective control groups using a fluorometric Caspase-Glo® 3/7 Assay Kit (Promega). A decreased caspase 3/7 levels were observed in MCF7_IQGAP2_KD group compared to the control ($p \leq 0.0001$, IQGAP2_KD - 35.06 ± 0.64 RLU × 10^5, Control_Sc - 49.25 ± 0.93 RLU × 10^5) (Fig. 5.2.8.3A). A similar trend was also observed in MDA-MB-468 cells ($p \leq 0.001$, IQGAP2_KD - 31.0 ± 3.41 RLU × 10^5, Control_Sc - 42.12 ± 2.3 RLU × 10^5) (Fig. 5.2.8.3B).

These results suggest that IQGAP2 activates apoptosis and restricts the proliferation of breast cancer cells. Mechanistically, IQGAP2 promotes ROS generation which subsequently activates phospho-p53/phospho-p38 and caspase 3/7, leading to apoptosis of breast cancer cells.

5.2.9 Reduced IQGAP2 expression increases migration and invasion of breast cancer cells via triggering epithelial to mesenchymal transition

Next, we examined the mechanism responsible for IQGAP2 mediated cell migration and invasion in breast cancer cells. It is well established that epithelial cells acquire the invasive mesenchymal property by a key process, EMT [120]. The loss of epithelial marker E-cadherin and gain of mesenchymal markers N-cadherin are characteristics of EMT [214]. Therefore, we inspected the status of E-cadherin and N-cadherin in MCF7 and MDA-MB-468 cells using Western blot.

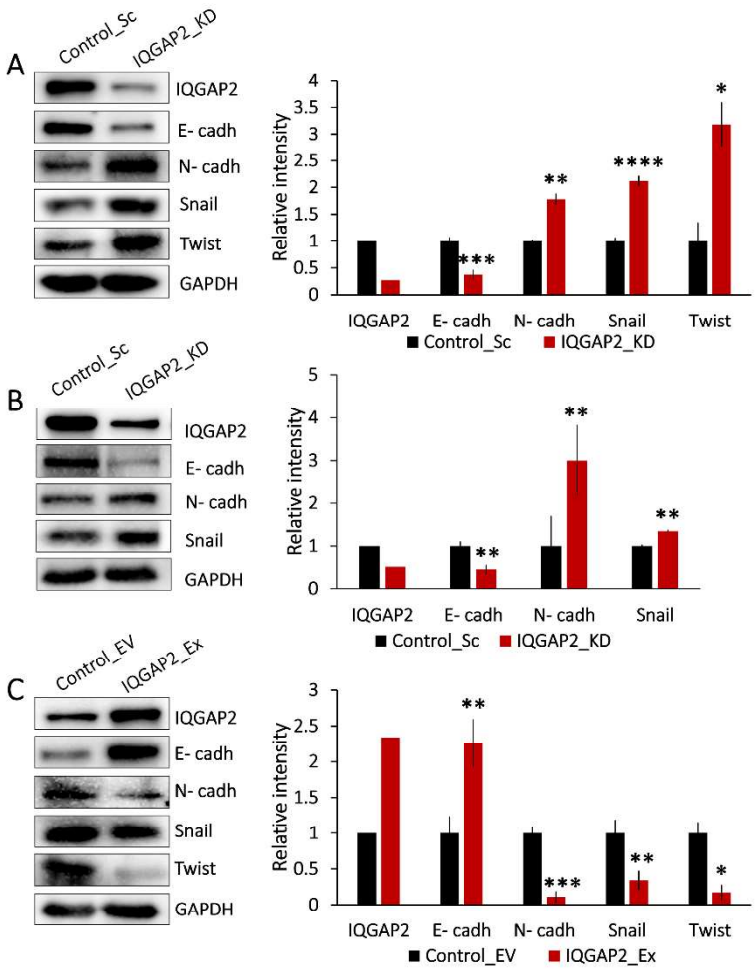

Figure 5.2.9.1. Effect on expression of epithelial to mesenchymal transition markers with IQGAP2 expression change. A) Representative Western blot images of EMT markers, N-cadherin, Snail, Twist and epithelial marker E-cadherin in MCF7 IQGAP2_KD and Control_Sc (left panel). Densitometry bar graph showing differences in expression of N-cadherin, Snail, Twist and E-cadherin, between Control_Sc and IQGAP2_KD groups (n = 3, 2-tailed unpaired t-test) (right panel). **B)** Representative Western blot images of N-cadherin, Snail and E-cadherin in MDA-MB-468 IQGAP2_KD and control (left panel). Densitometry bar graph showing differences in expression of N-cadherin, Snail and E-cadherin between Control_Sc and IQGAP2_KD groups (n = 3, 2-tailed unpaired t-test). **C)** Representative Western blot images of EMT markers, N-cadherin, Snail, Twist and epithelial marker E-cadherin in MCF7 IQGAP2_Ex and Control_Sc group (left panel). Densitometry bar graph showing differences in expression of N-cadherin, Snail, Twist and E-cadherin between Control_EV and IQGAP2_Ex groups (n = 3, 2-tailed unpaired t-test) (right panel). * represents $p \leq 0.05$, ** represents $p \leq 0.01$, *** represents $p \leq 0.001$, **** represents $p \leq 0.0001$.

MCF7 cells with IQGAP2 depletion showed a reduced level of E-cadherin ($p \leq 0.001$, IQGAP2_KD - 0.37 ± 0.08, Control_Sc - 1.0 ± 0.06) and elevated levels of N-cadherin

($p \leq 0.01$, IQGAP2_KD - 1.78 ± 0.09, Control_Sc - 1.0 ± 0.01) (Fig. 5.2.9.1A). A similar pattern of E- cadherin ($p \leq 0.01$, IQGAP2_KD - 0.45 ± 0.09, Control_Sc - 1.0 ± 0.09) and N-cadherin ($p \leq 0.01$, IQGAP2_KD - 3.0 ± 0.81, Control_Sc - 1.0 ± 0.68) was also observed in the IQGAP2_KD group of MDA-MB-468 cells (Fig. 5.2.9.1B). Subsequently, the expression levels of EMT-activating transcription factors, Twist and Snail were also examined by Western blot.

The elevated expression level of Twist ($p \leq 0.05$, IQGAP2_KD - 3.18 ± 0.4, Control_Sc - 1.0 ± 0.33) and Snail ($p \leq 0.0001$, IQGAP2_KD - 2.12 ± 0.08, Control_Sc - 1.0 ± 0.05) were observed in the IQGAP2_KD group of MCF7. In MDA-MB-468 cells, a similar expression pattern of Snail ($p \leq 0.01$, IQGAP2_KD - 1.34 ± 0.01, Control_Sc - 1.0 ± 0.01) was observed with depletion of IQGAP2 level.

In contrast to IQGAP2_KD group of MCF7, the ectopic expression of IQGAP2 in MCF7 cells led to the opposite expression pattern of EMT markers. The expression of E-cadherin was increased ($p \leq 0.01$, IQGAP2_Ex - 2.26 ± 0.32, Control_EV - 1.0 ± 0.22) while the levels of N-cadherin ($p \leq 0.001$, IQGAP2_Ex - 0.11 ± 0.07, Control_EV - 1.0 ± 0.08), Twist ($p \leq 0.05$, IQGAP2_Ex - 0.17 ± 0.09, Control_EV - 1.0 ± 0.15) and Snail ($p \leq 0.01$, IQGAP2_Ex - 0.34 ± 0.12, Control_EV - 1.0 ± 0.18) were reduced with the ectopic expression of IQGAP2 in MCF7 (Fig. 5.2.9.1C). Overall, these findings indicate that IQGAP2 regulates EMT in breast cancer cells.

5.2.10 Reduced IQGAP2 expression affects EMT via activation of ERK pathway

Next, we examined the key signaling molecules affecting the EMT process. The role of MAPK/ERK and PI3K/AKT signaling pathways in EMT is well established in cancer. Thus we hypothesized that deregulation of MAPK/ERK and/or PI3K/AKT pathways with

IQGAP2 expression changes, leads to EMT. To test this speculation, we examined the expression levels of phospho-ERK1/2, phospho-MEK and phospho-AKT by Western blot. We found that the reduction of IQGAP2 level in MCF7 increased the expression level of phospho-MEK ($p \leq 0.05$, IQGAP2_KD - 1.73 ± 0.23, Control_Sc - 1.0 ± 0.45) and phospho-ERK1/2 ($p \leq 0.0001$, IQGAP2_KD - 1.93 ± 0.09, Control_Sc - 1.0 ± 0.04) (Fig. 5.2.10.1A). In MDA-MB-468 cells, a similar result was observed where the depletion of IQGAP2 level resulted in increase in expression of phospho-MEK ($p \leq 0.05$, IQGAP2_KD - 3.15 ± 0.88, Control_Sc - 1.0 ± 0.28) and phospho-ERK1/2 ($p \leq 0.05$, IQGAP2_KD - 1.49 ± 0.20, Control_Sc - 1.0 ± 0.16). (Fig. 5.2.10.1B). In contrast, ectopic expression of IQGAP2 decreased the phospho-MEK ($p \leq 0.0001$, IQGAP2_Ex - 0.61 ± 0.02, Control_EV - 1.0 ± 0.02) and phospho-ERK1/2 ($p \leq 0.0001$, IQGAP2_Ex - 0.52 ± 0.05, Control_EV - 1.0 ± 0.02) expression level in MCF7 (Fig. 5.2.10.1C). Further, the analysis of phospho-AKT^{473} and phospho-AKT^{308} expression was carried out in MCF7_IQGAP2_KD, MDA-MB-468_IQGAP2_KD and, MCF7_IQGAP2_Ex cells. We did not observe a significant change in the expression level of phospho- AKT^{473} ($p \geq 0.05$, IQGAP2_KD - 0.95 ± 0.03, Control_Sc - 1.0 ± 0.02) or phospho-AKT^{308} ($p \geq 0.05$, IQGAP2_KD - 0.79 ± 0.44, Control_Sc - 1.0 ± 0.35) in MCF7_IQGAP2_KD group (Fig. 5.2.10.1D). Similarly, in MDA-MB-468_IQGAP2_KD, no remarkable change was observed in the expression level of phospho-AKT^{473} ($p \geq 0.05$, IQGAP2_KD - 1.13 ± 0.13, Control_Sc - 1.0 ± 0.12) or phospho-AKT^{308} ($p \leq 0.05$, IQGAP2_KD - 1.03 ± 0.14, Control_Sc - 1.0 ± 0.12) (Fig. 5.2.10.1E). The level of phospho-AKT^{473} ($p \geq 0.05$, IQGAP2_Ex - 0.97 ± 0.15, Control_EV - 1.0 ± 0.14) or phospho-AKT^{308} ($p \geq 0.05$, IQGAP2_Ex - 0.79 ± 0.14, Control_EV - 1.0 ± 0.14) were also not significantly altered in MCF7-IQGAP2_Ex group compared to their controls (Fig. 5.2.10.1F).

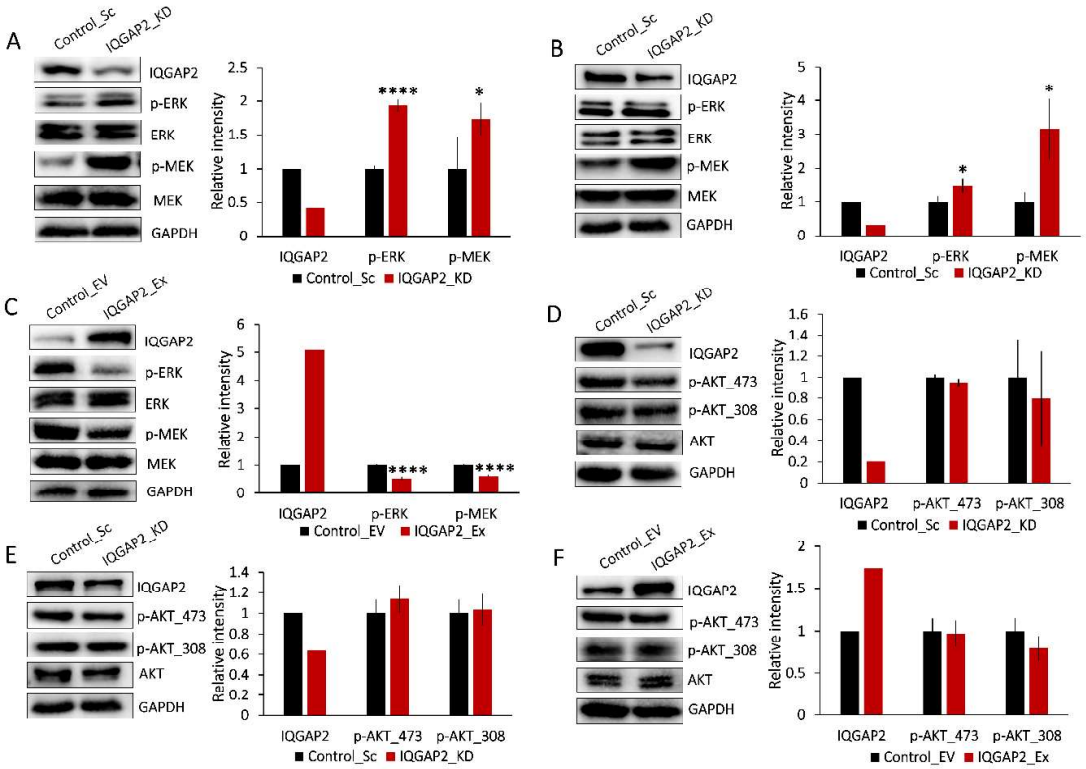

Figure 5.2.10.1. Effect of reduced IQGAP2 levels on EMT molecules, phospho MEK/ phospho-ERK and phospho-AKT levels. Representative Western blot images (left panel) and densitometry bar graph (right panel, n = 3, 2-tailed unpaired t-test) showing the phospho-MEK and phospho-ERK expression levels in **A)** MCF7 IQGAP2_KD and Control_Sc groups. **B)** MDA-MB-468_IQGAP2_KD and Control_Sc groups, and **C)** MCF7 IQGAP2_Ex and Control_EV groups. Representative Western blot images (left panel) and densitometry bar graph (right panel, n = 3, 2-tailed unpaired t-test) showing the phospho-AKT^{473} and phospho-AKT^{308} expression levels in **D)** MCF7 IQGAP2_KD and Control_Sc group, **E)** MDA-MB-468 IQGAP2_KD and Control_Sc group, and **F)** MCF7 IQGAP2_Ex and Control_EV group. * represents $p \leq 0.05$, **** represents $p \leq 0.0001$.

Next we checked whether, balancing the expression level of IQGAP2 in IQGAP2_KD group, rescued the phospho-ERK level in MCF7. That was done by a transient transfection of ectopic IQGAP2 expression vectors and a control vector in MCF7-IQGAP2-KD cells. The expression level of phospho-ERK was analysed by Western blot. The results show a rescue of the phospho-ERK level in the IQGAP2_KD group transfected with the ectopic IQGAP2 expression vector but not in the vehicle control,

indicating the regulatory role of IQGAP2 expression in phospho-ERK pathway. (Fig. 5.2.10.2A)

To further verify the specificity of IQGAP2 on ERK pathway in EMT regulation, the ERK pathway in MCF7-IQGAP2-KD cells was inhibited with the treatment of ERK inhibitor, U0126 (Calbiochem, Sigma-aldrich, USA) at 10 µM concentration for 30 min. U0126 is a very selective inhibitor of MEK1 and the MAP kinase cascade [29].

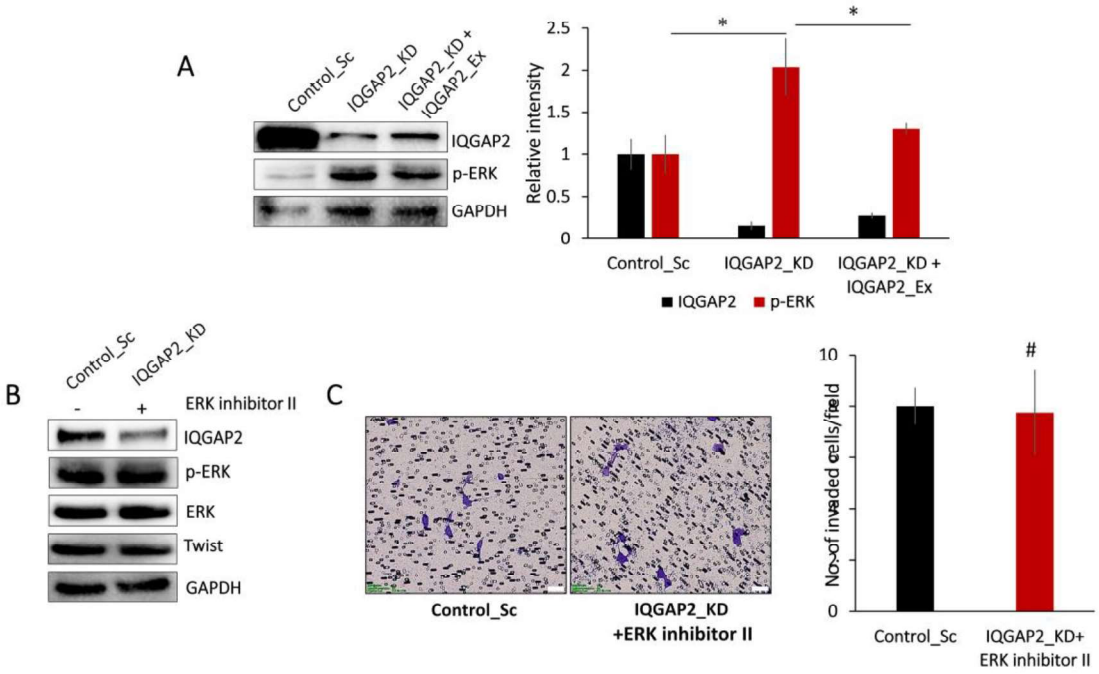

Figure 5.2.10.2. IQGAP2 restricts EMT upon inhibition of ERK pathway. A) Representative Western blot images showing the expression of phospho-ERK after ectopic expression of IQGAP2 in MCF7 IQGAP2_KD cells (left panel). Right panel shows the relative densitometry of phospho-ERK in MCF7_KD cells upon IQGAP2 expression (2-tailed unpaired t-test). **B)** Western blot images showing rescue of Twist (phospho-ERK downstream target) after treating MCF7 IQGAP2_KD cells with phospho-ERK inhibitor II. **C)** Cell invasion assay after treating MCF7 IQGAP2_KD cells with phospho-ERK inhibitor II (left panel). Right panel, bar graph showing no significant difference in the number of cells invaded in control and IQGAP2_KD with phospho-ERK inhibitor II (Student's t-test, unpaired, 2-tailed, n = 3). * represents $p \leq 0.05$, # represents non-significant.

We observed a significant inhibition of phospho-ERK level in the IQGAP2_KD group upon treatment of U0126. We next examined the level of Twist, an EMT marker in U0126

inhibitor treated and untreated groups of MCF7 IQGAP2_KD cells and, observed rescue of Twist expression level in U0126 inhibitor group, confirming the specificity of IQGAP2 mediated ERK pathway in EMT regulation (Fig. 5.2.10.2B).

This hypothesis is further supported by the finding where the inhibition of ERK abrogated the higher invasion observed with IQGAP2 knockdown (Fig. 5.2.10.2C). These results suggest that IQGAP2 expression inhibits cell migration, invasion, and EMT through MEK/ERK signaling pathways.

5.2.11 Reduction in IQGAP2 activates ER in MCF7 cells through ERK

The role of IQGAP1 in ERα-specific transcriptional activation through the ERK pathway is well reported [30]. In our study, the suppressive effect of IQGAP2 in the ERK pathway further led us to speculate the possible role of IQGAP2 in ERα-specific transcriptional regulation. To examine this conjecture, estrogen receptor 1 (ESR1) transcript level and phospho-ERα protein levels were investigated via qRT-PCR and Western blots in IQGAP2_KD and IQGAP2_Ex group of MCF7 with their controls.

We observed a significant change in transcript levels of ESR1 in IQGAP2_KD and IQGAP2_Ex groups of MCF7 compared to their controls. Decrease in IQGAP2 expression led to a 3.1 ± 0.33 fold ($p \leq 0.05$) upregulation of ESR1 transcript level. In contrast, an increased IQGAP2 expression led to a 12.5 ± 0.06 fold ($p \leq 0.001$) downregulation of ESR1 transcript level in MCF7 (Fig. 5.2.11.1A). Further, investigation on the effect of IQGAP2 in ERα phosphorylation showed an increase in phospho-ERα level in MCF7 IQGAP2_KD compared to its control ($p \leq 0.05$, IQGAP2_KD - 1.25 ± 0.08, Control_Sc - 0.78 ± 0.02) (Fig. 5.2.11.1B). In contrast, a decreased phospho-ERα level was observed in MCF7 IQGAP2_Ex group as compared to control ($p \leq 0.01$, IQGAP2_Ex - 0.72 ± 0.03, Control_EV - 1.23 ± 0.02) (Fig. 5.2.11.1C).

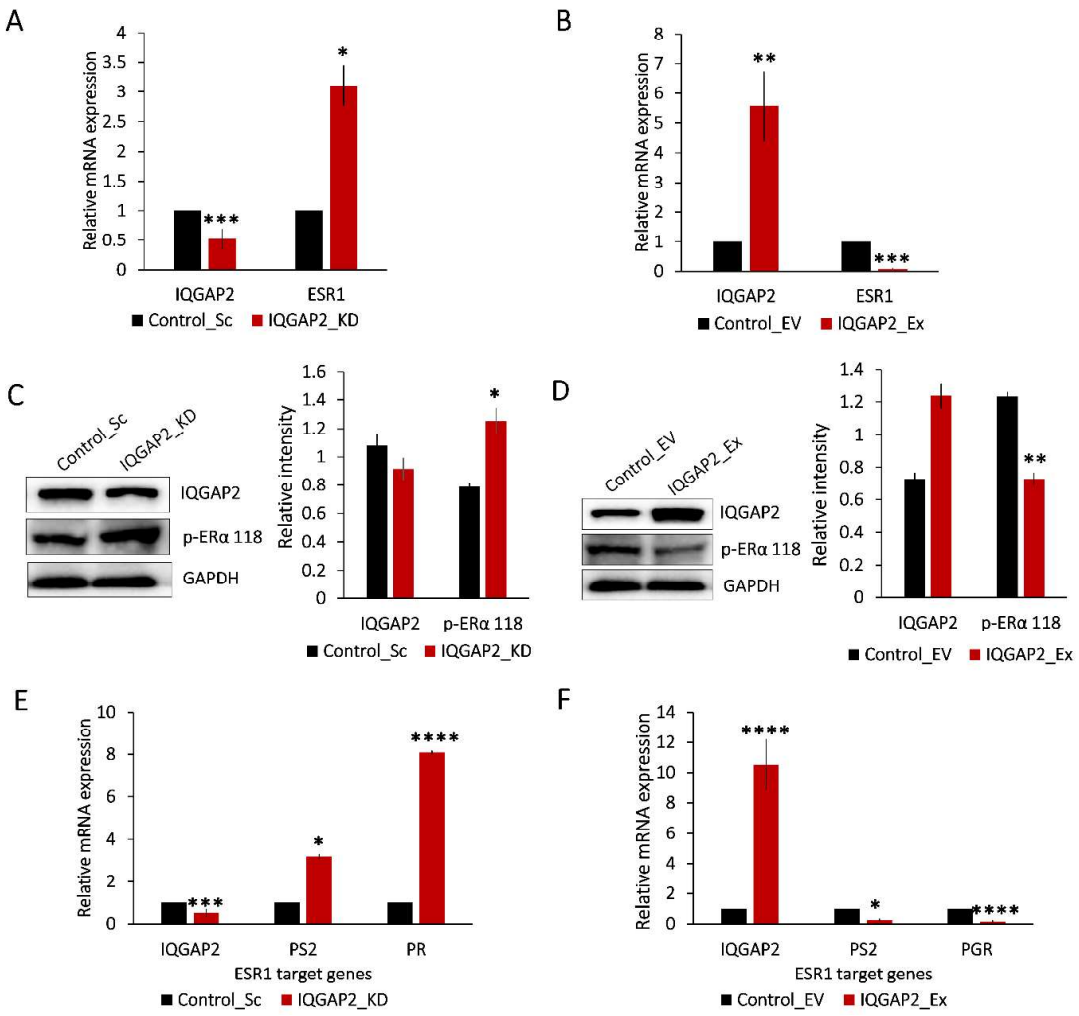

Figure 5.2.11.1. Reduction in IQGAP2 upregulates ER expression in MCF7 cells and induces its downstream signaling. qRT-PCR data showing ESR1 mRNA expression in **A)** MCF7 IQGAP2_KD and MCF7_Control_Sc (n = 3, 2-tailed unpaired t-test). **B)** MCF7 IQGAP2_Ex and MCF7_Control_EV (n = 3, 2-tailed unpaired t-test). **C)** Representative Western blot images of phospho ERα^{ser118} in MCF7 IQGAP2_KD and MCF7_Control_Sc cells (left panel). In right panel, the bar graph representing significant differences in mRNA level of phospho ERα^{ser118} between IQGAP2_KD and control groups (n = 3, 2-tailed unpaired t-test). **D)** Representative Western blot images of phospho ERα^{ser118} in MCF7 IQGAP2_Ex and MCF7_Control_EV cells (left panel). In right panel, the bar graph representing significant differences in mRNA level of phospho ERα^{ser118} between IQGAP2_Ex and control groups (n = 3, 2-tailed unpaired t-test). **E)** qRT-PCR data showing PS2 and PR mRNA level in MCF7 IQGAP2_KD and MCF7_Control_Sc groups (n = 3, 2-tailed unpaired t-test). **F)** qRT-PCR data showing PS2 and PR mRNA level in MCF7 IQGAP2_Ex and MCF7_Control_EV group (n = 3, 2-tailed unpaired t-test). All experiments performed with n = 3. * represents $p \leq 0.05$, ** represents $p \leq 0.01$, *** represents $p \leq 0.001$, **** represents $p \leq 0.0001$.

Next, we inspected the effect of IQGAP2 expression on ERα downstream transcriptional targets, pS2/trefoil factor 1 [33] and progesterone receptor (PR) [32] in MCF7 IQGAP2_KD, IQGAP2_Ex and their controls by qRT-PCR. A significantly increased pS2 (fold change = 3.19 ± 0.09, $p \leq 0.05$) transcript level was observed in MCF7 IQGAP2_KD group compared to the control. Similarly, an increased PR transcript level (8.09 ± 0.05 fold, $p \leq 0.0001$) was observed in the IQGAP2 knockdown group of MCF7 (Fig. 5.2.11.1E). In comparison to the IQGAP2_KD groups, ectopic expression of IQGAP2 significantly reduced the transcript level of pS2 and PR by 3.62 ± 0.22 ($p \leq 0.05$) and 6.26 ± 0.27 ($p \leq 0.0001$) fold, respectively (Fig. 5.2.11.1F).

We next explored whether reduced expression of IQGAP2 first activates estrogen receptor alpha followed by downstream activation of ERK or vice versa. To achieve this, we first blocked the ER pathway with the tamoxifen in MCF7 IQGAP2_KD cells and examined the change in phospho-ERK level.

Thereafter, the ERK pathway was blocked using ERK inhibitor (U0126) and the phospho-ER alpha level was checked in MCF7 IQGAP2_KD cells. The ER pathway inhibition with tamoxifen did not show a significant change in phospho-ERK level in MCF7 IQGAP2_KD cells (Fig. 5.2.11.2A). Interestingly, we observed a significant reduction of phospho-ER alpha level ($p \leq 0.01$) with ERK inhibition in MCF7 IQGAP2_KD cells (Fig. 5.2.11.2B).

The above findings suggest that reduced expression of IQGAP2 activates ERα pathway through ERK in ER positive, MCF7 cells.

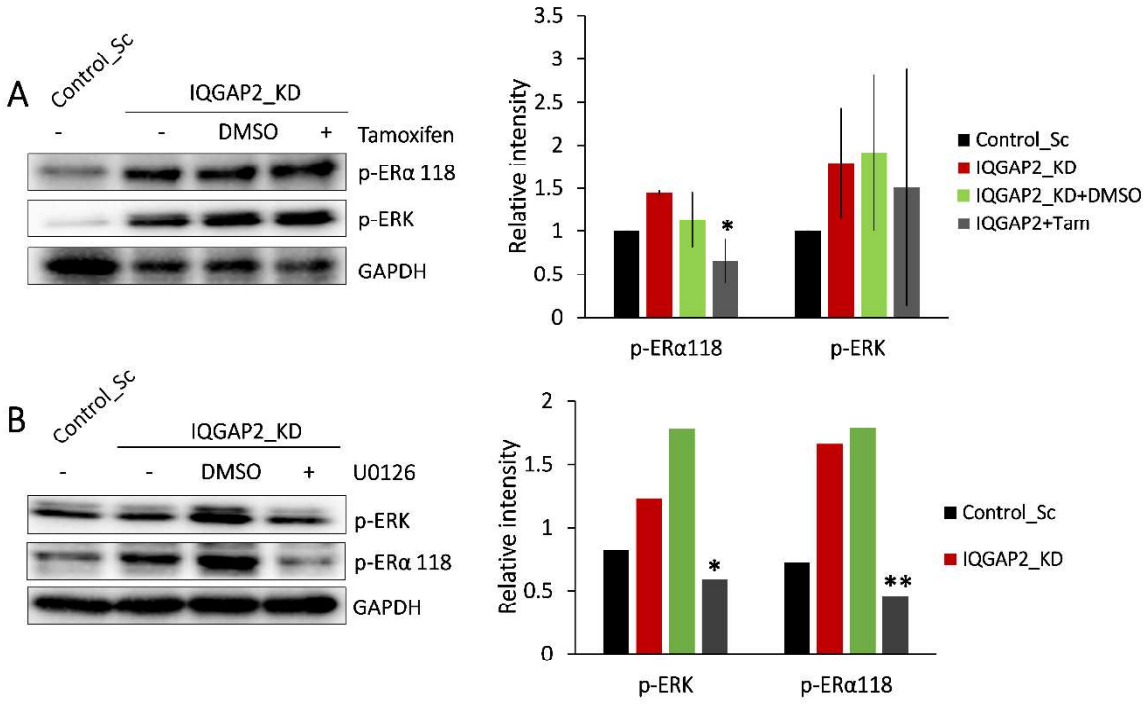

Figure 5.2.11.2. Reduction in IQGAP2 activates ER in MCF7 cells through ERK pathway. **A)** Western blot showing expression of phospho ERα^{ser118} and phospho-ERK in MCF7 IQGAP2_KD cells after tamoxifen treatment (left panel). Right graph showing no reduced phospho ERα^{ser118} (n = 3, 2-tailed unpaired t-test) and statistically non-significant difference of phospho-ERK (n = 3, 2-tailed unpaired t-test) levels in control vs tamoxifen treated groups. **B)** Western blot showing expression of phospho ERα^{ser118} and phospho-ERK in MCF7 IQGAP2_KD cells after treatment with ERK inhibitor II, U0126 (left panel). Graph showing phospho-ERα^{ser118} (n = 3, 2-tailed unpaired t-test) and phospho-ERK (n = 3, 2-tailed unpaired t-test) level in control vs ERK inhibitor II treated groups. * represents $p \leq 0.05$, ** represents $p \leq 0.01$.

5.2.12 Low IQGAP2 expression induces the pro-inflammatory cytokine expression in breast cancer cells

Many key cytokines tightly regulate tumor milieu. Inflammatory cytokines like CXCR1, IL-3, IL-5, IL-6, IL-8, IL-9, IL-10, CCL2, CCL3 and CCL11 have indispensable function in tumor initiation, progression as well as in metastasis [215] .Therefore, we examined the role of IQGAP2 on the expression levels of the above key inflammatory cytokines. To achieve this, qRT-PCR was performed using cytokine specific primers in MCF7-IQGAP2-Ex, MDA-MB-468-IQGAP2-KD and respective controls.

The analysis of qRT-PCR results showed a significant difference in the expression levels of IL-6, IL-8 and CCL2 in the MCF7_IQGAP2_Ex group compared to the control. The mRNA level was reduced in IL-6 by 0.33 ± 0.06 fold ($p \leq 0.01$), IL-8 by 0.47 ± 0.23 fold ($p \leq 0.01$), and CCL2 by 0.57 ± 0.24 fold ($p \leq 0.01$) (Fig. 5.2.12.1A). In contrast, reduction in the protein level of IQGAP2 in MDA-MB-468 lead to increased transcript level of IL-6 ($p \leq 0.01$, fold change = 2.67 ± 0.0001), CCL2 ($p \leq 0.001$, fold change = 2.21 ± 0.005), CCL3 ($p \leq 0.05$, fold change = 2.62 ± 0.12) and CCL11 ($p \leq 0.0001$, fold change = 2.60 ± 0.02). In case of IL-8, we did not observe a remarkable change in its mRNA level in

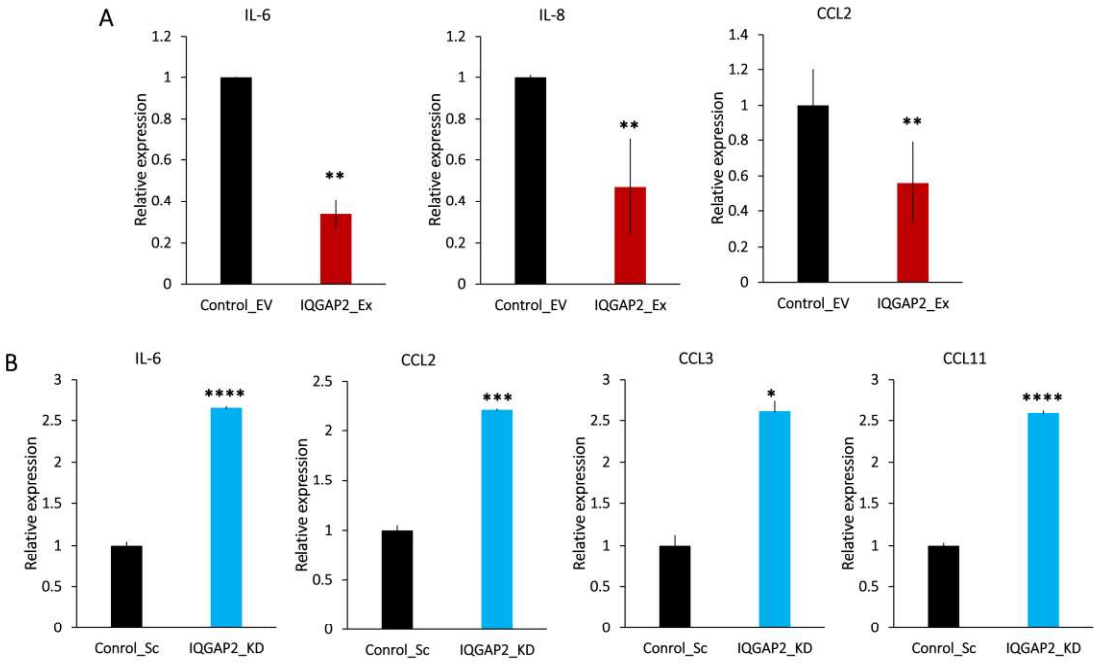

Figure 5.2.12.1. IQGAP2 expression reduces the pro-inflammatory cytokine expression in breast cancer cells. A) Bar graph showing the differential transcript level of IL-6, IL-8 and CCL2 between MCF7_IQGAP2_Ex and MCF7_Control_EV group (n = 3, 2-tailed unpaired t-test). **B)** Bar graph showing the differential transcript level of IL-6, CCL2, CCL3, CCL11 and IL-8 between MDA-MB-468_IQGAP2_KD and MDA-MB-468_Control_Sc group (n = 3, 2-tailed unpaired t-test). The experiment was performed with three technical replicates. * represents $p \leq 0.05$, ** represents $p \leq 0.01$, *** represents $p \leq 0.001$, **** represents $p \leq 0.0001$.

MDA-MB-468_IQGAP2_KD group compared to control ($p \leq 0.01$, fold change = 0.8 ± 0.01) (Fig. 5.2.12.1B). A higher IL-6 expression induces EMT and invasiveness of MCF7

[216, 217]. Likewise, IL-8 promotes EMT of both ER positive and ER negative breast cancer cells [218] . CCL2, CCL3 and CCL11 are well known key protumorigenic inflammatory cytokines in breast cancer [219-222]. Our results show coherence with the previous reports and explain how IQGAP2 might be affecting key cellular processes like proliferation and invasion through cytokines.

The above results underline the pivotal role of IQGAP2 in regulation of pro-inflammatory cytokine in breast cancer.

5.2.13 Reduced expression of IQGAP2 promotes the tumor growth in mouse model

To further validate the *in vitro* findings we used mouse xenograft model. The MCF7_IQGAP2_KD and control cells were injected into the mammary fat-pad of 6-8 weeks old female nude mice. The tumor growth in both groups was monitored for 30 days (day of euthanization). A visible difference in growth of tumor between both the groups can be seen in Fig. 5.2.13.1A.

The analysis of tumor size showed a significant increase in tumor volume in MCF7 IQGAP2_KD group compared to controls ($p \leq 0.01$, IQGAP2_KD - 1311.03 ± 389.37 mm^3, Control_Sc - 234.31 ± 124.60 mm^3) (Fig. 5.2.13.1B). The tumor weight was also calculated at day 30 and an elevated tumor weight was observed in MCF7_IQGAP2_KD group compared to the control ($p \leq 0.01$, IQGAP2_KD - 1407.5 ± 453.97 mg, Control_Sc - 272.5 ± 123.39 mg) (Fig. 5.2.13.1C). Additionally, we analysed the phospho-ERK levels in tumor sections of xenografts from nude mice, by IHC. The phospho-ERK expression was much higher in the MCF7_IQGAP2_KD derived xenograft group compared to the control (Fig. 5.2.13.1D). These findings were in support with our *in vitro* results. Overall,

the above *in vitro* and *in vivo* results suggest the tumor suppressor role of IQGAP2 in breast cancer.

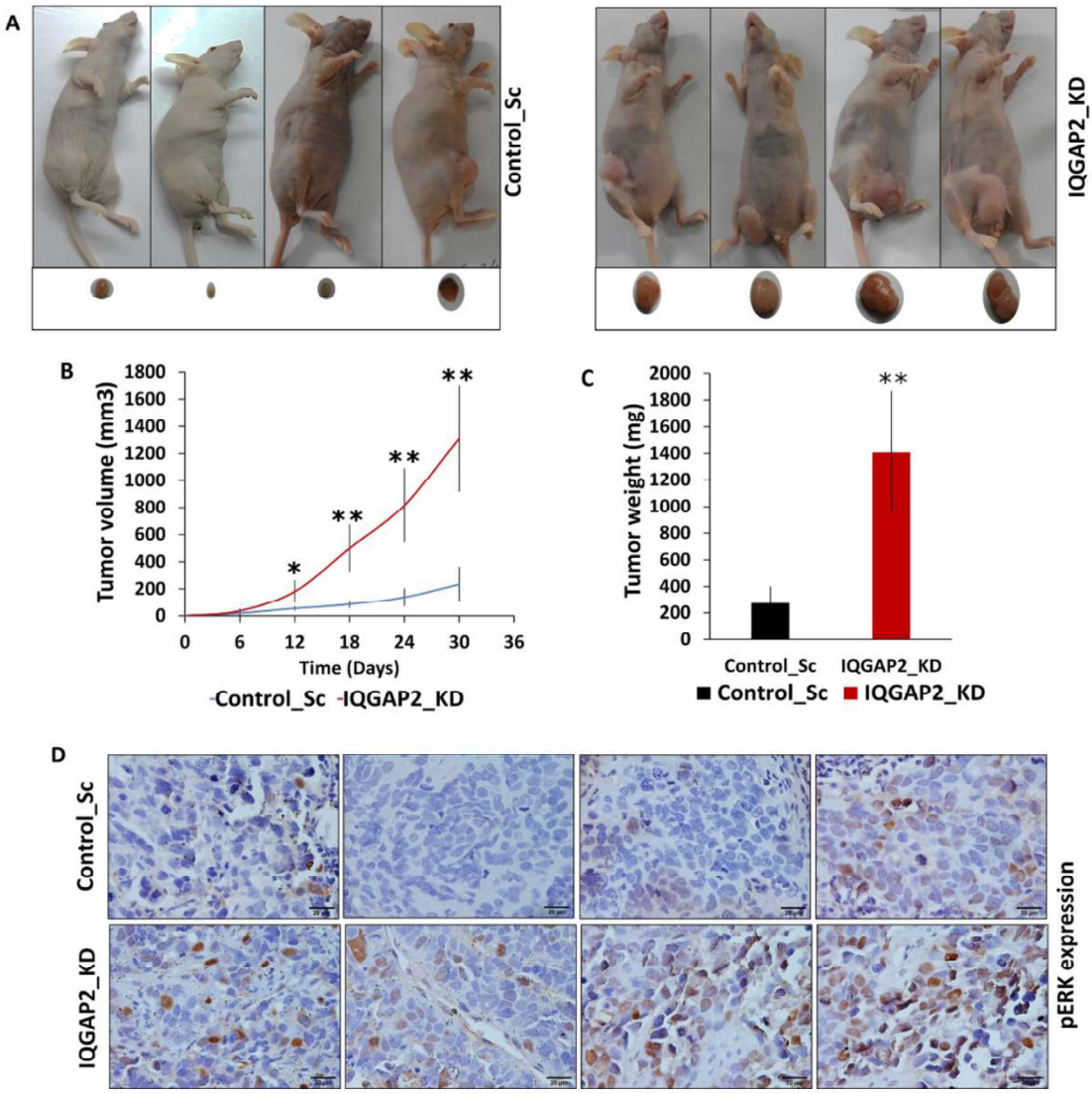

Figure 5.2.13.1. Reduced expression of IQGAP2 promotes the tumor growth in mouse model. A) Representative images of MCF7 xenograft nude mice showing progression in tumor volume in IQGAP2_KD group (right) and Control_Sc group (left) (n = 4). **B)** The comparative tumor volume of IQGAP2 knockdown group and control group at the interval of every 6 days (n = 4, 2-tailed unpaired t-test). **C)** Tumor weight of IQGAP2 knockdown mice and control mice group at day 30 (n = 4, 2-tailed unpaired t-test). **D)** Representative IHC images of phospho-ERK in xenograft tissues of MCF7_Control_Sc and MCF7_IQGAP2_KD groups. Images were captured using 40X objective lens. The scale bar is 20 µm. * represents $p \leq 0.05$, ** represents $p \leq 0.01$.

5.2.14 IQGAP2 is negatively correlated with phospho-ERK and IQGAP1 in breast cancer tissues

In breast cancer, the higher expression of IQGAP1 is well reported, where IQGAP1 serves to activate the ERK phosphorylation and protumorigenic signaling [20] [41]. In contrast, our findings have revealed the low expression of IQGAP2 in breast cancer tissues where it functions to suppress the ERK-phosphorylation and subsequent downstream signaling. Interestingly, the reciprocal expression pattern and function of these two members is well established in HCC [26, 27]. The above information prompted us to examine the correlation between the expression of IQGAP1 and IQGAP2 in breast cancer clinical specimens and association with phospho-ERK level, to decipher any regulatory circuit. Initially, the correlation between IQGAP1/ phospho-ERK and IQGAP2/ phospho-ERK was examined from publicly available dataset, Breast Invasive Carcinoma, TCGA, Firehose Legacy using cBioPortal site. This breast cancer dataset has the mass-spectrometry data of 74 breast cancer patients.

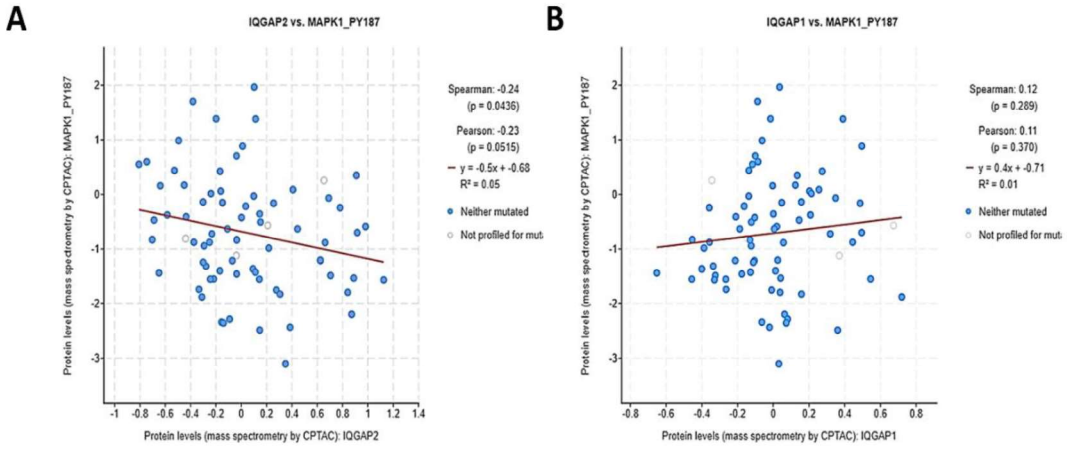

Figure 5.2.14.1. IQGAP2 negatively correlates with phospho-ERK level in TCGA, Firehose Legacy, cBioPortal dataset. A) Graph showing a negative correlation between IQGAP2 and phospho-ERK ($r = -0.23$, $p \leq 0.05$, $n = 74$, Pearson correlation). **B)** Graph showing a positive but non-significant correlation between IQGAP1 and phospho-ERK ($r = 0.11$, $p = 0.37$, $n = 74$, Pearson correlation).

The analysis showed a negative correlation between IQGAP2 and phospho-ERK (MAPK1_PY187) (Pearson, $p = 0.05$, $r = -0.23$,) (Fig. 5.2.14.1A). In contrast, a non-significant but positive correlation was noticed between IQGAP1 and phospho-ERK (MAPK1_PY187) (Pearson, $p = 0.37$, $r = 0.11$) (Fig. 5.2.14.1B).

To validate our data-mining based findings, we further analysed the correlation between these two isoforms in 38 breast cancer patient tissues samples using IHC. The Pearson correlation analysis showed a strong negative correlation between these two isoforms in breast tumor tissues ($r = -0.5654$, $R^2 = 0.3197$, $p \leq 0.001$, and 95% CI -0.7496 to -0.2998) (Fig. 5.2.14.2A).

Further, we checked the correlation between IQGAP1/ phospho-ERK and IQGAP2/ phospho-ERK in ten breast cancer patient tissue samples. Here, we observed a strong negative correlation between phospho-ERK and IQGAP2 (Pearson, $p \leq 0.05$, $r = -0.6342$, and 95% CI -0.9032 to -0.007497) (Fig. 5.2.14.2B). In contrast, a non-significant but strong positive correlation was noticed between phospho-ERK and IQGAP1 (Pearson, $p \geq 0.05$, correlation, $r = 0.4949$, $R^2 = 0.2449$ and 95% CI -0.1959 to 0.8574) (Fig. 5.2.14.2C). Interestingly, the phospho-ERK and the ratio of IQGAP2/IQGAP1 expression, showed a strong negative correlation (Pearson, $p \leq 0.05$, $r = -0.6489$, and 95% CI -0.9077 to -0.03240) (Fig. 5.2.14.2D). A representative IHC image shows the expression pattern of phospho-ERK, IQGAP2 and IQGAP1 in the tumor and normal regions of two breast cancer patient tissues (Fig. 5.2.14.2E, F).

The above in-silico and immunohistochemistry results together suggest that IQGAP2 and IQGAP1 are inversely associated with phospho-ERK level in breast cancer patients.

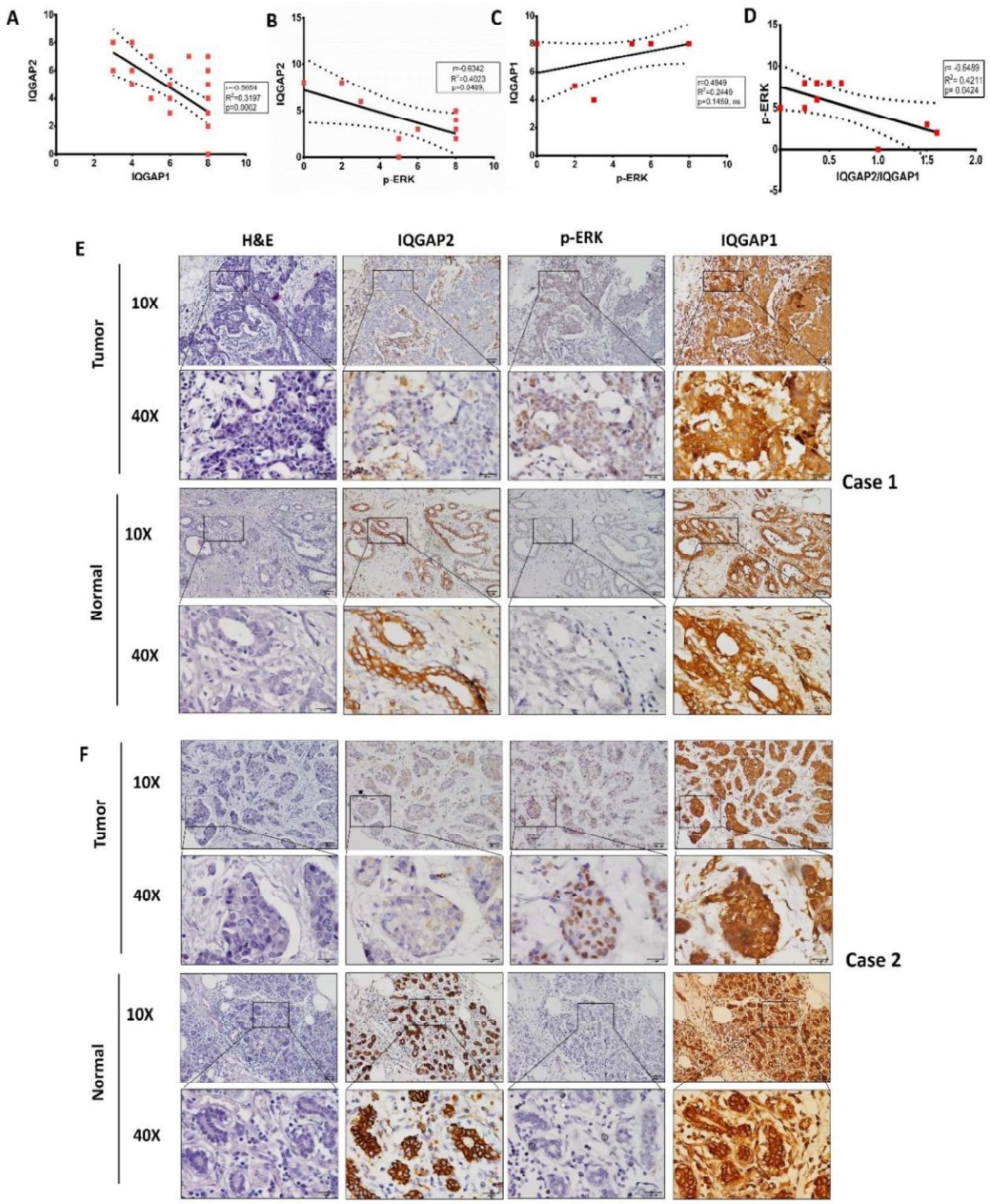

Figure 5.2.14.2. IQGAP2/IQGAP1 ratio is negatively correlated with phospho-ERK levels in breast cancer patients A). Pearson correlation between the expression levels of IQGAP2 and IQGAP1 in tumor tissues of breast (n = 38). **B)** Pearson correlation between the expression of IQGAP2 and phospho-ERK (n = 10). **C)** Pearson correlation between the expression of IQGAP1 and phospho-ERK (n = 10). **D)** Pearson correlation between the expression of the ratio of IQGAP2/IQGAP1 and phospho-ERK (n = 10). **E)** Representative images of H&E (left most) and IHC staining for IQGAP2, phospho-ERK and IQGAP1 in tumor and normal region of case 1 (breast cancer). **F)** Representative images of H&E (left most) and IHC for IQGAP2, phospho-ERK and IQGAP1 in tumor and normal region of case 2 (breast cancer). H&E and IHC images were captured with upright bright field microscope at 10X and 40X objective lens. Bar scale- 50 µm for 10X images, 20 µm for 40X images.

Interestingly, the inverse expression of IQGAP2 and IQGAP1 in same tumor tissue hints the possibility of opposite function of both the isoforms in phospho-ERK mediated cancer growth and metastasis.

5.2.15 IQGAP2 interacts with IQGAP1

Our findings led us to hypothesize that a common cancer signaling pathway is possibly affected by IQGAP2 and IQGAP1 in breast cancer wherein the function of one isoform may be regulated by the other and *vice-versa.* We prospect a physical interaction between the two isoforms that could be leading to the sequestering effect. To prove this hypothesis, IQGAP1-GST based pulldown experiments were conducted with MCF7-IQGAP2-Ex cell lysate. We observed a band of IQGAP2 at 180 kDa in pull downs with IQGAP1_GST but no such band was identified in pull downs with GST alone (Fig. 5.2.15.1A). Further, we repeated the pull downs assay in another cancer cell line, HeLa to confirm whether the interaction between these isoforms is organ specific or not. Interestingly, the results of HeLa were similar to MCF7 (Fig. 5.2.15.1B). Thus, these results suggest that IQGAP1 and IQGAP2 interact with each other.

5.2.16 The ratio of IQGAP2/IQGAP1 in breast cancer cells modulates ERK activation

In HCC, the interbreeding of Iqgap2−/− mice and Iqgap1−/− backgrounds have reported to decreases in the incidence and sizes of tumors, and the normalization of overall survival rates compared to those of Iqgap2−/− mice [38]. This indicates the possibility of alteration in common signaling and development of cancer with the change in the ratio of IQGAP2/IQGAP1. Keeping this in mind, we hypothesised that whether the ratio of these two isoforms could affect the activity of a common signaling molecule ERK *in vitro*.

To examine this, IQGAP1 was ectopically over expressed in MCF7 cells; on this background, IQGAP2_Ex and Control_EV vectors were transiently transfected to change the ratio of IQGAP2 to IQGAP1. We observed a high phospho-ERK level in IQGAP1_Ex group with vehicle control. Interestingly, MCF7 cells with increased IQGAP2 level showed a reduced phospho-ERK level (Fig. 5.2.15.1C). These results suggest that the ratio of IQGAP2 and IQGAP1 affects the level of common key signaling molecule phospho-ERK and maintains the balance.

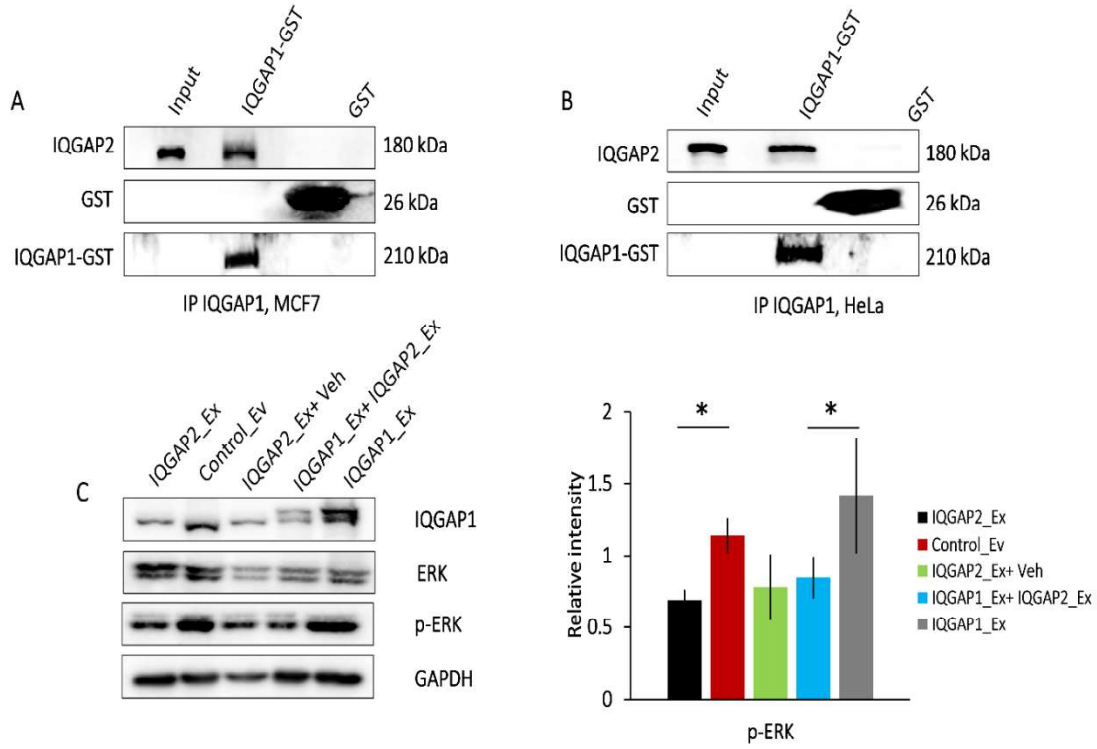

Figure 5.2.15.1. IQGAP2 and IQGAP1 interact and their ratio modulates IQGAP1 mediated ERK activation. A) Western blot images showing status of IQGAP2 in pull down assay performed with IQGAP1_GST and GST only in MCF7 cell lysates. The blot of different sizes probed with anti-IQGAP1, anti-IQGAP2 and GST antibodies. **B)** Western blot images showing status of IQGAP2 in pull down assay performed with IQGAP1_GST and GST only in HeLa cell lysates. The blot of different sizes probed with anti-IQGAP1, anti-IQGAP2 and GST antibodies. **C)** Representative images showing Western blots of phospho-ERK, IQGAP1 and total ERK in MCF7 cells, differing in ratio of IQGAP2 and IQGAP1. GAPDH was used as a loading control (left panel). The densitometry bar graph (right panel) showing the differences in expression of phospho-ERK in MCF7 cells differing in ratio of IQGAP2 and IQGAP1 expression (n = 3, 2-tailed unpaired t-test). * represents $p \leq 0.05$.

5.3 Discussion

The identification of molecular targets, which could help in early diagnosis of breast cancer and provide a very effective treatment regime in later stages of cancer, prompted us to explore the role of IQGAP2, in breast cancer.

Our IHC results in a large proportion of breast cancer cases revealed that the expression of IQGAP2 decreases with the progression of the disease. Additionally, our IHC data indicated the negative association of IQGAP2 expression with lymphovascular invasion positivity. Lymphovascular invasion is a characteristic of metastasis and poor survivability of the patients [223]. So, a negative association of IQGAP2 with lymphovascular invasion positivity hints at the possible protective role of IQGAP2 against the invasive phenotype in breast cancer patients, which is an evidence of the crucial tumor-suppressing ability of this protein.

The protective role of IQGAP2 in cancer metastasis is further substantiated by the finding that patients with advanced stage, III or IV, show a frequent weak/negative IQGAP2 expression in comparison to early stage breast cancer patients. Although, the analysis of patients IHC data did not show a statistically significant association between IQGAP2 expression and size of the tumor but a trend of larger tumors in patients with low IQGAP2 expression was observed. Additionally, our xenograft tumor model showed the correlation of reduced IQGAP2 expression with larger tumor size. These findings are in favour of the tumor suppressor role of IQGAP2 in breast cancer where IQGAP2 not only restricts the tumor growth but also the metastatic spread.

Our *in vitro* study in different breast cancer cell lines showed that IQGAP2 expression is not associated with a specific molecular subtype of breast cancer which is further supported by the tumor suppressor activity of IQGAP2 in both, ER/PR positive MCF7

cells as well as in triple negative MDA-MB-468 cells of breast cancer. Our finding is very helpful in the identification of new molecular targets that protect breast cancer irrespective of molecular subtypes. ERK and AKT are crucial pathways that promote EMT in breast cancer cells [224]. The role of IQGAP2 in AKT pathways is known in prostate cancer [41]. So, screening of both ERK and AKT was carried out in our study to examine the major pathway involved in IQGAP2 mediated EMT in breast cancer.

Our results revealed that IQGAP2 regulates EMT through MEK-ERK signaling pathways, without affecting the AKT pathway. The activation of MEK-ERK cascade is well reported to decrease E-cadherin and increase of EMT markers, N-cadherin, Snail and Twist [225]. Our results are also in agreement to this, where upon IQGAP2 depletion, higher protein levels of N-cadherin, Snail and Twist and lower E-cadherin level was observed. The role of the IQGAP2 mediated ERK pathway in EMT was further confirmed by the rescue of invasive character upon inhibition of the ERK pathway.

Thus, our results indicate that the negative effect of IQGAP2 on oncogenic characteristics of breast cancer cells, could be achieved primarily by inhibition of the ERK pathway, independent of the molecular subtype. However, in ER-positive cells, simultaneous reduction of the ERK and ER pathway and associated target genes, pS2 and PR are reported to cause more pronounced cumulative effect in tumor growth and EMT [226, 227]. We found activation of ERK and ER pathway and, further upregulation of the downstream targets pS2 and PR, which are completely in agreement with the previous reports and indicate the additional role of IQGAP2 in ER positive breast cancer. Previous literature has shown the interaction of IQGAP1 with ERα, which results in the activation of ERα [204]. In our study, IQGAP2 and IQGAP1 interaction resulted in loss of ERK activation. The reason of IQGAP1-IQGAP2 interaction mediated ERK activity loss may

be that IQGAP2 sequesters ERK binding site of IQGAP1, this eventually may affect ERα activation also. After analysis of IHC images, it seems like that in breast tumor cells, where expression of IQGAP2 was low, the expression of phospho-ERK was high and vice-versa. But further experiments will be required in order to validate it at cellular level.

Search of key inflammatory cytokines and chemokines, upon IQGAP2 alterations in MCF7 and MDA-MB-468 cells, led to the identification of possible role of IQGAP2 in suppression of pro-inflammatory cytokine signature, which further supports the protective role of IQGAP2 in disease progression. IL-6, CCL2, IL-8, CLL3 and CCL11 are crucial cytokines/chemokines that maintain the aggressive traits in less invasive luminal as well as invasive basal like cells [216, 217, 228, 229]. In our study, a change in mRNA levels of IL-6 and CCL2 was observed in MCF-7 and MDA-MB-468 cells whereas IL-8 levels were altered only in MCF7 cells. Interestingly, CCL3 and CCL11 chemokines were specifically altered in MDA-MB-468. Here, we predict that IL-6 and CCL2 are common regulatory cytokines that affect aggressiveness of breast cancer cells independent of its molecular subtype, whereas CCL3 and CCL11 may provide the added aggressiveness in MDA-MB-468 cells, specifically. The role of IL-6 and CCL2 is well characterised in cell motility and survival of breast cancer through the MAPK pathway [228-230].

Previous study in HCC, have shown the interaction between IQGAP2 and IQGAP1 where IQGAP2 was sequestering the pro-oncogenic effects of IQGAP1 in the same [38]. Our *in vitro* GST-Pull down results also suggest the possibility of the presence of a IQGAP2-IQGAP1 scaffold complex in breast cancer, and a similar sequestering effect of IQGAP2 upon IQGAP1 resulting in the reduction of phospho-ERK levels. However, we were not able to specifically explore the domains responsible for the physical interaction witnessed

or rule out the presence of intermediary binding partners in the complex. The paradoxical phenomenon of opposing functional roles of IQGAP1 and IQGAP2 in cancer progression, despite sharing a homologous domain structure, has been attributed to different binding partners in the past [17]. For instance, while both of these proteins bind Rac1 and cdc42, IQGAP2 binds indiscriminately to both the active GTP-bound as well as inactive GDP-bound forms of these proteins [168, 231], IQGAP1 binds selectively to the inactive form only [170, 171]. In addition, the different IQ-motifs in different IQGAPs determine their interaction with calmodulin and related proteins [163]. Another possible explanation of the different functional roles of IQGAP1 and IQGAP2, is their affinity to be phosphorylated by different kinases, which in turn regulates their binding to key interacting partners mediating cell-cell adhesion, like Cdc42 [232]. Understanding the divergent functions of IQGAP1 and IQGAP2 in breast cancer progression, with regards to their affinity to be differentially phosphorylated by specific kinases, and interaction with different binding partners like GTPases such as Cdc42 and Rac, is of utmost importance to develop them into molecular targets for breast cancer therapy in the near future.

In conclusion, IQGAP2 restricts tumor growth and EMT, by regulating the pro-inflammatory cytokine milieu mainly through inactivation of the MEK-ERK pathway. The tumor suppressive characteristics of IQGAP2, irrespective of molecular subtype of breast cancer cells, shows its candidature as a therapeutic target in breast cancer. The physical interaction between IQGAP2 and IQGAP1 may provide a sequestering effect on IQGAP1 mediated ERK pathway.

CHAPTER 2

To decipher the role and molecular signaling of IQGAP2 in tumor angiogenesis

Findings of this section have been communicated.

Kumar D, Chawla S, Mohapatra N, Dixit M., Reduced expression of IQ motif-containing GTPase-activating protein 2 activates VEGF-A/VEGFR2-AKT signaling and regulates angiogenesis in breast cancer.

6.1 Introduction

Tumor angiogenesis is a crucial event in growth and development of cancer which is characterised by the formation of new blood vessels in solid tumors to provide oxygen and nutrients to the tumor cells [233, 234]. Angiogenesis is a key element of the metastasis process [235, 236]. Increased microvascular density (MVD), is an independent prognostic indicator of metastatic potential of cancers [187, 237-240]. In breast cancer, high MVD is well known risk factor for metastasis and a predictor of poor prognosis [56, 239]. Thus, breast cancer angiogenesis is a promising diagnostic and therapeutic target that should be explored [241, 242] .

The role of pro-angiogenic activators is well established in the event of angiogenesis. Currently many angiogenic activators have been identified including, vascular endothelial growth factor (VEGF), TGF-β, tumor necrosis factor (TNF)-α, basic fibroblast growth factor (bFGF), platelet-derived endothelial growth factor, angiogenin transforming growth factor (TGF)-α [243]. Among these agents, VEGF is a strong angiogenic activator that is secreted by tumor tissues and the adjacent stroma, leading to tumor vascularisation and growth [94, 244, 245]. The VEGF family comprises of VEGF-A, VEGF-B, VEGF-C, VEGF-D and VEGF-E. Among VEGF family, VEGF-A is potent and highly specific mitogen that stimulates the full cascade of events required for angiogenesis [246, 247], and is overexpressed in a variety of tumors [248].

Anti-angiogenic agents like bevacizumab, ramucirumab and sorafenib have advantageous effect in VEGF and VEGFR target therapy that limits the tumor vessel growth and metastasis of breast cancer. But they show many side effects in patients (hypertension, congestive heart failure, proteinuria caused by renal failure, bone marrow depression, rash

and sensory neuropathy) and resistance towards VEGF-VEGFR during the course of treatment [249]. Therefore, new anti-angiogenic targets need to be explored.

Previous studies have found the tumor suppressor role of IQGAP2 in lung, liver, prostate and stomach cancer. Our study highlighted that IQGAP2 restricts the tumor growth, migration and metastasis of breast cancer by regulating the another IQGAP isoform, IQGAP1 which a well-established pro-angiogenic regulator [53-55]. Despite being reported as a tumor suppressor in few solid tumors the role of IQGAP2 in regulating tumor angiogenesis is completely unexplored. A comprehensive study with IQGAP2 in tumor angiogenesis could help in uncovering the role of IQGAP2 and its mechanism in the inhibition of breast cancer.

In this chapter, we have highlighted the paracrine role of IQGAP2 in breast cancer angiogenesis. All *in vitro* angiogenesis studies were performed on the primary Human Umbilical Vein Endothelial Cells (HUVECs). For the paracrine breast cancer model, we selected ER/PR positive MCF7 and ER negative MDA-MB-468 breast cancer cell lines. This selection of breast cancer cell lines of different molecular subtypes was taken to explore the possibility of differential role (if any) of IQGAP2 in angiogenesis.

Additionally, the *in vitro* findings of the role IQGAP2 in breast cancer angiogenesis was further validated in ex-ovo and *in vivo* model systems. Most importantly, we have carried out IHC to ascertain the correlation between IQGAP2 expression levels and microvessel density (MVD), which is a surrogate marker for the level of vascularity in normal and tumor tissues. Further, we explored the IQGAP2 mediated signaling pathways responsible for angiogenesis in breast cancer. We believe, objectives of this chapter will provide a thorough understanding of the role of IQGAP2 in aiding the process of angiogenesis in breast cancer, and in assertion of its therapeutic and prognostic value.

6.2 Results

6.2.1 Reduced IQGAP2 expression in breast cancer cells enhances angiogenesis *in vitro*

Tumor angiogenesis is well characterised by the higher proliferation, migration and tubule formation ability of endothelial cells in response to the pro-angiogenic factors released from the tumor cells. The proliferation of endothelial cells is very crucial to maintain the growth of capillaries, whereas the migration and tubule formation of endothelial cells are pivotal for sprouting and tubule formation, respectively.

Therefore, to check the effect of IQGAP2 expression on tumor angiogenesis we performed cell proliferation, migration and tubule formation assays on HUVECs with conditioned media collected from breast cancer cells, MCF7 (ER+) and MDA-MB-468 (triple negative). These cell lines reflect the intracellular signaling in less invasive ER positive breast cancer and highly invasive ER negative breast cancer systems, respectively. So, examining the effect of IQGAP2 with the background of these cell lines may help in segregating the effect on IQGAP2 in angiogenesis in ER positive and ER negative breast cancer. The conditioned media (CM) was harvested from MCF7_IQGAP2_KD, MCF7_IQGAP2_Ex, MDA-MB-468_IQGAP2_KD and their respective control cells. Then, this media was applied to HUVECs (primary endothelial cells). The results of each assay are described below:

6.2.1.1 Reduced expression of IQGAP2 in breast cancer cells promotes proliferation of HUVECs

The effect of IQGAP2 expression on cell proliferation of HUVECs was accessed by a colorimetric method (MTS assay). HUVECs treated with the conditioned media from MCF7_IQGAP2_KD showed significantly higher proliferation compared to the

HUVECs treated with conditioned media from MCF7_Control_Sc ($p \leq 0.01$, OD_{495nm} at day 4, IQGAP2_KD - 1.09 ± 0.049, Control_Sc - 0.80 ± 0.047) (Fig. 6.2.1.1A).

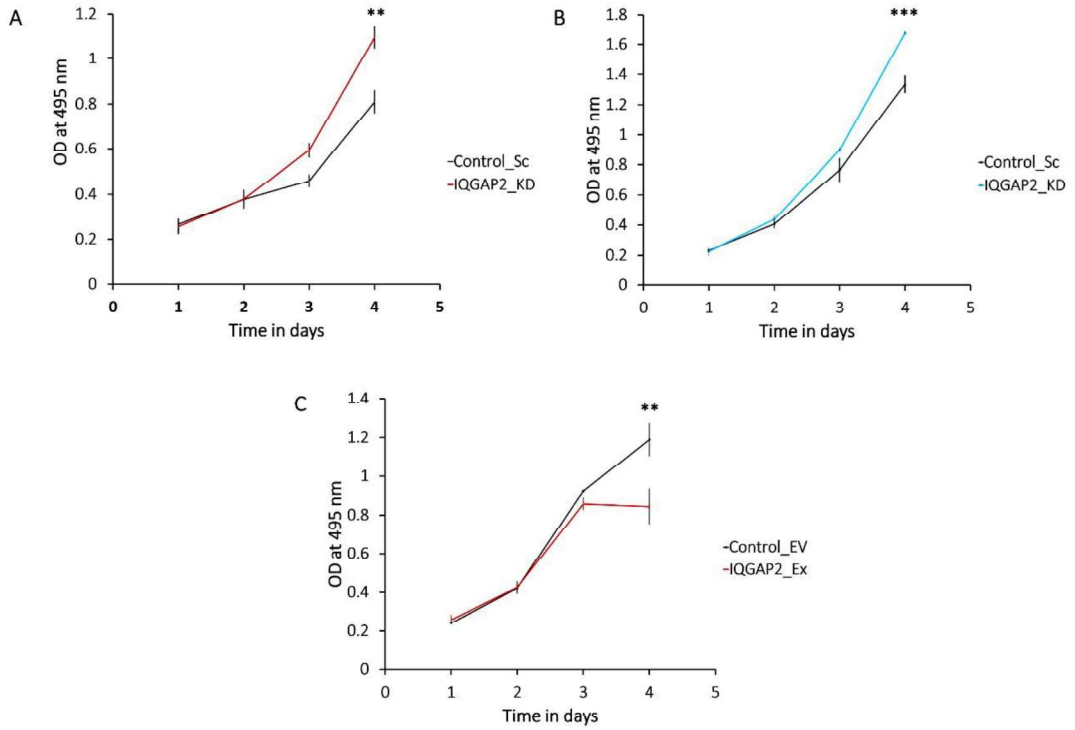

Figure 6.2.1.1. Low IQGAP2 expression in breast cancer cells increases proliferation of HUVECs. A) Graph showing results of MTS assay of HUVECs supplemented with conditioned media from MCF7_IQGAP2_KD and MCF7_Control_Sc. **B)** Graph showing results of MTS assay of HUVECs supplemented with conditioned media from MDA-MB-468_IQGAP2_KD and MDA-MB-468_Control_Sc. **C)** Graph showing results of MTS assay of HUVECs supplemented with conditioned media from MCF7_IQGAP2_Ex and MCF7_Control_EV. All assays were performed in triplicate, n = 3. In graph, X-axis represents time in days, Y-axis represents absorbance of cells post MTS assay at 495nm. Here, two-tailed Student's t-test was performed for statistical analysis. ** represents $p \leq 0.01$, *** represents $p \leq 0.001$.

A similar pattern of HUVEC proliferation was observed with the conditioned media from MDA-MB-468_IQGAP2_KD ($p \leq 0.001$, OD_{495nm} at day 4, IQGAP2_KD - 1.67 ± 0.05, Control_Sc - 1.33 ± 0.01) (Fig. 6.2.1.1B). In contrast, the conditioned media from MCF7_IQGAP2_Ex showed a decrease in cell proliferation of HUVECs compared to the conditioned media of MCF7_Control_EV ($p \leq 0.01$, OD_{495nm} at day 4, IQGAP2_Ex - 0.84 ± 0.08, Control_Sc - 1.19 ± 0.08) (Fig. 6.2.1.1C).

The above results suggest that the expression of IQGAP2 in breast cancer cells affects the proliferation of endothelial cells. The depletion of IQGAP2 in ER positive or ER negative breast cancer cells promotes proliferation of HUVECs, parallelly, its ectopic expression leads to inhibition of proliferation.

6.2.1.2 Low IQGAP2 expression in breast cancer cells enhances migration of HUVECs

To examine the effect of IQGAP2 expression levels on migration of endothelial cells, a transwell migration assay was performed. We noticed that the migration in HUVECs, treated with conditioned media from MCF7_IQGAP2_KD cells, was significantly higher than in HUVECs treated with conditioned media from MCF7_Control_Sc ($p \leq 0.0001$, IQGAP2_KD - 290.55 ± 33.10, Control_Sc - 179.71 ± 29.86) (Fig. 6.2.1.2A). Further, cell migration assay was performed with the conditioned media from MDA-MB-468_IQGAP2_KD cells, which showed enhanced migration of HUVECs compared to the those treated with conditioned media from MDA-MB-468_Control_Sc cells ($p \leq 0.0001$, IQGAP2_KD - 316.33 ± 50.02, Control_Sc - 234.44 ± 31.09) (Fig. 6.2.1.2B). This indicates that the reduction of IQGAP2 increases the migration of endothelial cells irrespective of the ER status of breast cancer cells. On the other hand, the HUVECs treated with the conditioned media from MCF7_IQGAP2_Ex showed a reduced cell migration compared to the HUVECs treated with the conditioned media from MCF7_Control_EV cells ($p \leq 0.01$, IQGAP2_Ex - 173 ± 44.70, Control_EV - 219.88 ± 45.02) (Fig. 6.2.1.2C).

The results from above section suggest that migratory property of HUVECs increases with the depletion of IQGAP2 in breast cancer cells and vice-versa. This highlights the

role of IQGAP2 in migration of endothelial cells which is a crucial event during angiogenesis.

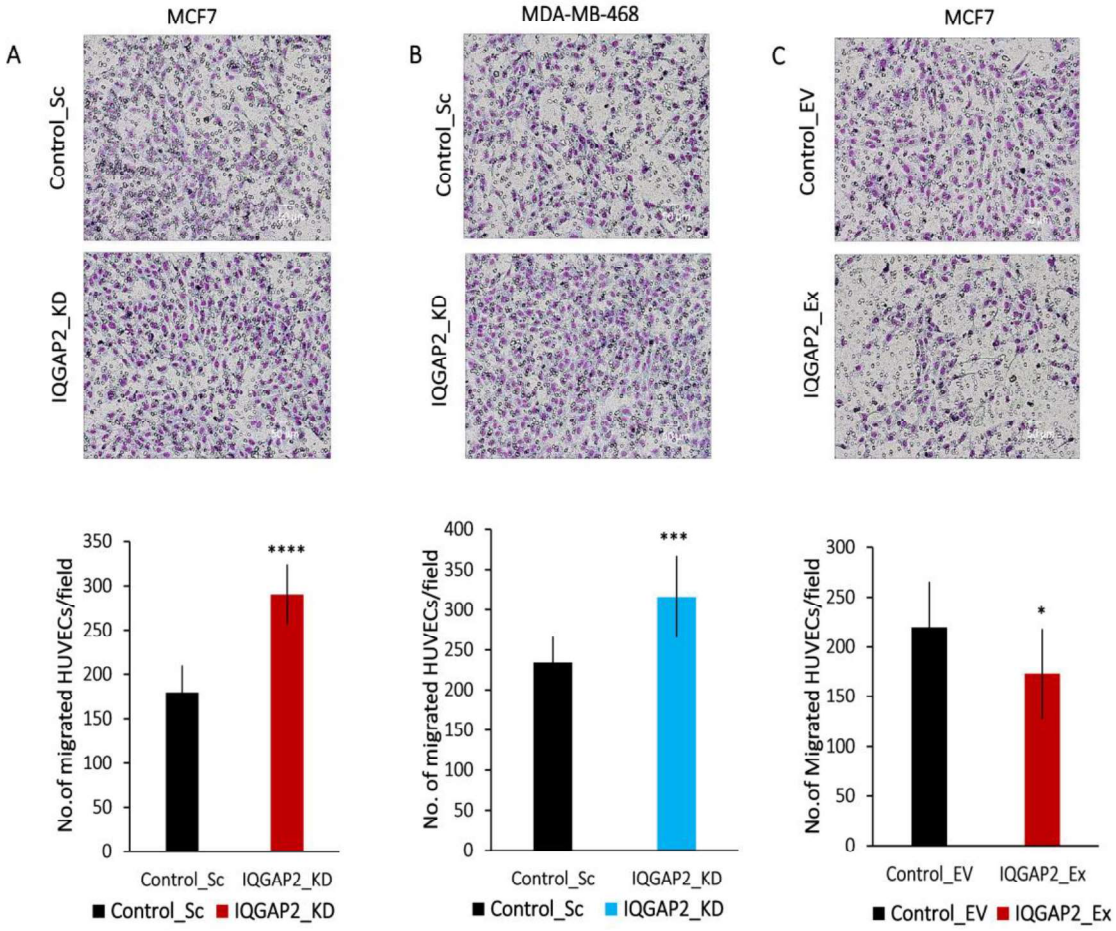

Figure 6.2.1.2. Low IQGAP2 expression in breast cancer cells enhances migration of HUVECs. A) The upper panel shows the representative images of transwell migration assay in HUVECs supplemented with the CM from MCF7_IQGAP2_KD and respective control. In lower panel, the bar graph showing differences in the migratory cells between the two experimental groups (n = 3, 2-tailed unpaired t-test). **B)** The upper panel shows the representative images of transwell migration assay in HUVECs treated with the CM from MDA-MB-468_IQGAP2_KD and respective control. In lower panel, the bar graph showing differences in the migratory cells between the experimental groups (n = 3, 2-tailed unpaired t-test). **C)** The upper panel shows the representative images of transwell migration assay in HUVECs treated with the CM from MCF7_IQGAP2_Ex and respective control. In lower panel, the bar graph showing differences in the migratory cells between two experimental groups (n = 3, 2-tailed unpaired t-test). * represents $p \leq 0.05$, *** represents $p \leq 0.001$, **** represents $p \leq 0.0001$.

6.2.1.3 Reduced expression of IQGAP2 in breast cancer cells promotes tubule formation of HUVECs

Next, we checked the effect of IQGAP2 on the tubulogenesis property of endothelial cells. For this, HUVECs were incubated with the conditioned media from MCF7_IQGAP2_KD, MCF7_IQGAP2_Ex, MDA-MB-468_IQGAP2_KD and their respective control cells. The images of tubules were captured at 4 hours and analysis of different angiogenesis parameters was carried out using Angiogenesis analyser tool in ImageJ software.

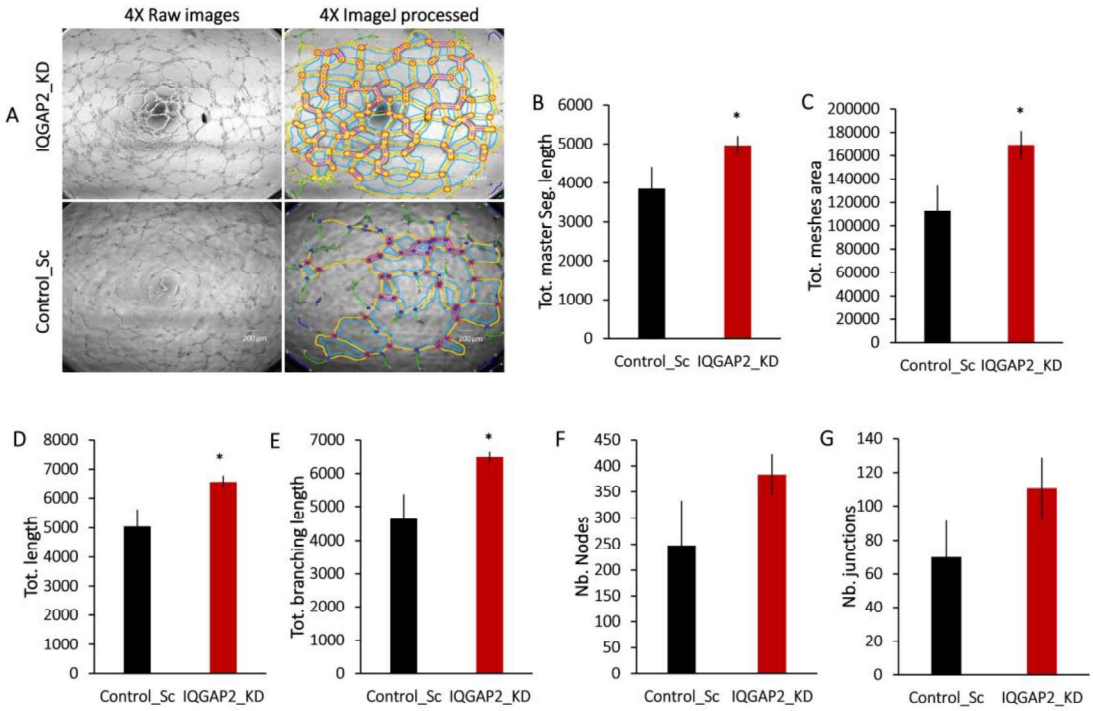

Figure 6.2.1.3.1. Reduced expression of IQGAP2 in MCF7 cells promotes tubule formation of HUVECs. A) Representative images of tubule formation in HUVECs treated with conditioned media of MCF7_IQGAP2_KD and MCF7_Control_Sc, (n = 3). The images on left side were captured with 4X objective lens. The images on right side are the representative skeletonised images after processing with Angiogenesis analyser, ImageJ software. Bar graph showing the difference in the following angiogenic parameters; **B)** master segment length of tubules (n = 3, 2-tailed unpaired t-test), **C)** meshes area of tubes (n = 3, 2-tailed unpaired t-test), **D)** total length of tubes (n = 3, 2-tailed unpaired t-test), **E)** total branching length of tubes (n = 3, 2-tailed unpaired t-test), **F)** branching nodes (n = 3, 2-tailed unpaired t-test), and **G)** number of junctions (n = 3, 2-tailed unpaired t-test). * represents $p \leq 0.05$. n represents experiment replicates.

The results showed that IQGAP2 knockdown significantly increased vessel network formation in MCF7 (Fig. 6.2.1.3.1A) which was evident by increased, total master segment length ($p \leq 0.05$, IQGAP2_KD - 4962 ± 230, Control_Sc - 3851.5 ± 546.60) (Fig. 6.2.1.3.1B), total meshe area ($p \leq 0.05$, IQGAP2_KD - 169253 ± 11483.31, Control_Sc - 112872 ± 21068.95) (Fig. 6.2.1.3.1C), total length of tube ($p \leq 0.05$, IQGAP2_KD - 6569.33 ± 193.89, Control_Sc - 5048 ± 555.08) (Fig. 6.2.1.3.1D) and total branching length of tubules ($p \leq 0.05$, IQGAP2_KD - 6569.33 ± 193.89, Control_Sc - 5048 ± 555.08) (Fig. 6.2.1.3.1E). Although, we did not observe a significant difference in number of nodes ($p \geq 0.05$, IQGAP2_KD - 383.66 ± 38.37, Control_Sc - 248 ± 83.43) (Fig. 6.2.1.3.1F), and number of junctions ($p \geq 0.05$, IQGAP2_KD - 110.33 ± 18.14, Control_Sc - 70 ± 21.21) (Fig. 6.2.1.3.1G) but a trend of increase was observed in the IQGAP2_KD group.

A similar trend of tubule formation was observed in HUVECs that were incubated with the conditioned media from MDA-MB-468_IQGAP2_KD group (Fig. 6.2.1.3.2A). The angiogenesis parameters like number of nodes ($p \leq 0.05$, IQGAP2_KD - 918.67 ± 197.41, Control_Sc - 437 ± 97.96) (Fig. 6.2.1.3.2B), number of junction ($p \leq 0.05$, IQGAP2_KD - 259.33 ± 47.54, Control_Sc - 122.67 ± 23.0) (Fig. 6.2.1.3.2C), total meshes area ($p \leq 0.05$, IQGAP2_KD - 1487994.5 ± 111150.82, Control_Sc - 383014 ± 284649.92) (Fig. 6.2.1.3.2D), total length of tube ($p \leq 0.01$, IQGAP2_KD - 31556.5 ± 2817.82, Control_Sc - 19036.33 ± 1532.40) (Fig. 6.2.1.3.2E), and total branching length of tubules ($p \leq 0.05$, IQGAP2_KD - 30834.5 ± 2939.44, Control_Sc - 17748 ± 2188.29) (Fig. 6.2.1.3.2F) were elevated in HUVECs cells supplemented with the conditioned media from MDA-MB-468_ IQGAP2_KD cells compared to the control. The difference in total master segment length of tubes was not significant but it showed trend similar to the above angiogenic

parameters ($p \geq 0.05$, IQGAP2_KD - 23892 ± 2641.75, Control_Sc – 10358 ± 840.04) (Fig. 6.2.1.3.2G).

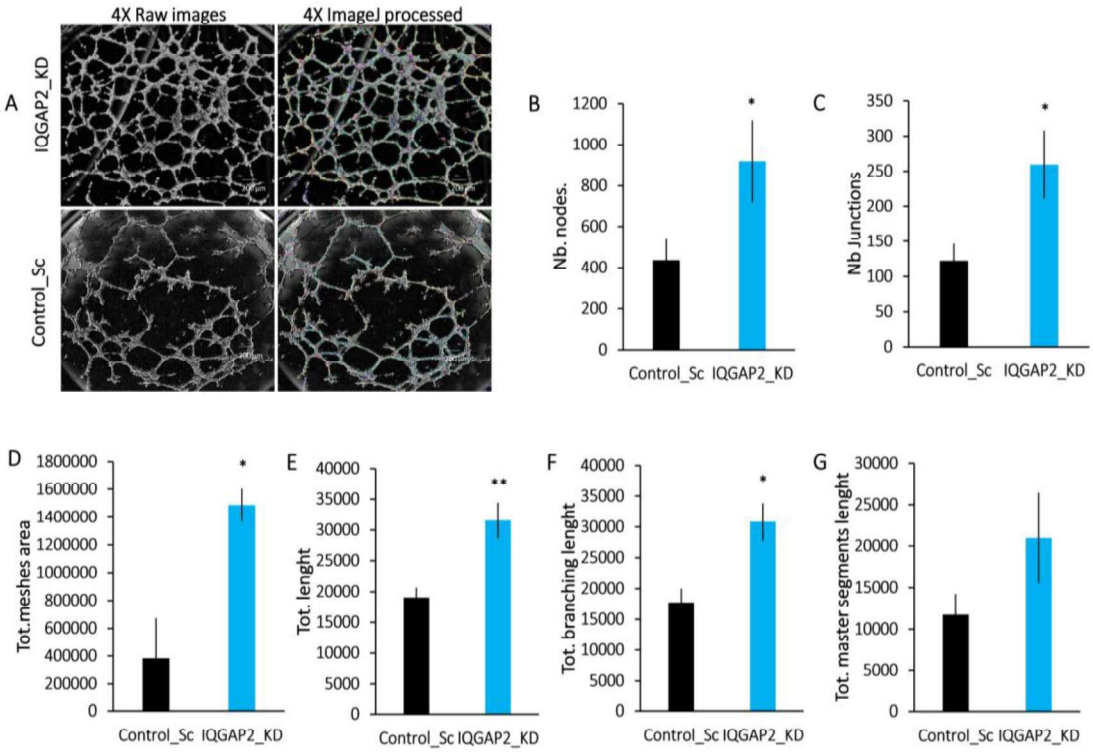

Figure 6.2.1.3.2. Reduced expression of IQGAP2 in MDA-MB-468 cells promotes tubule formation of HUVECs. A) Representative images of HUVECs tubule formation in response to conditioned media of MDA-MB-468_IQGAP2_KD and MDA-MB-468_Control_Sc, (n = 3). The images on left side were captured with 4X objective lens. The images on right side are the representative skeletonised images after processing with Angiogenesis analyser, ImageJ software. Bar graph showing the difference in the following angiogenic parameters; **B)** branching nodes (n = 3, 2-tailed unpaired t-test), **C)** number of junctions (n = 3, 2-tailed unpaired t-test), **D)** meshes area of tubes (n = 3, 2-tailed unpaired t-test), **E)** total length of tubes (n = 3, 2-tailed unpaired t-test), **F)** total branching length of tubes (n = 3, 2-tailed unpaired t-test) and, **G)** master segment length of tubules (n = 3, 2-tailed unpaired t-test). The results were considered significant at $p \leq 0.05$. * represents $p \leq 0.05$, ** represents $p \leq 0.01$.

As expected, fewer and smaller tubes were observed in HUVECS cells that were incubated with the conditioned media from MCF7_IQGAP2_Ex cells (Fig. 6.2.1.3.3A). The parameters of angiogenesis such as number of nodes ($p \leq 0.01$, IQGAP2_Ex - 234.66 ± 25.09, Control_EV - 388 ± 14.14) (Fig. 6.2.1.3.3B), number of junction ($p \leq 0.05$, IQGAP2_Ex - 69.67 ± 11.47, Control_EV - 113 ± 1.41) (Fig. 6.2.1.3.3C), total master segment length ($p \leq 0.001$, IQGAP2_Ex - 3469 ± 2.0, Control_EV - 5235 ± 69.30) (Fig.

6.2.1.3.3D), total meshes area ($p \leq 0.01$, IQGAP2_Ex - 76656.5 ± 1471.5, Control_EV - 170494 ± 12347.50) (Fig. 6.2.1.3.3E), total length of tube ($p \leq 0.01$, IQGAP2_Ex - 5563 ± 15, Control_EV - 6829.5 ± 153.44) (Fig. 6.2.1.3.3F) and total branching length of tubules ($p \leq 0.01$, IQGAP2_Ex - 4873 ± 81, Control_EV - 6662 ± 213.55) (Fig. 6.2.1.3.3G) were significantly reduced in tubule network of HUVECs cells supplemented with the conditioned media from MCF7_IQGAP2_Ex cells compared to the control.

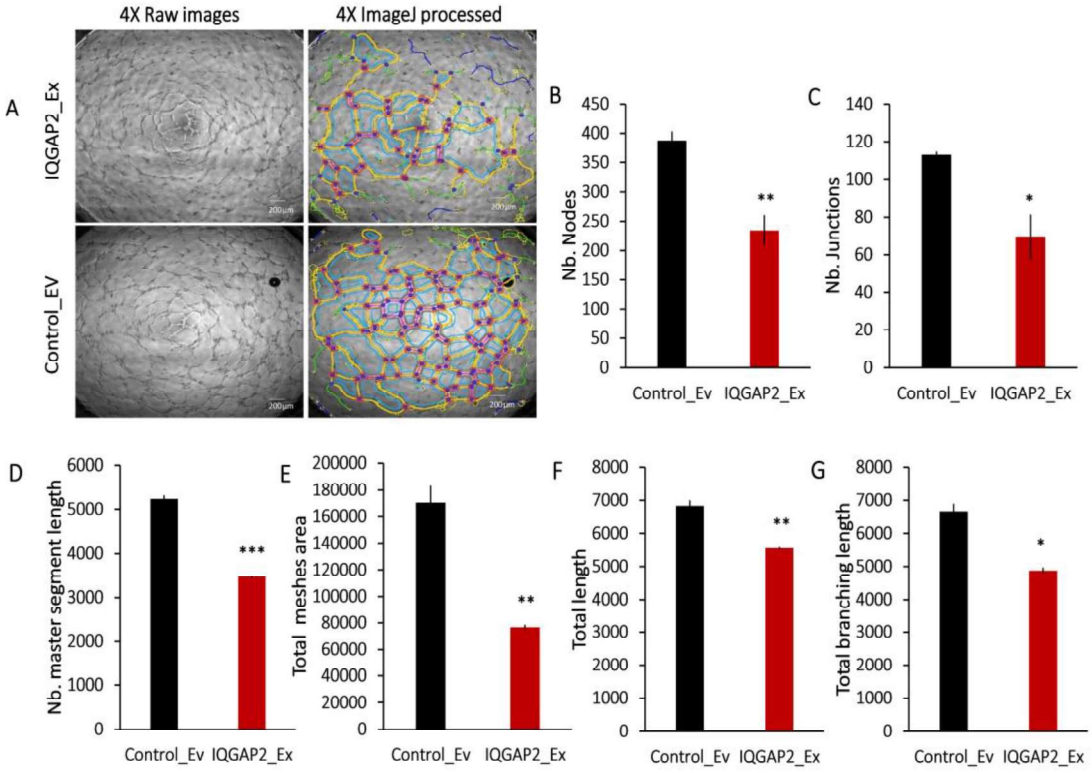

Figure 6.2.1.3.3. Increased expression of IQGAP2 in MCF7 cells reduces tubule formation of HUVECs. A) Representative images of HUVECs tubule formation in response to conditioned media of MCF7_IQGAP2_Ex and MCF7_Control_EV, (n = 3). The images on left side were captured with 4X objective lens. The images on right side are the representative skeletonised images after processing with Angiogenesis analyser, ImageJ software. Bar graph showing the difference in the following angiogenic parameters; **B)** branching nodes (n = 3, 2-tailed unpaired t-test), **C)** number of junctions (n = 3, 2-tailed unpaired t-test), **D)** master segment length of tubules (n = 3, 2-tailed unpaired t-test), **E)** meshes area of tubes (n = 3, 2-tailed unpaired t-test), **F)** total length of tubes (n = 3, 2-tailed unpaired t-test), and **G)** total branching length of tubes (n = 3, 2-tailed unpaired t-test). The results were considered significant at $p \leq 0.05$. * represents $p \leq 0.05$, ** represents $p \leq 0.01$, *** represents $p \leq 0.001$, n represents experiment replicates.

The results from above tubule formation assay, using the conditioned media from MCF7 and MDA-MB-468 cells, indicate that IQGAP2 reduction in breast cancer strongly activates the tubule formation ability of endothelial cells and favours angiogenesis.

6.2.2 Low IQGAP2 level in breast cancer cells enhances angiogenesis in ex-ovo model

To validate the *in vitro* findings of IQGAP2 in tumor angiogenesis, we performed Chick Chorioallantoic Membrane (CAM) assay.

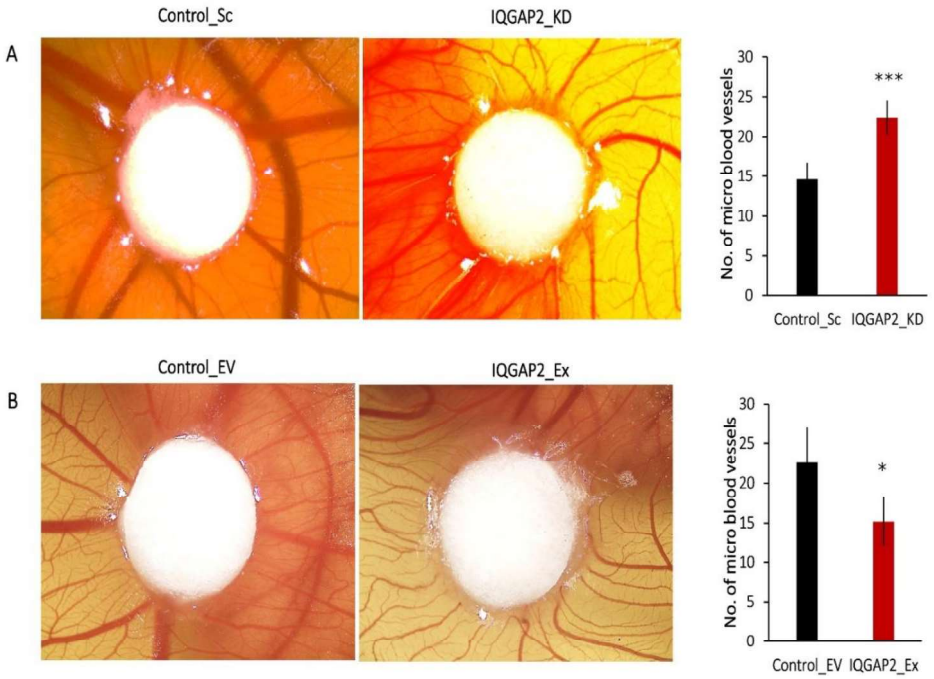

Figure 6.2.2.1. Low IQGAP2 level in breast cancer cells enhances angiogenesis in ex-ovo model system. A) The images of left show the number of blood vessels of the chorioallantoic membrane around the paper disc that was shocked with conditioned media from MCF7_IQGAP2_KD and MCF7_Control_Sc group (n = 5). The images were captured at day 13 using stereo microscope. The bar graph on the right showing the difference in number of micro blood vessels between the two groups (n = 5, 2-tailed unpaired t-test). **B)** The images of left show the number of blood vessels of the chorioallantoic membrane around the paper disc that was soaked with conditioned media of MCF7_IQGAP2_Ex and MCF7_Control_EV group (n = 5). The bar graph on the right showing the difference in number of micro blood vessels between the two groups (n = 5, 2-tailed unpaired t-test). The results were considered significant at $p \leq 0.05$. * represents $p \leq 0.05$, *** represents $p \leq 0.001$, n represents experiment replicates.

Here, we examined the microvessel count in CAM, which was supplemented with the conditioned media from MCF7_IQGAP2_KD, MCF7_IQGAP2_Ex and their respective control cells. The comparative analysis showed significantly higher number of microvessel count in CAM of MCF7_IQGAP2_KD compared to MCF7_Control_Sc ($p \leq 0.001$, IQGAP2_KD - 22.4 ± 2.07, Control_Sc - 14.6 ± 2.07) (Fig. 6.2.2.1A). In contrast, the number of microvessel count was significantly reduced in CAM supplemented with the CM from MCF7_IQGAP2_Ex compared to the control ($p \leq 0.05$, IQGAP2_Ex - 15.2 ± 3.03, Control_Sc - 22.6 ± 4.27) (Fig. 6.2.2.1B).

The results of CAM assay (animal system) indicate that reduction of IQGAP2 level increases the angiogenesis in breast cancer and hence support its inhibitory role in angiogenesis.

6.2.3 Reduced IQGAP2 expression in breast cancer cells enhances angiogenesis in *in vivo* model system

To further validate our *in vitro* and ex-ovo findings, we performed matrigel plug assay (MPA) in C57/BL6 mice. In this assays, a cocktail of reduced Matrigel and conditioned media from MCF7_IQGAP2_KD and MCF7_Control_Sc were injected into the right flank of C57/BL6 mice (6-8 weeks old). The plugs were removed on day 10 and images were captured. Further Haematoxylin and Eosin staining was carried out to check the number of blood vessels in plugs.

Matrigel plug assay directly shows the neo-vascularization potential of a molecule/ gene *in vivo*. Our results showed clearly visible increased vasculature in the Matrigel plugs which were supplemented with the MCF7_IQGAP2_KD conditioned media, on the other hand control plugs were almost transparent (Fig. 6.2.3.1A).

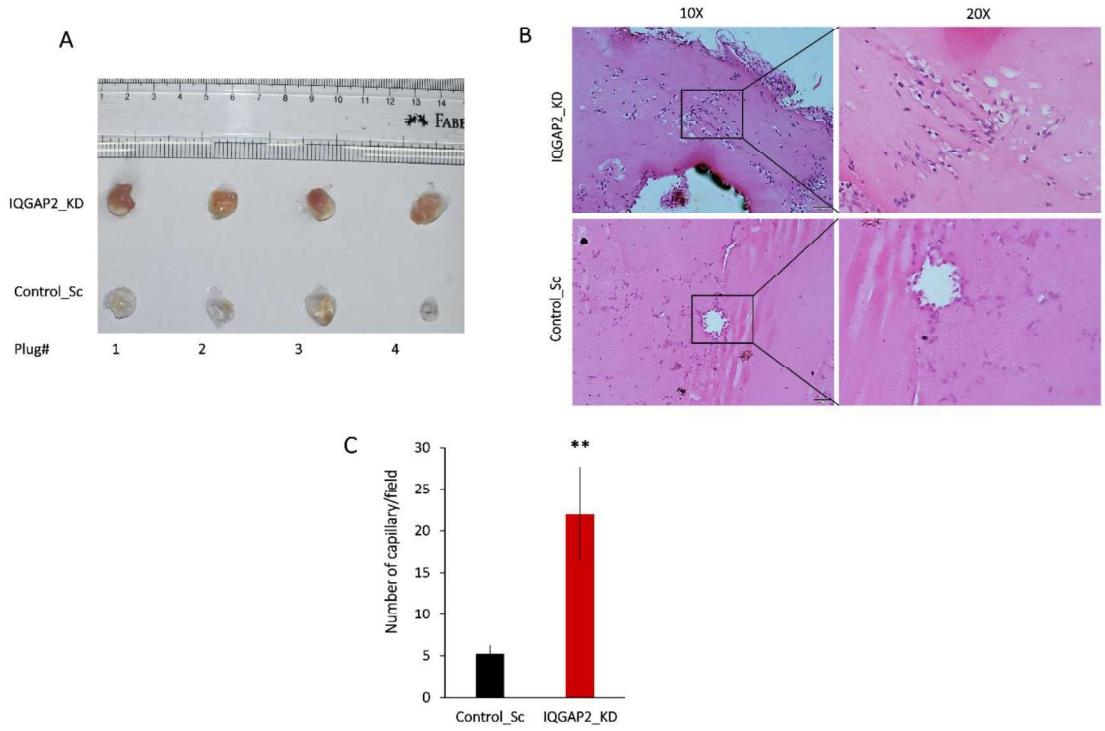

Figure 6.2.3.1 IQGAP2 inhibits angiogenesis in the Matrigel plug assay. Matrigel was mixed with the conditioned media from MCF7_IQGAP2_KD or MCF7_Control_EV. The Matrigel plugs were injected subcutaneously in the right flank of C57/BL6 mice. Ten days later, the plugs were harvested. **A)** Representative images showing the matrigel plugs taken from four mice of each treatment group. **B)** Representative Haematoxylin and Eosin images showing blood vessels formed in matrigel plugs. **C)** The bar graph showing statistical differences in the number of capillaries/ field formed in control and IQGAP2_KD groups (n = 4, 2-tailed unpaired t-test).

Further, Haematoxylin and Eosin staining showed significantly more number of blood vessels in Matrigel plugs which were supplemented with the conditioned media from MCF7_IQGAP2_KD groups compared to the control ($p \leq 0.01$, IQGAP2_KD - 22 ± 5.56, Control_Sc - 5.25 ± 0.95) (Fig. 6.2.3.1B, C).

6.2.4 Wound healing assay in mice supports the anti-angiogenic role of IQGAP2 in breast cancer

For further validation of our results, wound healing assay was also performed. Wound healing is a multi-step process, characterized by three overlapping phases: the inflammatory, proliferative, and the remodelling phase. In the inflammatory phase,

recruitment of neutrophils and macrophages takes place in wound area, where foreign particles, and damaged tissue phagocytosed by these cells [250, 251]. In the proliferative phase, the proliferation and movement of fibroblasts cells towards the wound area happens where they secrete new extracellular matrix (ECM), and form granulation tissue [251, 252]. In this step, epithelialization and angiogenesis take place that is characterised by the proliferation and migration of keratinocytes from the wound edges to the centre. Angiogenesis promotes blood supply to the newly formed tissue. In final remodelling phase collagen bundles increase in diameter and mature.

In this assay, a wound was created on the back skin of Balb/c mice and further it was treated with a cocktail of matrigel and conditioned media from MCF7_IQGAP2_KD and MCF7_Control_EV cells. A schematic of the wound formation is shown in Figure 6.2.4.1A The mice were euthanized on day 3, 6 and 9 and wound closure was measured. Further, H & E staining was carried out to check the epithelisation of wound area. The mouse treated with MCF7_IQGAP2_KD conditioned media show the gradual healing of wound which reached to complete closure by day 9 after injury. In control group, the complete wound closure was not observed on day 9. The wound size was lesser at day 3 ($p \leq 0.05$, unhealed wound area (%) - IQGAP2_KD - 61.4 ± 6.52, Control_Sc - 76.14 ± 4.70) and day 6 ($p \leq 0.05$, unhealed wound area (%) - IQGAP2_KD - 43.46 ± 11.91, Control_Sc - 65.0 ± 3.50) in mouse treated with MCF7_IQGAP2_KD conditioned media compared to MCF7_Control_Sc conditioned media (Fig. 6.2.4.1B, C).

Further, H & E analysis of tissue sections from wound area of mice showed more keratin layer accumulation in the epithelial layers, above the regenerating skin in MCF7_IQGAP2_KD conditioned media group compared to those treated with the conditioned media from MCF7_Control_Sc group (Fig. 6.2.4.1D).

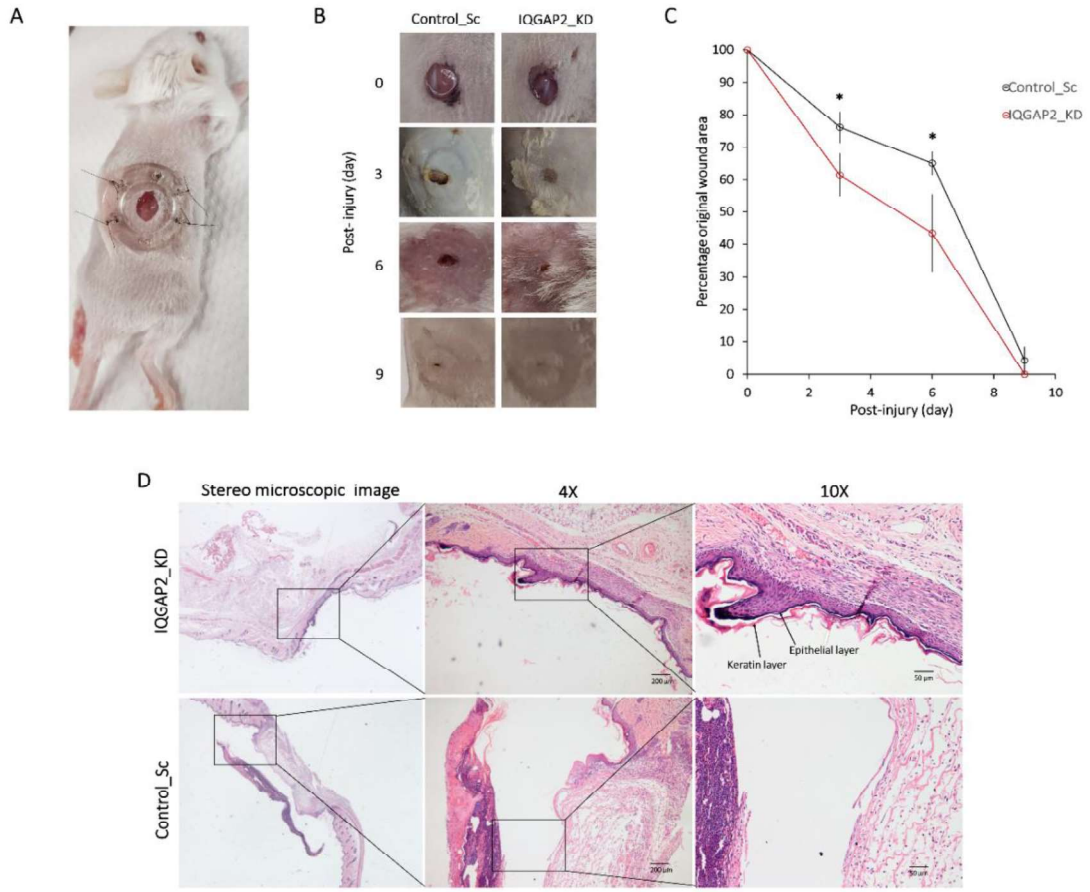

Figure 6.2.4.1. IQGAP2 reduction increases the wound healing process in mice. A) A representative image of wound created in the skin of mice (day 0). **B)** Representative photographs captured in IQGAP2_KD and Control_Sc treated mice groups showing the macroscopic wound closure on different days' post injury. **C)** Bar graph showing the difference in percentage of wound recovery between IQGAP2_KD and Control_Sc mouse group (n = 3, 2-tailed unpaired t-test). **D)** H & E staining showing the status of keratin layer with the epithelisation of wounded tissue in IQGAP2_KD and Control_Sc mice (day 6). The image of gross wound and normal area was taken with stereo microscope (left). The magnified images of wound area were taken at 4X (middle) and 10X objectives (right) in bright field microscope. The newly generated keratin and epithelial layer is shown with arrows at 10X magnified image (upper-right). Scale bar- 200 µm (4X), 50 µm (10X).

The results from this animal wound healing based assay, corroborate the anti-angiogenic role of IQGAP2 in breast cancer.

6.2.5 IQGAP2 expression levels negatively correlate with microvessel density in breast cancer tissues

After exploring the role of IQGAP2 using *in vitro*, ex-ovo and *in vivo* model systems, we explored the correlation of IQGAP2 expression with microvessel density (MVD), in breast cancer patient tissues. To achieve this, IHC of IQGAP2 and CD31 was performed in 188 archival, breast cancer FFPE tissue followed by calculation of Allred scoring for both the proteins.

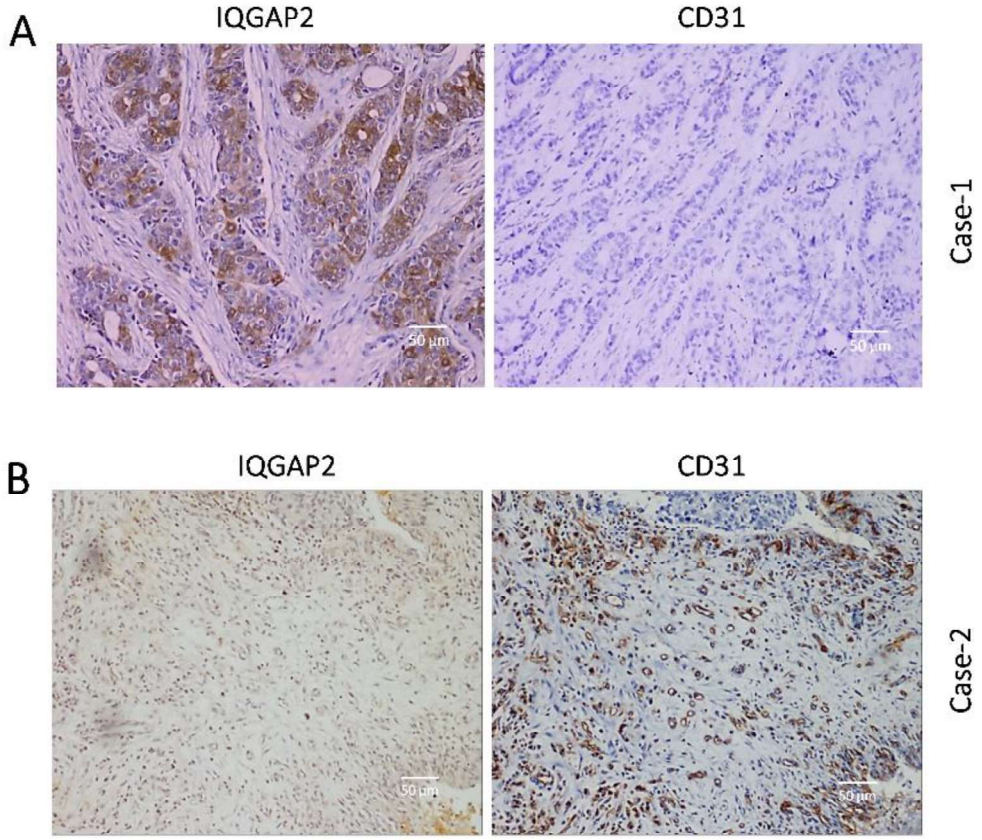

Figure 6.2.5.1. IQGAP2 and CD31 show inverse expression pattern in breast cancer. A) The representative IHC images showing the expression of IQGAP2 (left) and CD31 (right) in the tumor region of a low grade breast cancer tissue (Case-1). **B)** The representative IHC images showing the expression of IQGAP2 (left) and CD31 (right) in the tumor region of a high grade breast cancer tissue (Case-2). The images were captured using 10X objective of bright field upright microscope. Scale bar- 50 µm.

The visualisation of IQGAP2 and CD31 IHC images showed higher expression of IQGAP2 and low expression of CD31 in the tumorigenic region of the low grade breast cancer tissue (Fig. 6.2.5.1A). In contrast, low expression of IQGAP2 and higher expression of CD31 was observed in the tumorigenic region of high grade breast cancer tissues (Fig. 6.2.5.1B).

The microscopic examination of IQGAP2 and CD31 IHC images showed an inverse expression pattern in tumor tissues.

Further, IQGAP2 expression level and MVD count were categorised into two groups (low or high) depending on Allred score of IQGAP2 and, MVD count in tumor region. Chi-square test between IQGAP2 and MVD was performed.

Table 6.2.5.1. Association between the expression of IQGAP2 and MVD in breast cancer patients*

	MVD low	**MVD high**	**Total**
IQGAP2 low	47	88	135
IQGAP2 high	46	7	53
Total	93	95	188
$\chi 2 = 41.13, p \leq 0.0001$			

Chi-square test*

The analysis showed that patient with low IQGAP2 expression had significantly higher MVD (88/135, 65.1%) compared to those with high IQGAP2 expression (7/53, 13.2%) ($p \leq 0.0001$) (Table 6.2.5.1). To further examine a negative or positive correlation between the two, Pearson correlation analysis between IQGAP2 expression and MVD was performed. The analysis showed a significant negative correlation between MVD and IQGAP2 expression in breast cancer ($r = -0.31$, $n = 188$, p-value ≤ 0.0001) (Fig. 6.2.5.2).

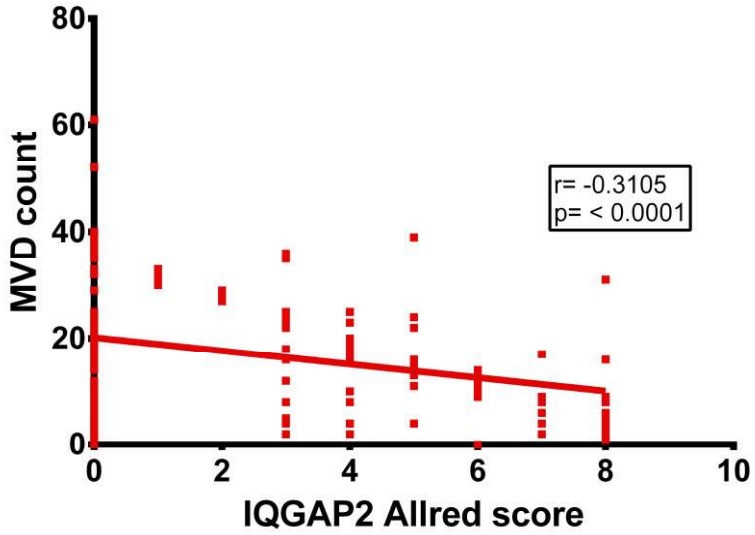

Figure 6.2.5.2. IQGAP2 negatively correlates with micro blood vessel density in breast cancer patient tissues. Graph showing results of Pearson correlation analysis between IQGAP2 and MVD count in breast cancer clinical samples. The analysis indicates a significant negative correlation between IQGAP2 and MVD in tumor region of breast cancer patients ($r = -0.31$, $n = 188$, $p \leq 0.0001$). Here, X-axis represents the MVD count in tumor region of breast cancer patients and Y-axis represents the Allred score of IQGAP2 in tumor region of breast cancer patients.

These results show an inverse correlation between the expression of IQGAP2 and MVD in breast cancer patient. These results also validate anti-angiogenic activity of IQGAP2 observed in our *in vitro* and animal based results.

6.2.6 Reduced IQGAP2 expression in breast cancer cells increases the levels of pro-angiogenic factors

To find out the molecular mechanism behind the effect of IQGAP2 on angiogenesis, we first inspected the expression level of key regulatory cytokines in MCF7_IQGAP2_Ex, MDA-MB-468_IQGAP2_KD and their respective control cells. Angiogenesis is induced by a milieu of pro-angiogenic cytokines or chemokines including IL-1, IL-6, IL-8, CCL1, CCL2, CCL3, CCL9, CCL11 and growth factors like VEGF, TGF-β, tumor necrosis factor (TNF)-α [253]. We checked the status of these angiogenic regulators by qRT-PCR in MCF7_IQGAP2_Ex and MDA-MB-468_IQGAP2_KD cells. In our study, the analysis

of cytokines and chemokines data revealed a decrease in the expression levels of IL-6, IL-8 and CCL2 in MCF7_IQGAP2_Ex compared to the control. In contrast, depletion of IQGAP2 level in MDA-MB-468 cells resulted in an increased expression of IL6, CCL2, CCL3 and CCL11 (Figure 5.2.12.1 of chapter 1). Further the analysis of pro-angiogenic growth factor including VEGF-A, VEGF-C, VEGF-D, TGF-β, TNF-α were carried out in MCF7 and MDA-MB468. The analysis did not show any significant difference in the expression of these pro-angiogenic growth factor except VEGF-A.

The expression level of VEGF-A was high in MCF7_IQGAP2_KD group compared to its control ($p \leq 0.01$, fold change = 1.78 ± 0.13) (Fig. 6.2.6.1A), whereas an opposite expression pattern of VEGF-A was observed with MCF7_IQGAP2_Ex compared to its control ($p \leq 0.001$, fold change = 0.23 ± 0.03) (Fig. 6.2.6.1B). The qRT-PCR data did not show a significant expression change of VEGF-A in MDA-MB-468_IQGAP2_KD ($p \geq 0.05$, fold change = 0.99 ± 0.02) (Fig. 6.2.6.1C).

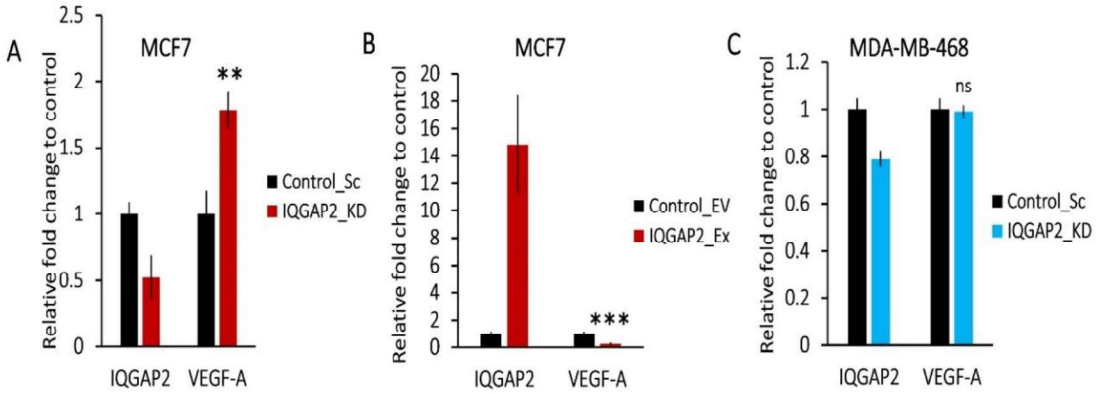

Figure 6.2.6.1. Low IQGAP2 expression in breast cancer cells increases the mRNA levels of VEGF-A. The bar graph representing the relative fold change in the mRNA level of VEGF-A in- **A)** MCF7_IQGAP2_KD group compared to the MCF7_Control_Sc group (n = 3, 2-tailed unpaired t-test). **B)** MCF7_IQGAP2_Ex group compared to the MCF7_Control_EV group (n = 3, 2-tailed unpaired t-test). **C)** MDA-MB-468_IQGAP2_KD group compared to the MDA-MB-468_Control_Sc group (n = 3, 2-tailed unpaired t-test). ** represents $p \leq 0.01$, *** represents $p \leq 0.001$.

In tumor angiogenesis, VEGF is secreted from the tumor cells in the local environment and binds to the specific receptor present on the surface of endothelial cells that ultimately stimulate the angiogenic signal cascade. Therefore, we inspected the level of secreted VEGF-A in the conditioned media of MCF7_IQGAP2_KD and MDA-MB-468_IQGAP2_KD cells using VEGF-A ELISA kit.

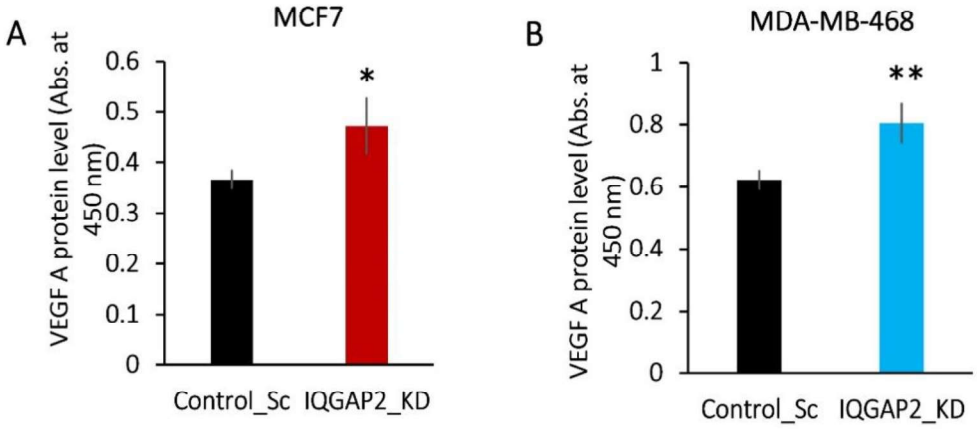

Figure 6.2.6.2. Reduced IQGAP2 expression in breast cancer cells increases the secreted protein levels of VEGF-A. A) The bar graph showing the protein level of VEGF-A in the conditioned media of MCF7_IQGAP2_KD and MCF7_Control_Sc groups. **B)** The bar graph showing the protein level of VEGF-A in the conditioned media of MDA-MB-468_IQGAP2_KD and MDA-MB-468_Control_Sc groups. Here, X-axis represents the IQGAP2_KD and Control_Sc groups, Y-axis represents the absorbance of ELISA reaction mix at 450nm. * represents $p \leq 0.05$, ** represents $p \leq 0.01$, n represents experiment replicates.

The analysis of ELISA results showed an elevated expression level of VEGF-A in the conditioned media of MCF7_IQGAP2_KD compared to the MCF7_Control_Sc group ($p \leq 0.05$, OD_{450nm} IQGAP2_KD - 0.47 ± 0.05, Control_Sc - 0.37 ± 0.01) (Fig. 6.2.6.2A). Similarly, the protein level of VEGF-A was also significantly enhanced in the conditioned media of MDA-MB-468_IQGAP2_KD cells compared to the MDA-MB-468_Control_Sc group ($p \leq 0.01$, OD_{450nm} IQGAP2_KD - 0.80 ± 0.06, Control_Sc - 0.62 ± 0.029) (Fig. 6.2.6.2B).

These results suggest that the depletion of IQGAP2 level in breast cancer cells increases the expression of pro-angiogenic cytokines (IL-6, IL-8), chemokines (CCL2, CCL-3, CCL-11) and growth factors like VEGF-A that may activate the angiogenesis event.

6.2.7 Reduced IQGAP2 level in breast cancer cells induces angiogenesis through VEGF-A-VEGFR2-AKT axis

To examine the signaling pathway involved in HUVECs in response to expression changes of IQGAP2 in breast cancer cells, the conditioned media from MCF7_IQGAP2_KD and MCF7_IQGAP2_Ex along with their control cells were applied to HUVECs. Protein lysates were prepared post 24 hours of incubation followed by Western blot for key angiogenic molecules of endothelial cells. VEGF is the primary pro-angiogenic growth factor that binds to the tyrosine kinase VEGF receptors (VEGFRs) and activates the angiogenic downstream signaling pathways by ERK or AKT mediated signaling. Till date, many VEGFs have been identified (VEGF-A, VEGF-B, VEGF-C and VEGF-D) that interact with different VEGF receptors such as VEGFR1, VEGFR2 and VEGFR3. Among all, the VEGF-A/VEGFR-2 angiogenesis signaling is the most prominent signaling cascade that regulate the angiogenesis process in endothelial cells [254].

Since, our qRT-PCR and ELISA results show a change in VEGF-A level, we checked the status of phosphorylated form of its primary receptor, VEGFR2 in HUVECs. The Western blot results showed a reduced expression level of phospho-VEGFR2 in HUVECs supplemented with the conditioned media of MCF7_IQGAP2_Ex cells as compared to the HUVECs treated with respective control conditioned media (Fig. 6.2.7.1A). As expected, the expression of phospho-VEGFR2 increased in HUVECs supplemented with

the conditioned media from MCF7_IQGAP2_KD cells compared to those supplemented with the conditioned media from MCF7_Control_Sc cells (Fig. 6.2.7.1B).

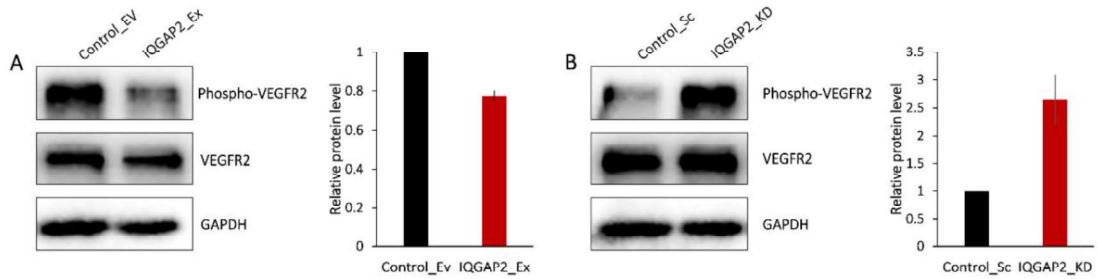

Figure 6.2.7.1. Reduced IQGAP2 expression in breast cancer cells increases the protein levels of phospho-VEGFR2 in HUVECs. A) Western blot images showing the expression of phospho-VEGFR2, total-VEGFR2 and GAPDH in MCF7_IQGAP2_Ex and MCF7_Control_EV cell groups. Here, the Western blot shows a decrease in phospho-VEGFR2 protein level in MCF7_IQGAP2_Ex group compared to the control. **B)** Western blot images representing the protein level of phospho-VEGFR2, total-VEGFR2 and GAPDH in MCF7_IQGAP2_KD and MCF7_Control_Sc cell groups. The Western blot results show an elevated protein level of phospho-VEGFR2 in MCF7_IQGAP2_KD group compared to the control. Here, GAPDH has been used as the loading control.

Further, we examined the primary downstream key molecules of VEGFR2 in endothelial cells, ERK and AKT. It is well reported that the activation of VEGFR2 leads to the phosphorylation of ERK and/or AKT molecules that ultimately increases the proliferation, migration and tubule formation ability of endothelial cells.

The analysis of Western blots showed a reduction of phospho-AKT^{473} in HUVECs cells supplemented with the conditioned media from MCF7_IQGAP2_Ex compared to those supplemented with the conditioned media from MCF7_Control_Ev (Fig. 6.2.7.2A). Concurrently, the HUVECs supplemented with the conditioned media from MCF7_IQGAP2_KD showed an elevated expression level of phospho-AKT^{473} compared to HUVECs supplemented with the conditioned media from MCF7_Control_Sc cells (Fig. 6.2.7.2B). We did not observe a change in protein levels of phospho-AKT^{308} or

phospho-ERK1/2 in HUVECs cells supplemented with the conditioned media from MCF7_IQGAP2_Ex (Fig. 6.2.7.2C, E) or MCF7_IQGAP2_KD cells (Fig. 6.2.7.2D, F).

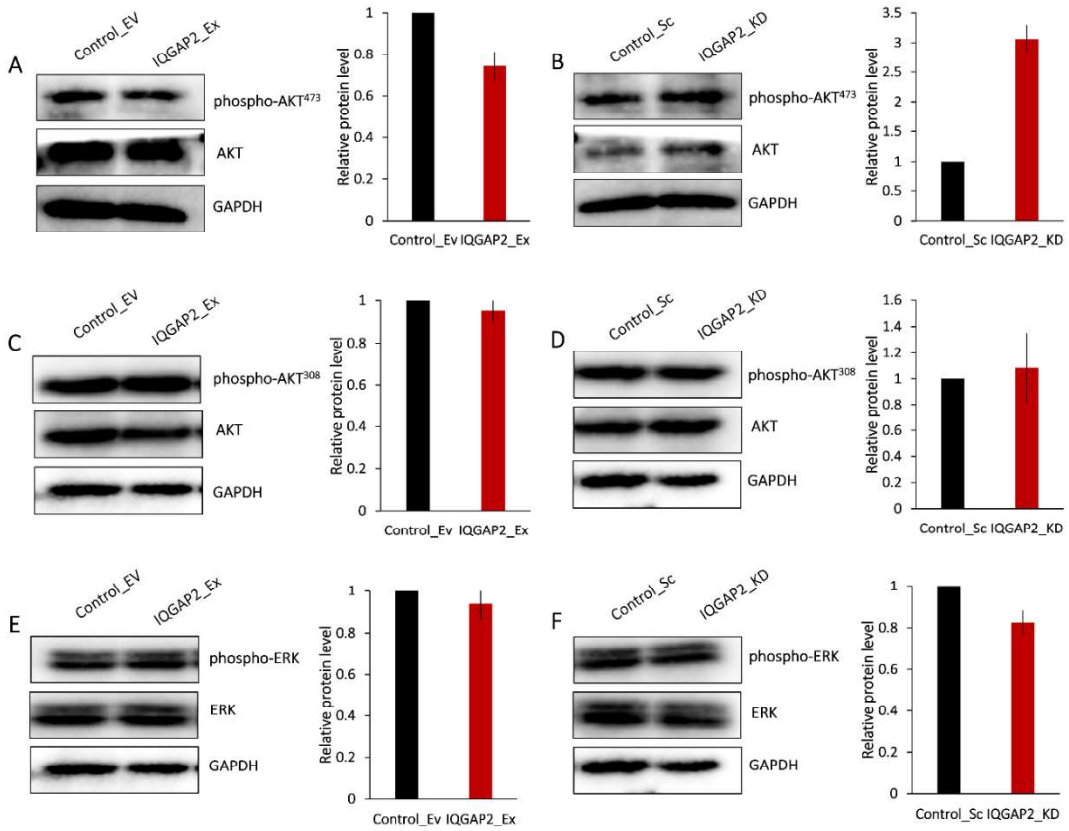

Figure 6.2.7.2. Reduced IQGAP2 expression in breast cancer cells induces phospho-AKT^{473} levels in HUVECs. A) Western blot images displaying the expression levels of phospho-AKT^{473}, total-AKT and GAPDH in MCF7_IQGAP2_Ex and MCF7_Control_EV cells group. **B)** Western blot images showing the protein levels of phospho-AKT^{473}, total-A and GAPDH in MCF7_IQGAP2_KD and MCF7_Control_Sc cells group. **C)** Western blot images representing the expression level of phospho-AKT^{308}, total-AKT and GAPDH in MCF7_IQGAP2_Ex and MCF7_Control_EV cells group. **D)** Western blot images showing the protein levels of phospho-AKT^{308}, total-AKT and GAPDH in MCF7_IQGAP2_KD and MCF7_Control_Sc cells group. **E)** Western blot images representing the expression level of phospho-ERK, total-ERK and GAPDH in MCF7_IQGAP2_Ex and MCF7_Control_EV cells group. **F)** Western blot images showing the protein level of phospho-ERK, total-ERK and GAPDH in MCF7_IQGAP2_KD and MCF7_Control_Sc cells group. Here, GAPDH is used as the loading control.

From the above results we imply that the reduction of IQGAP2 level in breast cancer cells promote the release of VEGF-A that binds and phosphorylates VEGFR2 receptor present

on the membrane of endothelial cells; this results in the activation of VEGFR2 mediated angiogenic signaling in endothelial cell through phospho-AKT^{473}.

Finally, to confirm whether IQGAP2 affects angiogenesis through VEGF-A-VEGFR2-AKT axis, we treated HUVECs (growing with the conditioned media of MCF7_IQGAP2_KD) cells with VEGFR2 inhibitor or its vehicle control (DMSO). After addition of these agents, the expression level of VEGFR2 and phospho-AKT^{473} in HUVECs were analysed using Western blot. The addition of VEGFR2 inhibitor resulted in the inhibition of VEGFR2 receptor in HUVECs cells and subsequently a decrease in phospho-AKT^{473} level. On the other hand, the HUVECs cells cultured with the vehicle control, DMSO did not show any change in the expression level of VEGFR2 or phospho-AKT^{473} in HUVECs. (Fig. 6.2.7.3).

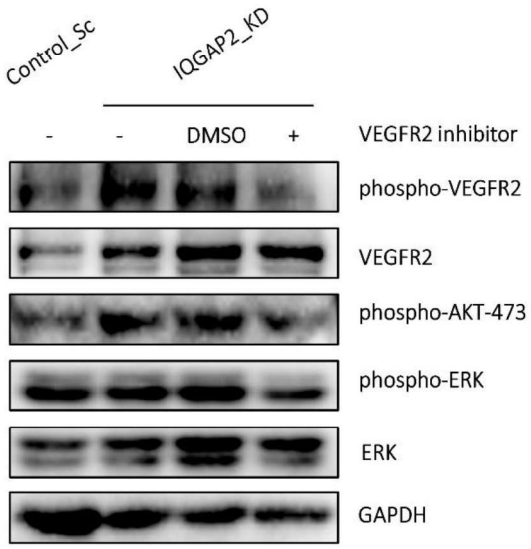

Figure 6.2.7.3. IQGAP2 affects breast cancer angiogenesis through VEGFR2 receptor. The Western blot images showing the expression levels of phospho-VEGFR2, total-VEGFR2, phospho-ERK, total-ERK and, phospho-AKT^{473} in HUVECs treated with CM from MCF7 cells with IQGAP2 perturbation. GAPDH was used a loading control.

The results were further, validated by tubule formation assay. Here, we observed that inhibition of VEGFR2 in HUVECs cells supplemented with VEGFR2 inhibitor and conditioned media from MCF7_IQGAP2_KD drastically reduced the tubule formation

ability of HUVECs compared to those supplemented with the vehicle control and conditioned media from MCF7_IQGAP2_KD cells (Fig. 6.2.7.4). The results obtained from VEGFR2 inhibition in HUVECs indicate that IQGAP2 depletion increases the angiogenic process of breast cancer by VEGF-A-VEGFR2 axis.

So from all the above results we conclude that IQGAP2 depletion in breast cancer cells increases the angiogenic properties (proliferation, migration and tubule formation) of nearby endothelial cells. The data from animal experiment like CAM assay, Matrigel plug assay and wound healing assay further support the anti-angiogenesis property of IQGAP2 in breast cancer.

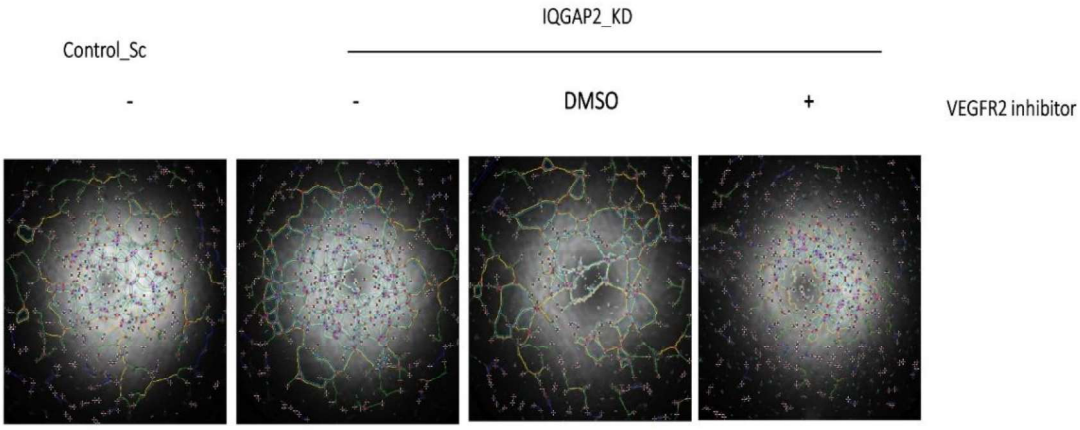

Figure 6.2.7.4. IQGAP2 modulates breast cancer angiogenesis specifically through VEGFR2 receptor. The tubule formation assay images showing the status of tubes in HUVECs after treatment with VEGFR2 inhibitor or vehicle control in MCF7_IQGAP2_KD background. These images are the representative images of tubules post processing in Angiogenesis analyser software, ImageJ analyser Here, the tubule formation assay results indicating the reduction of tube network in HUVECs supplemented with VEGFR2 inhibitor and conditioned media from IQGAP2_KD.

The inverse correlation of IQGAP2 expression with the MVD in breast cancer patients further support these findings. The mechanistic studies highlighted that IQGAP2 reduction increases the expression of certain cytokines/ chemokines and VEGF-A growth factor in tumor cells and activates VEGFR2 receptor, present on the membrane of

endothelial cells, in tumor microenvironment. Finally, activation of VEGFR2 leads to angiogenesis cascade through phospho-AKT^{473} axis.

6.3 Discussion

The growth and aggressiveness of breast cancer is supported by different molecular processes including angiogenesis. Angiogenesis helps tumor cells to survive by providing nutrients and oxygen [241]. This process is balanced by numerous angiogenic activators and inhibitors; tripping of the "angiogenic switch" feeds tumor. Anti-angiogenic therapy primarily targets the angiogenic activators to minimise their effect in angiogenesis [255, 256]. In recent years, the development and use of anti-angiogenic inhibitors have attracted much attention, in which VEGF-A and VEGFR inhibitors are on the top among all the approved angiogenesis inhibitors in human cancers [257-259].

Despite VEGF-targeted cancer therapy have shown a promising clinical success, these do not respond to patients having intrinsic resistance or patients acquire resistance for them during the course of treatment [260]. It has been observed that tumor cells find some alternate ways and activate oncogenic signals to escape from the effect of anti-VEGF drugs. For instance, resistance against VEGF therapy occurred due to activation of MAPK, EGFR and AKT mediated oncogenic signaling [261-264]. Therefore, the drugs targeting these pathways would be more beneficial in patients having resistance against the anti-VEGF therapy.

In the first section of our study, we observed the tumor suppressive role of IQGAP2 in breast cancer and its association with the invasiveness of the clinical specimen. The invasiveness of breast cancer is a cumulative effect of EMT and angiogenesis. In previous chapter we could establish that IQGAP2 decreases breast cancer invasiveness by effecting the EMT process via ERK pathway. This pathway is established to promote angiogenesis

via VEGF-A activation [265, 266]. Therefore, we explored the role of IQGAP2 in angiogenesis process.

In the present study, we found that IQGAP2 depletion significantly increased angiogenesis *in vitro*, *in vivo* and ex-ovo, in a paracrine manner. The elevated expression of IQGAP2 strongly decreased VEGF-A level in breast cancer cells and subsequently the phosphorylation of VEGFR2 in endothelial cells and vice-versa. These findings indicate that IQGAP2 could regulate tumor angiogenesis by controlling the activation of VEGF-A/ VEGFR2 signaling. A reduction in the activation of AKT, but not ERK, was observed, which explained the anti-angiogenic paracrine effects of IQGAP2 on endothelial cells.. The activation of AKT pathway promotes several key endothelial cell (EC) functions, including migration, cell growth and survival [267, 268]. In breast cancer patients, microvessel density, which is a direct indicator of tumor vascularisation and often significantly associated with survival outcome [269], was found to be negatively associated with IQGAP2 protein levels, highlighting the clinical significance of IQGAP2 in breast tumor neovascularisation.

It is noteworthy that the role of IQGAP1 is well established in angiogenesis. In previous reports it was found that the elevated expression of IQGAP1 in Esophageal squamous cell carcinoma (ESCC) increases the VEGF-A level and induces angiogenesis process by activating VEGFR2 mediated AKT and ERK signaling in endothelial cells [54]. The direct role of IQGAP1 in proliferation and migration of endothelial cells was also established by Yamaoka et al., 2006 [55] and Meyer R et al., 2008 [53], and suggested as an attractive anti-angiogenesis target in cancer treatment.

It is very important to note that we have observed an opposite function of IQGAP2 and IQGAP1 in breast cancer where former restricts IQGAP1 mediated ERK pathway.

Interestingly, they share a common signaling pathway where one activates VEGF-A-VEGFR2 pathway of angiogenesis and another restricts the same, the possibilities of interplay between IQGAP1 and IQGAP2 in breast cancer angiogenesis cannot be overlooked. Therefore, controlling IQGAP2 could be very promising effect in tumor angiogenesis, because of its role in suppressing the VEGF-VEGFR2 signaling cascade, as well as the negative effect on the transcript levels of other pro-angiogenic factors, which assume more significant roles in promoting neovascularisation in an *in vivo* setting.

In summary, we have shown that IQGAP2 inhibits angiogenesis in breast cancer by targeting the VEGF-VEGFR2-AKT signaling pathway. Our study demonstrated that IQGAP2 could regulate angiogenesis in breast cancer via tumor-stromal interactions, further highlighting the benefits associated with targeting IQGAP2 for breast cancer treatment.

CHAPTER 3

To find out the relative differential expression pattern of IQGAP2 and IQGAP3 in cancers

Findings of this chapter is published.

Kumar, D., Hassan, M. K., Pattnaik, N., Mohapatra, N., & Dixit, M. (2017). Reduced expression of IQGAP2 and higher expression of IQGAP3 correlates with poor prognosis in cancers. PLOS ONE, 12(10), e0186977.

7.1 Introduction

Findings in the previous chapter prompted us to look at the expression levels of IQGAP2 in different cancers. In past years, IQGAP1 has attracted much attention with regards to its involvement in carcinogenesis [14]. As opposed to IQGAP1, studies investigating the contribution of IQGAP2 in the onset and progression of different cancers are very limited. The third IQGAP member, IQGAP3 is misexpressed at the mRNA or protein level in certain cancers. IQGAP3 has been found to be overexpressed in lung [33], liver [270], breast [48] and pancreatic cancers [37]. These pioneering studies revealed that apart from IQGAP1 and IQGAP2, the third member, IQGAP3 is also involved in multiple cancers. Moreover, the role of relative expression level of IQGAP1 and IQGAP2 has been reported in HCC.

This is very interesting to note that despite structural similarity between IQGAP2 and IQGAP3, these isoforms show tissue specific expression and perform opposite functions. For instance, 1) IQGAP2 expresses predominantly in liver tissue whereas IQGAP3 expression is very limited in liver [16]. 2) IQGAP2 restricts the growth and spread of HCC [38], IQGAP3 promotes these event in HCC [270]. 3) while, low IQGAP2 level promotes invasion of gastric cancer cells [40], depletion of IQGAP3 level reduces the growth and spheroid formation in the same [271]. 4) IQGAP2 restricts the cancerous properties of ovarian tumor lines [42] whereas these cancerous properties get activated with increased level of IQGAP3 [35].

These examples indicate the possibility of contrasting role of both the isoforms in cancers. The status of the relative expression of these isoforms in same tumor tissue may serve as a prognostic marker. So far, no report is available that has extensively investigated the relative expression of these two isoforms. Therefore, in addition to finding the expression

pattern of IQGAP2 across multiple cancers, a thorough analysis of the association of mRNA levels of IQGAP3 was also carried out. In this chapter, we have undertaken a pan-cancer approach for analysing transcript levels of IQGAP2 and IQGAP3 using public mRNA databases (Oncomine and TCGA). These findings were further confirmed by immunohistochemistry in cancers of prostate, colorectal, stomach and brain. We also checked the genomic alteration and, carried out analysis of promoter methylation for IQGAP2 and IQGAP3 using cBioportal and Wanderer web tool, respectively. Further, we examined the prognostic significance of these factors in different cancer types with the help of survival data available in Kaplan-Meier Plotter (KM Plotter) and SurvExpress databases.

7.2 Results

7.2.1 IQGAP2 and IQGAP3 expression in different cancers

Initially, the differential transcript level of IQGAP2 and IQGAP3 in cancer and normal regions of different cancers types was examined by Oncomine database (Fig. 7.2.1.1). The results of the Oncomine analysis displayed a total of 354 and 192 unique analyses for IQGAP2 and IQGAP3 respectively. Further analysis with following parameters (p-value ≤ 0.01, fold change ≥ 2 fold, gene rank $\leq 10\%$) showed a significant change in 69 and 16 analyses/ studies for IQGAP2 and IQGAP3 respectively.

In case of IQGAP2, only 27 analyses displayed higher mRNA expression in cancer, while more analyses (42 analyses) showed a reduced transcript levels of the same in cancer. In case of IQGAP3, all 16 analyses (including breast cancer, bladder cancer, oesophageal cancer, colorectal cancer, liver cancer and lung cancer) displayed higher mRNA expression of IQGAP3 in tumor, as compared to normal tissue.

The detailed analysis of the expression pattern of IQGAP2 and IQGAP3 and their association with the survivability of the cancer patients of different types have been shown under the following headings;

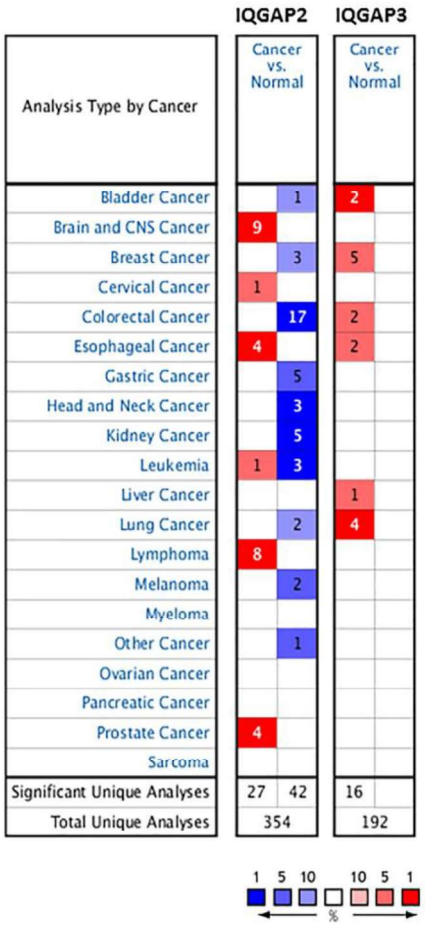

Figure 7.2.1.1. The mRNA expression patterns of IQGAP2 and IQGAP3 in cancers. Differences in the transcript level, between cancer and normal tissues, were investigated using Oncomine with following parameters, p-value ≤ 0.01, fold change ≥ 2 fold, gene rank ≤ 10%. The coloured values denote total analyses count satisfying the set thresholds. The red colour specifies elevated transcript levels of the genes and blue colour indicates decreased transcript level of gene in tumor tissues compared to normal. Here, colour depth signifies the gene rank. The darker colour indicate higher score for the analysis.

7.2.2 Lung cancer

Lung cancer is categorised into small cell lung cancer (SCLC), lung carcinoid tumor and non-small cell lung cancer (NSCLC). Among all, NSCLC is the most common (85%), which is further divided into lung squamous cell carcinoma (LUSC, 25–30% of lung

cancers), large cell lung carcinoma, (LCLC, 10% of lung cancers) and lung adenocarcinoma (AC, 40% of lung cancers). The other two lung cancer types, lung carcinoid tumor (5%) and SCLC (10-15%) are less frequent.

7.2.2.1 The expression levels of IQGAP2 and IQGAP3 in lung cancer

The analysis of expression pattern between normal and cancer tissues from Oncomine database showed a significant change in transcript levels of IQGAP2 and IQGAP3 in lung cancer subtypes in different datasets. Reduced IQGAP2 mRNA level was observed in lung carcinoid tumor (fold change = -4.96) and lung adenocarcinoma (fold change = -2.60) in Bhattacharjee lung dataset [272] (Fig. 7.2.2.1.1A).

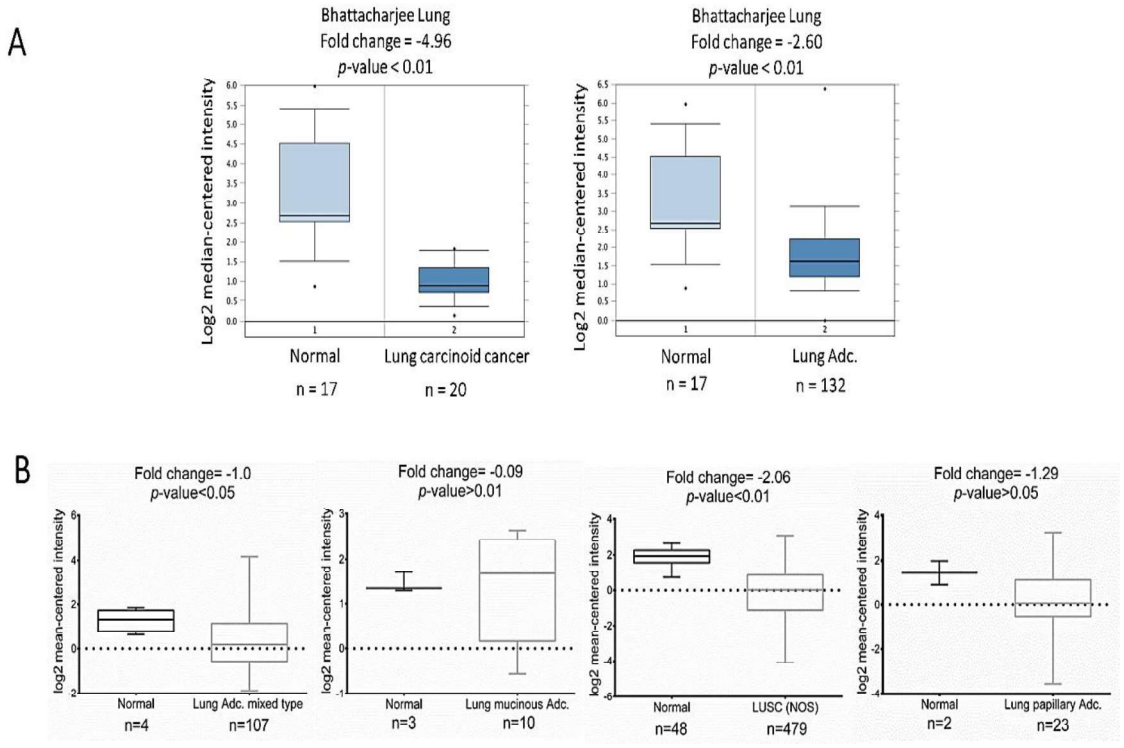

Figure 7.2.2.1.1 The mRNA level of IQGAP2 in lung cancer subtypes. A) Box and whisker plots showing the transcript level of IQGAP2 in lung cancer subtypes from Oncomine database. **B)** IQGAP2 expression in lung cancer subtypes from TCGA database has been shown as box and whisker plots. Here, X-axis denotes normal vs cancer group, Y-axis denotes mRNA expression of IQGAP2 in log2 median/mean centred intensity. The middle line represents the median value. A two-tailed Student's t-test was carried out to ascertain the statistical differences of expression between normal and cancerous region of lung cancer patients.

Additionally, analysis of TCGA-LUNG dataset, showed a significantly reduced IQGAP2 expression in lung adenocarcinoma mixed type (fold change = -1.0) and in lung squamous cell carcinoma (fold change = -2.06). No significant difference in IQGAP2 expression was observed between normal and cancer tissues in papillary adenocarcinoma and mucinous cell lung carcinoma (Fig. 7.2.2.1.1B).

In contrast, elevated IQGAP3 transcript level was observed in SCLC (fold change = 2.91), LCLC (fold change = 3.81), lung adenocarcinoma (fold change = 3.2) and LUSC (fold change = 2.67) (Fig. 7.2.2.1.2A) in Garber dataset (26). In agreement with these Oncomine results, an elevated expression level of IQGAP3 was also observed in the TCGA datasets (Fig. 7.2.2.1.2B).

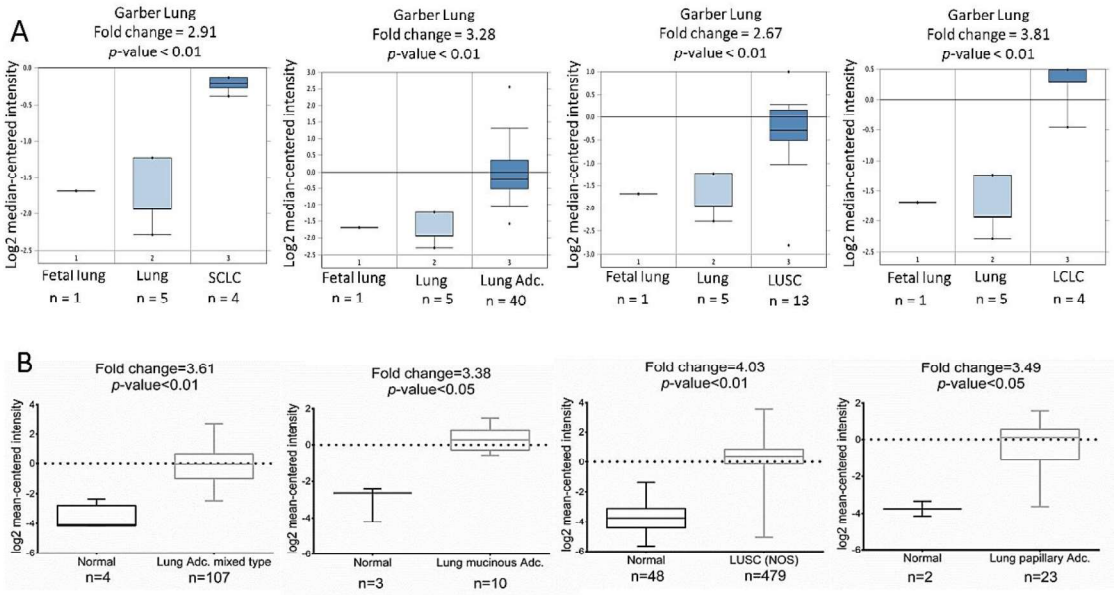

Figure 7.2.2.1.2. The mRNA expression of IQGAP3 in lung cancer subtypes. A) Box and whisker plots displaying transcript level of IQGAP3 in different subtypes of lung cancer in Oncomine database. **B)** Box and whisker plots representing the transcript level of IQGAP3 in subtypes of lung cancer in TCGA database. Here, X-axis denotes normal and cancer group; Y-axis represents transcript level of IQGAP3 in log2 median/mean centred intensity. Median value is represented by a line in the middle of the graph. A two-tailed Student's t-test was carried out to ascertain the statistical differences of expression between normal and cancerous region of lung cancer patients.

7.2.2.2 Prognostic significance of IQGAP2 and IQGAP3 in lung cancer

Next, the correlation between mRNA levels of both genes, with first progression survival (FP), overall survival (OS) and post-progression survival (PPS) of lung cancer patients were carried out using Kaplan-Meier plotter database. The results indicated a decreased OS ($p \leq 0.0001$, HR- 0.71, 95% CI 0.63-0.81) and FP ($p \leq 0.05$, HR- 0.82, 95% CI 0.68-0.99), for patients with reduced IQGAP2 expression (Fig. 7.2.2.2.1A).

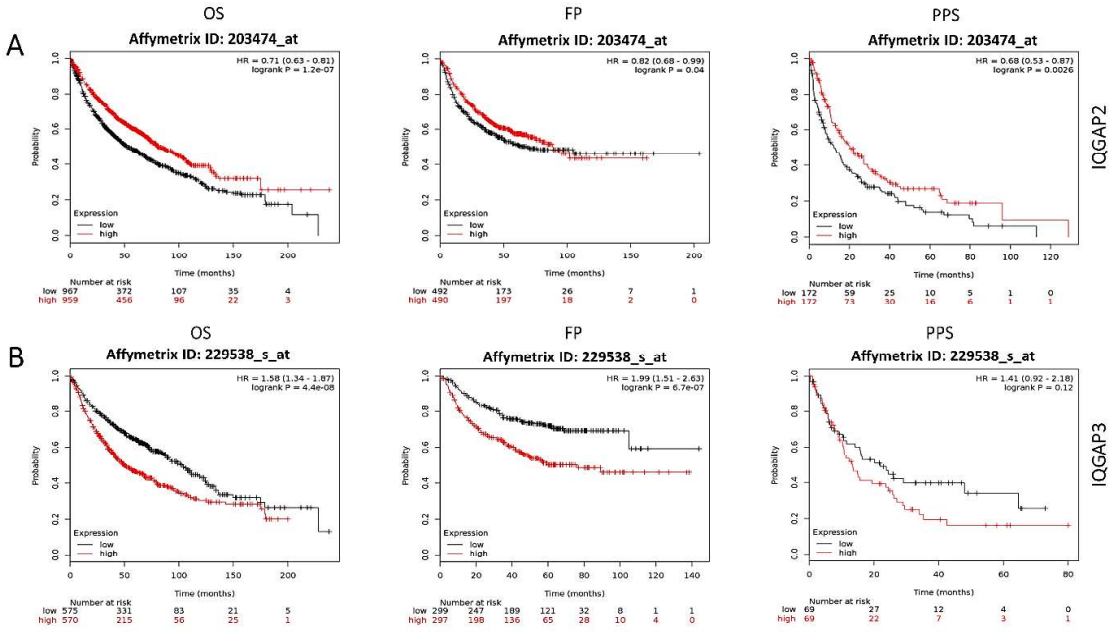

Figure 7.2.2.2.1. The mRNA expression of IQGAP2 and IQGAP3 in lung cancer and their correlation with survival of the patients. A) Kaplan-Meier plots showing a correlation between overall survival, first progression and post-progression survival of lung cancer patients with IQGAP2 expression. **B)** The overall survival and first progression and post-progression survival of lung cancer and their correlation with IQGAP3 expression have been shown by Kaplan-Meier plots. Here X-axis indicates number of patients at risk at specific time (in months) and Y-axis denotes the probability of survival. The red and black lines represent patients with expression above the median value and patients with expressions below the median value, respectively. The probe ID used for survival analysis are shown on top of the graphs. HR represents hazard ratio, 95% CI represents to confidence interval, p-value ≤ 0.05 was considered significant.

Similarly, PPS was also reduced in patients with low IQGAP2 expression ($p \leq 0.01$, HR- 0.68, 95% CI 0.53-0.87). In contrast, survivability of lung cancer patients was inversely associated with the expression of IQGAP3. A reduced OS ($p \leq 0.0001$, HR- 1.58, 95%

CI 1.34-1.87) of the lung cancer patients was observed with high IQGAP3 transcript level. Additionally, a reduced FP ($p \leq 0.0001$, HR- 1.99, 95% CI 1.51-2.63) was also observed in lung cancer patients with higher IQGAP3 expression. In case of PPS, the trend of survivability of the patient was similar to the OS and FP but data was non-significant ($p \geq 0.05$, HR- 1.41, 95% CI 0.92-2.18) (Fig. 7.2.2.2.1B).

Hence, our findings indicate that reduced IQGAP2 transcript levels in lung cancer associate with worse survival outcome, while IQGAP3 transcript levels are elevated in the same, and predict poor prognosis.

7.2.3 Breast cancer

Multiple studies have revealed that breast cancer has mainly two classes namely ductal and lobular which are further categorised into different subtypes explicitly luminal A, luminal B, basal-like and HER2-enriched. Accumulating evidence has suggested that breast cancers with different intrinsic subtypes show diverse treatment responses and require different therapeutic strategies. Therefore, accurate grouping of breast cancer into subtypes is very vital for the prediction of treatment response and the survival outcomes of the patient. With this information, we carried out the expression analysis of IQGAP2 and IQGAP3 in different subtypes of breast cancer and performed a correlation analysis with the survivability of breast cancer patients.

7.2.3.1 Expression of IQGAP2 and IQGAP3 in breast cancer

The analysis of different datasets of Oncomine showed a significant change in mRNA expression of both the genes in breast cancer. The expression of IQGAP2 was reduced in ductal breast carcinoma *in situ* (fold change = -2.65), as well as in invasive ductal breast carcinoma (fold change = -2.86) (Ma Breast dataset) [273] (Fig. 7.2.3.1.1A). The analysis of TCGA dataset showed a significant but very little change in expression of IQGAP2 in

invasive ductal carcinoma (fold change = -0.97). No significant difference in the expression of IQGAP2 in ductal, mixed lobular or invasive lobular breast carcinoma was observed (Fig. 7.2.3.1.1B).

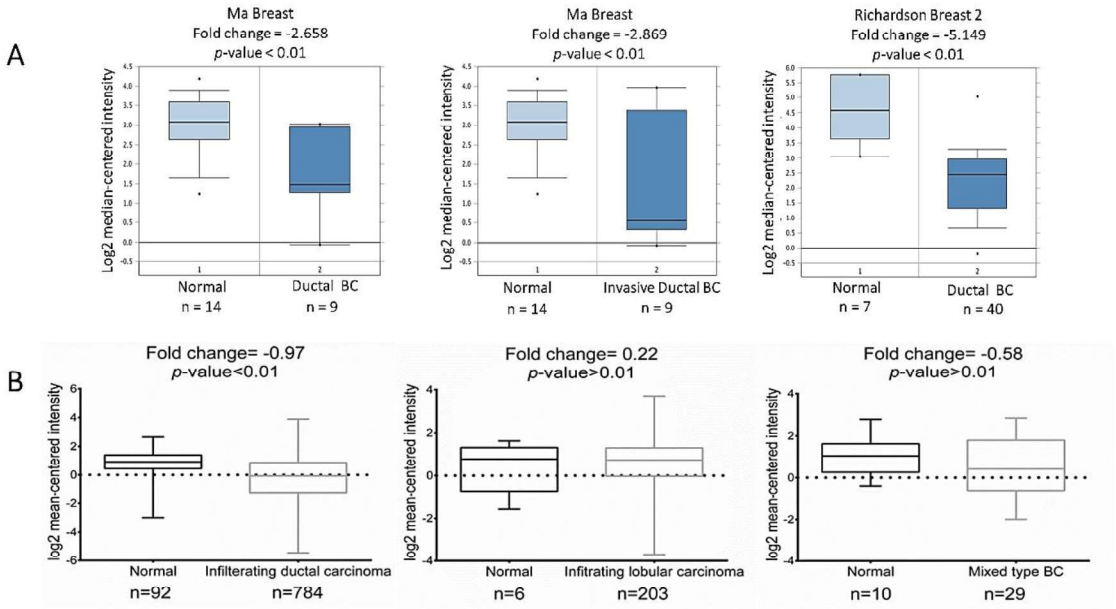

Figure 7.2.3.1.1. Expression of IQGAP2 in subtypes of breast cancer. A) The bar graphs showing transcript level of IQGAP2 in different subtypes of breast cancer post analysis with Oncomine database. **B)** Bar graph showing IQGAP2 transcript levels in breast cancer subtypes in TCGA database. In bar graph, X-axis displays the type of samples for breast cancer, normal or cancer. Y-axis showing the mRNA expression of IQGAP2 or IQGAP3 in log2 median/mean centred intensity (median value depicted as middle line in each box and whisker plot). To ascertain a statistically significant difference between the groups, two-tailed Student's t-test was used.

The analysis of Oncomine and TCGA datasets (version: 2011/09/02) showed an elevated level of IQGAP3 in infiltrating lobular (fold change = 3.84), infiltrating ductal (fold change = 5.68) and, mixed type breast carcinoma (fold change = 3.99) (Fig. 7.2.3.1.2A). In agreement with this, the TCGA dataset (TCGA dataset, version: 2016-08-16) also showed higher expression of IQGAP3 in infiltrating lobular (fold change = 4.08), infiltrating ductal (fold change = 4.22) and, mixed lobular and ductal breast carcinoma (fold change = 2.93) (Fig. 7.2.3.1.2B).

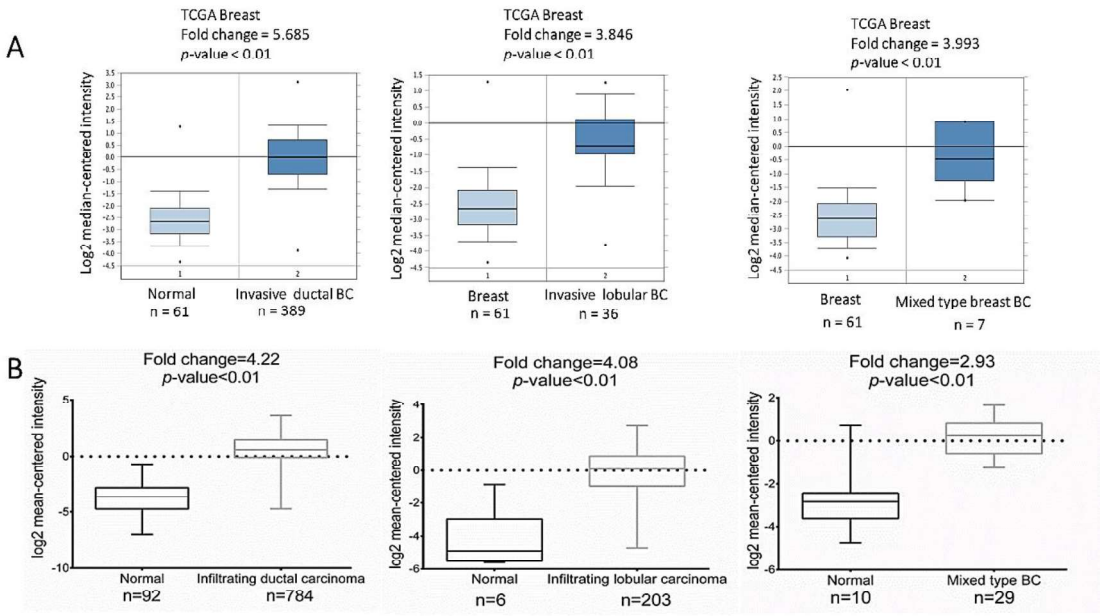

Figure 7.2.3.1.2. IQGAP3 transcript levels in different subtypes of breast cancer. A) Bar graph showing results of IQGAP3 mRNA expression as seen in breast cancer subtypes in Oncomine database. **B)** Bar graph showing results of IQGAP3 mRNA expression in different breast cancer subtypes with TCGA database. In bar graph, X-axis represents the type of samples for breast cancer, namely normal or cancer. Y-axis showing the mRNA expression of IQGAP2 or IQGAP3 in log2 median/mean centred intensity. Median value depicted as middle line in each box and whisker plot. To ascertain a statistically significant difference, two-tailed Student's t-test was performed.

7.2.3.2 Survival analysis of IQGAP2 and IQGAP3 in breast cancer

We analysed the prognostic significance of IQGAP2 and IQGAP3 isoforms in breast cancer with the help of Kaplan-Meier Plotter. The results showed that reduced IQGAP2 and elevated IQGAP3 level significantly correlated with poor survival of the patient. High IQGAP2 expression in patients was associated with the prolonged OS ($p \leq 0.01$, HR- 0.72, 95% CI 0.58-0.9), RFS ($p \leq 0.0001$, HR- 0.78, 95% CI 0.69-0.86), DMFS ($p \leq 0.001$, HR- 0.70, 95% CI 0.57-0.85). In PPS the trend was similar but the data was non-significant ($p \geq 0.05$, HR- 0.87, 95% CI 0.68- 1.1) (Fig. 7.2.3.2.1 A).

In contrast, high IQGAP3 expression in patients were associated with the poor OS ($p \leq 0.01$, HR- 1.57, 95% CI 1.14-2.15), RFS ($p \leq 0.0001$, HR- 1.53, 95% CI 1.31-1.79),

DMFS ($p \leq 0.05$, HR- 1.44, 95% CI 1.04-2.0). The PPS show a similar trend but data was non-significant ($p \geq 0.05$, HR- 1.27, 95% CI 0.89-1.81) (Fig. 7.2.3.2.1 B).

Overall, IQGAP2 transcript levels were reduced in infiltrating ductal and ductal carcinoma but not in mixed type or infiltrating lobular breast carcinoma. Whereas, IQGAP3 were increased in all the subtypes of breast cancer patients. While expression levels of the former were associated with good survival, increased transcript levels of the latter significantly associated with reduced patient survival.

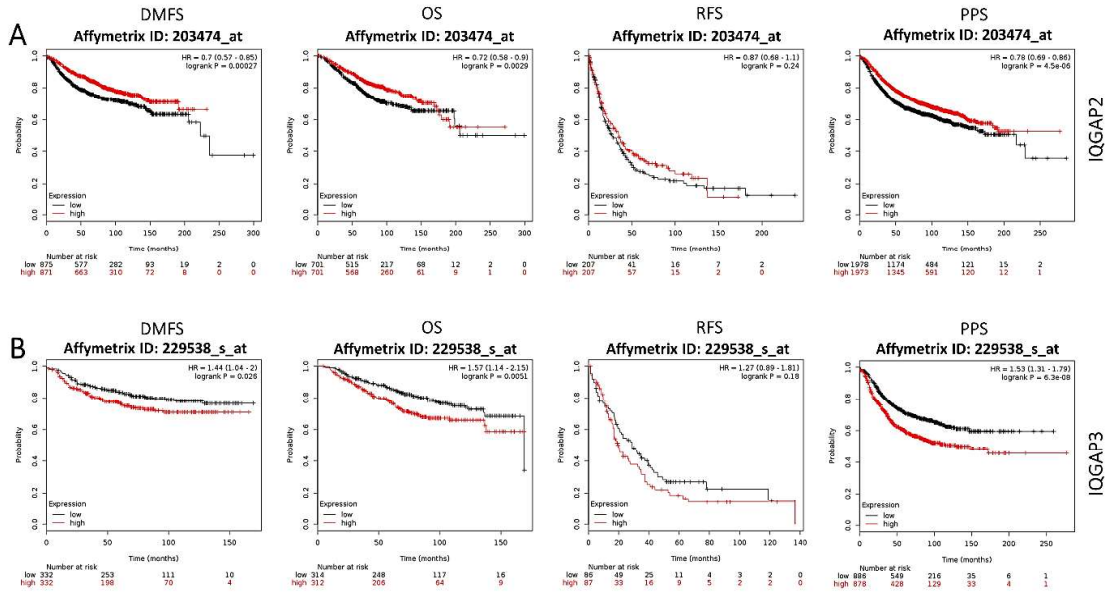

Figure 7.2.3.2.1 Association between patient's survival and IQGAP2/IQGAP3 expression in breast cancer. A) The graph of Kaplan-Meier plotter showing an association between IQGAP2 expression and DMFS, OS, PPS and RFS in breast cancer. **B)** Kaplan-Meier plotter graph representing the association of IQGAP3 expression with DMFS, OS, PPS and RFS in breast cancer. Here X-axis represents the number of patients at risk at different time intervals (in months). The probe ID used for survival analysis are shown on top of the graphs. Y-axis isshowing the probability of survivability of patient in percentage. Patients with transcript level higher than the median value have been indicated by red line whereas those having transcript level lower than the median value have been shown in black line. CI represents confidence interval; HR represents hazard ratio.

7.2.4 Gastric cancer

Gastric cancer is broadly categorised into, intestinal type gastric adenocarcinoma, mixed type gastric adenocarcinoma and diffuse type gastric adenocarcinoma, according to Lauren's classification. These subtypes exhibit distinct clinical, molecular and biological characteristics and show differences in prognosis and sensitivity to chemotherapy. So, the stratification of gastric cancer in subtypes is crucial not only for the prediction of treatment sensitivity but also for the survival outcomes of the patient. Therefore, we analysed the expression of these isoforms in subtypes of gastric cancer and analysed the association of these isoforms with survivability of the gastric cancer patient.

7.2.4.1 Expression of IQGAP2 and IQGAP3 in gastric cancer

The analysis of different datasets in Oncomine revealed significantly low expression of IQGAP2 in intestinal type gastric adenocarcinoma (fold change = 2.34, Cho Gastric

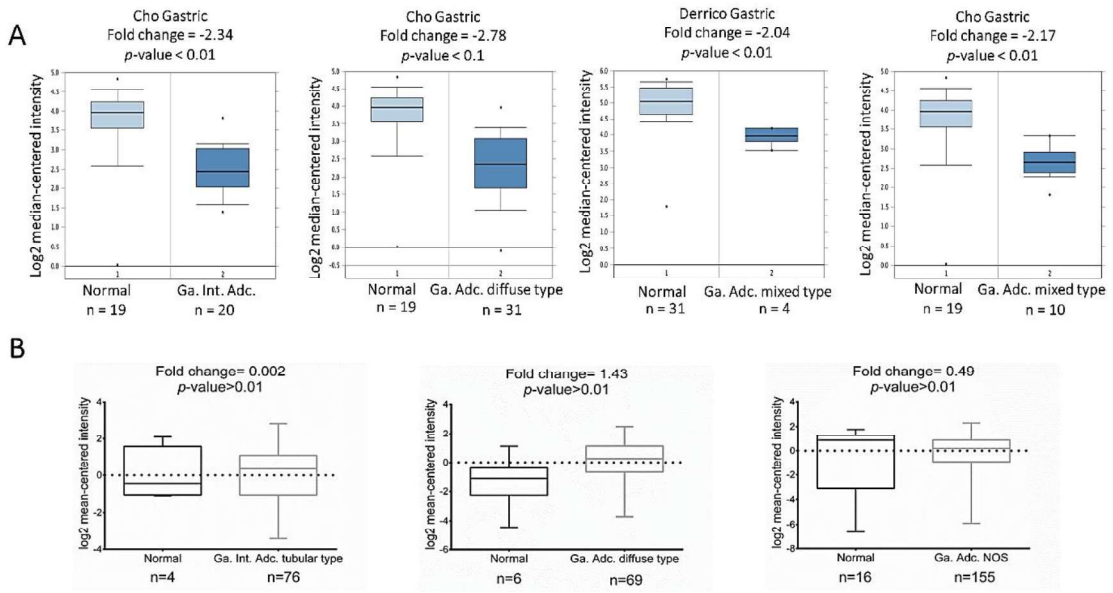

Figure 7.2.4.1.1. IQGAP2 expression in gastric cancer subtypes. A) The bar graphs showing mRNA expression of IQGAP2 in gastric cancer subtypes analysed from different datasets of Oncomine database. **B)** The bar graphs displaying the transcript level of IQGAP2 in gastric cancer subtypes analysed from TCGA database. X-axis of the graph displaying normal and cancer group;

Y-axis showing the mRNA expression of IQGAP2 in log2 median/mean centred intensity. The middle line in graphs represents the median value. A two-tailed Student's t-test was performed for the analysis of statistical differences between normal and cancer group.

datasets), diffuse type gastric adenocarcinoma (fold change = 2.78, Cho Gastric datasets) and mixed type gastric adenocarcinoma (fold change = 2.17, Cho Gastric datasets; 2.04, DErrico Gastric dataset) (Fig. 7.2.4.1.1A). But, no substantial change in IQGAP2 transcript level was observed in gastric cancer subtypes of TCGA datasets (Fig. 7.2.4.1.1B).

In contrast, analysis of TCGA datasets indicated an elevated IQGAP3 level in diffuse gastric adenocarcinoma (fold change = 2.51), gastric intestinal adenocarcinoma (fold change = 3.25) and gastric mixed adenocarcinoma (fold change of 2.43) (Fig. 7.2.4.1.2). However, no significant change was observed in IQGAP3 mRNA levels in gastric cancer types with set threshold parameters in Oncomine database.

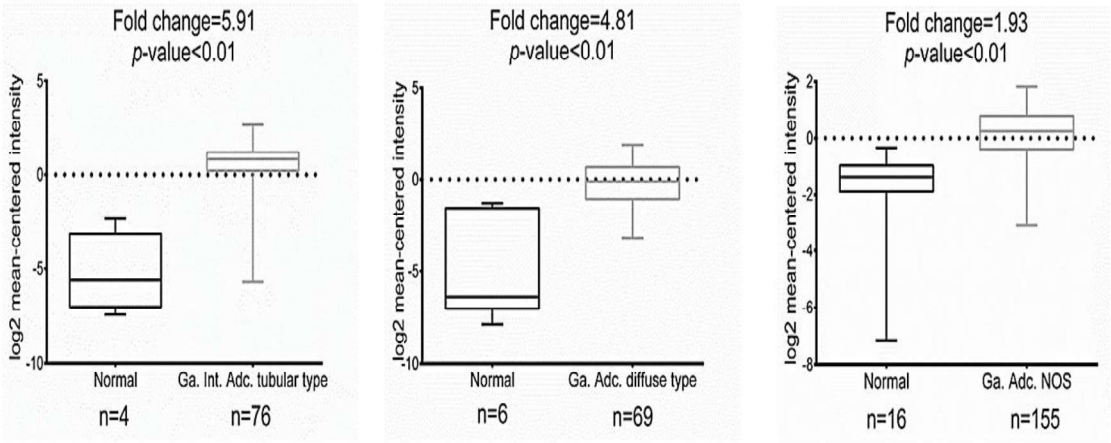

Figure 7.2.4.1.2. The mRNA expression of IQGAP3 in different subtypes of gastric cancer. The bar graphs showing transcript levels of IQGAP3 in gastric cancer subtypes analysed from TCGA. Here, X-axis of the graph displaying normal and cancer groups; Y-axis showing the mRNA expression of IQGAP3 in log2 median/mean centred intensity. The middle line in graphs represents the median value. A two-tailed Student's t-test was performed for the analysis of statistical differences between normal and cancer group.

7.2.4.2 Prognostic significance of IQGAP2 and IQGAP3 in gastric cancer

The Kaplain-Meier plotter survival analysis of gastric cancer patients showed low probability of OS ($p \leq 0.0001$, HR- 0.58, 95% CI 0.48-0.72) and FP ($p \leq 0.0001$, HR- 0.59, 95% CI 0.47-0.74) with the lower transcript level of IQGAP2 (Fig. 7.2.4.2.1A).

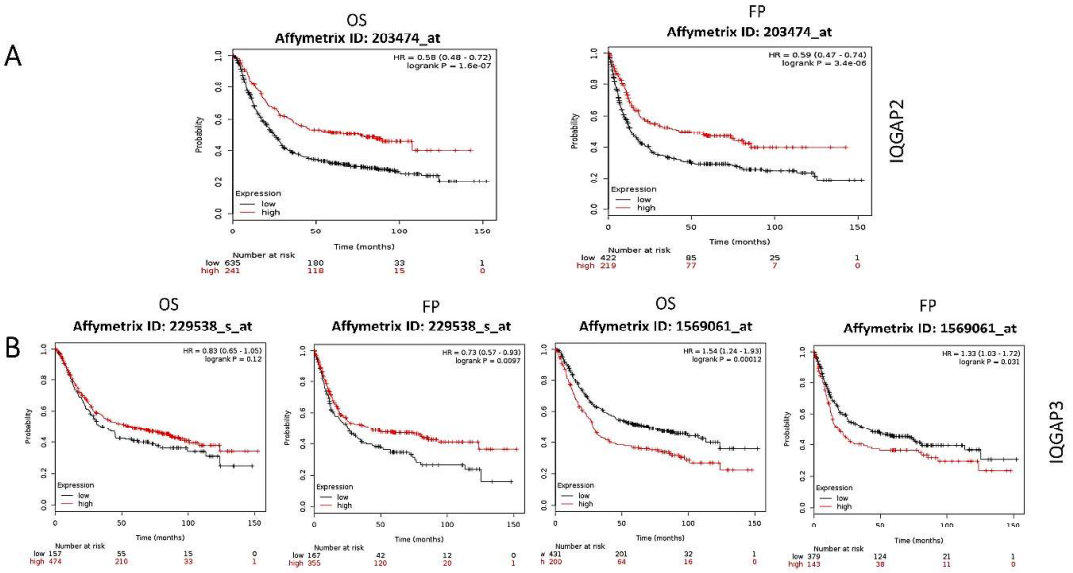

Figure 7.2.4.2.1. An association between the survival and expression of IQGAP2 and IQGAP3 in gastric cancer patients. A) Kaplan-Meier plots showing a correlation between the expression of IQGAP2 and overall survival (OS) and first progression (FP) survivability of gastric cancer patients. **B)** Kaplan-Meier plots depicting overall survival (OS) and first progression (FP) survival of gastric cancer patients with the expression levels of IQGAP3. In this graph, X-axis represents number of patients at risk at different time intervals (in months) and Y-axis shows the probability of patient survivability in percentage. The probe ID used for survival analysis are shown on top of the graphs. Red line denotes the patients who have expression of IQGAP2/IQGAP3 above the median whereas the black line represents patients with expressions below the median for IQGAP2/IQGAP3. HR represents hazard ratio, CI represents confidence interval.

Interestingly, the survival analysis of IQGAP3 in gastric cancer resulted in an opposite outcome from two different probes. A poor, non-significant OS ($p \geq 0.05$, HR- 0.83, 95% CI 0.65-1.05) and significant FP ($p \leq 0.01$, HR- 0.73, 95% CI 0.57-0.93) survival was observed with the reduced expression of IQGAP3 in one probe (229538_s_at), whereas a prolonged OS ($p \leq 0.001$, HR- 1.54, 95% CI 1.24-1.93) and FP ($p \leq 0.05$, HR- 1.33,

95% CI 1.03-1.72) survivability was observed with the low IQGAP3 expression from another probe (1569061_at) (Fig. 7.2.4.2.1B).

Similar to lung and breast cancer, increased expression of IQGAP2 and reduced level of IQGAP3 was associated with good prognosis of gastric cancer patients but with some exceptions.

7.2.5 Colorectal cancer

The cancer originated from rectal or colon is known as colorectal cancer. This cancer has been categorised into different subtypes depending on the molecular or physiological changes namely colon adenocarcinoma, rectal adenocarcinoma, lymphoma, neuroendocrine tumors, leiomyosarcoma and melanoma. Colon and rectal adenocarcinoma are the most common (95%) colorectal cancer types which can be further categorised into mucinous adenocarcinoma and signet ring cell adenocarcinoma.

7.2.5.1 Expression of IQGAP2 and IQGAP3 in colorectal cancer

The analysis of Oncomine database for the expression pattern of IQGAP2 and IQGAP3 resulted in low expression of IQGAP2 in 17 unique analyses whereas a higher expression of IQGAP3 in 2 unique analyses of colorectal cancer (Fig. 7.2.1.1). Kaiser Colon dataset [274] showed a significantly low mRNA levels of IQGAP2 in rectal adenocarcinoma (fold change = -2.67), colon adenocarcinoma (fold change = -3.25), rectal mucinous adenocarcinoma (fold change = -2.86) and colon mucinous adenocarcinoma (fold change = -2.13) (Fig. 7.2.5.1.1A).

Additionally, the analysis of TCGA colorectal cancer datasets (TCGA-COADREAD) displayed a reduced expression of IQGAP2 in rectal adenocarcinoma (fold change = -

1.90), colon adenocarcinoma (fold change = -2.04) and colon mucinous adenocarcinoma (fold change = -1.18) but not in rectal mucinous adenocarcinoma (Fig. 7.2.5.1.1B).

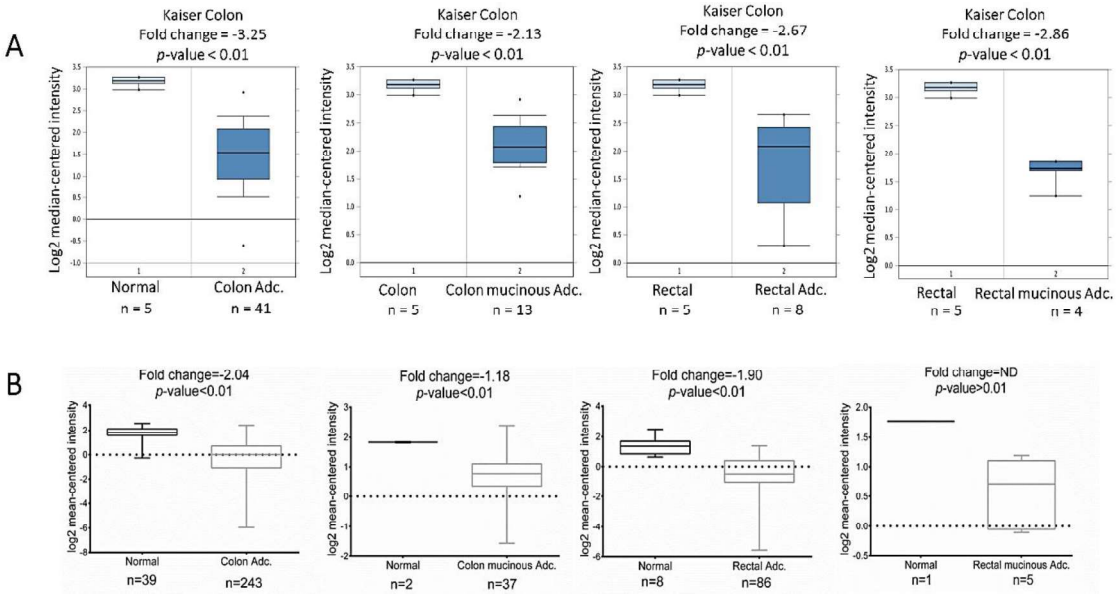

Figure 7.2.5.1.1. The mRNA expression of IQGAP2 in colorectal cancer subtypes. A) Box and whisker plots displaying the mRNA expression of IQGAP2 in colorectal cancer subtypes in Oncomine database. **B)** Box and whisker plots showing IQGAP2 transcript levels in colorectal cancer subtypes in TCGA database. Here, X-axis displaying normal vs. cancer group while Y-axis representing the mRNA level of IQGAP2 in log2 median/mean centred intensity. The middle line in the box plots represents the median value. To ascertain statistical difference between the normal and cancer groups, two-tailed Student's t-test was carried out.

The reduced transcript level of IQGAP2 was also observed in colon and rectal adenocarcinoma in other colorectal datasets of Oncomine which are summarised in Table 7.2.5.1.1.

Table 7.2.5.1.1. IQGAP2 transcript levels in colorectal cancer

Dataset	**Normal (Cases)**	**Tumor (Cases)**	**Fold change**	***p*-value**
Kaiser Colon	Colon (5)	Colon Adenocarcinoma (41)	-3.25	2.2e-16
	Colon (5)	Cecum Adenocarcinoma (17)	-2.65	1.5e-7
	Colon (5)	Colon Mucinous Adenocarcinoma (13)	-2.13	4.1e-7
	Colon (5)	Rectal Mucinous Adenocarcinoma (4)	-2.86	3.6e-4

	Colon (5)	Rectosigmoid Adenocarcinoma (10)	-2.93	2.8e-5
	Colon (5)	Rectal Adenocarcinoma (8)	-2.66	9.2e-4
Ki Colon	Colon (28) Liver (13)	Colon Adenocarcinoma (50)	-2.82	2.1e-14
Hong Colorectal	Colon (12)	Colorectal Carcinoma (70)	-5.39	7.1e-23
Gaedcke Colorectal	Rectum (65)	Rectal Adenocarcinoma (65)	-3.87	1.2e-36
TCGA Colorectal	Colon (19) Rectum (3)	Colon Adenocarcinoma (101)	-3.52	1.1e-24
	Colon (19) Rectum (3)	Rectosigmoid Adenocarcinoma (3)	-5.54	2.4e-9
	Colon (19) Rectum (3)	Rectal Adenocarcinoma (60)	-3.58	1.0e-19
Skrzypczak Colorectal 2	Colon (10)	Colon Adenoma Epithelia (5)	-4.41	1.4e-7
	Colon (10)	Colon Carcinoma (5)	-2.73	5.4e-8
	Colon (10)	Colon Carcinoma Epithelia (5)	-2.19	5.2e-8
TCGA-COADREAD*	Normal (39)	Colon Adenocarcinoma (243)	-2.04	≤ 0.0001
	Normal (2)	Colon mucinous Adenocarcinoma (37)	-1.18	≤ 0.0001
	Normal (8)	Rectal Adenocarcinoma (86)	-1.90	≤ 0.0001
	Normal (1)	Rectal mucinous Adenocarcinoma (5)	ND	ND

Oncomine analysis of IQGAP3 expression in colorectal cancer showed an elevated transcript levels of same in colorectal carcinoma (fold change = 2.58) and rectal mucinous adenocarcinoma (fold change = 2.38) (Fig. 7.2.5.1.2A).

A similar trend of IQGAP3 transcript level was observed in TCGA datasets for colon adenocarcinoma (fold change = 2.03) and rectal adenocarcinoma (fold change = -2.25).

No remarkable change in IQGAP3 mRNA expression was detected in rectal mucinous or colon mucinous adenocarcinoma in TCGA database (Fig. 7.2.5.1.2B) (Table 7.2.5.1.2).

Overall, the expression analysis of IQGAP2 and IQGAP3 showed reduced expression of former and elevated expression of later in colorectal cancer with some exceptions.

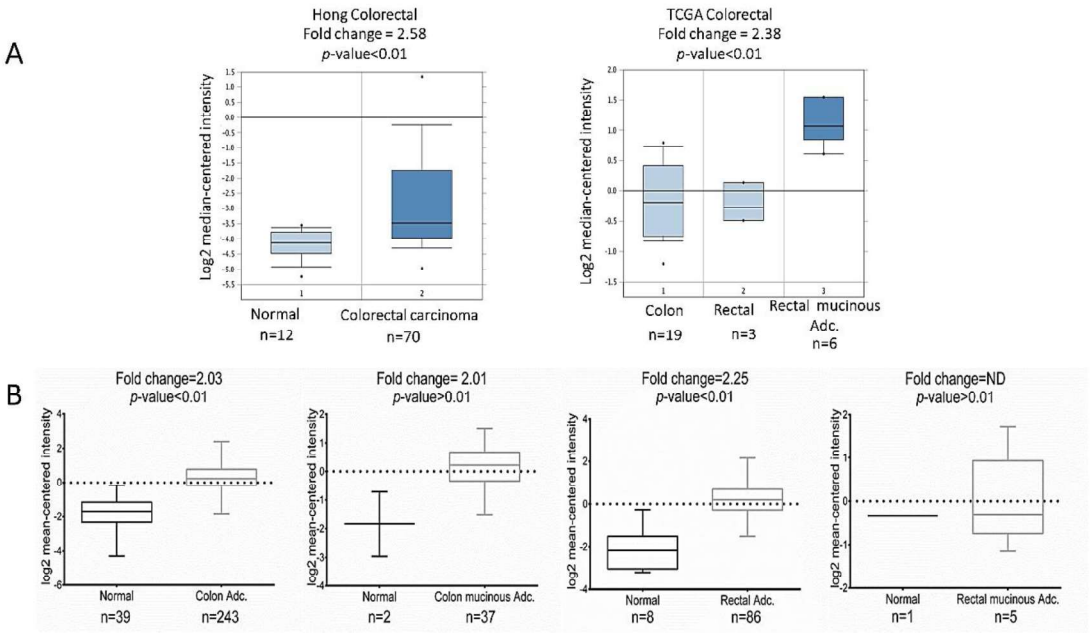

Figure 7.2.5.1.2. IQGAP3 mRNA expression in colorectal cancer subtypes. A) Oncomine database analysis showing the transcript level of IQGAP3 in different colorectal cancer subtypes in Box and whisker plots. **B)** The transcript level of IQGAP3 in different subtypes of colorectal cancer, analysed from TCGA databases are shown in plots. Here, X-axis is displaying normal and cancer groups. Y-axis represents the mRNA level of IQGAP3 in log2 median/mean centred intensity. The median value is displayed by the middle line of box plots. Two-tailed Students t-test was used to calculate signicance of difference.

Table 7.2.5.1.2. IQGAP3 mRNA expression in colorectal cancer

Dataset	**Normal (Cases)**	**Tumor (Cases)**	**Fold change**	***p*-value**
TCGA Colorectal	Rectum (3) Colon (19)	Adenocarcinoma (6) Rectal Mucinous	2.38	7.7e-6
Hong Colorectal	Colon (12)	Colorectal Carcinoma (70)	2.58	1.7e-7
TCGA-COADREAD*	Normal (39)	Colon Adenocarcinoma (243)	2.03	≤ 0.0001
	Normal (2)	Colon mucinous Adenocarcinoma (37)	2.01	0.32
	Normal (8)	Rectal Adenocarcinoma (86)	2.25	0.002
	Normal (1)	Rectal mucinous Adenocarcinoma (5)	ND	ND

7.2.5.2 Survival analysis of IQGAP2 and IQGAP3 in colorectal cancer

Due to non-availability of survival data in Kaplain Meier plotter for colorectal cancer, the survival analysis of colorectal cancer with IQGAP2 and IQGAP3 expression was carried out with the help of SurvExpress database. The survival analysis of the two TCGA datasets (COAD-TCGA and COADREAD-TCGA) did not show a significant correlation between OS of the colorectal cancer patients with the expression of either IQGAP2 or IQGAP3 (Fig. 7.2.5.2.1A, B).

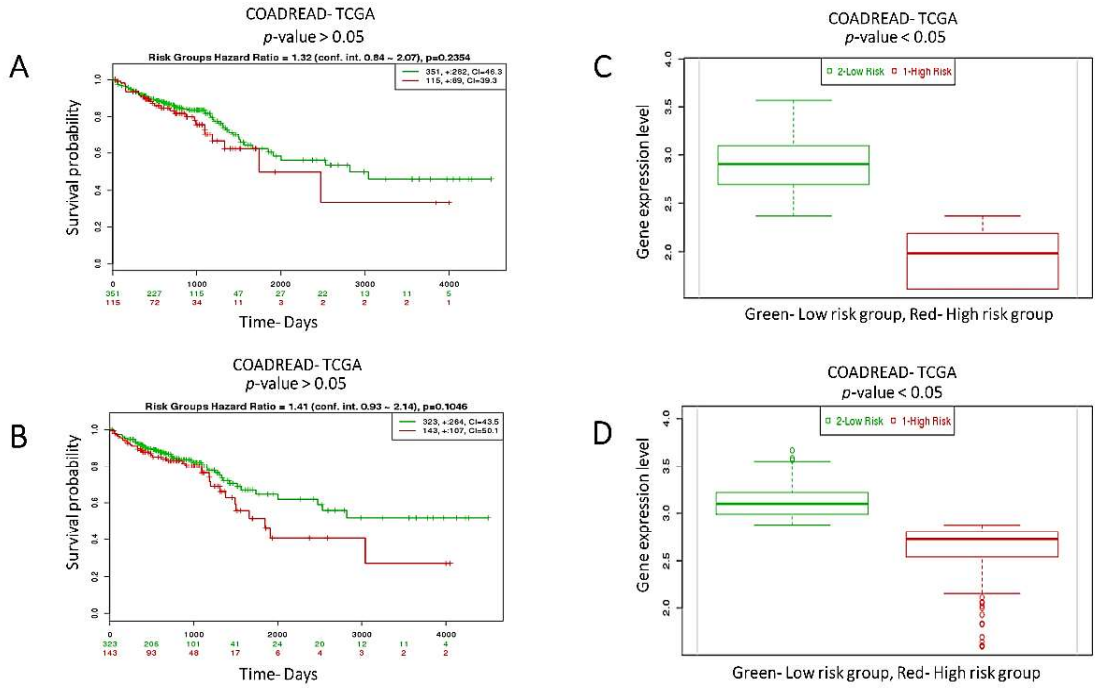

Figure 7.2.5.2.1. The correlation between the expression of IQGAP2/IQGAP3 with survival of the colorectal cancer patients. A) The graph showing correlation between overall patient survival (OS) in colorectal cancer with IQGAP2 expression (SurvExpress analysed). **B)** SurvExpress database showing overall patient survival (OS) in colorectal cancer with IQGAP3 expression. Here at the top of each graph, the p-value and 95% CI have been shown for selected dataset. Survival risk curves are shown for each group in two different colours. The line in green represents the low risk group whereas the line in red represents the high risk group. The X-axis display the time (days) to event. **C)** and **D)** show box plot of IQGAP2 and IQGAP3 gene expression levels in the two risk groups. The X-axis shows low and high risk groups. The Y-axis shows the expression levels.

Despite a non-significant correlation with survival, the trend of reduced IQGAP2 expression in high-risk group was observed compared to the low-risk group (Fig. 7.2.5.2.1C). An opposite trend with IQGAP3 expression was observed where elevated IQGAP3 expression was associated with high-risk group (Fig. 7.2.5.2.1D).

To summarise, in colorectal cancers increased IQGAP2 expression associated with low risk the disease, while those with increased IQGAP3 expression had high risk of the same.

7.2.6 Brain and CNS cancer

Brain cancer is a highly aggressive, difficult to treat and deadliest cancer. This cancer is mainly categorised into primary and secondary depending on the origin. Among malignant primary tumors, gliomas (glial cell origin) are most frequent types that further classify into different sub-types depending on the type of glial cell explicitly, ependimomas, oligodendroglioma, astrocytoma, and mixed glioma. Based on the grade of the tumor, astrocytoma is further classified into anaplastic astrocytoma, diffuse astrocytoma, pilocytic astrocytoma and glioblastoma multiforme (GBM).

7.2.6.1 IQGAP2 and IQGAP3 expression in Brain and CNS cancer

The Oncomine database analysis showed an elevated level of IQGAP2 in glioblastoma (GMB), in Sun brain [275], Murat brain [276] and, in TCGA brain dataset (Table 7.2.6.1.1). Similarly, the transcript level of IQGAP2 was elevated in oligodendroglioma (fold change = 2.05), anaplastic oligoastrocytoma (fold change = 4.83), diffuse astrocytoma (fold change = 3.78) (Fig. 7.2.6.1.1A) and anaplastic oligodendroglioma (fold change = 2.77) (Table 2). The analysis of TCGA brain cancer datasets (GBM, LGG and GBMLGG) also displayed higher transcript level of IQGAP2 in astrocytoma (fold change = 3.55), oligodendroglioma (fold change = 2.54), glioblastoma (fold change = 4.80) and oligoastrocytoma (fold change = 2.80) (Fig. 7.2.6.1.1B).

Table 7.2.6.1.1. IQGAP2 expression in Brain and CNS cancer

Dataset	**Normal (Cases)**	**Tumor (Cases)**	**Fold change**	***p*-value**
Sun Brain	Brain (23)	Glioblastoma (81)	5.614	8.8e-24
	Brain (23)	Diffuse Astrocytoma (7)	3.789	0.002
	Brain (23)	Anaplastic Astrocytoma (19)	3.11	2.7e-5
	Brain (23)	Oligodendroglioma (50)	2.05	4.3e-6
French Brain	Brain (6)	Anaplastic Oligodendroglioma (23)	2.77	7.5e-7
	Brain (6)	Anaplastic Oligoastrocytoma (4)	4.83	8.3e-4
Murat Brain	Brain (4)	Glioblastoma (80)	4.36	1.3e-6
TCGA Brain	Brain (10)	Glioblastoma (5)	3.59	0.005
	Brain (10)	Brain Glioblastoma (542)	4.78	7.5e-8
TCGA-LGG*	Normal (5)	Glioblastoma (151)	4.80	≤ 0.0001
	Normal (5)	Astrocytoma (194)	3.55	≤ 0.0001
	Normal (5)	Oligodendroglioma (191)	2.54	0.0002
	Normal (5)	Oligoastrocytoma (130)	2.80	≤ 0.0001

Table 7.2.6.1.2. IQGAP3 expression in Brain and CNS cancer

Dataset	**Normal (Cases)**	**Tumor (Cases)**	**Fold change**	***p*-value**
TCGA-LGG*	Normal (5)	Glioblastoma (151)	3.08	0.0027
	Normal (5)	Astrocytoma (194)	1.30	0.05
	Normal (5)	Oligodendroglioma (191)	0.92	0.12
	Normal (5)	Oligoastrocytoma (130)	1.09	0.08

The Oncomine database analysis at threshold parameters did not display a substantial change in the IQGAP3 expression for brain cancer subtypes. However, increased transcript level of IQGAP3 was observed in glioblastoma (fold change = 3.08) with TCGA database analysis. The TCGA analysis did not show such change in other subtypes of brain cancer (Table 7.2.6.1.2) (Fig. 7.2.6.1.1C).

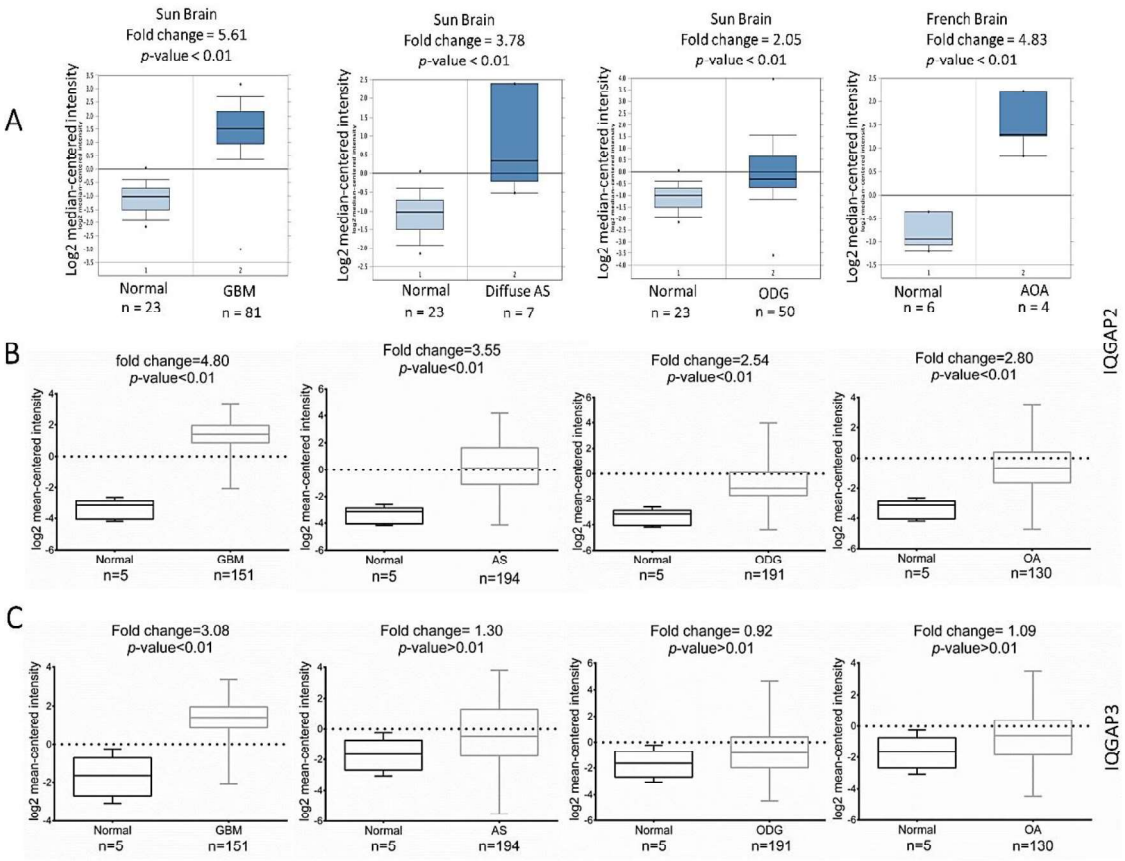

Figure 7.2.6.1.1. The mRNA expression of IQGAP2 and IQGAP3 in brain cancer. A) Box and whisker plots presenting the mRNA level of IQGAP2 in brain cancer subtypes (Source- Oncomine database). **B)** The box and whisker plots displaying IQGAP2 expression in different brain cancer subtypes (Source- TCGA database). **C)** Box and whisker plots showing transcript level of IQGAP3 from TCGA database in subtypes of brain cancer. Here, X-axis represents normal and cancer groups. Y-axis displaying the log2 median/mean centred intensity of IQGAP2 or IQGAP3 transcript levels. Line in the middle represents the median/mean value. Two-tailed student's t-test was used to analysis the differences.

7.2.6.2 Prognostic significance of IQGAP2 and IQGAP3 in brain and CNS cancer

The SurvExpress analysis of LGG-TCGA brain cancer dataset showed a correlation between poor OS survivability of the patient and higher expression of IQGAP2 ($p \leq 0.0001$, HR- 4.58, 95% CI 3.16-6.65) (Fig. 7.2.6.2.1A).

Likewise, the increased expression of IQGAP3 was associated with the poor OS survivability of the patients in LGG-TCGA dataset ($p \leq 0.0001$, HR- 5.08, 95% CI 3.42-

7.55) (Fig. 7.2.6.2.1B). The survival analysis of GBMLGG-TCGA dataset also showed similar pattern ($p \leq 0.0001$, HR- 5.49, 95% CI 3.51-8.59) (Table 7.2.6.2.1).

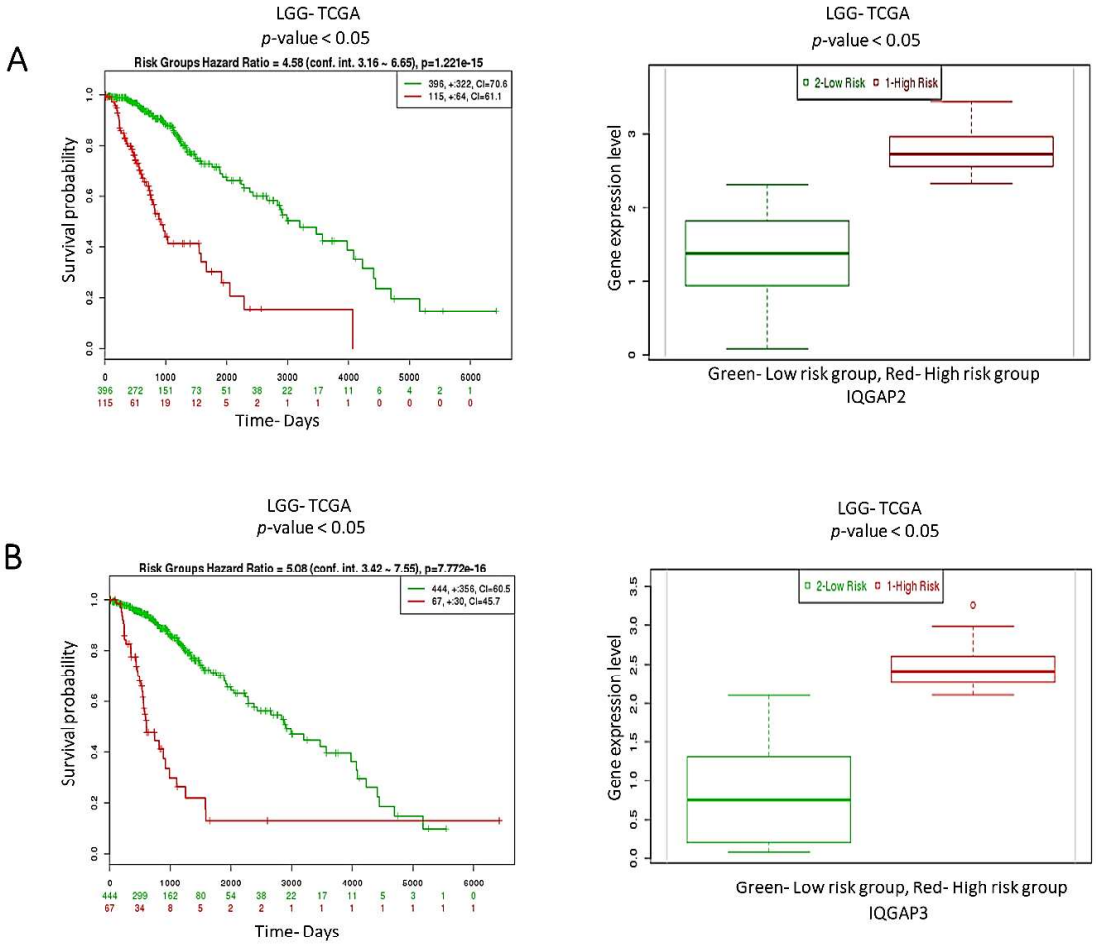

Figure 7.2.6.2.1. IQGAP2 and IQGAP3 mRNA expression and survival of the brain cancer patients. A) The survival plot (left panel) showing the correlation between overall survival (OS) of the brain cancer patients and IQGAP2 expression (SurvExpress analysed). Box and whisker plot (right) showing the association of IQGAP2 expression and risk groups of brain cancer patients. **B)** The survival plot (left panel) showing the correlation between overall survival (OS) of the brain cancer patient and IQGAP3 expression (SurvExpress analysed). Box and whisker plot (right panel) showing the association of IQGAP3 expression and risk groups of patients. Here at the top of each graph, the p-value and 95% CI have been shown for selected dataset. Survival risk curves are shown in green (low risk group) and red (high risk groups). The X-axis shows the time (days) to event.

Table 7.2.6.2.1. The association between IQGAP3 expression and overall survival of Brain and CNS cancer patients

Database	Dataset/ Affymetrix ID	Survival outcome	No. of Cases	HR	95% CI	*p*-value
SurvExp	LGG-TCGA	OS	512	5.08	3.42-7.55	7.7e-16
SurvExp	GBMLGG-TCGA	OS	660	5.49	3.51-8.59	9.3e-14

Interestingly we observed just opposite differential expression trends for IQGAP2 in brain tumors; IQGAP2 levels were elevated in the tumor region and associated with poor prognosis. In general, the expression of IQGAP3 was elevated in tumors and was associated with the low survivability of the patients as seen in other cancers.

7.2.7 Prostate Cancer

Adenocarcinoma is the predominant type (about 90%) of prostate cancer, which can further be categorised into colloid, atrophic and signet ring carcinoma. The minority of prostate cancer (10%) include squamous cell cancer, sarcomas, carcinoid, sarcomatoid cancers, transitional cell cancer and small cell cancer.

7.2.7.1 Expression of IQGAP2 and IQGAP3 in prostate cancer

The four datasets of Oncomine showed elevated mRNA levels of IQGAP2 in prostate cancer compared to the normal.

Table 7.2.7.1.1. IQGAP2 and IQGAP3 mRNA expression in Prostate cancer

Dataset	Normal (Cases)	Tumor (Cases)	Fold change	*p*-value
IQGAP2				
Varambally Prostate	Prostate Gland (6)	Prostate Ca.(7)	2.901	2.8e-6
Welsh Prostate	Prostate Gland (9)	Prostate Carcinoma (25)	2.064	1.7e-6
Singh Prostate	Prostate Gland (50)	Prostate Ca. (52)	2.716	1.3e-4

Grasso Prostate	Prostate Gland (28)	Prostate Ca. (59)	2.052	2.4e-5
TCGA Prostate cancer (PRAD)*	Prostate Gland (51)	Prostate Ca. acinar type (482)	0.23	0.843
IQGAP3				
TCGA Prostate cancer (PRAD)*	Prostate Gland (51)	Prostate Ca. acinar type (482)	1.937	≤ 0.00001

*TCGA Datasets (version: 2016-08-16)

But the analysis of TCGA dataset (PRAD-TCGA) did not show any significant difference in the expression pattern of IQGAP2 in prostate cancer (Table 7.2.7.1.1).

7.2.7.2 Survival analysis of IQGAP2 and IQGAP3 in prostate cancer

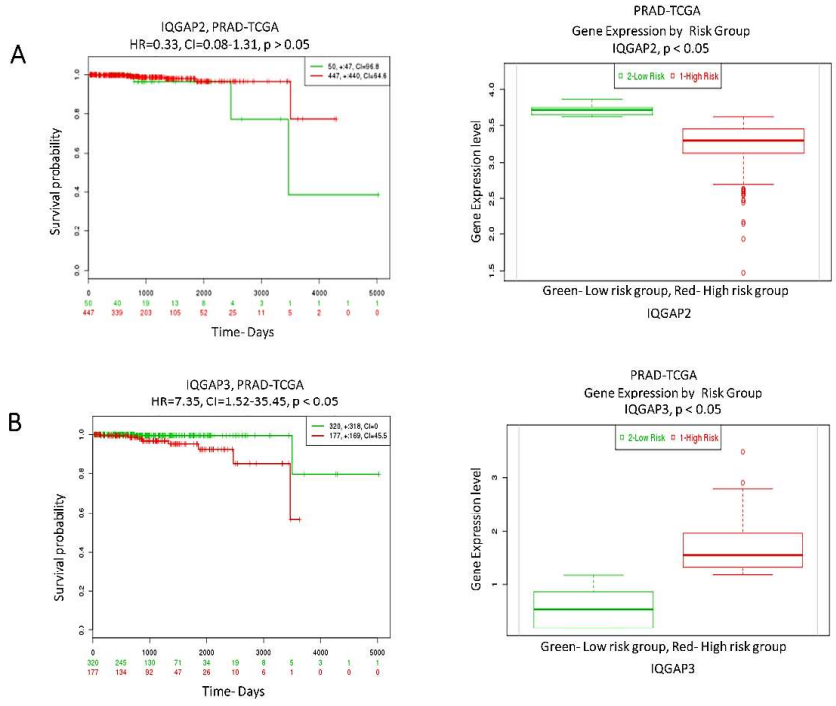

Figure 7.2.7.2.1. IQGAP2 and IQGAP3 expression and survival of the prostate cancer patients. A) The survival plot (left panel) showing the correlation between overall survival (OS) of the prostate cancer patient and IQGAP2 expression (SurvExpress analysed). Box and whisker plot (right) showing the association between IQGAP2 expression and risk groups of prostate cancer patients. **B)** The survival plot (left panel) showing the correlation between overall survival (OS) of the prostate cancer patient and IQGAP3 expression (SurvExpress analysed). Box and whisker plot (right panel) showing the association between IQGAP3 transcript levels and risk groups of patients. Here at the top of each graph, the p-value and 95% CI have displayed. Survival risk curves are shown in green (low risk group) and red (high risk groups). The X-axis shows the time (days) to event.

The analysis of PRAD-TCGA dataset using SurvExpress, showed no substantial correlation between the IQGAP2 expression and the survivability of the prostate cancer patients ($p \geq 0.05$, HR- 0.33, 95% CI 0.08-1.31) (Fig. 7.2.7.2.1A). But, the analysis displayed an association between higher IQGAP3 expression and the poor survivability of the patient ($p \leq 0.05$, HR- 7.35, 95% CI 1.52-35.4) (Fig. 7.2.7.2.1B).

Overall, as seen in brain tumors, IQGAP2 levels were higher in the tumor region and indicated worse patient survival. IQGAP3 was also elevated, and associated with worse patient survival as seen in other cancers.

7.2.8 Liver Cancer

Based on the origin, liver cancer has been categorised into the primary and the secondary liver cancer. The cancer of first type, primary liver cancer further classified into angiosarcoma, hepatocellular cancer, hemangiosarcoma and intrahepatic cholangiocarcinoma. In secondary liver cancer, tumor cells originated from other body parts reach to the liver and form cancer.

7.2.8.1 Expression of IQGAP2 and IQGAP3 in liver cancer

No substantial change in IQGAP2 expression was observed in liver cancer subtypes with the set thresholds parameters in Oncomine.

Table 7.2.8.1.1 IQGAP2 and IQGAP3 mRNA expression in liver cancer

Gene	Dataset	Normal (Cases)	Tumor (Cases)	Fold change	*p*-value
IQGAP2	TCGA Liver Cancer (LIHC)*	Liver (49)	HCC (361)	-1.025	≤ 0.0001
IQGAP3	TCGA Liver Cancer (LIHC)*	liver (49)	HCC (361)	4.192	≤ 0.0001

But, the TCGA database analysis of liver cancer (LIHC-TCGA) showed a significant reduction in mRNA level of IQGAP2 (fold change = -1.02) in liver cancer. In contrast, higher IQGAP3 expression (fold change = 4.19) was detected in liver cancer. (Table 7.2.8.1.1).

7.2.8.2 Survival analysis of IQGAP2 and IQGAP3 in liver cancer

To check the correlation between survivability of the liver cancer patients and the expression of IQGAP2 or IQGAP3, two datasets namely LIHC-TCGA and LIVER-TCGA were analysed from SurvExpress.

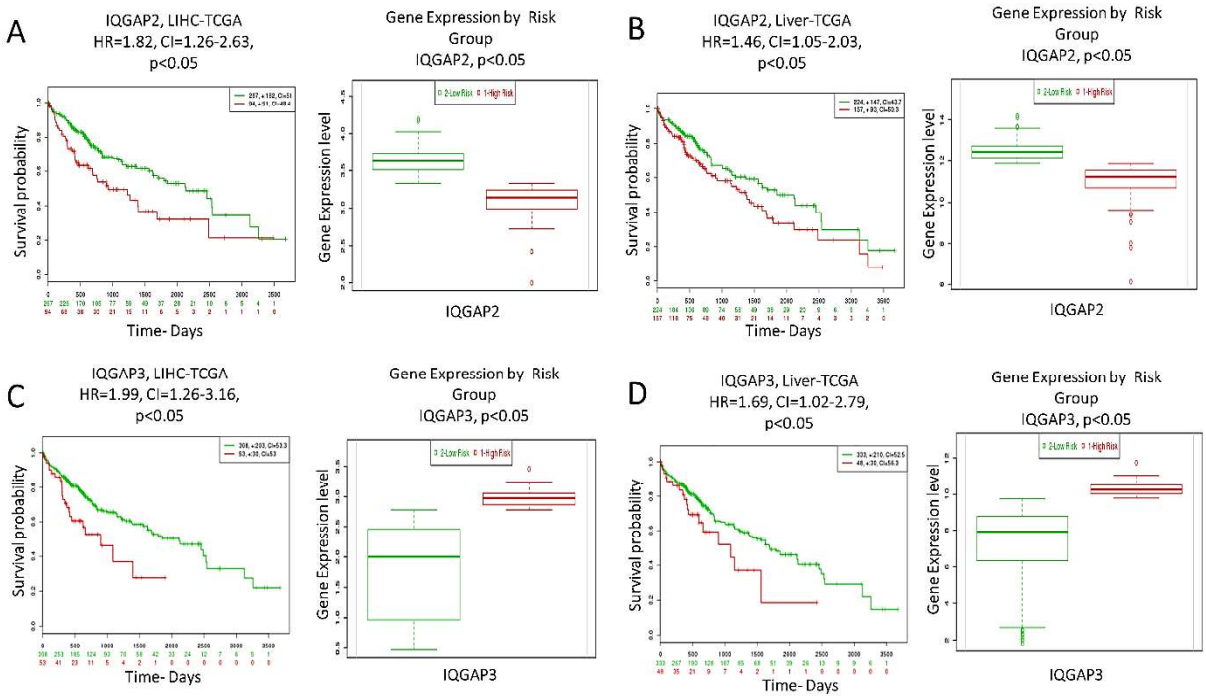

Figure 7.2.8.2.1. The expression of IQGAP2 and IQGAP3 and their correlation with survival of the liver cancer patients. A-B) The survival plot (left panel) showing the association between overall survival of the liver cancer patients and IQGAP2 expression in LIHC-TCGA and LIVER-TCGA datasets, respectively (SurvExpress analysed). Box and whisker plot (right) showing the association between IQGAP2 expression and risk groups of patients. **C-D)** The survival plot (left panel) showing the correlation between overall survival of the liver cancer patient and IQGAP3 expression in LIHC-TCGA and LIVER-TCGA datasets respectively (SurvExpress analysed). Box and whisker plot (right) showing the association between IQGAP3 expression and risk groups of patients. Survival curves are shown in green (low risk group) and red (high risk groups). The X-axis displays the time (days) to event.

Here, we observed that low IQGAP2 expression were correlated with the poor OS survivability of liver cancer patients (LIHC-TCGA- $p \leq 0.001$, HR- 1.82, 95% CI 1.26-2.63 and LIVER-TCGA- $p \leq 0.05$, HR- 1.46, 95% CI 1.05-2.03) (Fig. 7.2.8.2.1A, B).

In contrast, elevated IQGAP3 transcript level was associated with the low survivability of the patients (LIHC-TCGA- $p \leq 0.001$, HR- 1.99, 95% CI 1.26-3.16 and LIVER-TCGA- $p \leq 0.05$, HR- 1.69, 95% CI 1.02-2.79) (Fig. 7.2.8.2.1C, D).

To summarise, IQGAP2 was downregulated, while IQGAP3 was significantly increased in liver cancer. While expression levels of the former associated with good survivability, transcript levels of the latter predicted poor prognosis.

7.2.9 Kidney Cancer

Kidney cancer also known as the renal cancer is categorised into, renal cell carcinoma (RCC) and transitional cell carcinoma of renal pelvis (TCC). RCC is further sub-grouped into, papillary, clear cell and chromophobe on the basis of histology of RCC. Among the major types, RCC is the predominant type (80%) compared to TCC (10%).

7.2.9.1 Expression of IQGAP2 and IQGAP3 in kidney cancer

The Oncomine dataset analysis showed reduced expression of IQGAP2 in clear RCC and papillary RCC. A similar IQGAP2 expression pattern was observed in TCGA datasets. The analysis showed low expression of IQGAP2 in KIRC-TCGA and KIRP-TCGA datasets (Table 7.2.9.1.1).

No substantial change in expression of IQGAP3 was observed in kidney cancer at the set threshold parameters of Oncomine.

Table 7.2.9.1.1. IQGAP2 mRNA expression in kidney cancer

Dataset	Normal (Cases)	Tumor (Cases)	Fold change	*p*-value
Yesenko Renal	Kidney (3), Fetal Kidney (2)	Papillary Renal Cell Ca. (19)	-3.568	1.1e-7
Higgins Renal	Kidney (3)	Clear Renal Cell Ca. (25)	-2.105	2.4e-4
Beroukhim Renal	Renal Cortex (10), Renal Tissue (1)	Non-Hereditary Clear Renal Cell Ca. (27)	-2.886	1.6e-6
Gumz Renal	Kidney (10)	Clear Renal Cell Ca. (10)	-2.598	2.7e-5
Lenburg Renal	Kidney (9)	Clear Renal Cell Ca. (9)	-2.623	4.7e-4
TCGA Kidney Papillary Cell Ca. (KIRP)*	Kidney (32)	Papillary Renal Cell Ca. (290)	-2.225	≤ 0.0001
TCGA Kidney Clear Cell Ca. (KIRC)*	Kidney (72)	Clear Renal Cell Ca. (533)	-1.057	≤ 0.0001

However, the analysis of TCGA datasets (KIRC-TCGA and KIRP-TCGA), showed significantly elevated levels of IQGAP3 in renal cancer (Table 7.2.9.1.2).

Table 7.2.9.1.2. The mRNA expression of IQGAP3 in kidney cancer

Dataset	Normal (Cases)	Tumor (Cases)	Fold change	*p*-value
TCGA Kidney Papillary Cell Ca. (KIRP)*	Kidney (32)	Papillary Renal Cell Ca. (290)	2.67	≤ 0.0001
TCGA Kidney Clear Cell Ca. (KIRC)*	Kidney (72)	Clear Renal Cell Ca. (533)	2.935	≤ 0.0001

7.2.9.2 Prognostic significance of IQGAP2 and IQGAP3 in kidney cancer

The survival data were analysed from SurvExpress KIRC-TCGA and KIPAN-TCGA datasets. In both TCGA datasets, we observed poor OS of the patients with reduced

IQGAP2 expression (KIPAN-TCGA- $p \leq 0.0001$, HR- 2.54, 95% CI 1.83-3.52 and KIRC-TCGA- $p \leq 0.0001$, HR- 3.03, 95% CI 2.09-4.4) (Figs 7.2.9.2.1A, B). In contrast, with higher expression of IQGAP3 the OS of the patient was reduced (KIPAN-TCGA- $p \leq 0.0001$, HR- 3.17, 95% CI 2.4-4.2 and KIRC-TCGA- $p \leq 0.0001$, HR- 3.45, 95% CI 2.29-5.21) (Fig. 7.2.9.2.1C, D).

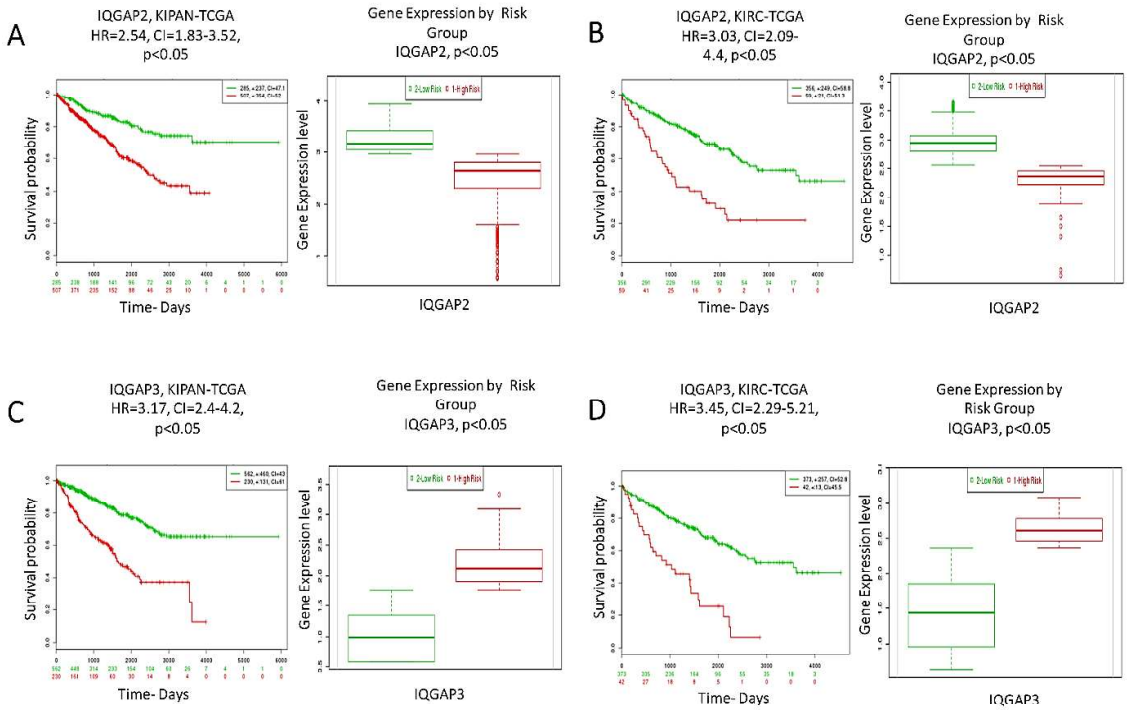

Figure 7.2.9.2.1. Expression of IQGAP2 and IQGAP3 and their association with prognosis of the renal cancer. A-B) The survival plot (left panel) showing the correlation between overall survival of the renal cancer patient and IQGAP2 expression in KIPAN-TCGA and KIRC-TCGA datasets respectively (SurvExpress analysed). Box and whisker plot (right) showing the association between IQGAP2 expression and risk groups of patients. **C-D)** The survival plot (left panel) showing the correlation between overall survival (OS) of the liver cancer patient and IQGAP3 expression in KIPAN-TCGA and KIRC-TCGA datasets respectively (SurvExpress analysed). Box and whisker plot (right) showing the association between the expression level of IQGAP3 and risk groups of patients. Here at the top of each graph, the p-value and 95% CI have been shown for selected dataset. Survival risk curves are shown in green (low risk group) and red (high risk groups). The X-axis shows the time (days) to event.

To summarise, IQGAP2 mRNA levels were significantly reduced, while IQGAP3 mRNA levels were overexpressed in kidney cancer. Increased IQGAP2 transcript levels

associated with good survivability, while increased IQGAP3 mRNA levels predicted poor disease outcome.

7.2.10 Expression of IQGAP2 and IQGAP3 in different stages of cancer

To examine the status of IQGAP2 and IQGAP3 mRNA expression in various stages of cancers (I to IV), the expression analysis of these genes was carried out in breast, colorectal, lung, brain, liver, stomach, kidney and prostate cancer. Due to lack of stage wise data in brain cancer, the expression analysis was done among the histologic grades (G2 and G3).

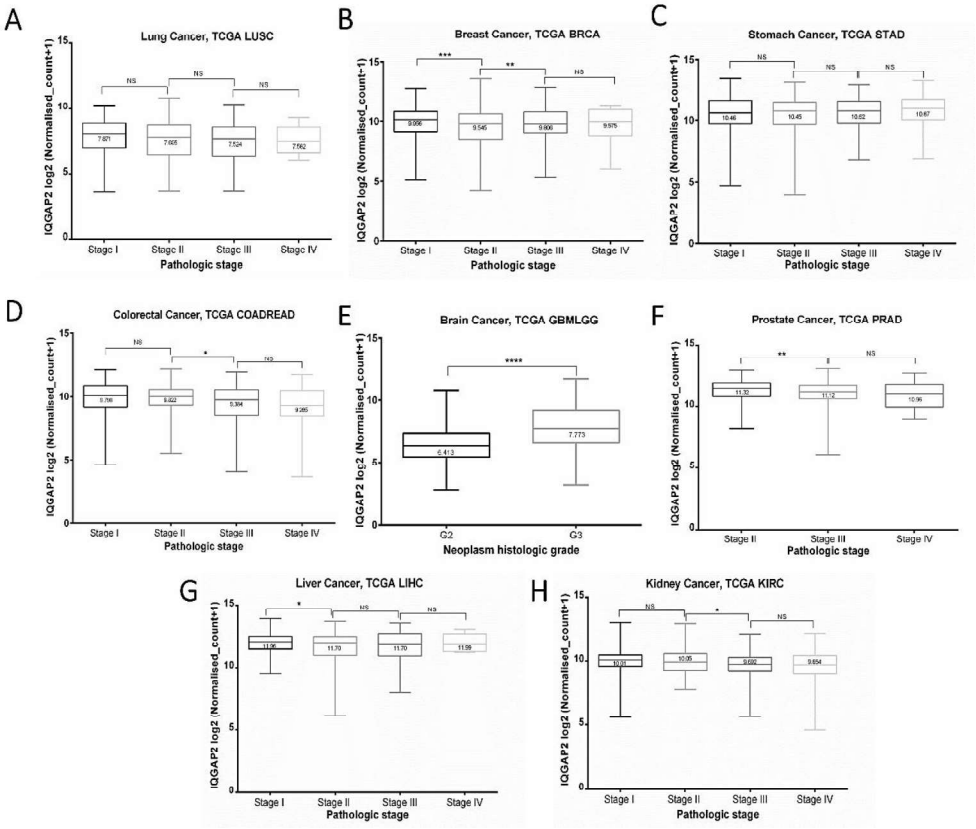

Figure 7.2.10.1. Expression levels of IQGAP2 in different stages of cancers. Box plots showing the trend of IQGAP2 expression with stages of (A) lung cancer (B) breast cancer (C) stomach cancer (D) colorectal cancer (E) brain cancer (F) prostate cancer (G) liver cancer and, (H) kidney cancer. The TCGA dataset selected for analysis of each cancer type is highlighted in box plot. In plot, X-axis shows the log2 normalised mRNA expression of gene. Y-axis represents diffrent pathological stage of cancer.

The mRNA level of IQGAP2 was significantly reduced in stage II than stage I in breast and liver cancer. Similarly, low IQGAP2 level was also observed in stage III compared to II in liver, prostate, colorectal, and kidney cancer. In contrary, elevated IQGAP2 mRNA level was found in higher grade of brain cancer (G3) than the low grade brain cancer (G2). In case of lung cancer, no substantial differences were observed between the stages in respect to IQGAP2 levels (Fig. 7.2.10.1).

In contrast to IQGAP2, elevated IQGAP3 expression was observed in stage II compared to the stage I in lung and breast cancer. Similarly, increased expression of IQGAP3 was detected in stage III compared to stage I in kidney and prostate cancer. In case of brain cancer, IQGAP3 mRNA level was elevated in higher grade (G3) compared to the lower grade (G2) of brain cancer. No such significant differences in IQGAP3 expression among stages of stomach and liver cancer were observed (Fig. 7.2.10.2).

As a whole the results in this section highlight that IQGAP2 levels show a significant reduction with disease progression, with brain and prostate tumors as exceptions. IQGAP3 levels on the other hand show upregulation with increasing stage of tumor. We speculate that IQGAP2 and IQGAP3 may play crucial role in the initiation or progression of cancers in tissue specific manner. The results indicate the role of IQGAP2 in initiation in neoplasm like breast cancer, liver and lung cancer whereas in tumor progression in kidney and colorectal cancer. Similarly, IQGAP3 might have role in initiation of liver, breast, colorectal, lung and stomach cancer whereas, in progression of prostate, brain and kidney cancer.

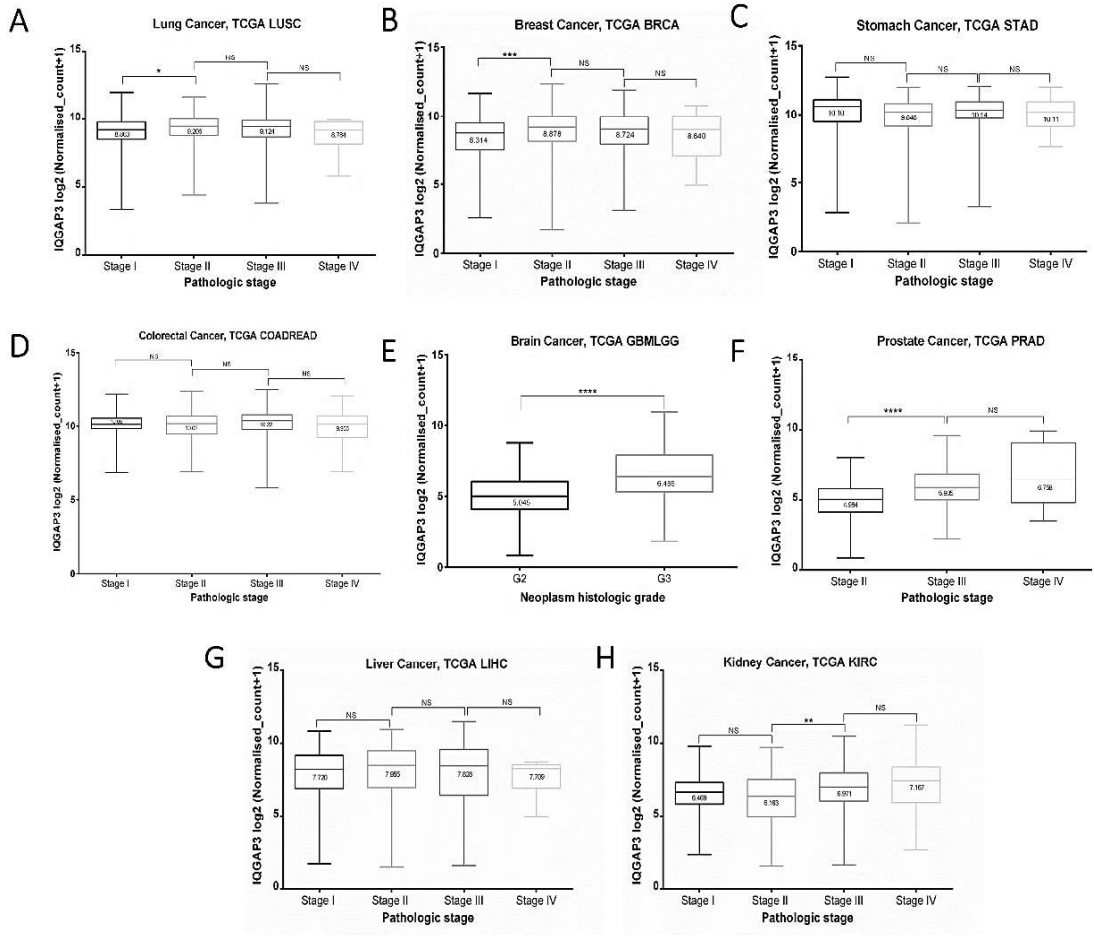

Figure 7.2.10.2. Expression analysis of IQGAP3 with stages in different cancers. Box plots showing the stages wise expression of IQGAP3 in (A) lung cancer (B) breast cancer (C) stomach cancer (D) colorectal cancer (E) brain cancer (F) prostate cancer (G) liver cancer and (H) kidney cancer. The TCGA dataset selected for analysis of each cancer type is highlighted in box plot. X-axis displays the log2 normalised mRNA expression of gene. Y-axis represents the different pathological stage of cancer.

7.2.11 IQGAP2 and IQGAP3 mutations and copy number alterations

Further, to examine the cause of expression changes of both the genes, we performed mutation and copy number analysis in all eight cancer types using TCGA datasets. The studies which were included for the nutation and copy number analysis have been summarised in Table 7.2.11.1. The results showed different frequency of somatic mutations, deletion or gene amplification associated with both the genes, which are summarised in Table 7.2.11.1.

In case of IQGAP2, no remarkable change in copy number was observed in cancers, except prostate cancer (Table 7.2.11.1A). In prostate cancer the copy number was reduced in 4.2% cases.

Table 7.2.11.1. Genomic alterations associated with IQGAP2 and IQGAP3 in cancers

A. Frequency of genomic alterations of IQGAP2 in cancers

Data source	Cancer type	Number of cases (N)	Alteration frequency (%) (n)	Amp (%) (n)	Del (%) (n)	Missense and other mutations (%)(n)
Metabric, Nature	Breast	2051	0.6 (12)	0.5 (11)	0 (1)	0
TCGA, Cell 2015	Breast	816	2.2 (18)	0	1.6 (13)	0.6 (5)
TCGA, Nature 2013	Kidney	418	1.2 (5)	0.2 (1)	0	1 (4)
TCGA, Nature 2012	colorectal	212	5.2 (11)	0	0.5 (1)	**4.7** (10)
TCGA, Cell 2016	Brain	794	0.4 (3)	0	0.3 (2)	0.1 (1)
TCGA Provisional	Liver	366	1.9 (7)	0.5 (2)	0.3 (1)	1.1 (4)
TCGA, Nature 2014	Lung	230	5.2 (12)	0	0.9 (2)	**4.3** (10)
TCGA, Nature 2012	Lung	178	4.5 (8)	0	0.6 (1)	**3.9** (7)
TCGA, Cell 2015	Prostate	333	4.5 (15)	0	**4.2** (14)	0.3 (1)
TCGA, Nature 2014	Stomach	287	4.9 (14)	0.3 (1)	1.7 (5)	2.8 (8)

B. Frequency of genomic alterations of IQGAP3 in cancers

Data source	Cancer type	Number of cases (N)	Alteration frequency (%) (n)	Amp (%) (n)	Del (%) (n)	Missense and other mutations (%)(n)
Metabric, Nature	Breast	2051	20.7 (424)	**20.7** (424)	0	0
TCGA, Cell 2015	Breast	816	12.9 (105)	**11.9** (97)	0	0.9 (8)
TCGA, Nature 2013	Kidney	418	1 (4)	0.2 (1)	0	0.7 (3)
TCGA, Nature 2012	colorectal	212	5.7 (12)	0.5 (1)	0	**5.2** (11)
TCGA, Cell 2016	Brain	794	1.1 (9)	1.1 (9)	0	0
TCGA Provisional	Liver	366	14.2 (52)	**12.3** (45)	0	1.9 (7)
TCGA, Nature 2014	Lung	230	14.3 (33)	**12.6** (29)	0	1.7 (4)
TCGA, Nature 2012	Lung	178	9 (16)	1.7 (3)	0	**7.3** (13)
TCGA, Cell 2015	Prostate	333	1.8 (6)	0.6 (2)	0.9 (3)	0.3 (1)
TCGA, Nature 2014	Stomach	287	7.3 (21)	2.1 (6)	0	**5.2** (15)

Abbreviations used- N- total number of cases, n- cases showing genetic alterations.

In case of IQGAP3, the analysis revealed higher frequency of gene amplification in liver cancer (12.3%), lung adenocarcinoma (12.6%), and breast cancer (11.9% in TCGA

dataset, 20.7% in Metabric dataset), whereas low frequency of copy number was observed in stomach, prostate, lung squamous cell carcinoma, kidney and brain cancer (Table 7.2.11.1B).

Furthermore, a correlation analysis between expression of IQGAP3 and copy number was carried out to verify the effect of former on later in those cancer types where we observed high copy number changes. The analysis showed a positive correlation between the two (Fig. 7.2.11.1).

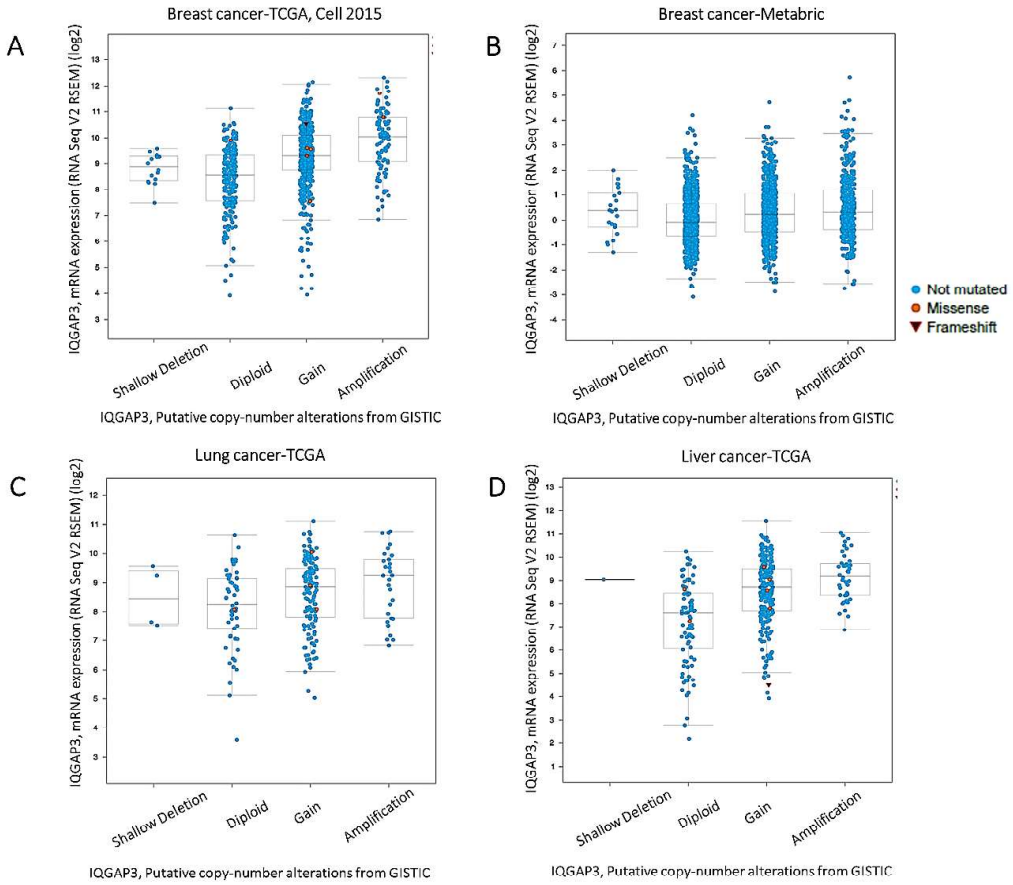

Figure 7.2.11.1. The association of IQGAP3 expression and copy number. Box and whisker plot showing the association of IQGAP3 transcript level with copy number in; **A)** Breast cancer-TCGA, Cell 2015 dataset. **B)** Breast cancer-Metabric dataset. **C)** Lung cancer-TCGA dataset and **D)** Liver cancer-TCGA datasets. X-axis displaying putative copy number alterations. Y-axis represents the mRNA expression Z-scores.

The mutation analysis of IQGAP2 showed, high frequency of pan-mutations in colorectal cancer, lung squamous cell carcinoma and lung adenocarcinoma (Fig. 7.2.11.2A).

However, no specific single point mutation with high frequency was observed on in-depth analysis (Fig. 7.2.11.2C).

Mutation analysis of IQGAP3 showed high frequency of mutations in colorectal (5.2%), lung squamous cell carcinoma (7.3%) and stomach cancer (5.2%), where the frequency of copy number change was very low (Fig. 7.2.11.2B). Here it is noteworthy that one frequent mutation (V293I/X293_splice) was present in four stomach cancer cases, at the splice site of IQGAP3(Fig. 7.2.11.2D).

Here it is worth mentioning that we observed one specific mutation in four gastric cancers (V293I/X293_splice). This mutation was located at the splice site of IQGAP3.

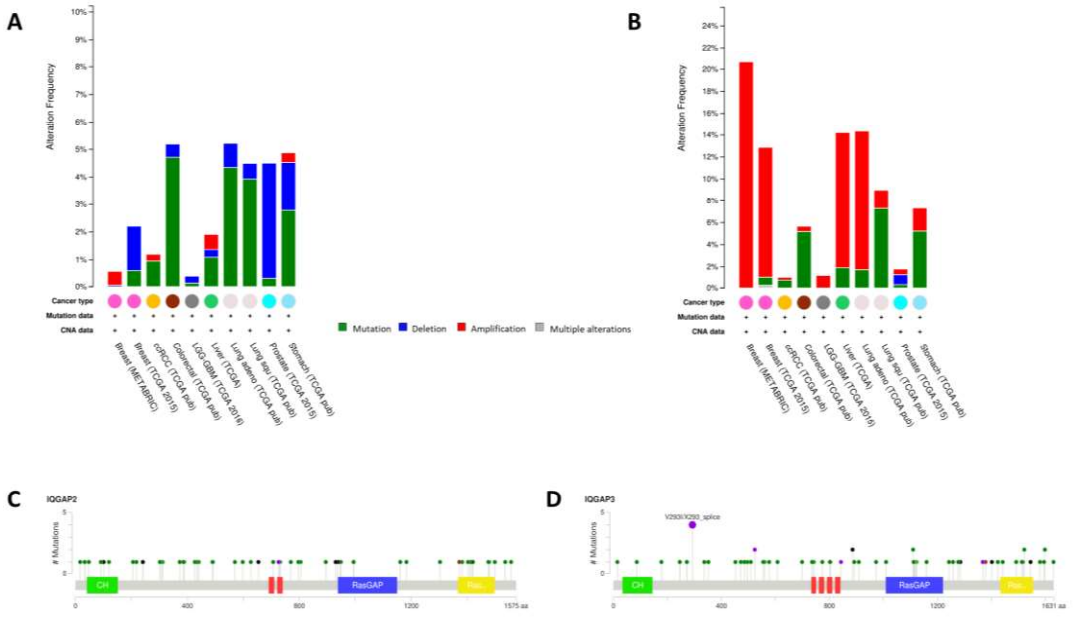

Figure 7.2.11.2. Frequency of Genetic alterations in IQGAP2 and IQGAP3 in different cancers. The percentage frequency of various genetic changes associated with; **A)** IQGAP2 gene. **B)** IQGAP3 gene. Colours shown in figure represent a particular genetic change. In figure, X-axis represents the studies selected for analysis. Y-axis display the percentage of genetic alteration in each cancer type. **C)** graphical summary displaying all nonsynonymous mutations of IQGAP2. The position and frequency of mutations displayed in the graphical summary are in context of Pfam protein domains. **D)** graphical summary showing nonsynonymous mutations of IQGAP3. Here, most frequent mutation at 293_splice site has been shown in purple colour.

7.2.12 Methylation status of IQGAP2 and IQGAP3 promoters

Epigenetic modification is very crucial event that regulates the expression of a gene. In cancer, hyper methylation of promoter of a tumor suppressor gene results in loss of expression and, progression of disease. So, next we checked the status of methylation at the CpG islands of promoter region of both genes, in different cancer types. Initially, the status of methylation at promotor region of IQGAP2 and IQGAP3 in various cancer was compared with the normal. The probes displaying significant changes (table 7.2.12.1 and 7.2.12.2), were further subjected to correlation analyses with the transcript levels.

Overall, a significant change in methylation pattern of IQGAP2/IQGAP3 promoter region in cancer, with the exception of glioblastoma multiforme and stomach cancer, was observed. This might be because of the low sample size in normal group (n = 2). A weak correlation was observed between the mRNA expression and methylation pattern at promoter region of these isoforms in all cancer types.

Table 7.2.12.1. Methylation status of IQGAP2 promoter region and its correlation with the mRNA expression

Data source	**Cancer type**	**No. of cases (N)**	**Probes significantly altered in methylation level at p ≤ 0.05**	**Pearson coefficient (Meth vs mRNA)**	**Correlation (Strong/Weak)**
		Normal/ Cancer		Normal/ Cancer	
TCGA LUAD	Lung adenocarcinoma	32/463	cg19828169	-0.097/ -0.21	Weak
			cg05060672	0.188/ -0.235	Weak
TCGA LUSC	Lung squamous cell carcinoma	43/361	cg02294176	0.101/ 0.008	Weak
			cg19828169	-0.09/ 0.029	Weak
			cg05060672	0.19/ -0.051	Weak
			cg02387679	-0.248/ -0.182	Weak

TCGA BRCA	Breast Invasive Carcinoma	98/743	cg19828169	-0.049/ -0.202	Weak
			cg05060672	0.063/ -0.29	Weak
			cg02387679	0.119/ -0.359	Weak
TCGA COAD	Colorectal Cancer	38/302	cg19828169	0.431/ -0.121	Weak
TCGA STAD	Stomach Cancer	2/339	ns	-	-
TCGA KRIC	Kidney renal clear cell carcinoma	160/324	cg02294176	-0.249/ -0.261	Weak
			cg19828169	-0.08/ -0.158	Weak
			cg05060672	-0.178/ -0.162	Weak
			cg02387679	-0.232/ -0.4	Weak
TCGA LIHC	Liver hepatocellular Carcinoma	50/256	cg26024851	0.458/ -0.004	Weak
			cg12262564	0.504/ 0.048	Weak
			cg12441221	-0.173/ -0.147	Weak
			cg17722719	-0.11/ -0.112	Weak
			cg12124478	0.437/ 0.054	Weak
TCGA GBM	Glioblastoma multiforme	2/129	ns	-	-
TCGA PRAD	Prostate adenocarcinoma	49/340	cg02294176	-0.249/ 0.116	Weak
			cg19828169	-0.073/ 0.051	Weak
			cg05060672	-0.408/ -0.067	Weak
			cg02387679	-0.231/ -0.061	Weak

Table 7.2.12.2. Methylation status of IQGAP3 promoter region and its correlation with the mRNA expression

Data source	Cancer type	Number of cases (N)	Probes significantly altered in methylation level at p≤ 0.05	Pearson coefficient (Meth vs mRNA)	Correlation (Strong/Weak)
		Normal/ Cancer		Normal/ Cancer	
TCGA LUAD	Lung adenocarcinoma	32/ 463	cg26024851	-0.106/ 0.019	Weak
			cg12441221	0.165/ -0.115	Weak
			cg17722719	0.084/ -0.01	Weak
TCGA LUSC	Lung squamous cell carcinoma	43/ 361	cg26024851	0.124/ -0.136	Weak
			cg12441221	0.299/ -0.03	Weak
			cg17722719	-0.195/ -0.117	Weak
			cg12124478	0.597/ -0.093	Weak
TCGA BRCA	Breast Invasive Carcinoma	98/ 743	cg26024851	-0.027/ 0.006	Weak
			cg12262564	0.002/ 0.008	Weak
			cg12441221	-0.047/ -0.183	Weak
			cg17722719	-0.113/ -0.1	Weak
TCGA COAD	Colorectal Cancer	38/ 302	cg26024851	0.215/ -0.057	Weak
			cg12262564	0.228/ -0.092	Weak
TCGA STAD	Stomach Cancer	2/ 339	ns	_	_
TCGA KRIC	Kidney renal clear cell carc.	160/ 324	cg26024851	0.56/ 0.206	Weak
			cg12262564	0.67/ 0.222	Weak
			cg12441221	-0.076/ -0.087	Weak
			cg17722719	-0.209/ -0.094	Weak
			cg12124478	0.265/ 0.146	Weak
		50/	cg26024851	0.458/	Weak

TCGA LIHC	Liver hep. Carcinoma	256		-0.004	
			cg12262564	0.504/ -0.048	Weak
			cg12441221	-0.173/ -0.147	Weak
			cg17722719	-0.11/ -0.112	Weak
			cg12124478	0.437/ 0.054	Weak
TCGA GBM	Glioblastoma multiforme	2/ 129	Ns	–	–
TCGA PRAD	Prostate adenocarcinoma	49/ 340	cg26024851	-0.008/ -0.02	Weak
			cg12262564	0.084/ 0.004	Weak
			cg12441221	0.232/ -0.024	Weak
			cg17722719	0.078/ -0.028	Weak
			cg12124478	-0.084/ 0.041	Weak

7.2.13 IQGAP2 and IQGAP3 expression validation by IHC

Next, the in-silico findings of IQGAP2 and IQGAP3 mRNA expression in cancers, were validated by protein expression level analysis by immunohistochemistry (IHC). We also examined the localization of these isoforms in cancer patients. We compared IQGAP2 and IQGAP3 expression between tumor tissue and the adjacent normal region, in prostate, colorectal, stomach and brain cancer. To check the localization of these proteins, nucleus was counter stained with hematoxylin.

The results showed that IQGAP2 expression was predominant in cytoplasm and membrane. But the expression of IQGAP3 was predominant in the nucleus (Fig. 7.2.13.1). In colorectal and gastric cancer, the expression of IQGAP2 was low in tumor tissues. In contrast, in brain and prostate cancer the pattern of IQGAP2 expression was opposite. The expression of IQGAP3 was high in cancer tissue in all four types of cancer under investigation.

The IRS score analysis indicated low expression of IQGAP2 in stomach cancer (23/47) and colorectal (42/53). In support of the in-silico finding showing high transcript level of IQGAP2 in prostate cancer, IHC results also displayed the higher IQGAP2 protein level in prostate cancer (28/32). In brain cancer, IQGAP2 expression pattern was very similar to the expression in prostate cancer (Fig. 7.2.13.2). The strong IRS score for IQGAP2 was observed in tumor region of only 1.9 % colorectal cancer patients whereas the normal region showed strong IRS score in most of the colorectal cancer patients (78.2 %).

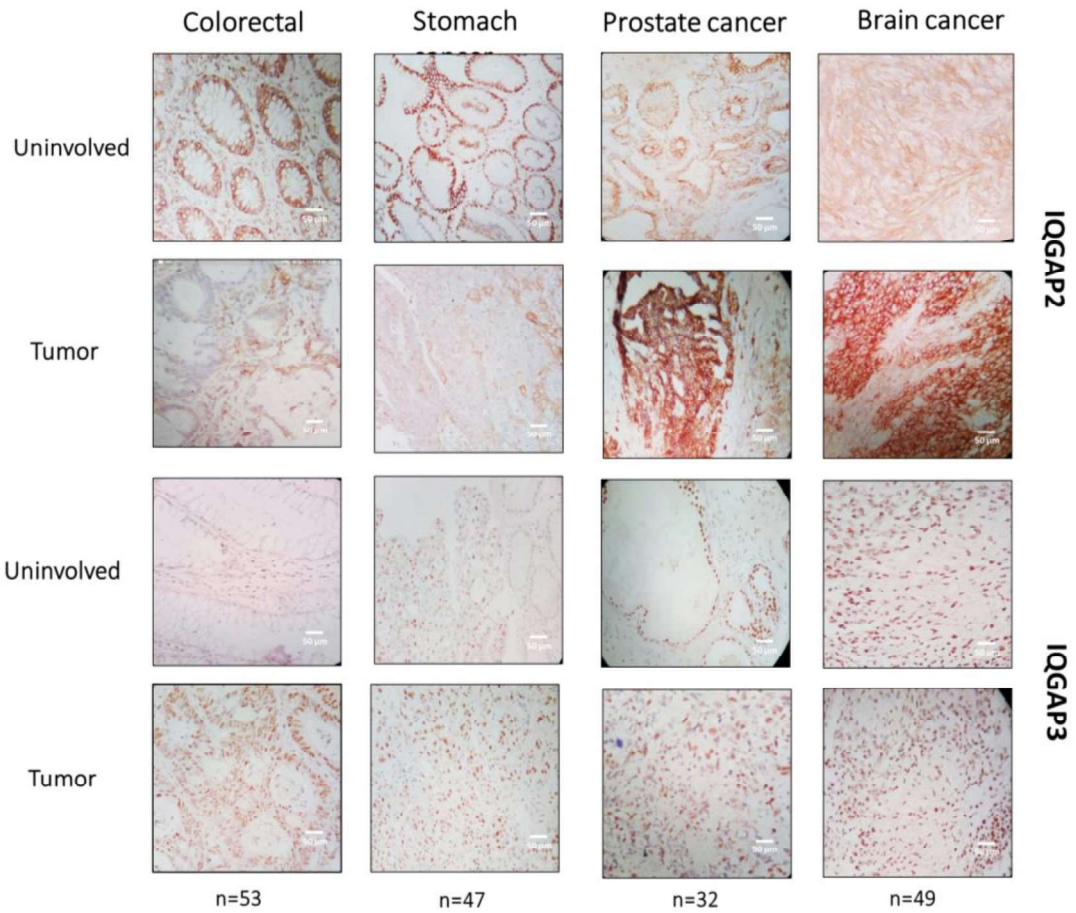

Figure 7.2.13.1. Immunohistochemistry based expression analysis for IQGAP2 and IQGAP3 in different cancers. These images show IHC staining of IQGAP2 and IQGAP3 in tumor or uninvolved/normal areas for colorectal, stomach, prostate and brain cancer. The brown color represents positive staining. Here, 'n' represents the number of cases. Images were taken at 10X objective.

Similarly, in stomach cancer a strong IRS score of IQGAP2 was observed in normal region of majority of the patients (95.56 %). In contrast, in prostate cancer most patients

(87.5 %) showed strong IRS score in tumor region compared to the 47.37 % of BPH patients. Likewise, in brain cancer weak staining was observed in normal region of all brain cancer patient (100%) whereas the tumor region of the brain showed strong, moderate, and weak IRS score in 12.25 %, 26.5 % and, 61.2 % brain cancer patients, respectively.

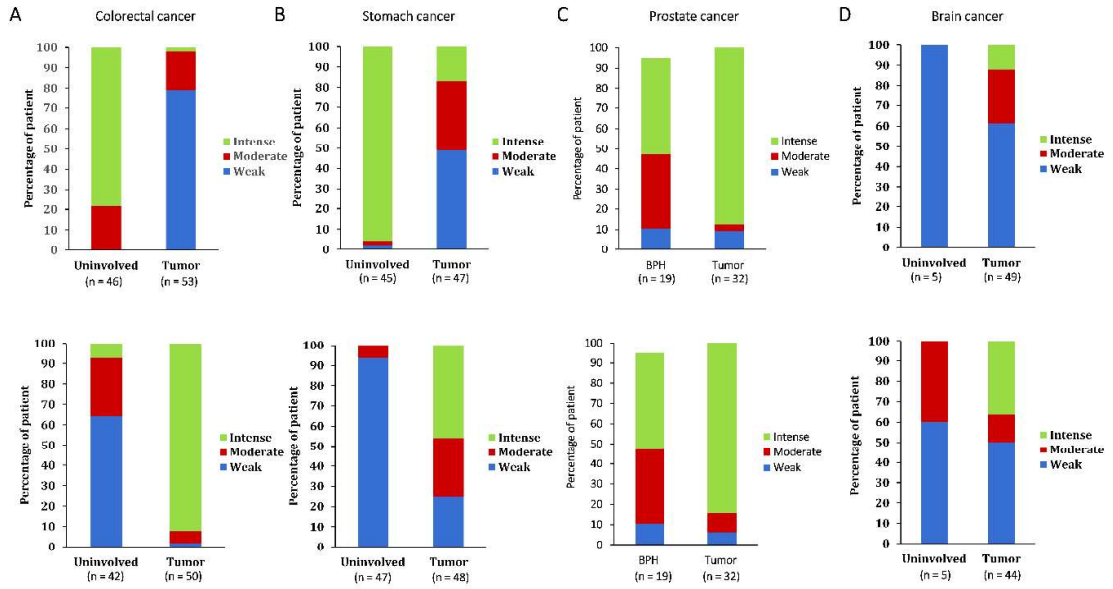

Figure 7.2.13.2. Distribution pattern of IQGAP2 and IQGAP3 expression intensity (IHC based) in normal and cancer tissue. Bar graphs display IQGAP2 and IQGAP3 staining intensity in cancer and normal tissue. Staining intensity represented in three colors (blue- weak, red- moderate and green- strong). X-axis shows normal and tumor tissue type. Y-axis shows the % positivity of patients for specific IQGAPs intensity level. A, B, C and D show expression pattern of IQGAP2 (upper panel) and IQGAP3 (lower panel) in normal vs tumor tissue in colorectal cancer, stomach cancer, prostate cancer and brain cancer, respectively.

On the other hand, IQGAP3 showed an increased expression of this isoform in stomach cancer (22/48), prostate cancer (27/32), colorectal cancer (46/50) and brain cancer (16/44) (Fig. 24). The IRS score of IQGAP3 was strong and moderate in 45.8% and 29.2%, respectively, in tumor region of stomach cancer patients. Whereas, 93.6% of the normal region of the patient showed weak staining for this protein. Similarly, in colorectal cancer, strong IRS score was observed in tumor region of most of the (92%) patients compared

to normal region of the patients (7%). In brain cancer, the trend was very similar to other two cancer types. Strong IRS score was observed in the tumor region of 36.7% patients, whereas in normal region no such strong intensity for IQGAP3 was observed. In case of prostate cancer, we did not find the normal region and therefore, BPH tissue were treated as control in our study. The results showed strong IRS score of IQGAP3 in tumor region of most of the prostate cancer patients (84.4%) compared to the tumor region of BPH patients (47.4%).

Hence we infer that our IHC results are in complete agreement with the results obtained by database analysis, indicating that mRNA levels of both IQGAP isoforms correlate directly with their protein levels.

Overall we found that role of IQGAP2 might be tissue specific but IQGAP3 might work as an oncogene irrespective of tissue type. We did not find their consistent inverse differential expression pattern across all cancer types, rather it was tissue specific.

7.3 Discussion

As opposed to IQGAP1, which has garnered significant importance for its role in carcinogenesis, the role of the other two IQGAP isoforms is relatively less explored. A pan cancer analysis of the expression levels of these isoforms was warranted to understand the significance of these proteins with regard to their role in disease progression and prognosis. Using publically available databases, we were able to show that mRNA levels of IQGAP2 are reduced with some exceptions, while those of IQGAP3 are elevated in all cancer types. The observed expression pattern of these IQGAP isoforms further substantiates the notion that IQGAP2 possibly acts as tumor suppressor gene but in tissues specific manner, whereas IQGAP3 acts as an oncogene an all tissue types.

While IQGAP2 was found to associate with good survival outcome in most of the cancer types, IQGAP3 was associated with worse prognosis in all cancers. It is important to discuss the tissues specific role of IQGAP2 as it was downregulated in most cancers but it showed upregulation in brain and prostate cancers. The answers to this anomaly could lie in the tissue-specific expression pattern inherent to members of this protein family, which hints at their differential functions in specific tissue types. For instance, IQGAP1 expresses ubiquitously, IQGAP3 expresses primarily in the brain, while IQGAP2 expresses predominantly in the liver [16]. It is possible that the relative expression levels of IQGAP1, 2 and 3 determine certain signaling events. Depending upon the growth rate or specialised function of cells, some cell might have high total concentration of pro-proliferation IQGAP isoforms and less concentration of anti-proliferative isoform and vice versa. The another cause behind the specialised function of IQGAPs may be the variations in the amino acid sequences of IQGAP isoforms. It is possible that post-translational modifications in non-conserved region residues among three isoforms, regulate the function differentially. For example, phosphorylation at Serine- 123, 330, 124, residues in IQGAP1 is observed. Interestingly these residue are not conserved in IQGAP2 or IQGAP3 [277, 278]. In this study we have shown that IQGAP2 may inhibit, IQGAP1 mediated signaling, which supports the role of their relative expression levels. Another possibility is IQGAP2 interacts with other molecules in tissue specific manner, which decides its function in that tissue.

While prospecting possible explanations for the altered expression levels of these IQGAP isoforms in different cancer types, we found gene amplification and promoter methylation to be possible factors responsible for the same. The effect of hyper methylation in IQGAP2 silencing, is reported in the pathogenesis of gastric [40] and ovarian cancers [42]. Our results show a weak negative correlation between IQGAP2 expression and

methylation status in lung adenocarcinoma, breast, colorectal and kidney cancer, but no such correlation was observed with liver, prostate, glioblastoma and gastric cancer. Our results in HCC and prostate cancer are in line with the previous reports where no significant correlation between promoter methylation and expression status of IQGAP2 was observed [39, 41]. In HCC the methylation of promoter may not be the principle mechanism of IQGAP2 depletion. Some specific miRNAs have been reported which silence IQGAP1 in HCC [39], so the possibilities of IQGAP2 expression depletion by some kind of specific miRNAs cannot be overlooked. In our study a positive correlation between IQGAP3 mRNA level and gene copy number was observed in breast, liver and lung cancers. In other cancers, this type of correlation was not observed, indicating the other possible mechanism/s behind the upregulated mRNA level of IQGAP3. In HCC E2F1, a retinoblastoma protein binding transcription factor, has been reported to bind to the promoter region of IQGAP3 and subsequent transactivation of transcript level [279]. The possibility of this type of mechanism for upregulated expression of IQGAP3 in other cancer types can never be underestimated.

Reduction of IQGAP2 levels and increase in IQGAP3 levels with disease progression further underscores the clinical significance of these proteins in disease progression. Corroboration of findings at mRNA levels with measurement of protein levels via IHC proves that there is a direct correlation between the transcript and protein levels of these proteins. This makes the significance of both of these genes as potential biomarkers, even more relevant. We have previously discussed about the reciprocal function of IQGAP2, as opposed to IQGAP1, in mediating oncogenic effects in breast cancer. Since, we observed that like IQGAP1, IQGAP3 also shows an almost opposite expression pattern to IQGAP2 in breast cancer tissues, it would be interesting to investigate the possibility of IQGAP2 being a potential hindrance to the oncogenic role of IQGAP3 in breast tumors

cells, just as we have seen with IQGAP1. The therapeutic significance of IQGAP2 in this context becomes even more promising as it is able to counteract the pro-metastatic tendencies of not just one protein, but two, in the same tissue.

SUMMARY AND CONCLUSION

DINESH KUMAR

NISER, Bhubaneswar

8. SUMMARY AND CONCLUSION

Members of the IQGAP protein family have become known as mediators of key processes linked to cancer. Much of the evidence in this regard, came from the study of IQGAP1, which established itself as a potent oncogene, overexpressed across a wide variety of cancer types, via triggering EMT and neoangiogenesis. Later, IQGAP3 was also found to play pro-tumorigenic role in many cancers. As expected, the levels of these proteins predicted poor survival outcome in cancers. In the midst of all this, contradictory findings regarding the role of IQGAP2 in cancer progression emerged; a couple of studies found overexpression of this protein, while most of the others reported downregulation in cancers. However, *in vitro* and *in vivo* function studies, weighed in on the tumor-suppressive role of IQGAP2. The tumor-suppressive ability of IQGAP2 was supported by findings in HCC, in which IQGAP2 showed a reciprocal expression pattern to IQGAP1 and functionally abrogated the pro-cancerous abilities of IQGAP1.

Despite the key finding of IQGAP1 neutralizing effect, IQGAP2 did not garner any attention with regard to its role in breast cancer. Investigating the role of IQGAP2 in EMT and angiogenesis in mammary carcinoma is highly beneficial in a therapeutic sense, more so because of the involvement of IQGAP1 in accelerating such processes. With these considerations in mind, we carried out this study to explore the role of IQGAP2 in breast cancer as a priority.

We found that as opposed to IQGAP1 and IQGAP3, the expression of IQGAP2 decreases with breast cancer progression, with more expression in early stages compared to later and more aggressive stages. IQGAP2 was also associated with decreased lymphovascular invasion in breast cancer patients. Using *in vitro* and *in vivo* approaches, we were able to show that IQGAP2 expression suppressed the ERK pathways in breast tumor cells,

leading to reduction of ERK dependent proliferation, migration and invasion abilities of these cells and vice versa. There was reduction in expression levels of key EMT molecules and inflammatory cytokines upon ectopic IQGAP2 expression. More importantly, the tumor-suppressive ability of IQGAP2 was independent of the molecular subtype of breast cancer cells. IQGAP2 was also found to activate estrogen receptor mediated signaling in luminal cells. GST-Pull downs suggested the possibility of the presence of a IQGAP2-IQGAP1 scaffold complex in breast cancer, leading to sequestering effect of IQGAP2 on IQGAP1, resulting in the reduction of phospho-ERK levels in the cells. We went on to show that IQGAP2 acts as an inhibitor of tumor angiogenesis in breast cancer, via repression of VEGF-A levels, thereby down regulating the VEGFA-VEGFR2-AKT pathway which is exploited by endothelial cells to proliferate, migrate and tabulate during the process of angiogenesis in the tumor. In breast cancer patients, microvessel density, which is a direct indicator of tumor vascularisation and often significantly associated with survival outcome, was found to be negatively associated with IQGAP2 protein levels, highlighting the clinical significance of IQGAP2 in breast tumor neovascularisation. A pan-cancer analysis of publically available databases showed that mRNA levels of IQGAP2 are reduced with some exceptions, while those of IQGAP3 are elevated in all cancer types. While IQGAP2 was found to associate with good survival outcome in most of the cancer types, IQGAP3 was associated with worse prognosis in all cancers. We showed that gene amplification and promoter methylation could be responsible for maintenance of IQGAP2/IQGAP3 levels in different caners. It is important to mention that for IQGAP2, the expression pattern was opposite in a couple of cancers, which needs to be investigated in the light of the tissue-specific roles of this protein. There was a correlation between the mRNA and protein levels of both of these genes in cancers.

To conclude, we have shown that IQGAP2 restricts tumor growth and EMT, independent of molecular subtype of breast cancer cells, primarily via repression of MEK-ERK pathway. The physical interaction between IQGAP2 and IQGAP1 may provide a sequestering effect on IQGAP1 mediated ERK pathway. Understanding the divergent functions of IQGAP1 and IQGAP2 with regards to their affinity to be differentially phosphorylated by specific kinases, and interaction with different binding partners like GTPases is of utmost importance to develop them into molecular targets for breast cancer therapy in the near future. We also show that IQGAP2 presents a promising therapeutic target for tumor angiogenesis, evident by its role in suppressing the VEGF-VEGFR2 signaling cascade, which plays significant role in promoting tumor angiogenesis. In addition to illustrating the reciprocal function of IQGAP2, as opposed to IQGAP1, in mediating oncogenic effects in breast cancer, we have also shown opposite expression pattern of IQGAP3 to IQGAP2 in multiple cancers, including breast cancer tissues. In the near future, it would be interesting to investigate the possibility of IQGAP2 being a potential hindrance to the oncogenic role of IQGAP3 in breast tumor cells, as we have seen with IQGAP1. This will add more weightage to the prospects of IQGAP2 being used in therapeutic intervention of breast cancer.

BIBLIOGRAPHY

DINESH KUMAR

NISER, Bhubaneswar

9. BIBLIOGRAPHY

1. Bray, F., et al., *Global cancer statistics 2018: GLOBOCAN estimates of incidence and mortality worldwide for 36 cancers in 185 countries.* CA Cancer J Clin, 2018. **68**(6): p. 394-424.
2. Rojas, K. and A. Stuckey, *Breast Cancer Epidemiology and Risk Factors.* Clin Obstet Gynecol, 2016. **59**(4): p. 651-672.
3. Brody, J.G., et al., *Environmental pollutants and breast cancer: epidemiologic studies.* Cancer, 2007. **109**(12 Suppl): p. 2667-711.
4. Waks, A.G. and E.P. Winer, *Breast Cancer Treatment: A Review.* JAMA, 2019. **321**(3): p. 288-300.
5. Pucci, C., C. Martinelli, and G. Ciofani, *Innovative approaches for cancer treatment: current perspectives and new challenges.* Ecancermedicalscience, 2019. **13**: p. 961.
6. Davies, E. and S. Hiscox, *New therapeutic approaches in breast cancer.* Maturitas, 2011. **68**(2): p. 121-8.
7. Utku, N., *New approaches to treat cancer - what they can and cannot do.* Biotechnol Healthc, 2011. **8**(4): p. 25-7.
8. Masoud, V. and G. Pages, *Targeted therapies in breast cancer: New challenges to fight against resistance.* World J Clin Oncol, 2017. **8**(2): p. 120-134.
9. Hedman, A.C., J.M. Smith, and D.B. Sacks, *The biology of IQGAP proteins: beyond the cytoskeleton.* EMBO Rep, 2015. **16**(4): p. 427-46.
10. Shannon, K.B., *IQGAP Family Members in Yeast, Dictyostelium, and Mammalian Cells.* Int J Cell Biol, 2012. **2012**: p. 894817.

11. Lee, I.J., V.C. Coffman, and J.Q. Wu, *Contractile-ring assembly in fission yeast cytokinesis: Recent advances and new perspectives.* Cytoskeleton (Hoboken), 2012. **69**(10): p. 751-63.

12. Noritake, J., et al., *IQGAP1: a key regulator of adhesion and migration.* J Cell Sci, 2005. **118**(Pt 10): p. 2085-92.

13. Brown, M.D. and D.B. Sacks, *IQGAP1 in cellular signaling: bridging the GAP.* Trends Cell Biol, 2006. **16**(5): p. 242-9.

14. White, C.D., H.H. Erdemir, and D.B. Sacks, *IQGAP1 and its binding proteins control diverse biological functions.* Cell Signal, 2012. **24**(4): p. 826-34.

15. Osman, M., *An emerging role for IQGAP1 in regulating protein traffic.* ScientificWorldJournal, 2010. **10**: p. 944-53.

16. Watanabe, T., S. Wang, and K. Kaibuchi, *IQGAPs as Key Regulators of Actin-cytoskeleton Dynamics.* Cell Struct Funct, 2015. **40**(2): p. 69-77.

17. White, C.D., M.D. Brown, and D.B. Sacks, *IQGAPs in cancer: a family of scaffold proteins underlying tumorigenesis.* FEBS Lett, 2009. **583**(12): p. 1817-24.

18. Kanada, M., A. Nagasaki, and T.Q. Uyeda, *Adhesion-dependent and contractile ring-independent equatorial furrowing during cytokinesis in mammalian cells.* Mol Biol Cell, 2005. **16**(8): p. 3865-72.

19. Wang, J.B., et al., *IQGAP1 regulates cell proliferation through a novel CDC42-mTOR pathway.* J Cell Sci, 2009. **122**(Pt 12): p. 2024-33.

20. Briggs, M.W. and D.B. Sacks, *IQGAP proteins are integral components of cytoskeletal regulation.* EMBO Rep, 2003. **4**(6): p. 571-4.

21. Mateer, S.C., N. Wang, and G.S. Bloom, *IQGAPs: integrators of the cytoskeleton, cell adhesion machinery, and signaling networks.* Cell Motil Cytoskeleton, 2003. **55**(3): p. 147-55.

22. Dong, P., et al., *Overexpression and diffuse expression pattern of IQGAP1 at invasion fronts are independent prognostic parameters in ovarian carcinomas.* Cancer Lett, 2006. **243**(1): p. 120-7.

23. Wang, X.X., et al., *Overexpression of IQGAP1 in human pancreatic cancer.* Hepatobiliary Pancreat Dis Int, 2013. **12**(5): p. 540-5.

24. Walch, A., et al., *Combined analysis of Rac1, IQGAP1, Tiam1 and E-cadherin expression in gastric cancer.* Mod Pathol, 2008. **21**(5): p. 544-52.

25. Liu, Z., et al., *IQGAP1 plays an important role in the invasiveness of thyroid cancer.* Clin Cancer Res, 2010. **16**(24): p. 6009-18.

26. Wang, X., et al., *IQGAP1 silencing suppresses the malignant characteristics of laryngeal squamous cell carcinoma cells.* Int J Biol Markers, 2018. **33**(1): p. 73-78.

27. Zeng, F., et al., *Ras GTPase-Activating-Like Protein IQGAP1 (IQGAP1) Promotes Breast Cancer Proliferation and Invasion and Correlates with Poor Clinical Outcomes.* Med Sci Monit, 2018. **24**: p. 3315-3323.

28. Nakamura, H., et al., *Expression pattern of the scaffold protein IQGAP1 in lung cancer.* Oncol Rep, 2005. **13**(3): p. 427-31.

29. Wang, X.X., et al., *Targeted knockdown of IQGAP1 inhibits the progression of esophageal squamous cell carcinoma in vitro and in vivo.* PLoS One, 2014. **9**(5): p. e96501.

30. Diao, B., et al., *IQGAP1siRNA inhibits proliferation and metastasis of U251 and U373 glioma cell lines.* Mol Med Rep, 2017. **15**(4): p. 2074-2082.

31. Jin, X., et al., *The Overexpression of IQGAP1 and beta-Catenin Is Associated with Tumor Progression in Hepatocellular Carcinoma In Vitro and In Vivo.* PLoS One, 2015. **10**(8): p. e0133770.

32. Jadeski, L., et al., *IQGAP1 stimulates proliferation and enhances tumorigenesis of human breast epithelial cells.* J Biol Chem, 2008. **283**(2): p. 1008-17.

33. Yang, Y., et al., *IQGAP3 promotes EGFR-ERK signaling and the growth and metastasis of lung cancer cells.* PLoS One, 2014. **9**(5): p. e97578.

34. Jinawath, N., et al., *Enhancement of Migration and Invasion of Gastric Cancer Cells by IQGAP3.* Biomolecules, 2020. **10**(8).

35. Dongol, S., et al., *IQGAP3 promotes cancer proliferation and metastasis in high-grade serous ovarian cancer.* Oncol Lett, 2020. **20**(2): p. 1179-1192.

36. Qian, E.N., et al., *Expression and diagnostic value of CCT3 and IQGAP3 in hepatocellular carcinoma.* Cancer Cell Int, 2016. **16**: p. 55.

37. Xu, W., et al., *Overexpression and biological function of IQGAP3 in human pancreatic cancer.* Am J Transl Res, 2016. **8**(12): p. 5421-5432.

38. Schmidt, V.A., et al., *Development of hepatocellular carcinoma in Iqgap2-deficient mice is IQGAP1 dependent.* Mol Cell Biol, 2008. **28**(5): p. 1489-502.

39. White, C.D., et al., *IQGAP1 and IQGAP2 are reciprocally altered in hepatocellular carcinoma.* BMC Gastroenterol, 2010. **10**: p. 125.

40. Jin, S.H., et al., *IQGAP2 inactivation through aberrant promoter methylation and promotion of invasion in gastric cancer cells.* Int J Cancer, 2008. **122**(5): p. 1040-6.

41. Xie, Y., et al., *IQGAP2, A candidate tumour suppressor of prostate tumorigenesis.* Biochim Biophys Acta, 2012. **1822**(6): p. 875-84.

42. Deng, Z., et al., *Epigenetic regulation of IQGAP2 promotes ovarian cancer progression via activating Wnt/beta-catenin signaling.* Int J Oncol, 2016. **48**(1): p. 153-60.

43. Xia, F.D., et al., *Differential expression of IQGAP1/2 in Hepatocellular carcinoma and its relationship with clinical outcomes.* Asian Pac J Cancer Prev, 2014. **15**(12): p. 4951-6.

44. Xie, Y., L. Zheng, and L. Tao, *Downregulation of IQGAP2 Correlates with Prostate Cancer Recurrence and Metastasis.* Transl Oncol, 2019. **12**(2): p. 236-244.

45. Ernst, T., et al., *Decrease and gain of gene expression are equally discriminatory markers for prostate carcinoma: a gene expression analysis on total and microdissected prostate tissue.* Am J Pathol, 2002. **160**(6): p. 2169-80.

46. Ohmachi, T., et al., *Clinical significance of TROP2 expression in colorectal cancer.* Clin Cancer Res, 2006. **12**(10): p. 3057-63.

47. White, C.D., et al., *IQGAP1 protein binds human epidermal growth factor receptor 2 (HER2) and modulates trastuzumab resistance.* J Biol Chem, 2011. **286**(34): p. 29734-47.

48. Hu, G., et al., *RNA Interference of IQ Motif Containing GTPase-Activating Protein 3 (IQGAP3) Inhibits Cell Proliferation and Invasion in Breast Carcinoma Cells.* Oncol Res, 2016. **24**(6): p. 455-461.

49. Hu, G., et al., *IQ Motif Containing GTPase-Activating Protein 3 (IQGAP3) Inhibits Kaempferol-Induced Apoptosis in Breast Cancer Cells by Extracellular Signal-Regulated Kinases 1/2 (ERK1/2) Signaling Activation.* Med Sci Monit, 2019. **25**: p. 7666-7674.

50. Hu, W., et al., *IQGAP1 promotes pancreatic cancer progression and epithelial-mesenchymal transition (EMT) through Wnt/beta-catenin signaling.* Sci Rep, 2019. **9**(1): p. 7539.

51. Su, D., Y. Liu, and T. Song, *Knockdown of IQGAP1 inhibits proliferation and epithelial-mesenchymal transition by Wnt/beta-catenin pathway in thyroid cancer.* Onco Targets Ther, 2017. **10**: p. 1549-1559.

52. Liu, J., et al., *Downregulation of IQGAP1 inhibits epithelial-mesenchymal transition via the HIF1alpha/VEGF-A signaling pathway in gastric cancer.* J Cell Biochem, 2019. **120**(9): p. 15790-15799.

53. Meyer, R.D., D.B. Sacks, and N. Rahimi, *IQGAP1-dependent signaling pathway regulates endothelial cell proliferation and angiogenesis.* PLoS One, 2008. **3**(12): p. e3848.

54. Li, C.H., et al., *Overexpression of IQGAP1 promotes the angiogenesis of esophageal squamous cell carcinoma through the AKT and ERKmediated VEGFVEGFR2 signaling pathway.* Oncol Rep, 2018. **40**(3): p. 1795-1802.

55. Yamaoka-Tojo, M., et al., *IQGAP1 mediates VE-cadherin-based cell-cell contacts and VEGF signaling at adherence junctions linked to angiogenesis.* Arterioscler Thromb Vasc Biol, 2006. **26**(9): p. 1991-7.

56. Bielenberg, D.R. and B.R. Zetter, *The Contribution of Angiogenesis to the Process of Metastasis.* Cancer J, 2015. **21**(4): p. 267-73.

57. Hanahan, D. and R.A. Weinberg, *Hallmarks of cancer: the next generation.* Cell, 2011. **144**(5): p. 646-74.

58. Rakha, E.A., et al., *Morphological and immunophenotypic analysis of breast carcinomas with basal and myoepithelial differentiation.* J Pathol, 2006. **208**(4): p. 495-506.

59. Althuis, M.D., et al., *Etiology of hormone receptor-defined breast cancer: a systematic review of the literature.* Cancer Epidemiol Biomarkers Prev, 2004. **13**(10): p. 1558-68.

60. Banin Hirata, B.K., et al., *Molecular markers for breast cancer: prediction on tumor behavior.* Dis Markers, 2014. **2014**: p. 513158.

61. UK, C.R. *In situ breast carcinoma incidences by anatomical site*. 2015 December 17; Available from: https://www.cancerresearchuk.org/health-professional/cancer-statistics/statistics-by-cancer-type/breast-cancer/incidence-in-situ#heading-Three.

62. Avagliano, A., et al., *Mitochondrial Flexibility of Breast Cancers: A Growth Advantage and a Therapeutic Opportunity.* Cells, 2019. **8**(5).

63. Grander, D., *How do mutated oncogenes and tumor suppressor genes cause cancer?* Med Oncol, 1998. **15**(1): p. 20-6.

64. De Ieso, M.L. and A.J. Yool, *Mechanisms of Aquaporin-Facilitated Cancer Invasion and Metastasis.* Front Chem, 2018. **6**: p. 135.

65. Neagu, M., et al., *Proteomic Technology "Lens" for Epithelial-Mesenchymal Transition Process Identification in Oncology.* Anal Cell Pathol (Amst), 2019. **2019**: p. 3565970.

66. Prat, A. and C.M. Perou, *Deconstructing the molecular portraits of breast cancer.* Mol Oncol, 2011. **5**(1): p. 5-23.

67. Micalizzi, D.S. and H.L. Ford, *Epithelial-mesenchymal transition in development and cancer.* Future Oncol, 2009. **5**(8): p. 1129-43.

68. Scimeca, M., et al., *Emerging prognostic markers related to mesenchymal characteristics of poorly differentiated breast cancers.* Tumour Biol, 2016. **37**(4): p. 5427-35.

69. Felipe Lima, J., et al., *EMT in Breast Carcinoma-A Review.* J Clin Med, 2016. **5**(7).

70. Pomp, V., et al., *Differential expression of epithelial-mesenchymal transition and stem cell markers in intrinsic subtypes of breast cancer.* Breast Cancer Res Treat, 2015. **154**(1): p. 45-55.

71. Zimta, A.A., et al., *The Role of Angiogenesis and Pro-Angiogenic Exosomes in Regenerative Dentistry.* Int J Mol Sci, 2019. **20**(2).

72. Folkman, J., *Tumor angiogenesis: therapeutic implications.* N Engl J Med, 1971. **285**(21): p. 1182-6.

73. Holmgren, L., M.S. O'Reilly, and J. Folkman, *Dormancy of micrometastases: balanced proliferation and apoptosis in the presence of angiogenesis suppression.* Nat Med, 1995. **1**(2): p. 149-53.

74. Carmeliet, P., *Angiogenesis in life, disease and medicine.* Nature, 2005. **438**(7070): p. 932-6.

75. Maj, E., D. Papiernik, and J. Wietrzyk, *Antiangiogenic cancer treatment: The great discovery and greater complexity (Review).* Int J Oncol, 2016. **49**(5): p. 1773-1784.

76. Hanahan, D. and J. Folkman, *Patterns and emerging mechanisms of the angiogenic switch during tumorigenesis.* Cell, 1996. **86**(3): p. 353-64.

77. Volpert, O.V., K.M. Dameron, and N. Bouck, *Sequential development of an angiogenic phenotype by human fibroblasts progressing to tumorigenicity.* Oncogene, 1997. **14**(12): p. 1495-502.

78. Madu, C.O., et al., *Angiogenesis in Breast Cancer Progression, Diagnosis, and Treatment.* J Cancer, 2020. **11**(15): p. 4474-4494.

79. Arbiser, J.L., et al., *Oncogenic H-ras stimulates tumor angiogenesis by two distinct pathways.* Proc Natl Acad Sci U S A, 1997. **94**(3): p. 861-6.

80. Pugh, C.W. and P.J. Ratcliffe, *Regulation of angiogenesis by hypoxia: role of the HIF system.* Nat Med, 2003. **9**(6): p. 677-84.

81. Stein, I., et al., *Stabilization of vascular endothelial growth factor mRNA by hypoxia and hypoglycemia and coregulation with other ischemia-induced genes.* Mol Cell Biol, 1995. **15**(10): p. 5363-8.

82. North, S., M. Moenner, and A. Bikfalvi, *Recent developments in the regulation of the angiogenic switch by cellular stress factors in tumors.* Cancer Lett, 2005. **218**(1): p. 1-14.

83. Tonini, T., F. Rossi, and P.P. Claudio, *Molecular basis of angiogenesis and cancer.* Oncogene, 2003. **22**(42): p. 6549-56.

84. Mukhopadhyay, D., L. Tsiokas, and V.P. Sukhatme, *Wild-type p53 and v-Src exert opposing influences on human vascular endothelial growth factor gene expression.* Cancer Res, 1995. **55**(24): p. 6161-5.

85. Zhang, L., et al., *Wild-type p53 suppresses angiogenesis in human leiomyosarcoma and synovial sarcoma by transcriptional suppression of vascular endothelial growth factor expression.* Cancer Res, 2000. **60**(13): p. 3655-61.

86. Galy, B., et al., *p53 directs conformational change and translation initiation blockade of human fibroblast growth factor 2 mRNA.* Oncogene, 2001. **20**(34): p. 4613-20.

87. Galy, B., et al., *Tumour suppressor p53 inhibits human fibroblast growth factor 2 expression by a post-transcriptional mechanism.* Oncogene, 2001. **20**(14): p. 1669-77.

88. Sun, Y., et al., *Wild type and mutant p53 differentially regulate the gene expression of human collagenase-3 (hMMP-13).* J Biol Chem, 2000. **275**(15): p. 11327-32.

89. Subbaramaiah, K., et al., *Inhibition of cyclooxygenase-2 gene expression by p53.* J Biol Chem, 1999. **274**(16): p. 10911-5.

90. Dameron, K.M., et al., *Control of angiogenesis in fibroblasts by p53 regulation of thrombospondin-1.* Science, 1994. **265**(5178): p. 1582-4.

91. Lawler, J., et al., *Thrombospondin-1 gene expression affects survival and tumor spectrum of p53-deficient mice.* Am J Pathol, 2001. **159**(5): p. 1949-56.

92. Fukushima, Y., et al., *Brain-specific angiogenesis inhibitor 1 expression is inversely correlated with vascularity and distant metastasis of colorectal cancer.* Int J Oncol, 1998. **13**(5): p. 967-70.

93. Bian, J. and Y. Sun, *Transcriptional activation by p53 of the human type IV collagenase (gelatinase A or matrix metalloproteinase 2) promoter.* Mol Cell Biol, 1997. **17**(11): p. 6330-8.

94. Folkman, J., *Angiogenesis in cancer, vascular, rheumatoid and other disease.* Nat Med, 1995. **1**(1): p. 27-31.

95. Carmeliet, P., *Angiogenesis in health and disease.* Nat Med, 2003. **9**(6): p. 653-60.

96. Li, Y., et al., *Long non-coding RNA MALAT1 promotes gastric cancer tumorigenicity and metastasis by regulating vasculogenic mimicry and angiogenesis.* Cancer Lett, 2017. **395**: p. 31-44.

97. Shen, J., et al., *DUSP1 inhibits cell proliferation, metastasis and invasion and angiogenesis in gallbladder cancer.* Oncotarget, 2017. **8**(7): p. 12133-12144.

98. Xu, H., et al., *Six1 promotes colorectal cancer growth and metastasis by stimulating angiogenesis and recruiting tumor-associated macrophages.* Carcinogenesis, 2017. **38**(3): p. 281-292.

99. Joukov, V., et al., *A novel vascular endothelial growth factor, VEGF-C, is a ligand for the Flt4 (VEGFR-3) and KDR (VEGFR-2) receptor tyrosine kinases.* EMBO J, 1996. **15**(2): p. 290-98.

100. Qi, J.H., et al., *A novel function for tissue inhibitor of metalloproteinases-3 (TIMP3): inhibition of angiogenesis by blockage of VEGF binding to VEGF receptor-2.* Nat Med, 2003. **9**(4): p. 407-15.

101. Voelkel, N.F., et al., *Janus face of vascular endothelial growth factor: the obligatory survival factor for lung vascular endothelium controls precapillary artery remodeling in severe pulmonary hypertension.* Crit Care Med, 2002. **30**(5 Suppl): p. S251-6.

102. Meyer, M., et al., *A novel vascular endothelial growth factor encoded by Orf virus, VEGF-E, mediates angiogenesis via signalling through VEGFR-2 (KDR) but not VEGFR-1 (Flt-1) receptor tyrosine kinases.* EMBO J, 1999. **18**(2): p. 363-74.

103. Relf, M., et al., *Expression of the angiogenic factors vascular endothelial cell growth factor, acidic and basic fibroblast growth factor, tumor growth factor beta-1, platelet-derived endothelial cell growth factor, placenta growth factor, and pleiotrophin in human primary breast cancer and its relation to angiogenesis.* Cancer Res, 1997. **57**(5): p. 963-9.

104. Lin, Y., et al., *Identification of interleukin-8 as estrogen receptor-regulated factor involved in breast cancer invasion and angiogenesis by protein arrays.* Int J Cancer, 2004. **109**(4): p. 507-15.

105. Marjon, P.L., E.V. Bobrovnikova-Marjon, and S.F. Abcouwer, *Expression of the pro-angiogenic factors vascular endothelial growth factor and interleukin-8/CXCL8 by human breast carcinomas is responsive to nutrient deprivation and endoplasmic reticulum stress.* Mol Cancer, 2004. **3**: p. 4.

106. Razmkhah, M., et al., *Expression profile of IL-8 and growth factors in breast cancer cells and adipose-derived stem cells (ASCs) isolated from breast carcinoma.* Cell Immunol, 2010. **265**(1): p. 80-5.

107. Claesson-Welsh, L. and M. Welsh, *VEGFA and tumour angiogenesis.* J Intern Med, 2013. **273**(2): p. 114-27.

108. Srabovic, N., et al., *Vascular endothelial growth factor receptor-1 expression in breast cancer and its correlation to vascular endothelial growth factor a.* Int J Breast Cancer, 2013. **2013**: p. 746749.

109. Guo, S., et al., *Vascular endothelial growth factor receptor-2 in breast cancer.* Biochim Biophys Acta, 2010. **1806**(1): p. 108-21.

110. Lushnikova, A.A., et al., *VEGFR-2 expression in tumor tissue of breast cancer patients.* Dokl Biol Sci, 2010. **434**: p. 363-7.

111. Linardou, H., et al., *The prognostic and predictive value of mRNA expression of vascular endothelial growth factor family members in breast cancer: a study in primary tumors of high-risk early breast cancer patients participating in a randomized Hellenic Cooperative Oncology Group trial.* Breast Cancer Res, 2012. **14**(6): p. R145.

112. Fidler, I.J. and L.M. Ellis, *Chemotherapeutic drugs--more really is not better.* Nat Med, 2000. **6**(5): p. 500-2.

113. Li, A., et al., *IL-8 directly enhanced endothelial cell survival, proliferation, and matrix metalloproteinases production and regulated angiogenesis.* J Immunol, 2003. **170**(6): p. 3369-76.

114. Liekens, S., E. De Clercq, and J. Neyts, *Angiogenesis: regulators and clinical applications.* Biochem Pharmacol, 2001. **61**(3): p. 253-70.

115. Martin, D., R. Galisteo, and J.S. Gutkind, *CXCL8/IL8 stimulates vascular endothelial growth factor (VEGF) expression and the autocrine activation of VEGFR2 in endothelial cells by activating NFkappaB through the CBM (Carma3/Bcl10/Malt1) complex.* J Biol Chem, 2009. **284**(10): p. 6038-42.

116. Brady, N., et al., *The FGF/FGFR axis as a therapeutic target in breast cancer.* Expert Rev Endocrinol Metab, 2013. **8**(4): p. 391-402.

117. Heppner, K.J., et al., *Expression of most matrix metalloproteinase family members in breast cancer represents a tumor-induced host response.* Am J Pathol, 1996. **149**(1): p. 273-82.

118. Bartsch, J.E., E.D. Staren, and H.E. Appert, *Matrix metalloproteinase expression in breast cancer.* J Surg Res, 2003. **110**(2): p. 383-92.

119. Woessner, J.F., Jr., *The family of matrix metalloproteinases.* Ann N Y Acad Sci, 1994. **732**: p. 11-21.

120. Hanahan, D. and R.A. Weinberg, *The hallmarks of cancer.* Cell, 2000. **100**(1): p. 57-70.

121. Kerr, J.F., A.H. Wyllie, and A.R. Currie, *Apoptosis: a basic biological phenomenon with wide-ranging implications in tissue kinetics.* Br J Cancer, 1972. **26**(4): p. 239-57.

122. Wong, R.S., *Apoptosis in cancer: from pathogenesis to treatment.* J Exp Clin Cancer Res, 2011. **30**: p. 87.

123. Vikhanskaya, F., et al., *Cancer-derived p53 mutants suppress p53-target gene expression--potential mechanism for gain of function of mutant p53.* Nucleic Acids Res, 2007. **35**(6): p. 2093-104.

124. Avery-Kiejda, K.A., et al., *P53 in human melanoma fails to regulate target genes associated with apoptosis and the cell cycle and may contribute to proliferation.* BMC Cancer, 2011. **11**: p. 203.

125. Creagh, E.M., H. Conroy, and S.J. Martin, *Caspase-activation pathways in apoptosis and immunity.* Immunol Rev, 2003. **193**: p. 10-21.

126. Fink, S.L. and B.T. Cookson, *Apoptosis, pyroptosis, and necrosis: mechanistic description of dead and dying eukaryotic cells.* Infect Immun, 2005. **73**(4): p. 1907-16.

127. Shen, X.G., et al., *Downregulation of caspase-9 is a frequent event in patients with stage II colorectal cancer and correlates with poor clinical outcome.* Colorectal Dis, 2010. **12**(12): p. 1213-8.

128. Devarajan, E., et al., *Down-regulation of caspase 3 in breast cancer: a possible mechanism for chemoresistance.* Oncogene, 2002. **21**(57): p. 8843-51.

129. Fong, P.Y., et al., *Caspase activity is downregulated in choriocarcinoma: a cDNA array differential expression study.* J Clin Pathol, 2006. **59**(2): p. 179-83.

130. Cohen, G.M., *Caspases: the executioners of apoptosis.* Biochem J, 1997. **326 (Pt 1)**: p. 1-16.

131. Baburski, A.Z., S.A. Andric, and T.S. Kostic, *Luteinizing hormone signaling is involved in synchronization of Leydig cell's clock and is crucial for rhythm robustness of testosterone productiondagger.* Biol Reprod, 2019. **100**(5): p. 1406-1415.

132. Blazquez, S., et al., *Caspase-3 and caspase-6 in ductal breast carcinoma: a descriptive study.* Histol Histopathol, 2006. **21**(12): p. 1321-9.

133. Pu, X., et al., *Caspase-3 and caspase-8 expression in breast cancer: caspase-3 is associated with survival.* Apoptosis, 2017. **22**(3): p. 357-368.

134. Kaminska, M., et al., *Breast cancer risk factors.* Prz Menopauzalny, 2015. **14**(3): p. 196-202.

135. Gnerlich, J.L., et al., *Poorer survival outcomes for male breast cancer compared with female breast cancer may be attributable to in-stage migration.* Ann Surg Oncol, 2011. **18**(7): p. 1837-44.

136. Bagnardi, V., et al., *Light alcohol drinking and cancer: a meta-analysis.* Ann Oncol, 2013. **24**(2): p. 301-308.

137. Soroush, A., et al., *The Role of Oral Contraceptive Pills on Increased Risk of Breast Cancer in Iranian Populations: A Meta-analysis.* J Cancer Prev, 2016. **21**(4): p. 294-301.

138. Bethea, T.N., et al., *A case-control analysis of oral contraceptive use and breast cancer subtypes in the African American Breast Cancer Epidemiology and Risk Consortium.* Breast Cancer Res, 2015. **17**: p. 22.

139. Balmana, J., et al., *BRCA in breast cancer: ESMO Clinical Practice Guidelines.* Ann Oncol, 2011. **22 Suppl 6**: p. vi31-4.

140. Paluch-Shimon, S., et al., *Prevention and screening in BRCA mutation carriers and other breast/ovarian hereditary cancer syndromes: ESMO Clinical Practice Guidelines for cancer prevention and screening.* Ann Oncol, 2016. **27**(suppl 5): p. v103-v110.

141. Davis, N.M., et al., *Deregulation of the EGFR/PI3K/PTEN/Akt/mTORC1 pathway in breast cancer: possibilities for therapeutic intervention.* Oncotarget, 2014. **5**(13): p. 4603-50.

142. Elizalde, P.V., et al., *ErbB-2 nuclear function in breast cancer growth, metastasis and resistance to therapy.* Endocr Relat Cancer, 2016. **23**(12): p. T243-T257.

143. Alanazi, I.O. and Z. Khan, *Understanding EGFR Signaling in Breast Cancer and Breast Cancer Stem Cells: Overexpression and Therapeutic Implications.* Asian Pac J Cancer Prev, 2016. **17**(2): p. 445-53.

144. Chen, Y. and O.I. Olopade, *MYC in breast tumor progression.* Expert Rev Anticancer Ther, 2008. **8**(10): p. 1689-98.

145. Jung, M., et al., *A Myc Activity Signature Predicts Poor Clinical Outcomes in Myc-Associated Cancers.* Cancer Res, 2017. **77**(4): p. 971-981.

146. DeSantis, C.E., et al., *Breast cancer statistics, 2019.* CA Cancer J Clin, 2019. **69**(6): p. 438-451.

147. Coleman, M.P., et al., *Cancer survival in five continents: a worldwide population-based study (CONCORD).* Lancet Oncol, 2008. **9**(8): p. 730-56.

148. Abbas, Z. and S. Rehman, *An Overview of Cancer Treatment Modalities*, in *Neoplasm*. 2018.

149. Lumachi, F., et al., *Endocrine therapy of breast cancer.* Curr Med Chem, 2011. **18**(4): p. 513-22.

150. Cameron, D., et al., *11 years' follow-up of trastuzumab after adjuvant chemotherapy in HER2-positive early breast cancer: final analysis of the HERceptin Adjuvant (HERA) trial.* Lancet, 2017. **389**(10075): p. 1195-1205.

151. Tolaney, S.M., et al., *Adjuvant paclitaxel and trastuzumab for node-negative, HER2-positive breast cancer.* N Engl J Med, 2015. **372**(2): p. 134-41.

152. Slamon, D., et al., *Adjuvant trastuzumab in HER2-positive breast cancer.* N Engl J Med, 2011. **365**(14): p. 1273-83.

153. Masuda, N., et al., *Adjuvant Capecitabine for Breast Cancer after Preoperative Chemotherapy.* N Engl J Med, 2017. **376**(22): p. 2147-2159.

154. Weissbach, L., et al., *Identification of a human rasGAP-related protein containing calmodulin-binding motifs.* J Biol Chem, 1994. **269**(32): p. 20517-21.

155. Ho, Y.D., et al., *IQGAP1 integrates Ca2+/calmodulin and Cdc42 signaling.* J Biol Chem, 1999. **274**(1): p. 464-70.

156. Smith, J.M., A.C. Hedman, and D.B. Sacks, *IQGAPs choreograph cellular signaling from the membrane to the nucleus.* Trends Cell Biol, 2015. **25**(3): p. 171-84.

157. Pathmanathan, S., et al., *The interaction of IQGAPs with calmodulin-like proteins.* Biochem Soc Trans, 2011. **39**(2): p. 694-9.

158. Ren, J.G., et al., *Self-association of IQGAP1: characterization and functional sequelae.* J Biol Chem, 2005. **280**(41): p. 34548-57.

159. Ren, J.G., Z. Li, and D.B. Sacks, *IQGAP1 modulates activation of B-Raf.* Proc Natl Acad Sci U S A, 2007. **104**(25): p. 10465-9.

160. Roy, M., Z. Li, and D.B. Sacks, *IQGAP1 is a scaffold for mitogen-activated protein kinase signaling.* Mol Cell Biol, 2005. **25**(18): p. 7940-52.

161. Roy, M., Z. Li, and D.B. Sacks, *IQGAP1 binds ERK2 and modulates its activity.* J Biol Chem, 2004. **279**(17): p. 17329-37.

162. Abel, A.M., et al., *IQGAP1: insights into the function of a molecular puppeteer.* Mol Immunol, 2015. **65**(2): p. 336-49.

163. Atcheson, E., et al., *IQ-motif selectivity in human IQGAP2 and IQGAP3: binding of calmodulin and myosin essential light chain.* Biosci Rep, 2011. **31**(5): p. 371-9.

164. Li, Z. and D.B. Sacks, *Elucidation of the interaction of calmodulin with the IQ motifs of IQGAP1.* J Biol Chem, 2003. **278**(6): p. 4347-52.

165. Pathmanathan, S., et al., *IQ motif selectivity in human IQGAP1: binding of myosin essential light chain and S100B.* Mol Cell Biochem, 2008. **318**(1-2): p. 43-51.

166. Adachi, M., et al., *Involvement of IQGAP family proteins in the regulation of mammalian cell cytokinesis.* Genes Cells, 2014. **19**(11): p. 803-20.

167. Hart, M.J., et al., *IQGAP1, a calmodulin-binding protein with a rasGAP-related domain, is a potential effector for cdc42Hs.* 1996. **15**(12): p. 2997-3005.

168. Joyal, J.L., et al., *Calmodulin modulates the interaction between IQGAP1 and Cdc42. Identification of IQGAP1 by nanoelectrospray tandem mass spectrometry.* J Biol Chem, 1997. **272**(24): p. 15419-25.

169. Wang, S., et al., *IQGAP3, a novel effector of Rac1 and Cdc42, regulates neurite outgrowth.* J Cell Sci, 2007. **120**(Pt 4): p. 567-77.

170. Brill, S., et al., *The Ras GTPase-activating-protein-related human protein IQGAP2 harbors a potential actin binding domain and interacts with calmodulin and Rho family GTPases.* Mol Cell Biol, 1996. **16**(9): p. 4869-78.

171. McCallum, S.J., W.J. Wu, and R.A. Cerione, *Identification of a putative effector for Cdc42Hs with high sequence similarity to the RasGAP-related protein IQGAP1 and a Cdc42Hs binding partner with similarity to IQGAP2.* J Biol Chem, 1996. **271**(36): p. 21732-7.

172. Zhao, H.Y., et al., *IQ-domain GTPase-activating protein 1 promotes the malignant phenotype of invasive ductal breast carcinoma via canonical Wnt pathway.* Tumour Biol, 2017. **39**(6): p. 1010428317705769.

173. Chuang, H.C., et al., *MAP4K3/GLK Promotes Lung Cancer Metastasis by Phosphorylating and Activating IQGAP1.* Cancer Res, 2019. **79**(19): p. 4978-4993.

174. Wei, T., et al., *A PI3K/AKT Scaffolding Protein, IQ Motif-Containing GTPase Associating Protein 1 (IQGAP1), Promotes Head and Neck Carcinogenesis.* Clin Cancer Res, 2020. **26**(1): p. 301-311.

175. Li, J.H., et al., *IQGAP1 Maintains Pancreatic Ductal Adenocarcinoma Clonogenic Growth and Metastasis.* Pancreas, 2019. **48**(1): p. 94-98.

176. Liang, Z., et al., *SUMOylation of IQGAP1 promotes the development of colorectal cancer.* Cancer Lett, 2017. **411**: p. 90-99.

177. Zoheir, K.M., et al., *Gene expression of IQGAPs and Ras families in an experimental mouse model for hepatocellular carcinoma: a mechanistic study of cancer progression.* Int J Clin Exp Pathol, 2015. **8**(8): p. 8821-31.

178. Lin, H., et al., *IQGAP3 overexpression correlates with poor prognosis and radiation therapy resistance in breast cancer.* Annals of Oncology, 2018. **29**.

179. Xu, L., et al., *IQGAP2 Inhibits Migration and Invasion of Gastric Cancer Cells via Elevating SHIP2 Phosphatase Activity.* Int J Mol Sci, 2020. **21**(6).

180. Casteel, D.E., et al., *Rho isoform-specific interaction with IQGAP1 promotes breast cancer cell proliferation and migration.* J Biol Chem, 2012. **287**(45): p. 38367-78.

181. Zoheir, K.M., et al., *IQGAP1 gene silencing induces apoptosis and decreases the invasive capacity of human hepatocellular carcinoma cells.* Tumour Biol, 2016. **37**(10): p. 13927-13939.

182. Vaitheesvaran, B., et al., *Role of the tumor suppressor IQGAP2 in metabolic homeostasis: Possible link between diabetes and cancer.* Metabolomics, 2014. **10**(5): p. 920-937.

183. DeBerardinis, R.J., et al., *The biology of cancer: metabolic reprogramming fuels cell growth and proliferation.* Cell Metab, 2008. **7**(1): p. 11-20.

184. Steiner, L., *Antibodies - a Laboratory Manual - Harlow,E, Lane,D.* Nature, 1989. **341**(6237): p. 32-32.

185. Fedchenko, N. and J. Reifenrath, *Different approaches for interpretation and reporting of immunohistochemistry analysis results in the bone tissue - a review.* Diagn Pathol, 2014. **9**: p. 221.

186. Rhodes, D.R., et al., *ONCOMINE: a cancer microarray database and integrated data-mining platform.* Neoplasia, 2004. **6**(1): p. 1-6.

187. Tomczak, K., P. Czerwinska, and M. Wiznerowicz, *The Cancer Genome Atlas (TCGA): an immeasurable source of knowledge.* Contemp Oncol (Pozn), 2015. **19**(1A): p. A68-77.

188. Aguirre-Gamboa, R., et al., *SurvExpress: an online biomarker validation tool and database for cancer gene expression data using survival analysis.* PLoS One, 2013. **8**(9): p. e74250.

189. Gao, J., et al., *Integrative analysis of complex cancer genomics and clinical profiles using the cBioPortal.* Sci Signal, 2013. **6**(269): p. pl1.

190. Cerami, E., et al., *The cBio cancer genomics portal: an open platform for exploring multidimensional cancer genomics data.* Cancer Discov, 2012. **2**(5): p. 401-4.

191. Diez-Villanueva, A., I. Mallona, and M.A. Peinado, *Wanderer, an interactive viewer to explore DNA methylation and gene expression data in human cancer.* Epigenetics Chromatin, 2015. **8**: p. 22.

192. Rivera, E. and H. Gomez, *Chemotherapy resistance in metastatic breast cancer: the evolving role of ixabepilone.* Breast Cancer Res. **12 Suppl 2**: p. S2.

193. Hulka, B.S., *Epidemiology of susceptibility to breast cancer.* Prog Clin Biol Res, 1996. **395**: p. 159-74.

194. Polyak, K., *Breast cancer: origins and evolution.* J Clin Invest, 2007. **117**(11): p. 3155-63.

195. Colditz, G.A., et al., *Family history and risk of breast cancer: nurses' health study.* Breast Cancer Res Treat. **133**(3): p. 1097-104.

196. Allison, K.H., *Molecular pathology of breast cancer: what a pathologist needs to know.* Am J Clin Pathol. **138**(6): p. 770-80.

197. Yang, Y., et al., *IQGAP3 promotes EGFR-ERK signaling and the growth and metastasis of lung cancer cells.* PLoS One. **9**(5): p. e97578.

198. Qian, E.N., et al., *Expression and diagnostic value of CCT3 and IQGAP3 in hepatocellular carcinoma.* Cancer Cell Int. **16**: p. 55.

199. Zhou, J., et al., *Development and evaluation of a rapid detection assay for severe fever with thrombocytopenia syndrome virus based on reverse-transcription recombinase polymerase amplification.* Mol Cell Probes, 2020: p. 101580.

200. Xu, W., et al., *Overexpression and biological function of IQGAP3 in human pancreatic cancer.* Am J Transl Res. **8**(12): p. 5421-5432.

201. Xie, Y., et al., *IQGAP2, A candidate tumour suppressor of prostate tumorigenesis.* Biochim Biophys Acta. **1822**(6): p. 875-84.

202. White, C.D., et al., *IQGAP1 and IQGAP2 are reciprocally altered in hepatocellular carcinoma.* BMC Gastroenterol. **10**: p. 125.

203. Deng, Z., et al., *Epigenetic regulation of IQGAP2 promotes ovarian cancer progression via activating Wnt/beta-catenin signaling.* Int J Oncol. **48**(1): p. 153-60.

204. Erdemir, H.H., Z. Li, and D.B. Sacks, *IQGAP1 binds to estrogen receptor-alpha and modulates its function.* J Biol Chem, 2014. **289**(13): p. 9100-12.

205. Chen, F., et al., *IQGAP1 is overexpressed in hepatocellular carcinoma and promotes cell proliferation by Akt activation.* Exp Mol Med, 2010. **42**(7): p. 477-83.

206. Kuroda, S., et al., *Role of IQGAP1, a target of the small GTPases Cdc42 and Rac1, in regulation of E-cadherin- mediated cell-cell adhesion.* Science, 1998. **281**(5378): p. 832-5.

207. Yamashiro, S., H. Abe, and I. Mabuchi, *IQGAP2 is required for the cadherin-mediated cell-to-cell adhesion in Xenopus laevis embryos.* Dev Biol, 2007. **308**(2): p. 485-93.

208. Carmon, K.S., et al., *RSPO-LGR4 functions via IQGAP1 to potentiate Wnt signaling.* Proc Natl Acad Sci U S A, 2014. **111**(13): p. E1221-9.

209. Gnatenko, D.V., et al., *Transcript profiling identifies iqgap2(-/-) mouse as a model for advanced human hepatocellular carcinoma.* PLoS One, 2013. **8**(8): p. e71826.

210. Choi, J.B., et al., *Reactive Oxygen Species and p53 Mediated Activation of p38 and Caspases is Critically Involved in Kaempferol Induced Apoptosis in*

Colorectal Cancer Cells. Journal of Agricultural and Food Chemistry, 2018. **66**(38): p. 9960-9967.

211. Schuler, M., et al., *p53 induces apoptosis by caspase activation through mitochondrial cytochrome c release.* J Biol Chem, 2000. **275**(10): p. 7337-42.

212. Fernandes-Alnemri, T., et al., *Mch3, a novel human apoptotic cysteine protease highly related to CPP32.* Cancer Res, 1995. **55**(24): p. 6045-52.

213. Rodriguez-Hernandez, A., et al., *Nuclear caspase-3 and capase-7 activation, and poly(ADP-ribose) polymerase cleavage are early events in camptothecin-induced apoptosis.* Apoptosis, 2006. **11**(1): p. 131-139.

214. Son, H. and A. Moon, *Epithelial-mesenchymal Transition and Cell Invasion.* Toxicol Res, 2010. **26**(4): p. 245-52.

215. Dranoff, G., *Cytokines in cancer pathogenesis and cancer therapy.* Nat Rev Cancer, 2004. **4**(1): p. 11-22.

216. Gyamfi, J., et al., *Interleukin-6/STAT3 signalling regulates adipocyte induced epithelial-mesenchymal transition in breast cancer cells.* Sci Rep, 2018. **8**(1): p. 8859.

217. Ortiz-Montero, P., A. Londono-Vallejo, and J.P. Vernot, *Senescence-associated IL-6 and IL-8 cytokines induce a self- and cross-reinforced senescence/inflammatory milieu strengthening tumorigenic capabilities in the MCF-7 breast cancer cell line.* Cell Commun Signal, 2017. **15**(1): p. 17.

218. Todorovic-Rakovic, N. and J. Milovanovic, *Interleukin-8 in breast cancer progression.* J Interferon Cytokine Res, 2013. **33**(10): p. 563-70.

219. Soria, G. and A. Ben-Baruch, *The inflammatory chemokines CCL2 and CCL5 in breast cancer.* Cancer Lett, 2008. **267**(2): p. 271-85.

220. Qian, B.Z., et al., *CCL2 recruits inflammatory monocytes to facilitate breast-tumour metastasis.* Nature, 2011. **475**(7355): p. 222-5.

221. Farmaki, E., et al., *Induction of the MCP chemokine cluster cascade in the periphery by cancer cell-derived Ccl3.* Cancer Lett, 2017. **389**: p. 49-58.

222. Wang, R. and K. Huang, *CCL11 increases the proportion of CD4+CD25+Foxp3+ Treg cells and the production of IL2 and TGFbeta by CD4+ T cells via the STAT5 signaling pathway.* Mol Med Rep, 2020. **21**(6): p. 2522-2532.

223. Shen, S.D., et al., *Correlation of lymphovascular invasion with clinicopathological factors in invasive breast cancer: a meta-analysis.* Int J Clin Exp Med, 2015. **8**(10): p. 17789-95.

224. Siersbaek, R., S. Kumar, and J.S. Carroll, *Signaling pathways and steroid receptors modulating estrogen receptor alpha function in breast cancer.* Genes Dev, 2018. **32**(17-18): p. 1141-1154.

225. Loh, C.Y., et al., *The E-Cadherin and N-Cadherin Switch in Epithelial-to-Mesenchymal Transition: Signaling, Therapeutic Implications, and Challenges.* Cells, 2019. **8**(10).

226. Aronica, S.M. and B.S. Katzenellenbogen, *Progesterone receptor regulation in uterine cells: stimulation by estrogen, cyclic adenosine 3',5'-monophosphate, and insulin-like growth factor I and suppression by antiestrogens and protein kinase inhibitors.* Endocrinology, 1991. **128**(4): p. 2045-52.

227. Brown, A.M., et al., *Activation of pS2 gene transcription is a primary response to estrogen in the human breast cancer cell line MCF-7.* Proc Natl Acad Sci U S A, 1984. **81**(20): p. 6344-8.

228. Fang, W.B., et al., *CCL2/CCR2 chemokine signaling coordinates survival and motility of breast cancer cells through Smad3 protein- and p42/44 mitogen-activated protein kinase (MAPK)-dependent mechanisms.* J Biol Chem, 2012. **287**(43): p. 36593-608.

229. Nam, J.S., et al., *Chemokine (C-C motif) ligand 2 mediates the prometastatic effect of dysadherin in human breast cancer cells.* Cancer Res, 2006. **66**(14): p. 7176-84.

230. De Luca, A., et al., *Mesenchymal stem cell-derived interleukin-6 and vascular endothelial growth factor promote breast cancer cell migration.* J Cell Biochem, 2012. **113**(11): p. 3363-70.

231. Hart, M.J., et al., *IQGAP1, a calmodulin-binding protein with a rasGAP-related domain, is a potential effector for cdc42Hs.* EMBO J, 1996. **15**(12): p. 2997-3005.

232. Grohmanova, K., et al., *Phosphorylation of IQGAP1 modulates its binding to Cdc42, revealing a new type of rho-GTPase regulator.* J Biol Chem, 2004. **279**(47): p. 48495-504.

233. Sato, Y., *Molecular diagnosis of tumor angiogenesis and anti-angiogenic cancer therapy.* Int J Clin Oncol, 2003. **8**(4): p. 200-6.

234. Weis, S.M. and D.A. Cheresh, *Tumor angiogenesis: molecular pathways and therapeutic targets.* Nat Med, 2011. **17**(11): p. 1359-70.

235. Carmeliet, P. and R.K. Jain, *Principles and mechanisms of vessel normalization for cancer and other angiogenic diseases.* Nat Rev Drug Discov, 2011. **10**(6): p. 417-27.

236. Carmeliet, P. and R.K. Jain, *Angiogenesis in cancer and other diseases.* Nature, 2000. **407**(6801): p. 249-57.

237. Potente, M., H. Gerhardt, and P. Carmeliet, *Basic and therapeutic aspects of angiogenesis.* Cell, 2011. **146**(6): p. 873-87.

238. Baeriswyl, V. and G. Christofori, *The angiogenic switch in carcinogenesis.* Semin Cancer Biol, 2009. **19**(5): p. 329-37.

239. Weidner, N., et al., *Tumor angiogenesis correlates with metastasis in invasive prostate carcinoma.* Am J Pathol, 1993. **143**(2): p. 401-9.

240. Mao, J.M., et al., *Glioblastoma vasculogenic mimicry: signaling pathways progression and potential anti-angiogenesis targets.* Biomark Res, 2015. **3**: p. 8.

241. van Hinsbergh, V.W., A. Collen, and P. Koolwijk, *Angiogenesis and anti-angiogenesis: perspectives for the treatment of solid tumors.* Ann Oncol, 1999. **10 Suppl 4**: p. 60-3.

242. Pietras, R.J. and O.K. Weinberg, *Antiangiogenic Steroids in Human Cancer Therapy.* Evid Based Complement Alternat Med, 2005. **2**(1): p. 49-57.

243. Meadows, K.L. and H.I. Hurwitz, *Anti-VEGF therapies in the clinic.* Cold Spring Harb Perspect Med, 2012. **2**(10).

244. Folkman, J., *What is the evidence that tumors are angiogenesis dependent?* J Natl Cancer Inst, 1990. **82**(1): p. 4-6.

245. Folkman, J., *Seminars in Medicine of the Beth Israel Hospital, Boston. Clinical applications of research on angiogenesis.* N Engl J Med, 1995. **333**(26): p. 1757-63.

246. Leung, D.W., et al., *Vascular endothelial growth factor is a secreted angiogenic mitogen.* Science, 1989. **246**(4935): p. 1306-9.

247. Conn, G., et al., *Amino acid and cDNA sequences of a vascular endothelial cell mitogen that is homologous to platelet-derived growth factor.* Proc Natl Acad Sci U S A, 1990. **87**(7): p. 2628-32.

248. Dvorak, H.F., *Vascular permeability factor/vascular endothelial growth factor: a critical cytokine in tumor angiogenesis and a potential target for diagnosis and therapy.* J Clin Oncol, 2002. **20**(21): p. 4368-80.

249. Kristensen, T.B., et al., *Anti-vascular endothelial growth factor therapy in breast cancer.* Int J Mol Sci, 2014. **15**(12): p. 23024-41.

250. Broughton, G., 2nd, J.E. Janis, and C.E. Attinger, *The basic science of wound healing.* Plast Reconstr Surg, 2006. **117**(7 Suppl): p. 12S-34S.

251. Robson, M.C., D.L. Steed, and M.G. Franz, *Wound healing: biologic features and approaches to maximize healing trajectories.* Curr Probl Surg, 2001. **38**(2): p. 72-140.

252. Witte, M.B. and A. Barbul, *General principles of wound healing.* Surg Clin North Am, 1997. **77**(3): p. 509-28.

253. Neufeld, G. and O. Kessler, *Pro-angiogenic cytokines and their role in tumor angiogenesis.* Cancer Metastasis Rev, 2006. **25**(3): p. 373-85.

254. Abhinand, C.S., et al., *VEGF-A/VEGFR2 signaling network in endothelial cells relevant to angiogenesis.* J Cell Commun Signal, 2016. **10**(4): p. 347-354.

255. Folkman, J., et al., *Isolation of a tumor factor responsible for angiogenesis.* J Exp Med, 1971. **133**(2): p. 275-88.

256. Mousa, S.A. and P.J. Davis, *Chapter 1 - Angiogenesis and Anti-Angiogenesis Strategies in Cancer*, in *Anti-Angiogenesis Strategies in Cancer Therapeutics*, S.A. Mousa and P.J. Davis, Editors. 2017, Academic Press: Boston. p. 1-19.

257. Comunanza, V. and F. Bussolino, *Therapy for Cancer: Strategy of Combining Anti-Angiogenic and Target Therapies.* Front Cell Dev Biol, 2017. **5**: p. 101.

258. Heath, V.L. and R. Bicknell, *Anticancer strategies involving the vasculature.* Nat Rev Clin Oncol, 2009. **6**(7): p. 395-404.

259. Cesca, M., et al., *Tumor delivery of chemotherapy combined with inhibitors of angiogenesis and vascular targeting agents.* Front Oncol, 2013. **3**: p. 259.

260. Bergers, G. and D. Hanahan, *Modes of resistance to anti-angiogenic therapy.* Nat Rev Cancer, 2008. **8**(8): p. 592-603.

261. Mizukami, Y., et al., *Induction of interleukin-8 preserves the angiogenic response in HIF-1alpha-deficient colon cancer cells.* Nat Med, 2005. **11**(9): p. 992-7.

262. Matsuo, Y., et al., *K-Ras promotes angiogenesis mediated by immortalized human pancreatic epithelial cells through mitogen-activated protein kinase signaling pathways.* Mol Cancer Res, 2009. **7**(6): p. 799-808.

263. Ciardiello, F., et al., *Inhibition of growth factor production and angiogenesis in human cancer cells by ZD1839 (Iressa), a selective epidermal growth factor receptor tyrosine kinase inhibitor.* Clin Cancer Res, 2001. **7**(5): p. 1459-65.

264. Ciardiello, F., et al., *Antitumor activity of ZD6474, a vascular endothelial growth factor receptor tyrosine kinase inhibitor, in human cancer cells with acquired resistance to antiepidermal growth factor receptor therapy.* Clin Cancer Res, 2004. **10**(2): p. 784-93.

265. Jung, Y.D., et al., *Extracellular Signal-regulated Kinase Activation Is Required for Up-Regulation of Vascular Endothelial Growth Factor by Serum Starvation in Human Colon Carcinoma Cells.* 1999. **59**(19): p. 4804-4807.

266. Liu, Y., et al., *Periostin promotes tumor angiogenesis in pancreatic cancer via Erk/VEGF signaling.* Oncotarget, 2016. **7**(26): p. 40148-40159.

267. Shiojima, I. and K. Walsh, *Role of Akt signaling in vascular homeostasis and angiogenesis.* Circ Res, 2002. **90**(12): p. 1243-50.

268. Lee, M.Y., et al., *Endothelial Akt1 mediates angiogenesis by phosphorylating multiple angiogenic substrates.* Proc Natl Acad Sci U S A, 2014. **111**(35): p. 12865-70.

269. Uzzan, B., et al., *Microvessel density as a prognostic factor in women with breast cancer: a systematic review of the literature and meta-analysis.* Cancer Res, 2004. **64**(9): p. 2941-55.

270. Shi, Y., et al., *Role of IQGAP3 in metastasis and epithelial-mesenchymal transition in human hepatocellular carcinoma.* J Transl Med, 2017. **15**(1): p. 176.

271. Oue, N., et al., *Overexpression of the Transmembrane Protein IQGAP3 Is Associated with Poor Survival of Patients with Gastric Cancer.* Pathobiology, 2018. **85**(3): p. 192-200.

272. Bhattacharjee, A., et al., *Classification of human lung carcinomas by mRNA expression profiling reveals distinct adenocarcinoma subclasses.* Proc Natl Acad Sci U S A, 2001. **98**(24): p. 13790-5.

273. Ma, X.J., et al., *Gene expression profiling of the tumor microenvironment during breast cancer progression.* Breast Cancer Res, 2009. **11**(1): p. R7.

274. Kaiser, S., et al., *Transcriptional recapitulation and subversion of embryonic colon development by mouse colon tumor models and human colon cancer.* Genome Biol, 2007. **8**(7): p. R131.

275. Sun, L., et al., *Neuronal and glioma-derived stem cell factor induces angiogenesis within the brain.* Cancer Cell, 2006. **9**(4): p. 287-300.

276. Murat, A., et al., *Stem cell-related "self-renewal" signature and high epidermal growth factor receptor expression associated with resistance to concomitant chemoradiotherapy in glioblastoma.* J Clin Oncol, 2008. **26**(18): p. 3015-24.

277. Dephoure, N., et al., *A quantitative atlas of mitotic phosphorylation.* Proc Natl Acad Sci U S A, 2008. **105**(31): p. 10762-7.

278. Olsen, J.V., et al., *Quantitative phosphoproteomics reveals widespread full phosphorylation site occupancy during mitosis.* Sci Signal, 2010. **3**(104): p. ra3.

279. Lin, M., et al., *E2F1 transactivates IQGAP3 and promotes proliferation of hepatocellular carcinoma cells through IQGAP3-mediated PKC-alpha activation.* Am J Cancer Res, 2019. **9**(2): p. 285-299.

APPENDIX

DINESH KUMAR

NISER, Bhubaneswar

10. APPENDIX I: PLASMID VECTORS

Vector name	Description	Plasmid #	Source	Bacterial resistance	Selection marker
pcDNA 3.1	Empty vector	V790-20	Invitrogen	Ampicillin	Neomycin
pcDNA 3- Myc-IQGAP1	IQGAP1 expression vector with myc tag at c-terminal	30118	Addgene	Ampicillin	Neomycin
IQGAP2-Myc-DDK	IQGAP2 expression vector with Myc-DDK tag at c-terminal	RC223783	OriGene	Ampicillin	Neomycin
pCMV6-Entry	Empty vector	PS100001	OriGene	Ampicillin	Neomycin
pLKO.1_IQGAP2-shRNA	IQGAP2 knockdown shRNA vector, TRCN0000047494	Clone ID: NM_006633.1-319s1c1	Sigma	Ampicillin	Puromycin
pLKO.1_Scrambled	Empty vector	1864	Sigma	Ampicillin	Puromycin

APPENDIX II: List of antibodies used in study

Antibody	Dilution	Cat. No	Brand	Host
IQGAP2	WB: 1:1000, IHC: 1:100	ab187153	Abcam	Rabbit
IQGAP2	ICC: 1:100, IP: 1:50	EB09511	Everest Biotech	Goat
CD31, (Autostainer Link 48)	Pre-diluted	Clone JC70A	Dako	Mouse
E-cadherin	WB: 1:1000	AB1416	Abcam	Mouse
N-cadherin	WB: 1:1000	AB98952	Abcam	Mouse
GAPDH	WB: 1:1000	10-10011	AbGenex	Mouse
Phospho-AKT Ser-473	WB: 1:1000	4060S	CST	Rabbit
Phospho-AKT Thr-308	WB: 1:1000	13038S	CST	Rabbit
Phospho-ERK1/2	WB: 1:1000	4370	CST	Rabbit
Phospho-P38MAPK Tyr180/ Y182	WB: 1:1000	9211S	CST	Rabbit
P38 MAPK	WB: 1:1000	9212S	CST	Rabbit
AKT (pan)	WB: 1:1000	SAB4301170	Sigma	Rabbit
Phospho-P38 MAPK	WB: 1:1000	9211S	CST	Rabbit
Sec-Anti-Rabbit	WB: 1:1000	A9169	Sigma	Goat
Sec-Anti- Mouse	WB: 1:20000	31452	Invitrogen	Rabbit
Slug (C19G7)	WB: 1:1000	9585S	CST	Rabbit
Snail (C1583)	WB: 1:1000	3879S	CST	Rabbit
Total-ER-alpha	WB: 1:1000	13258S	CST	Rabbit
Phospho-ER alpha Ser118	WB: 1:1000	2511	CST	Mouse
Total-ERK	WB: 1:1000	9102S	CST	Rabbit
Twist1	WB: 1:1000	3879S	CST	Rabbit
Alexa_fluor_488	ICC: 1:500	ab150141	Abcam	Rabbit
IQGAP1	WB: 1:1000 IP: 1:50	AB86064	Abcam	Rabbit
Anti-GST	WB: 1:2000	G7781	Sigma	Rabbit
VEGFR2	WB: 1:1000	2479	CST	Rabbit
Anti-phospho-VEGFR2 Tyr1175	WB: 1:1000	SAB4504567	Sigma	Rabbit
Anti-Cytokeratin 14	IHC: 1:2000	ab181595	Abcam	Rabbit
IQGAP3	IHC: 1:500	HPA030143	Sigma	Rabbit

APPENDIX III: List of primers used in study

Primer Name	Primer sequence (5' - 3')
GAPDH F	ACCCAGAAGACTGTGGATGG
GAPDH R	TCTAGACGGCAGGTCAGGTC
IQGAP2 F	TTCAGTCCTGGTTCCGAATGGC
IQGAP2 R	TGTTCGCTCTCAACAGTGACTGT
ANGIOSTATIN F	CTGGCCAGTCCCAAAATGGA
ANGIOSTATIN R	AGAGGCTCTCCTTGACCTGA
ANGPT1 F	TGCAGAGAGATGCTCCACAC
ANGPT2 R	CTCAGTGGCTAATGAAGCTTGAGA
ANGPT2 F	TCATCACAGCCGTCTGGTTC
ANGPT2 R	TCTCAAGTTTTTGCAGCCACTG
ANGPTL3 F	CCCAATGCAATCCCGGAAAAC
ANGPTL3 R	CACCAGCCTCCTGAATAACCC
ANPEP F	CCTGATGGACCAGTACAGCG
ANPEP R	TCCACTGCTTGAAAAGGCCA
CCL11 F	ACCCCTTCAGCGACTAGAGA
CCL11 R	CTTGAAGATCACAGCTTTCTGGG
CCL2 F	GCTCAGCCAGATGCAATCAAT
CCL2 R	CACTTGCTGCTGGTGATTCTT
CCL3 F	TTCCGTCACCTGCTCAGAAT
CCL3 R	GCAGCAAGTGATGCAGAGAAC
PGR F	GTGCCTATCCTGCCTCTCAATC
PGR R	CCCGCCGTCGTAACTTTCG
PS2 F	CATCGACGTCCCTCCAGAAGAG
PS2 R	CTCTGGGACTAATCACCGTGCTG
ESR1 F	GCTACGAAGTGGGAATGATGAAAG
ESR1 R	TCTGGCGCTTGTGTTTCAAC
CDK2 F	CCAGGAGTTACTTCTATGCCTGA
CDK2 R	TTCATCCAGGGGAGGTACAAC
CXCL1 Beta F	AACCTGCTGGTGTGTGACGTTC
CXCL1 Beta R	CAGCACGAGGCTTTTTTGTTGT
CXCL1 F	AACCGAAGTCATAGCCACAC
CXCL1 R	GTTGGATTTGTCACTGTTCAGC
CXCL10 F	AAGACCCAGACATCAAGGCG
CXCL10 R	AATCGATGACAGCGCCGTAG
CXCL3 F	GATACTGAACAAGGGGAGCAC
CXCL3 R	TTTTCAGCTCTGGTAAGGGCA
CXCL5 F	CAGACCACGCAAGGAGTTCA
CXCL5 R	TCTTCAGGGAGGCTACCACT
CXCL6 F	TGCGTTGCACTTGTTTACGC
CXCL6 R	GGAGGCTACCACTTCCACCT
CXCL8 F	ACCGGAAGGAACCATCTCAC

CXCL8 R	GGCAAAACTGCACCTTCACAC
CXCL9 F	GTGCAAGGAACCCCAGTAGT
CXCL9 R	GGGCTTGGGGCAAATTGTTT
ENDOGLIN F	GGACACAGGATAAGGCCCAG
ENDOGLIN R	TTCTGCAAGACTTGTGGGGC
ENDOSTATIN F	GTCCTGGGGAGAGCATGG
ENDOSTATIN R	CTGATGCGCTCTGGCTCC
ENDOTHELIN1 F	CAGAAACAGCAGTCTTAGGCG
ENDOTHELIN1 R	GACTGGGAGTGGGTTTCTCC
FGF1 F	GCGGTCCTCGGACTCACTA
FGF1 R	AGCCAATGGTCAAGGGAAC
FGF2 F	GCGGTCCTCGGACTCACTA
FGF2 R	AGCCAATGGTCAAGGGAAC
FGF4 F	TCTATGGCTCGCCCTTCTTC
FGF4 R	CATGCCGGGGTACTTGTAGG
FGF7 F	TGCAAAGAAAGAATGCAATGAAGA
FGF7 R	TTTCCCCTCCGTTGTGTGTC
GMCSF F	GCCCTGGGAGCATGTGAATG
GMCSF R	CTGTTTCATTCATCTCAGCAGCA
HGF F	GACGCAGCTACAAGGGAACA
HGF R	GGCAAAAAGCTGTGTTCGTG
MMP1 F	AGAGCAGATGTGGACCATGC
MMP1 R	TTGTCCCGATGATCTCCCCT
MMP10 F	AGTTTGGCTCATGCCTACCC
MMP10 R	TTGGTGCCTGATGCATCTTCT
MMP2 F	CGTCGCCCATCATCAAGTTC
MMP2 R	CAGGTATTGCACTGCCAACTC
MMP3 F	CACTCACAGACCTGACTCGG
MMP3 R	AGTCAGGGGGAGGTCCATAG
MMP8 F	AAGCCAGGAGGGGTAGAGTT
MMP8 R	TTTTCCAGGTAGTCCTGAACAGT
MMP9 F	TTCAGGGAGACGCCCATTTC
MMP9 R	AGCGAGAGACTCTACACCCA
NRP2 F	TCGGCTTTTGCAGGTGAGAA
NRP2 R	AGTCCACCTCGTATTCATCATCA
p21 F	CGATGGAACTTCGACTTTGTCA
p21 R	GCACAAGGGTACAAGACAGTG
PDGFA F	GCCAACCAGATGTGAGGTGA
PDGFA R	GGAGGAGAACAAAGACCGCA
PDGFB F	ACCTGCGTCTGGTCAGC
PDGFB R	ATCTTCCTCTCCGGGGTCTC
TGFB F	GCAACAATTCCTGGCGATACC
TGFB R	AAAGCCTCAATTTCCCCTCC
TWIST1 F	GGAGTCCGCAGTCTTACGAG
TWIST1 R	TCTGGAGGACCTGGTAGAGG

SIP1 F	TTCCTGGGCTACGACCATAC
SIP1 R	TGTGCTCCATCAAGCAATTC
VEGF-A F	AGGAGGAGGGCAGAATCATCA
VEGF-A R	CTCGATTGGATGGCAGTAGCT
VEGF-B F	GATCCGGTACCCGAGCAGTCAG
VEGF-B R	CACCTGCAGGTGTCTGGGTTGA
VEGF-D F	ATCTGTATGAACACCAGCACCTC
VEGF-D R	TGGCAACTTTAACAGGCACTAAT
FOXC2 F	GCCTAAGGACCTGGTGAAGC
FOXC2 R	TTGACGAAGCACTCGTTGAG
E-CADHERIN F	TGCCCAGAAAATGAAAAAGG
E-CADHERIN R	GTGTATGTGGCAATGCGTTC
N-CADHERIN F	ACAGTGGCCACCTACAAAGG
N-CADHERIN R	CCGAGATGGGGTTGATAATG
FN1 F	CAGTGGGAGACCTCGAGAAG
FN1 R	TCCCTCGGAACATCAGAAAC
VIMENTIN F	GAGAACTTTGCCGTTGAAGC
VIMENTIN R	GCTTCCTGTAGGTGGCAATC
SNAIL F	CCTCCCTGTCAGATGAGGAC
SNAIL R	CCAGGCTGAGGTATTCCTTG

APPENDIX IV: ASSAY PROCEDURES

Plasmid extraction (Midiprep)

Plasmid extraction was performed using QIAGEN Plasmid Midi Kit, Cat No./ID: 12145 (Qiagen, Germany). Below mentioned protocol is adapted from QIAGEN Plasmid Purification Handbook.

1. Overnight bacterial culture (100 ml) was harvested by centrifugation at 6000 x g for 15 minutes at 4°C.
2. Bacterial pellet was then resuspended in 4 ml Buffer P1.
3. 4 ml of Buffer P2 was added, thorough mixing was done by inverting 4–6 times and room temperature incubation was carried out for 5 minutes.
4. 4 ml of pre-chilled Buffer P3 was then added, and thoroughly mixed by inverting 4–6 times. Incubation on ice was done for 15 minutes.
5. Centrifugation was done at ≥ 20,000 x g for 30 minutes at 4°C. Then, supernatant was centrifuged at ≥ 20,000 x g for 15 minutes at 4°C.
6. QIAGEN-tip 100 was equilibrated by applying 4 ml Buffer QBT.
7. Supernatant was poured in the QIAGEN-tip, allowed to enter the raisin by gravity flow.
8. QIAGEN-tip was washed twice with 10 ml of QC buffer.
9. DNA was eluted with 5 ml Buffer QF into a 15 ml tube.
10. 3.5 ml room-temperature isopropanol was then added to the eluted DNA and, mixed for precipitation of DNA. Then centrifugation was done at ≥ 15,000 x g for 30 minutes at 4°C. The resulting supernatant was then carefully decanted.
11. Pellet was washed twice with 70% ethanol and centrifuged at ≥ 15,000 x g for 10 minutes. Supernatant was carefully decanted. The final pellet was air-dried for 5-10 minutes and DNA was dissolved in 100 µl of 1X TE buffer.

Plasmid extraction (Miniprep)

Plasmid extraction was done using QIAGEN Plasmid Mini Kit, Cat No./ID: 12125 (Qiagen, Germany). Below mentioned protocol is adapted from QIAGEN Plasmid Purification Handbook.

1. Bacterial cells were pelleted and the pellet was resuspended in 250 µl Buffer.
2. 250 µl of Buffer P2 was then added and thorough mixing was done by inverting the tube 4-6 times.
3. 350 µl of Buffer N3 was then added and thorough mixing was done by inverting the tube 4-6 times.
4. Centrifugation was done at 13,000 rpm (~17,900 x g) for 10 minutes in a table-top microcentrifuge.
5. A compact white pellet was formed, subsequently 800 µl of the supernatant was transferred to the QIAprep 2.0 spin column by pipetting.
6. Centrifugation for 30-60 seconds was done and the resulting flow through was discarded.
7. Washing of the QIAprep 2.0 spin column was carried out by adding 0.75 ml Buffer PE and centrifuging for 30–60 seconds.
8. The flow-through was discarded, and centrifugation at full speed for an additional 1 minutes to remove residual wash buffer, was carried out.
9. The QIAprep 2.0 column was then placed in a clean 1.5 ml microcentrifuge tube. DNA was eluted by adding 30 µl Buffer EB (10 mM Tris·Cl, pH 8.5) to the center of each QIAprep 2.0 spin column, and subsequently centrifugation was done for one minute.

Endotoxin free plasmid extraction

Plasmid extraction was done using EndoFree Plasmid Maxi Kit, Cat No./ID: 12362, (Qiagen, Germany). Below mentioned protocol is adapted from EndoFree Plasmid Purification Handbook.

1. A single colony was picked from a freshly streaked selective plate and inoculated onto a starter culture of 2-5 ml LB medium containing the appropriate selective antibiotic. Incubation was carried out for approx. 8 hours at 37°C with vigorous shaking
2. The starter culture was diluted into a selective LB medium. 100 ml medium was inoculated with 100–200 µl of starter culture and grown at 37°C for 12–16 hours with vigorous shaking.
3. The bacterial cells were then harvested by centrifugation at 6000 x g for 15 minutes at 4°C.
4. The bacterial pellet was resuspended in 10 ml Buffer P1.
5. 10 ml Buffer P2 was subsequently added, thorough mixing was done by vigorously inverting the tube 4–6 times, and incubated at room temperature (15–25°C) for 5 minutes.
6. Then, 10 ml chilled Buffer P3 was added to the lysate and mixed immediately by vigorously inverting 4–6 times.
7. The lysate was then poured into the barrel of the QIAfilter Cartridge and incubated at room temperature for 10 minutes.
8. Cap from the QIAfilter Cartridge outlet nozzle was removed. The plunger was gently inserted into the QIAfilter Maxi Cartridge. The cell lysate was filtered into a 50 ml tube.

9. 2.5 ml of Buffer ER was added to the filtered lysate, mixed by inverting the tube approximately 10 times, and incubated on ice for 30 minutes.
10. A QIAGEN-tip 500 was equilibrated by applying 10 ml Buffer QBT, and allowing the column to empty by gravity flow.
11. Apply the filtered lysate incubated with buffer ER from step 9 to the QIAGEN-tip and allow it to enter the resin by gravity flow.
12. The QIAGEN-tip was washed twice with 30 ml Buffer QC.
13. DNA was then eluted with 15 ml Buffer QN.
14. DNA was precipitated by adding 10.5 ml (0.7 volumes) room-temperature isopropanol to the eluted DNA. The mixture was centrifuged immediately at ≥ 15,000 x g for 30 minutes at 4°C and the supernatant was carefully decanted.
15. Finally, the DNA pellet was washed with 5 ml of endotoxin-free room-temperature 70% ethanol and centrifuged at ≥ 15,000 x g for 10 minutes. The supernatant was carefully decanted.
16. The pellet was air-dried for 5–10 minutes, and DNA was dissolved in a 100 µl of endotoxin-free Buffer TE.

RNA extraction

Plasmid extraction was performed using RNeasy Mini Kit, Cat No./ID: 74106 (Qiagen, Germany). Below mentioned protocol is adapted from RNeasy Mini Handbook.

1. Cells growing in a 60 mm dish were harvested by direct lysis in the vessel by adding 350 µl of Buffer RLT.
2. 1 volume of 70% ethanol was added to the lysate, and mixed well by pipetting.
3. Up to 700 µl of the sample was transferred to an RNeasy Mini spin column placed in a 2 ml collection tube, and centrifuged for 15 seconds at ≥ 8000 x g. The flow-through was discarded.

4. 700 µl Buffer RW1 was added to the RNeasy spin column and centrifuged for 15 seconds at ≥ 8000 x g. The flow-through was discarded.
5. 500 µl Buffer RPE was added to the RNeasy spin column and centrifuged for 15 seconds at ≥ 8000 x g. The flow-through was discarded.
6. 500 µl Buffer RPE was added to the RNeasy spin column and centrifuged for 15 seconds at ≥ 8000 x g. The flow-through was discarded.
7. The RNeasy spin column was subsequently placed in a new 1.5 ml collection tube. 30 µl RNase-free water was added directly to the spin column membrane, and centrifuged for 15 s at ≥ 8000 x g to elute the RNA.

ELISA

Plasmid extraction was performed using Human VEGF Quantikine ELISA Kit, Cat No./ID: DVE00 (R&D Systems, USA). Below mentioned protocol is taken from the datasheet of Quantikine®ELISA, Human VEGF Immunoassay.

1. 50 µl of Assay Diluent RD1W was added to each well.
2. 200 µl of standard, control, or sample as added per well. The strips were then covered with the adhesive strip provided and incubated for 2 hours at room temperature
3. Each well was aspirated and washed, repeating the process twice for a total of three washes. Washing was done by filling each well with Wash Buffer (400 µl). After the last wash, the remaining wash buffer was carefully decanted completely.
4. 200 µl of Human VEGF Conjugate was added to each well. The strip was covered with a new adhesive strip and subsequently incubated for 2 hours at room temperature.
5. The wash step was then repeated as described previously.

6. 200 µl of Substrate Solution was added to each well. Protect from light. Incubation for 20 minutes was done at room temperature.
7. 50 µl of Stop Solution was added to each well.
8. Optical density of each well was determined within 30 minutes, using a microplate reader set to 450 nm.

APPENDIX V: BUFFERS

Buffer name	Components	Weight/volume
Agarose gel electrophoresis		
6x DNA loading buffer (100 ml)	0.5 M EDTA, pH 8	12 ml
	Glycerol	60 ml
	Bromophenol blue	10 mg
	dH_2O	to 100 ml
50x TAE (1 L)	Glacial acetic acid	57.1 ml
	Tris base	242.2 g
	0.5 M EDTA, pH 8	100 ml
	dH_2O	to 1 L
SDS-PAGE and Western Blot		
30% Acrylamide (100 ml)	Bis-acrylamide	1 g
	Acrylamide	29 g
	dH_2O	to 100 ml
0.5 M Tris-Cl, pH 6.8 (100 ml)	Tris base	6 g
	pH 6.87 with 6 N HCl	
	dH_2O	to 100 ml
1.5 M Tris-Cl, pH-8.8 (100 ml)	Tris base	18.15 g
	dH_2O	80 ml
	pH 8.8 with 6 N HCl	
	dH_2O	to 100 ml
10% (w/v) APS (10 ml)	Ammonium persulfate	1 g
	dH_2O	to 10 ml
10% (w/v) SDS (100 ml)	SDS	10 g
	dH_2O	to 100 ml
Water-Saturated n-Butanol (55 ml)	n-Butanol	50 ml
	dH_2O	5 ml
2× SDS-PAGE (Laemmli, 30 ml)	50% Glycerol	15 ml
	1.0% Bromophenol blue	0.3 ml
	10% SDS	6 ml
	0.5 M Tris-HCl, pH 6.8	3.75 ml
	dH_2O	to 30 ml
	β-mercaptoethanol (50 µl to 950 µl sample buffer) before use	
TGS Running buffer (10x)	Tris base	30.2 g
	Glycine	144 g
	SDS	10 g
	dH_2O	to 1 L
10x Transfer buffer (4 L)	Tris base	121.1 g
	Glycine	576 g
	dH_2O	to 4 L
1x Transfer buffer (1 L)	10x Transfer buffer	100 ml
	dH_2O	700 ml
	Methanol	200 ml
10x TBS (1 L)	Tris base	24 g
	NaCl	88 g
	pH to 7.6 with concentrated HCl	
	dH_2O	to 1 L
0.1% TBST (1 L)	20x TBS	50 ml

	Tween 20	1 ml
	dH_2O	to 1 L
Other buffers and solutions		
4% Paraformaldehyde (1 L)	1x PBS	800 ml
	Paraformaldehyde powder	40 g
	1x PBS	to 1 L
10x PBS (1 L)	$Na_2HPO_4 \cdot 7H_2O$	25.6 g
	NaCl	80 g
	KCl	2 g
	KH_2PO_4	2 g
	dH_2O	to 1 L
Crystal violet stain (100 ml)	Crystal violet	2 g
	Ethyl alcohol	20 ml
	Ammonium citrate monohydrate	0.8 g
	dH_2O	80 ml